STUDIES ON FREE SURFACE FLOW OF CONCENTRATED SUSPENSION IN OPEN CHANNELS AND ROTATING CYLINDERS

A Thesis submitted in partial fulfillment of the requirements for the degree of

DOCTOR OF PHILOSOPHY

By

A. ASHOK KUMAR

DEPARTMENT OF CHEMICAL ENGINEERING

INDIAN INSTITUTE OF TECHNOLOGY GUWAHATI

GUWAHATI, INDIA

May 2011

DECLARATION

It is certified that the work contained in the thesis entitled **"Studies on free surface flow of concentrated suspension in open channels and rotating cylinders"** has been done by me, a student in the Department of Chemical Engineering, Indian Institute of Technology Guwahati under the guidance of **Prof. Anugrah Singh** for the award of Doctor of Philosophy and that this work has not been submitted elsewhere for a degree.

Date:

A. ASHOK KUMAR

Research Scholar

Department of Chemical Engineering

Indian Institute of Technology Guwahati

CERTIFICATE

DEPARTMENT OF CHEMICAL ENGINEERING

IIT GUWAHATI

ASSAM-781039

It is certified that the work contained in the thesis titled **"Studies on free surface flow of concentrated suspension in open channels and rotating cylinders"** by **A. Ashok Kumar,** a student of the Department of Chemical Engineering, India Institute of Technology Guwahati, for the award of the degree of Doctor of Philosophy has been carried out under my supervision and that this work has not been submitted elsewhere for a degree.

Date: 26 May 2011

Dr. ANUGRAH SINGH

Associate Professor

Department of Chemical Engineering

Indian Institute of Technology Guwahati

DEDICATION

To my parents

A. Manonmany & A. Annadurai

Without their support this would not have been possible

ABSTRACT

Free surface flow of concentrated suspension has been studied in open channel and rotating cylinders at low Reynolds number flow. In this work, the wall slip was characterized through flow visualization experiments. The conventional rheometers and Couette cells has been used for determining slip velocity for suspension of smaller particles. However, characterization of wall slip for suspensions of larger particles such as debris flow, concrete mixtures etc. cannot be performed in conventional rheometers. For such systems we have provided the technique of determining wall slip from the velocity profile measurements in open channel flow. To measure the velocity profiles in open channel flow, we have used the method of particle image velocimetry (PIV). Experiments have been carried out under the conditions of slip and no-slip conditions and velocity and surface corrugation patterns have been analyzed. Our study showed that the wall slip only changes the velocity profile and it has no apparent effect on the surface corrugation. This is because the slip layer affects are confined near the wall, the bulk shape of the surface remains unchanged. To measure the height of corrugation structures we have performed measurements in velocity-vorticity plane. The interface was seeded with hollow glass balloons which floated on the surface and their location was determined using an edge detection technique. Position of maximum gradient of image intensity determines the interface height. By comparing the interface profile between two consecutive image frames we determined the vertical velocity of the interface. It is observed that interface fluctuation increases linearly with increase in shear rate. The perturbation of the interface in the velocity-vorticity plane increases with increase in particle concentration until an optimum particle concentration, and thereafter the height of the free surface corrugation decreases continuously. These results also support the findings from the analysis of spectra of refracted light from the free surface. It is observed that the interface fluctuation increases with increase in particle size for a given suspending fluid whereas it decreases with increase in the viscosity of suspending fluid for suspension of given particle size. In another study we have, investigated the band formation during free surface flow of concentrated suspension of bi-dispersed particles in rotating cylinders. In this work, we have studied the behavior of bi-dispersed neutrally and non-neutrally buoyant suspension of non-colloidal particles in a horizontally rotating cylinder separately. Experiments were carried out at various filling fractions and angular speed of the cylinder. A number of distinct patterns of particle size

segregation were observed for various conditions. At low rotation speeds, the gravity force on the particles dominates and we observe that alternate bands of larger and smaller particles completely fill the tube. These bands also move axially and merge to form bigger bands. The number of bands decreases with rotation speed whereas the band width increases. At higher speeds the bands of smaller particles are disturbed by the bigger particles and no stable axial segregation is observed. On the other hand, at much higher speed when the centrifugal force on the both smaller and larger particles dominates, the particle bands segregate from the suspending fluid. The bands of larger and smaller particles are found to be side by side. The number of bands in this regime increases with the rotation speed of the cylinder. It was observed that the dry granular particles consisting of only bi-modal spherical particles of same density do not exhibit axial segregation. Thus, it can be concluded that the interplay between gravity, buoyancy, viscous drag and centrifugal force on the particles in suspension plays an important role in size segregation in rotating cylinder. The relation between free surface fluctuations and axial migration is also discussed.

ACKNOWLEDGEMENTS

எந்நன்றி கொன்றார்க்கும் உய்வுண்டாம் உய்வில்லை
செய்ந்நன்றி கொன்ற மகற்கு.

He who has killed every virtue may yet escape;
There is no escape for him who has killed gratitude.

I would first like to thank God for his/her grace to get me such a wonderful guide like Dr. Anugrah Singh. When I arrived at IITG, my intention was to do a PhD in any environmental area. I was thinking that doing PhD in environment might be easier than other core chemical engineering areas. I did not expect that I will do my PhD in fluid mechanics, where I was totally blank. But, when I was asked to meet each professor to choose our research guide, I met Dr. Anugrah Singh. When he talked with me about the research area, it gave me a confidence, and I was convinced myself to take such a challenging work. Here, I sincerely thank him for this opportunity, and also for his continuous support and encouragement. Once again, I express my sincere gratitude to him for his highly patience at me.

I would also like to thank Dr. G.Pugazhenthi for his continuous and deep support as my doctoral committee chairman and for his moral support in all my crucial times. I am very thankful to him that I never ever forget his all time support; moreover there are no words to express my thankfulness to him.

I want to acknowledge the effort made in reviewing this thesis work by Dr. Ujjwal K. Saha. I extend my hearty thanks to him for his effort to bring this thesis to perfection.

I have also been fortunate to have great technician Mr. Minesh Ch. Medhi from central workshop IITG who had made all my experimental setups. I would like to extend my gratitude to him for his great support and perfect understanding of my expectation to get in to real on the fabrication of experimental setups.

I wish to thank Mr. Bhaskar Jyoti Medhi who had given me daily encouragement and support. I am very thankful to him where he had shared my work from fabrications to conducting experiments in my research period.

I would like to express my special hearty thanks to M. Eswaran, Dr. Pichai Saravanan, Dr. Senthil Kumar, Shyam Anand, P. Monash, P. Aadaleesan, Biraj Kumar Kakati and N.

Vinothkumar for their technical help and moral support in all the ways. Without their contribution I would not have completed this work.

I wish to make a separate space to express my grateful thanks to Mr. Anto Pradeep for his help in grammatical correction which only can make the thesis meaningful. I am very thankful to him for his patience and effort in my thesis writing.

I would like to extend my sincere thanks to E. Suganya and Jansi for their all time moral support. Finally, I am very grateful and thankful to all my juniors and friends Yennam Rajesh, Laxmanan, Somnath Mondal, S. Yadav, Ashish Kumar Thokchom, Dr. Subramanian, Dr. Arumugaperumal, N. Sivarama Krishnan, D. Vasanth, R. Anantharaj, S. Murugavelh, Sakthivel for their all time support and encouragement.

CONTENTS

NOMENCLATURE

Symbol	Description
a	Particle radius
C_1	Concentration of larger particles
D	Shear induced diffusivity
d	Self diffusivity
d_p	Particle diameter
g	Gravity force
H	Channel width
I	Intensity value
I_0	Averaged intensity value
J_d	Drift flux
K	Crowding effect
κ	Relative roughness parameters
K_c	Diffusion coefficient in concentration
K_η	Diffusion coefficient in viscosity
L	Channel length scale
N	Rotation rate in rpm
N_c	Particle flux
N_t	Total diffusive flux
N_η	Viscosity gradient induced migration flux
R, R_i, R_a	Radius of cylinder, Inner radius, Outer radius
R_{ew}	Reynolds number based on cylinder radius and angular rotation
u	Velocity
u_s	Apparent wall slip velocity
X_f	Filling fraction
Y_m	Root mean squared fluctuation
ϕ	Particle volume fraction
ϕ_m	Maximum particle packing fraction

ρ	Density
ρ_s	Suspending fluid density
ρ_p	Particle density
η	Viscosity
η_{eff}	Effective viscosity
η_s	Suspending fluid viscosity
λ	Relative effective viscosity of suspension
β	Wall slip coefficients
β_1	Dynamic angle of repose
$\Delta\psi$	Difference in dynamic angle of repose between larger and smaller particles.
$\dot{\gamma}$	shear rate
δ	Slip layer thickness
τ	Shear stress tensor
ω	Vertical velocity of the interface
Ω	Angular speed of rotation

ABBREVIATIONS

CCD	Charged Coupled Device
LDA	Laser-Doppler Anemometer
LDV	Laser-Doppler Velocimetry
NMR	Nuclear Magnetic Resonance
OBC	Oscillatory Baffled Column
PCB	Printed Circuit Board
PIV	Particle Image Velocimetry
PSD	Power Spectral Density
PMMA	Poly-Methylmethacryalte
RBC	Red Blood Cells
SEM	Surface Elevation Mapping
Triton-X-100	t-Octylphenoxypoly-ethoxy-ethonal
WBC	White Blood Cells

LIST OF FIGURES

CHAPTER 1

INTRODUCTION

1.1 SUSPENSION

Suspension can be defined as a two phase mixture comprising of dispersion of one phase in another. The dispersed phase may be solid particles (Brownian or non-Brownian) and continuous phase may be a liquid or a gas. In general, suspensions can be divided in three categories: solid particles dispersed in a liquid medium, liquid droplets present in a liquid medium (emulsion) and gas in a liquid medium (such as foam). In our study by the term suspension we refer dispersion of solid particles in a viscous liquid medium. Examples of this type of suspensions are industrial slurries, paste, composite materials, ceramics, colloids, polymers, etc. Suspensions are commonly used in day to day human life such as chocolate (sugar crystals and coca dispersed in a continuous fat), milk, ice cream, tooth paste etc. Suspensions are also often encountered in many industrial applications and natural settings. Some common examples of suspension flow encountered in industrial applications are material processing, mineral processing, food processing, drilling mud, and in nature, the suspension flow can be found in the form of flood waves, debris flow, slurries flow, lava flow etc. It is also commonly found in the biological systems such as blood (RBC and WBC particles in plasma medium). Many industrial processes deal with slurry transport that is being mixed and pumped from one place to another without allowing the solids to precipitate. The presence of non-Brownian spherical particles in such suspension affects the properties of the whole mixture such as density, viscosity, thermal conductivity etc. Hence, the flow behavior of these suspensions is often complex and their rheological properties are often very different from those of the suspending fluid. Hence, these materials are also a part of the larger system of 'complex fluids'. A vast quantity of products and raw material in the form of complex fluids are handled by the chemical, bio-chemical and pharmaceutical industries. Thus, there is a clear need for an understanding of the flow behavior of these systems. This

would help us in better and more efficient handling of such materials in an industrial scenario.

As mentioned above a number of experimental evidences suggest that the characteristic of suspension flow is different from those of an equivalent homogeneous liquid. At moderate to high particle concentration, the hydrodynamic interactions between particles significantly alter the flow characteristics. These systems often exhibit many interesting phenomena, which are not seen in the flow of a Newtonian fluid. Now it is well known fact that even though the suspending fluid is Newtonian, the flowing suspensions exhibit non-Newtonian characteristics. Many interesting phenomena often observed in the suspension flow such as shear induced migration, particle segregation, blunted velocity profile, wall slip, surface corrugation etc. are not encountered in simple Newtonian homogenous liquid. Hence it is important to know the physics of such flows for better design and handling of suspension in process industries. From a practical point of view the study of such system is critical in dealing with current industrial problems. In the biological systems such as living cells, blood it is an even more exciting problem for practical application. Suspension exhibits the flow characteristics in a wide range, which is from solid-like (for example squeezing toothpaste out of a tube) to even gas-like (the bed of particles in gas-solid fluidized beds). The difficulty arises even more in the analysis of flow behavior of suspensions, where the suspending fluids are not a simple fluid like water and air (Newtonian fluids). In fact complex flow behavior of suspension can exist in nano, micro as well as macro scale level. The macroscopic flow behavior of a suspension depends on the dynamics at the micro-structural level. Thus, the inter-particle forces and hydrodynamic forces are essential to understand the micro-structure or micro-mechanics of particles in suspensions. In industrial applications an in-depth knowledge of their complex rheological behavior is required for the optimum manufacturing, processing, and design of the materials. Hence, the suspension flow problems are quite challenging, active and attractive are of research among fluid mechanic researchers.

1.2 SUSPENSION VISCOSITY

The suspension flow behavior can be very complex and it can exhibit non-Newtonian characteristics even if the suspending fluid is Newtonian. Suspension viscosity and particle fraction play a vital role in the flow behavior of suspensions. However in the beginning, suspensions were treated as Newtonian fluids with enhanced viscosity. One of the earliest contributions to the calculation of viscosity of suspensions in terms of the volume fraction of the dispersed particles was given by Einstein (1906). His theoretical analysis was valid for

suspensions so dilute that the movement of one sphere does not influence the fluid flow in the neighborhood of any other sphere. Then it suffices to analyze only the motion of the fluid around a single sphere, and the effects of the individual spheres are additive. The viscosity of such suspensions was found to be a function of the concentration of suspended particles, given in terms of particle volume fractions (ϕ). The theoretical expression of Einstein (1906) for the effective viscosity of suspension is as follows,

$$\eta_{eff} = \eta_S(1+2.5\phi), \tag{1.1}$$

where η_{eff} is the effective viscosity of suspension and η_S is the viscosity of suspending fluid. After the work of Einstein (1906), further advancements in the representation of suspension rheological properties in terms of particle volume fraction (ϕ) was provided by Batchelor (1969) who developed the ensemble volume average method for determining rheological properties from known properties of fluid and particles. When interactions between particles are included, the situation becomes more complicated. The presence of other particles is accounted for by higher-order terms in ϕ. Batchelor (1969) derived the expression for the effective viscosity of suspension as,

$$\eta = \eta_S(1+2.5\phi+6.2\phi^2) \tag{1.2}$$

In a review paper, Jeffery and Acrivos (1976) have discussed several factors other than ϕ which affects the suspension rheology at high particle concentrations. A great amount of work has been done on the dilute suspensions, but almost all conclude that these are of little relevance to suspensions of industrial importance. The theories of dilute suspensions cover the range below 10% phase volume. The situation for concentrated suspensions, where we expect higher-order terms than ϕ^2 to be important, is even more difficult to analyze. Ball and Richmond (1980) started from the assumption that in a concentrated suspension the effect of all the particles are additive and proposed the following correlation,

$$\eta = \eta_S(1-K\phi)^{-5/2K} \tag{1.3}$$

where, K accounts for the so-called "crowding" effect. Ball and Richmond's expression is effectively identical to that of Krieger and Dougherty (1959). Krieger and Dougherty's theory also states that, in the general case, the $5/2$ factor should be replaced by the intrinsic viscosity

(η). The value of $5/2$ is the intrinsic viscosity for an ideal dilute suspension of spherical particles. The Krieger-Dougherty correlation is as follows,

$$\eta = \eta_s \left(1 - \frac{\phi}{\phi_m}\right)^{-1[\eta]\phi_m} \tag{1.4}$$

where, ϕ_m denotes the maximum packing fraction. At extremely high concentration the particles in the suspension "jam up", giving continuous three-dimensional contact throughout the suspensions, thus making flow impossible, i.e. the viscosity tends to infinity. The particular phase volume at which this happens is called the maximum packing fraction ϕ_m. The value of this parameter depends on various factors that influence the arrangement of the particles. Even for mono-disperse sphere the value of ϕ_m range from approximately 0.5 to 0.75 (Krieger and Dougherty, 1959).

1.3 SOME FLOW PHENOMENA IN SUSPENSIONS

The concentrated suspensions even at low Reynolds number exhibit many interesting phenomena such as shear induced migration, particle segregation, wall slip, surface corrugation etc. These phenomena which results from particle-particle and fluid-particle interactions depends on various factors such as the concentration of the particles, surface tension and viscosity of the suspending fluid as well as applied shear rate. We describe here some of the interesting phenomena which has attracted wide attention in recent years.

1.3.1 Shear-induced particle migration

Among the several non-linear behaviors of flow phenomena with particulate suspensions, the shear-induced particle migration is one of the most widely studied in the recent years. Subsequent to the studies on viscosity of suspensions, a number of researchers showed several evidences which challenged the generalized Newtonian description of suspension of solid particles in Newtonian fluids. The first experimental evidence of particle migration at low Reynolds number was provided by the work of Gadala-maria and Acrivos (1980), when they detected shear-thinning of suspension of neutrally buoyant particles in cylindrical Couette geometry over prolonged shearing. Their experiments and subsequent experiments in pipe flow of suspension proved that when a well mixed suspension is subjected to inhomogeneous shear flow then the particles migrate from the higher shear rate region and establish a particle accumulation in the low shear rate region. In the pressure driven pipe flow

(Hampton *et al*., 1997) the particles migrate from the regions of high shear (near the walls) to regions of low shear (the centerline). In addition, a number of curvilinear flows have been studied including wide-gap circular Couette flow, parallel-plate torsional flow and small angle cone- and-plate torsional flow. In wide-gap Couette flow, Abbott *et al*. (1991) and Phillips *et al*. (1992) observed particles migrate away from the rotating inner cylinder, a region of high shear to the outer stationary wall where the shear rate is lower. Chapman (1990) and Chow *et al*. (1994) observed little to no particle migration in a parallel-plate torsional flow while Chow *et al*. (1995) observed migration that is radially outward from the cone apex in the torsional cone-and-plate flow. The last two studies did not follow the assumption of migration from regions of high to low shear which predicts that the particles would have migrated radially inward from the higher shear experienced on the outer edges of the plate in the parallel-plate torsional flow and there would have been no migration in the cone-and-plate torsional flow where the shear rate remains constant throughout the domain, leaving no shear rate gradients to drive particle migration.

To explain observations of particle migration in concentrated suspensions a phenomenological model called 'Diffusive flux Model' was developed by Phillips *et al*. (1992) based on the arguments of Leighton and Acrivos (1987b). This model works well for rectilinear flow such as channel and pipe flow but fails to explain anomalous migration in curvilinear flow. The 'Suspension balance model' of Nott and Brady (1994) which is based on conservation equation for the suspension phase and particle phase, overcomes the limitation of Diffusive Flux model. Morris and Boulay (1999) illustrated the importance of anisotropy and normal stress difference effects for predictions of migration in curvilinear flows. This model has been recently used by Miller and Morris (2006) to simulate suspension flow employing finite volume technique. Miller *et al.* (2009) have presented a frame-invariant formulation of the suspension balance model for general geometries. Zarraga *et al*. (2000) and Singh and Nott (2003) have experimentally measured normal stresses in particulate suspensions. In addition, simulations by Phung *et al*., (1996) and Singh and Nott (2000) have also revealed the existence of normal stresses over a broad range of parameters in both bounded and unbounded shear flow.

1.3.2 Axial segregation of particles

Axial segregation of particles in a partially filled horizontally rotating cylinder is a free surface instability phenomenon which has attracted several studies in the recent past due to its practical applications. For example mixing of different sizes of particles dispersed in fluid

medium is carried out in a rotating drum to prepare pastes for manufacture of composite materials. Cement kilns also employ rotating drums for mixing of particles. Pan coater (which is a rotating tube device) is commonly used in pharmaceutical industries for coating different sizes of capsules and tablets in pharmaceutical industry. To improve the coating performance of such devices it is essential to understand the motion of particles and fluid inside the pan coater. Tirumkudulu *et al*. (1999) in an experiment with partially filled horizontal Couette device found a new kind of instability in the flow of suspensions containing narrow-sized neutrally buoyant particles in a very viscous Newtonian liquid. It was observed that the whole suspension segregates into regions of high and low particle concentration along the length of the cylinder. Tirumkudulu *et al*. (2000) conducted similar experiments but in a different geometry (horizontal rotating cylinder) which was partially filled with the similar suspension and rotated about it horizontal axis. They found that within a certain range of parameter space, the initially uniform suspension divided into bands of high particle concentration separated by regions of pure liquid. They suggested that this instability is initiated by particle concentration fluctuations, which lead to fluctuations in the effective viscosity of the suspension.

In another experiment, Timberlake and Morris (2002) observed alternate bands of relatively concentrated and dilute particle fraction along the axis of a partially filled inclined concentric cylinder. The number of bands was found to increase with the rotation speed of the cylinder. In these studies the fluid-air interface is thought to be important for axial segregation as no segregation was observed when the tube was fully filled with the neutrally buoyant particles. Subsequent to these experiments, Breu *et al*. (2003) studied the flow of non-neutrally buoyant suspension of mono-dispersed particles in a completely filled cylinder. They observed similar instabilities and pattern formations at higher rotation speed where centrifugal forces on the particles dominated over other forces. The reason for this observation was thought to be the density difference between the fluid and particles. Matson *et al*. (2006) further demonstrated that a suspension of non-colloidal settling particles in a completely filled horizontal cylinder demonstrates a rich array of concentration and velocity patterns at various rotation rates. In case of non-neutrally buoyant, mono-dispersed suspension the particles approach in downward side and expel in upward side and the formation of clusters depends on the rotation speed (Pan *et al*., 2007). Kalyankar *et al*. (2008) have also observed unique concentration and velocity patterns in a horizontally rotating cylinder completely filled with a mono-dispersed suspension of non-Brownian particles. Jain *et al*. (2001) reported alternate

band formation in wet granular media or slurries as well as for dry granular mixtures. They found that particle segregation in dry granular mixture is significantly faster compared to that in suspensions in liquid media.

There are several studies on the axial segregation of bi-modal granular mixtures but not many on the particulate suspensions. To our knowledge, there are no reported studies on suspension of bi-dispersed non-neutrally buoyant particles in rotating cylinder. In most of the practical applications the suspensions often have particles of different sizes. This motivated us to study the segregation pattern for bi-dispersed system. On the other hand, the phenomenon of particle segregation also provides an easy way of separating the particles by taking advantage of segregation caused by simply rotation of the cylinder. In our study, we have investigated the bi-dispersed suspension dynamics and free surface effect for both neutrally and non-neutrally buoyant suspension present in rotating cylinder. Both dry granular system and solid-liquid suspensions were investigated under rotation in partially and fully filled cylinder. In fully filled case, the dry granular system of bi-dispersed particles did not show any instability whereas for the case of suspension flow we observed a number of distinct patterns. We have carried out detailed investigation of these issues in this thesis.

1.3.3 Surface corrugation

Free surface flow of non-colloidal suspension of rigid particles in Newtonian fluids even at low Reynolds number causes the interface to become highly corrugated and it has been found that the surface deformation depends on the concentration of particles, surface tension of the suspending fluid and applied shear rate (Loimer *et al.*, 2002). Subsequent to these findings, Singh *et al*. (2006) have carried out experiments to measure free surface velocity profiles as well as dynamics of flow structure during flow of concentrated suspension in open channels using the tool particle image velocimetry. The surface corrugation or surface deformation is one of the important phenomenon observed during the free surface flow of concentrated suspension. Analysis of the spectra of the refracted light from the free surface has shown that flow structures of many length scales are present (Singh *et al*., 2006). It was also observed that as the particle fraction increases the autocorrelation function decays slowly.

Knowledge of the free surface shape is of fundamental importance to application to material processing industries (e.g. food processing, polymer processing) as the surface effect is particularly manifest at the interface where the transport of mass, momentum and energy are

affected. In such process, an increase in the interfacial area at the free-surface would be desirable and a welcome effect. Free-surface flow of suspensions is also encountered during dip coating/blade coating where it is desirable to have a smooth layer of coat on the surface and any surface in-homogeneity or corrugation is undesirable. Understanding of such flow will also help to understand the dynamics of flood waves and mud flow carrying extremely high content of suspended matters. Limited experimental studies have shown that the corrugation appears as an ensemble of disturbances depends on the particle size, on particle concentration and on the suspending fluid viscosity. From the point of view of practical applications, it is very important to know the correlation between free-surface deformation and near surface velocities. It is also desired to study the role of other parameters such as surface tension, particle concentration, particle size on the corrugation pattern. To measure the amplitude and velocity of the free surface motion in the channel flow, the variation in the height of the interface is needed to quantify the free-surface deformation. Brady and Carpen (2002) argue that there is an instability mechanism in non-Newtonian fluids when a jump in normal stress is present between the two fluids. Using stability analysis they have shown that the fluids with a negative second normal stress difference can be unstable with respect to transverse and span wise perturbations.

Timberlake and Morris (2005) have carried out study on the gravity-driven free-surface flow of falling film of neutrally buoyant suspension. They have measured the free surface velocity profile and film thickness down the inclined channel. Their measurements using the technique of stereoscopic particle velocimetry show particle migration away from the solid surface, which results from gradient in shear rate across the film height. Their model predictions which is based on the suspension balance approach of Nott and Brady (1994), do show a concentration gradient across the film thickness, which is in qualitative agreement with the experimental results, but overestimates the concentration at the free-surface. Timberlake and Morris suggested that this could be due to an improper boundary condition at the free surface. This adds to the importance of understanding the correlation between the surface microstructure and velocity near the interface. Subsequent to the experiments of Loimer *et al*. (2002), Singh *et al*. (2006) have studied the free surface flow of concentrated suspension in channel flow with the tool of particle image velocimetry. It was observed that as the concentration increases the blunting of velocity profiles across the channel increases. In the absence of significant particle migration the velocity profile indicates the presence of slip between the fluid and suspension near the wall of the channel. In view of the observed

slip velocity at the wall it is important to measure wall slip to formulate proper boundary conditions.

1.3.4 Wall slip

As mentioned above, Singh *et al*. (2006) while studying the free surface corrugation reported blunted velocity profile in absence of significant particle migration. Blunted velocity profile was also reported in the experiments of Lyon and Leal (1998) when concentration profile showed no inhomogeneities. The velocity blunting in cases where bulk suspension shows uniform particle concentration is due to wall slip which has been studied widely for particulate suspensions in non-Newtonian fluids but there are only few studies on suspension of non-colloidal particles in Newtonian fluids. It was observed that as the concentration increases the blunting of velocity profiles across the channel increases. In the absence of significant particle migration, the velocity profile indicates the presence of apparent slip between the fluid and bulk suspension near the wall of the channel. Slip or wall depletion effects are generally observed in the flow of two-phase fluids in rheometers, in pipe or any channel. When a two-phase or multi-phase fluid is brought into contact with a smooth, solid boundary, the local microstructure is first affected by physical depletion because the suspended particles cannot penetrate solid walls. This phenomenon can also be observed if there is no flow and this is known as static geometric depletion effect. There may be many reasons behind this phenomenon like steric, hydrodynamic, viscoelastic, chemical and gravitational forces acting on the solid particles adjacent to the wall. In many cases, the walls themselves can repel adjacent particles because of various physico-chemical forces arising between the particles and the walls, like electrostatic and steric.

When flow takes place in the bulk fluid, the resulting hydrodynamic and entropic forces can move the particles away from walls. Gravity also plays an important role in enhancing the slip effects especially for liquid systems that show any tendency to sediment or cream with time, which is generally the case with suspensions and emulsions. The slip phenomenon is basically occurrence of relative velocity between the wall and the fluid at the wall. Since the fluid is continuum, even in concentrated suspension there is no “true slip”. In real it is an “apparent slip”. The apparent slip is created by a region of high velocity gradient close to the wall and bulk fluid. Thus it appears an apparent slippage of the suspension thorough a thin liquid-rich layer (slip layer) of thickness at the wall (Vand, 1948). This layer is depleted of suspended particles compared to the bulk suspension. It is also well known that non-collodial concentrated suspensions have non-zero normal stress differences. Many polymeric fluids

have large first normal stress difference. Under condition of no-slip polymeric fluids with negative (extensional) first normal stress difference will behave like a stretched membrane. The non-colloidal suspensions are known to have positive (in the compression sense) first and second normal stress difference. Whether the presence of wall slip causes the free surface to exhibit shape (like when a stretched membrane is suddenly relaxed) in the form of surface corrugation was the motivation behind studying the effect of wall slip on surface corrugation.

1.4 GOALS AND OBJECTIVES

Our objectives were to study the free surface flow of highly concentrated suspensions in open channel flow and horizontally rotating cylinder. In the open channel flow our aim was to measure the amplitude and velocity of the free surface motion. It was also desired to measure the variation in the height of the interface to quantify the free-surface deformation. To achieve these objectives we have followed an approach which is very similar to that adopted by Law *et al*. (1999) to study the free surface waves. The interface would be visualized by adding hollow glass microballons which will float at the surface of the suspension. Due to the presence of these tracers the air side will produce luminance when illuminated with laser light, which contrasts very sharply with the suspension side and this contrast line will be imaged by the CCD camera. This contrast indicates the location of the interface, which will be determined using an edge detection algorithm. The intensity gradient at each point will be calculated and the edge is defined as the location of the maximum gradient. The movement of the interface can be tracked by calculating the displacement between two successive images. At a single location, the displacement is equivalent to the shift of varying intensity profiles. The location of the interface averaged over many frames can be interpreted as the free surface perturbation whereas from the displacement of the interface in two successive images the velocity of the interface can be calculated.

To study the velocity of the particles near the free surface in the bulk, we plan to use the method of particle image velocimetry (PIV). The technique of PIV has been used effectively in the past for the pure fluids, but recently, we have demonstrated that this method is also suited for the suspension flow. PIV technique requires capturing the image of a set of particles at frequent interval of time and determines their positions from the images. The velocity of the individual particles can then be calculated from the differences in their positions and known time intervals. In our study, the bulk flow will be seeded with small tracer particles having the same density as that of suspended particles. The suspension will be illuminated with a sheet of laser light. To obtain a good quality image, it is desired that only

few particles are illuminated and general scattering is avoided. This requires that the refractive index of the particles and the suspending fluids be nearly same. The velocity profile measurements will also be used to characterize wall slip. This would be achieved by performing measurements under conditions of slip and no-slip and comparing the velocity profiles from the two measurements.

The studies on the free surface flow of suspension in rotating cylinder is aimed at understanding as what effect the bi-dispersed particles has on size segregation. To understand the role of free surface on the size segregation it is our objective to carry out experiments for various fill fractions in the cylinder. To understand the interplay between viscous drag, gravity and centrifugal forces on the particles in the rotating cylinder we have carried out experiments at various rotation speeds.

1.5 THESIS OUTLINE

This thesis is divided into seven chapters starting with the introduction of concentrated suspension flow that has been discussed here (Chapter 1). Important studies in the past on various aspects of suspension flow including the wall slip, surface corrugation and free surface flow in rotating cylinder has been discussed in Chapter 2. The experimental measurements on apparent wall slip velocity during free surface flow of concentrated suspension in open channel flow have been presented in Chapter 3. This is followed by the investigation of wall slip effects on free surface corrugation in Chapter 4. Measurement of the interface area in open channel flow of concentrated suspensions is reported in Chapter 5. In Chapter 6 we have presented experiments on free surface flow of bi-dispersed suspensions in rotating cylinders. Results have been presented for both neutrally and non-neutrally buoyant suspensions at various rotation speeds and different fill levels. This is followed by conclusion in the last Chapter 7.

CHAPTER 2

LITERATURE REVIEW

2.1 SUSPENSION FLOW AND WALL SLIP

The concentrated suspension may be composed of neutrally or non-neutrally buoyant and colloidal or non-colloidal rigid particles that are immersed in Newtonian fluid. In recent years, the free surface flow of suspension has drawn more attention among fluid mechanic researchers due to its importance in process industries and natural settings. In general, most of the free surface flow of suspension has been carried out in circular (closed) and rectangular (open/closed) conduits, which are more commonly practiced in industries. The properties, such as density, viscosity, thermal conductivity and surface tension of the suspension, play a vital role in the flow processes. In general, transport of suspensions is easier than that of dry powder. So many industries have processed the dry powders in terms of suspensions. Many industries are facing problems in processing concentrated suspensions due to the lack of information on the transport processes. One can effectively and economically handle these materials by understanding the transport properties of the suspensions and its influence by the parameters, such as particle diameter, particle fraction, effective viscosity and surface tension. Many theoretical and experimental studies have been conducted on the flow of suspension by varying the process parameters to get optimum effective flow conditions, which are useful for industrial applications. Significant efforts have been made in last two decades to study the concentrated suspensions. In most of the studies the viscosity of such suspensions is assumed to be a function of the concentration of suspended particles, which is given in terms of particle volume fractions (ϕ). A very first record of evaluation of suspension properties is found in the work of Einstein (1906). In this work, the viscosity of dilute suspension has been expressed as a function of particle concentration for a suspension of spherical particles in Newtonian fluid. In general the flow of concentrated suspension is characterized by the strong interaction between the neighboring particles and this leads to

various interesting phenomena such as wall slip, surface corrugation, shear induced migration of particles, particle segregation, etc.

In a recent experiment, Loimer *et al*. (2002) have studied the nature of the free surface during the simple shear flow of concentrated suspensions of small inertia-less particles in a viscous fluid using Laser-Doppler velocimetry technique. They have observed that the corrugation of the surface depends on the particle size, particle concentration and on the surface tension of the suspending fluid. It is interesting to note that such phenomenon is observed at flow conditions where the Reynolds number is very small. Timberlake and Morris (2005) have carried out the studies on gravity-driven free-surface film flow of neutrally buoyant suspension. They have measured the free surface velocity profile and film thickness down the inclined channel. Their measurements, using the technique of stereoscopic particle velocimetry, show particle migration away from the solid surface, which is due to the gradient in shear rate across the film height. Their model predictions, which are based on the suspension balance approach (Nott and Brady, 1994; Morris and Bouley, 1999), do show a concentration gradient across the film thickness. Their results are in qualitative agreement with the experimental observations, but overestimate the concentration at the free-surface. The authors have suggested that the over estimation of concentration at the free surface could be due to an improper boundary condition at the free surface. This adds to the importance of understanding the correlation between the surface microstructure and velocity near the interface. Subsequent to the experiments of Loimer *et al*. (2002), Singh *et al*. (2006) have studied the free surface flow of concentrated suspension in channel flow by using particle image velocimetry (PIV). They have observed the blunting of velocity profiles as the concentration increases, which indicates the presence of apparent slip velocities near the channel wall, in the absence of significant particle migration. In view of the observed slip velocity at the wall, it is important to properly characterize the wall slip.

Apparent wall slip of complex fluids has attracted large number of studies (Yoshimura and Prud'homme, 1988; Yilmazer and Kalyon, 1989; Kalyon *et al*., 1993; Aral and Kalyon, 1994; Jana *et al*., 1995; Lawal and kalyon, 1997; Ekere *et al*., 2001; Kalyon, 2005; Nickerson *et al*., 2005; Lam *et al*., 2007; Ahuja and Singh, 2009). Though the phenomenon of wall slip is quite old, but it still attracts significant attention due to its practical importance. Moreover, the nature of wall slip under various flow conditions is far from understood. The wall slip phenomenon is basically the occurrence of apparent relative velocity between the wall and the fluid at the wall. However, since the fluid is continuum, even in concentrated suspensions

there is no 'true slip'. It is in reality an 'apparent slip' created by a region of high velocity gradient close to the wall compared to the bulk. This appears as an apparent slippage of the suspension through a thin liquid-rich layer (slip layer) of thickness δ at the wall (Vand, 1948). The slip layer is depleted of suspended particles compared to the adjacent regions of bulk suspension. As a result, if the rheological measurements are carried out with smooth geometries, the measured viscosity (also called as apparent viscosity) is much lower than the true viscosity of suspensions. The wall slip effects are generally observed in the flow of two-phase liquids in rheometers, in pipe, or any channel with smooth wall. Near the smooth solid boundary, the local microstructure is depleted because the suspended particles cannot penetrate the solid walls. This particle deficient layer can also be observed if there is no flow and this is known as static geometric depletion effect. This could result from steric, hydrodynamic, viscoelastic, chemical and gravitational forces acting on the solid particles adjacent to the wall (Barnes, 1995). In some situations, the walls can also repel adjacent particles because of electrostatic forces arising between the particles and the walls. During the bulk flow, the resulting hydrodynamic and entropic forces can move the particles away from the walls. The presence of large particles as disperse phase, smooth walls, low speeds or flow rates and wall and particles carrying electrostatic charges are some of the reasons which enhance the slip effects. Shear induced migration (Leighton and Acrivos, 1987b) can also cause depletion of particles near the wall and enhance the wall slip. It is now well known that to prevent slip at the wall, roughned and serrated wall surfaces can be used (Barnes, 1995). Nickerson et al. (2005) have described the use of cleated surfaces on parallel disk tools to quantitatively measure the rheological properties of diverse slip-prone fluids and soft materials. They have shown that the densely packed protrusions (0.45 mm × 0.45 mm cross section of 0.6 mm length, 0.9 mm apart) penetrate the slip layer and prevent significant flow between cleats. This creates a no-slip boundary ~ 0.16 mm below their tips, which serves as the sample gap boundary. They have also shown the advantage of cleated tools over other slip-preventing methods using increasingly challenging materials - an emulsion (mayonnaise), a suspension (peanut butter), and a biological tissue (procine vitreous humor). Bilodeau and Bousfield (1998) have presented a Stokesian dynamics model for the prediction of effective viscosity and microstructure for concentrated suspensions. They have shown the presence of slip plane for the dispersed and flocculated suspensions with smooth walls; the presence of slip plane reduces the suspension viscosity. They have also modeled the boundary roughness by attaching two particles to each boundary. This boundary roughness increases the viscosity predictions by an order of magnitude. The classic analysis of wall slip

is given by Mooney (1931) in Couette and capillary geometries of Rheometer. Yoshimura and Prud'homme (1988) have given a new way to calculate the wall slip velocity with rheometer. In their analysis, they have assumed that the wall-layer thickness is very small compared to the rheometer dimensions. They have treated the wall slip velocity as a discontinuity in velocity i.e., actual slip, where the slip velocity is defined as the difference between the velocity of the wall and that of the fluid at the wall. They have also assumed that once the steady state is achieved, the slip velocity is only a function of stress. They also have worked with parallel disks having torsional flows in which the apparent shear rate at the edge is related to the true shear rate at the edge, and corrected for slip. Kalyon et al. (1993) have studied the rheological behavior of a very concentrated suspension (76.5 vol. %), which is widely used as a solid rocket fuel stimulant. This fuel is characterized using both capillary and torsional flows. The suspension showed shear thinning over the apparent shear rate range of 30-3000 s^{-1}. They have observed considerable amount of slip at the wall, which increases from 0.001 mm/s at a shear stress of 4 Pa to as high as 60 mm/s at 100 kPa. Then, they have used a flow visualization technique for the first time to determine the wall slip velocities in torsional flow, which can also provide the true deformation rate. They have also observed the contribution of the wall slip to the volumetric flow rate in capillary flow. They have found it to be increasing with decreasing shear stress, which gives rise to plug flow at very low shear stress values. Aral and Kalyon (1994) have carried out a systematic study, which is focused on the effects of temperature and surface roughness on the wall slip, in the flow of concentrated suspensions, containing 63 % by volume solid glass spheres and poly terpolymer matrix, using steady torsional flow. They have investigated the role of roughened surfaces for the elimination of wall slip in concentrated suspensions. They have used surfaces of different roughness and for defining the roughness; two relative roughness parameters (κ_1 and κ_2) were defined. It was observed that the increased surface roughness (increased value of κ_1) prevented the wall slip of the concentrated suspension. On the other hand for the lower values of κ_1 (for smooth surfaces) significant slip effects were observed. They found that the deformation rate, shear stress and wall slip velocity values during torsional flow were time dependent and asymptotically reached steady-state values. The characteristic time necessary to reach steady state decreased with increasing shear rate and temperature. Increasing temperature also increased the wall slip velocity.

Jana *et al*. (1995) determined the apparent wall slip coefficient of concentrated suspensions of 90 μm PMMA particles in a viscous Newtonian fluid in a narrow gap Couette device by measuring the particles velocities across the gap using a Laser-Doppler anemometer system and then extrapolating the results to two walls. This led directly to the apparent wall slip velocities as well as to the corresponding extrapolated wall shear rates. The slip coefficients thereby obtained were found to be insensitive to the magnitude of the applied shear that is approximately, λ/8 (λ refers to the relative effective viscosity of the suspension with respect to that of the pure fluid) for particle concentration in the range $0.45 \leq \phi \leq 0.52$. They observed the presence of significant shear induced particle migration. Jana et al. (1995) measured the wall slip using the following equation

$$\left(\beta = \frac{u_s}{a\dot{\gamma}} \right) \tag{2.1}$$

where, u_s is the apparent wall slip velocity, $\dot{\gamma}$ is the apparent wall shear rate and a is the radius of particles. Barnes *et al*. (2001) have presented a review paper on the use of rotating vane geometries for the measurement of very slip prone non-Newtonian liquids. Originally these geometries were used to measure the apparent yield stress of inorganic dispersions, but have more recently been also used to measure other rheological parameters. The particular advantages of the vane geometry are its simplicity of fabrication, ease of cleaning and more than anything else, its elimination of serious wall slip effects. Lawal and Kalyon (1997) developed an analytical non-isothermal model of the extrusion of viscoplastic fluids subject to wall slip. The model accommodates different slip coefficients at the screw and barrel surfaces. Lam et al. (2007) carried out the experiment to find the effect of wall slip of concentrated suspension melts in capillary flows at elevated temperature. The effect of particle concentration on wall slip was studied experimentally in a capillary rheometer. The result obtained that slip velocity increased with an increase of particle concentration.

Hay et al. (2000) have measure the shear stress and slip velocity of low density polyethylene in capillary and parallel plate geometry. They have compared the data from parallel plate measurements, where effects of pressure and temperature are negligible, to those from pressure driven flows where they are not. They provided the comparison of steady shear experiments to obtain the slip velocity and flow curve in three test geometries (slit, capillary, parallel plates). This became possible with the advent of a testing technique for parallel plates allowing higher shear rates to be achieved. Couetee flow of concentrated suspension of

viscoplastic fluid generally exhibit apparent wall slip in extrusion processing. Ekere *et al.* (2001) studied the effects of wall slip on the measurements of the viscosity of solder pastes using rheometer. Solder pastes are concentrated suspensions of spherical solder particles suspended in a flux-vehicle medium. Solder pastes are used as the main interconnection materials in electronics packaging and in assembly of printed circuit board (PCB). The printing of solder pastes through very small stencil apertures required for ultra-fine pitch and flip-chip applications is known to result in incomplete transfer of paste to the printed circuit pads. So, at these narrow aperture sizes, achieving consistent solder paste deposits from pad to pad, and from board to board becomes difficult, and solder paste rheology becomes very crucial for consistent paste withdrawal. They observed that, because of the presence of the wall slip, the measured viscosity (also called the apparent viscosity) is much lower than the true viscosity of the paste. Therefore, a correction needs to be applied to the measured viscosity in order to obtain the true viscosity of the solder paste. A model, for predicting the true viscosity based on measurements using parallel plate viscometer and the influence of wall slip on viscosity measurement, was presented. The apparent viscosity values was measured at two different plate gaps, but at the same applied shear rate (also called the apparent shear rate), is used for predicting the true viscosity, the wall slip velocity and the thickness of the boundary slip layer. The model was validated using results from solder paste samples measured at three different plate gaps (0.5 mm, 1.0 mm, and 1.5 mm). Ahuja and Singh (2009) presented the measurement of wall slip velocity in concentrated suspension of non-colloidal particles. The experiments were carried out in a cylindrical Couette device. They provided a simple methodology for the determination of slip velocity. The rheological measurements were carried out with smooth and serrated geometry of a Rheometer. The serrated geometry penetrated the slip layer creating no-slip boundary whereas smooth geometry showed significant slip at higher concentration of particles. Comparing the wall shear stresses from the two measurements they have determined the slip velocity and slip coefficients. The slip velocity varies linearly with the shear rate. They provided more insight into slip effects observed in the flow of concentrated suspensions.

The motivation of the present work comes from the above mentioned studies as well as some recent experiments on surface corrugation in free surface flow of concentrated suspensions (Loimer *et al.*, 2002; Timberlake and Morris, 2005). In a recent study, Singh *et al.* (2006) observed that the free surface velocity profile in a gravity driven open channel flow is blunted. The deviation of velocity profile from the Newtonian profile increased as the particle

concentration was increased. In the past Karnis *et al*. (1966) and Sinton & Chow (1991) have also reported velocity blunting but no measurable non-uniformity of particle concentration. Koh *et al*. (1994) have measured the velocity and concentration profiles in pressure driven flow of concentrated suspension in a closed rectangular channel. Based on their measurements they speculate that there could be a significant 'slip' between the particles and the suspending fluid which increases with increase in particle concentration and size. Blunted velocity profile was also reported in the experiments of Lyon and Leal (1998) when concentration profile showed no in-homogeneities. The motivation of our study on wall slip comes from these observations. It is also our objective to investigate further the work of Singh *et al*. (2006) and study the effect of apparent wall slip velocity on surface corrugation in the free surface flow of concentrated suspension in open channel. It is also well known that non-colloidal concentrated suspensions have non-zero normal stress differences. Many polymeric fluids have large first normal stress difference. Under condition of no-slip polymeric fluids with negative (extensional) first normal stress difference will behave like a stretched membrane. The non-colloidal suspensions are known to have positive (in the compression sense) first and second normal stress difference. Whether the presence of wall slip causes the free surface to appear (like when a stretched membrane is suddenly relaxed) in the form of surface corrugation was the motivation behind studying the effect of wall slip on surface corrugation.

2.2 PIV AND ITS APPLICATIONS

The flow visualization techniques such as Laser-Doppler velocimetry (LDV), Laser-Doppler anemometer (LDA) and Particle image velocimetry (PIV) are often difficult for studying the flow behavior of suspension due to the requirement of refractive index matching. Averbakh *et al*. (1997) have used LDV technique to study the particle velocities and particle migration for the suspension with particle fraction (ϕ) ranging from 0.3 to 0.5. Their qualitative result shows that the longitudinal profiles lose their Newtonian shape at high concentration. Lyon and Leal (1998) have reported the experimental results of velocity and concentration profiles for suspensions having a bi-dispersed distribution of particle size undergoing pressure driven flow through a parallel wall channel. At bulk particle volume fractions of 0.30 and 0.40, they have found non-uniform overall particle concentration distributions and blunted velocity profiles. They have observed that large particles are occupied in the centerline region of the channel. They have applied laser Doppler velocimetry technique for their study. The PIV technique in the recent years has become a very efficient tool for measuring the instantaneous

velocity field in various fluid dynamic applications. This is a nonintrusive method for experimental measurements, which measures local and instantaneous particle displacement vector in an illuminated fluid plane. When a continuous light is used to illuminate the fluid motion, the operator has to determine the optimal separation time between two successive exposures. In the case of small regions of flow field, the use of a common CCD video camera seems to be a convenient way. In the study of high speed fluid flows, PIV flow visualization technique uses a camera with very high frame acquisition rate. Northrup *et al.* (1993) has given a direct measurement of interstitial velocity field variations in a porous media using Florescent-Particle image velocimetry technique. Philip *et al*. (1994) have developed a high speed particle image velocimetry technique using florescent tracers to study steam bubble collapse. They have used appropriate filters to filter the unnecessary light rays from florescent seeds. The filters blocked most of the green light and passed the red light emitted by the florescent tracers. Kadambi *et al*. (1998) have described the major factors influencing the successful measurement of particle size from PIV image data. They have suggested employing a high resolution CCD camera, and Argon ion laser to capture the clear images of particles. The effect of Gaussian intensity profile across the depth of the light sheet and the optical collection system's depth of field were investigated using PIV technique. Their results have provided insight into designing a balanced illumination and optical system necessary to obtain constant particle size estimation, independent of their position within the light sheet. In our study, we have used similar high resolution CCD camera and Argon ion laser.

Desaubry and Gervais (2000) have constructed a PIV instrument using a video frame grabbing system and two unsynchronized CCD video arrays. In the optical device, the two CCDs are positioned at two perpendicular axes, with an image splitter located at their intersection and a single imaging lens in front of it. For an optical characterization of each CCD array the imaging lens is needed to ensure that the field of view is similar for each vision. First the simple experimental method is used to deduce the basic optical parameters of the imaging lens. A simple video model is then applied to extract the unknown optical parameters of the device such as the angular field of view, the efficient dimensions of each CCD array and the transfer function from the CCD to the TV screen. An identification method, which is based on global magnification measurements, allowed the resolution of the micrometric stages needed for the spatial calibration step of the final instrument to be deduced. Experimental tests have shown that the aberration in image formation is minimum in this configuration. The flow behavior of various commercial pulp fiber suspensions at fiber

mass concentrations range from 1 to 5% (weight %) was conducted in conventional rheometer coupled with local velocity measurements using ultrasonic Doppler velocimetry by Derakshandeh *et al*. (2010). They have obtained the experimental data using a stress-controlled rheometer. By implementing a vane in large cup geometry, it exhibits apparent yield stress values which are lower than those predicted values. This happened mainly due to existence of apparent slip. Pulp suspensions exhibit shear-thinning behavior up to a certain shear rate value after which Newtonian behavior prevails. Local velocity measurements prove the existence of significant wall slippage at the vane surface. By increasing the fiber mass concentration apparent yield stress and apparent wall slippage was found to increase.

A first order accurate method of extending the capability of particle image velocimetry to interface is presented by Tsuei and Savas (2000). In this method, the image fields are locally extended across interfaces to form an image pair. During this image parity exchange, the extension of the image fields amounts to locally reversing and reflecting the relative velocity field across the interface. This method can be employed for the study of Couette flow, laminar pipe flow, uniform flow past a sphere and a sphere moving in stagnant fluid demonstrating curved rigid surfaces, free surfaces flow and interface flow. Olsen and Adrian (2000) applied this technique for Brownian motion. The main disadvantage of PIV technique in Brownian suspension is that either Brownian effect diminishes the signal strength of PIV or PIV signal affects the reality of Brownian motion. Hence, we need to make sure the effects of light scattering from PIV or Brownian motion is very small. With proper selection of imaging and signal processing systems PIV is also being used in microfluidics. Heise *et al*. (2004) acquired the flow pattern, instantaneous velocity fields and shear stress distribution of distal end-to-side anastomoses, the local hemodynamics and pressure losses of crural bypass anastomoses by using PIV technique. Microscopic particle image velocimetry (microPIV) experiments were performed by Li *et al*. (2005) on a polydimethylsiloxane (PDMS) micro-channel with a cross-section measuring 320 µm to 330 µm for Reynolds numbers between 272 and 2853. They have taken the care to ensure that the seed particle density was great enough to get accurate instantaneous velocity vector fields for all the Reynolds numbers. Velocity fluctuations were calculated from ensembles of micro-PIV velocity fields. Paul *et al*. (2007) conducted an experimental investigation on turbulent cross-flow in a staggered tube bundle with transverse and longitudinal pitch-to-diameter ratios of 3.8 and 2.1, respectively. They employed a PIV technique to obtain detailed measurements in the bundle at inlet-velocity-based Reynolds numbers of 4800, 9300 and 14400.

The PIV analysis technique are used in various application area such as flow in channels, laminar mixed convection in a vertical ducts, granular flow, design of compact heat exchangers, solar collectors, nuclear reactors and the cooling of electronic equipment etc. Slominski *et al*. (2007) utilized the PIV technique to study the deformation measurements in dry cohesion-less sand during free flow in small rectangular model silo. The effect of the initial sand density and roughness of silo walls on the volumetric and deviatoric strain in sand was investigated using PIV technique. They discussed about accuracy, advantages and disadvantages of PIV technique. The PIV method can be used as an effective optical technique to measure deformations on the surface of granular materials on the basis of processing successive digital images without any physical contact. Their disadvantages are that strains inside of the material cannot be traced (only those on the surface of the specimen). Thus, in the case of silo flow (due to wall friction between the granulated and transparent wall), strains on the surface can differ from those inside of the material. In addition, the size of the plane specimen should not be too large. Tatum *et al*. (2005) used PIV technique to study the 3D flow field around a sphere sedimenting near a wall. The flow fields surrounding a sphere sedimenting through a liquid near a vertical wall were characterized using 3D stereoscopic PIV experiments. Three different fluids, a Newtonian reference fluid, a constant (shear) viscosity Boger fluid, and a shear-thinning elastic fluid, were used to determine the effects of both elasticity and shear-thinning on the flow field using PIV technique. All three fluids have similar zero shear viscosities. Kurada *et al*. (1997) proposed a new particle image velocimetry technique for 3D flow, which is a PC-based machine vision system for obtaining 3D particle co-ordinates using a single camera. Based on photogrammetric imaging, this system uniquely combines the advantages of stereo and orthogonal views to determine the accurate locations of the particles. They implemented a 3D cross-correlation algorithm to follow the particle from frame to frame and compute the velocity vectors. The effect of viscosity on mixing in an oscillatory baffled column (OBC) was studied using DPIV by Fitch *et al*. (2005). The results showed that a ratio of the plane-averaged axial over the radial velocity is defined to quantify the viscosity effects. For the given geometry the velocity ratio approaches very quickly at increased oscillatory Reynolds numbers, regardless of the Newtonian and non-Newtonian fluids used. An empirical critical ratio of 3.5 was identified, below which the system mixes sufficiently. They suggested that this would act as the guide for industrial applications where a viscous fluid is mixed in an aqueous solution in the OBC. Evaluation of multiphase flotation models in grid turbulence was studied via PIV by Brady *et al*. (2006). Multiphase flows such as floatation requires

understanding of the relationships between bubbles, solid particles and the flow. To measure all the three phases in turbulent flow with great accuracy they have employed DPIV that can record the velocity vectors of all three phases, namely, the fluid, the solid particles and the air bubbles with temporal resolution. They studied the interaction of three phases in homogeneous isotropic turbulence generated by cylindrical grids. Ramrez-Gilly *et al*. (2007) applied PIV technique for analysis the velocity fields near four-blade vane-in-a-large-cup in controlled-stress rheometer small particles suspended in four different fluids.

There are few techniques available to study the suspension flow which is based on light scattering spectroscopy. Muller (2002) presented a review paper on the different light scattering velocity field analysis technique such as LDV, PIV and NMR imaging techniques. He summarized the advantages and disadvantages of each method as well as discussed about their applications in non-Newtonian fluids. To investigate the flow characteristic and deformation behavior of viscoplastic materials, the knowledge of the relation between the wall slip and wall shear stress, under isothermal condition, is necessary (Tang and Kalyon, 2004). In our study, we have chosen PIV technique for quantitative analysis. The instantaneous measurements of the free surface velocity and velocity field in the bulk for various suspensions are performed through PIV technique. The details of PIV work can be found in Chapter 3.

2.3 SURFACE CORRUGATION AND INTERFACE FLUCTUATION

It is now well known that the free surface shape of a concentrated suspension undergoing simple shear (Loimer *et al.*, 2002) or gravity driven flow (Timberlake and Morris, 2005; Singh *et al.*, 2006) becomes highly corrugated. The surface deformation depends on the particle size, particle concentration, viscosity and surface tension of the suspending fluid. The deformation has many length scales above and below particle size and it appears in the form of waves traveling with the local surface fluid speed (Loimer *et al.*, 2002). The free surface flow of viscous Newtonian fluid is itself a very interesting and active area of research which has received some attention. Argyriadi *et al*. (2006) have conducted an experimental study in a gravity-driven viscous film flow along an inclined periodic wall with transverse rectangular corrugations. The steady interaction between the corrugated wall (bottom wall) and the flow led to a statically deformed free surface. They studied the film flow to get the deviation of flow characteristics for flat and plane wall. They observed that increasing or changing the corrugation height does not make any affect in free surface corrugation of film flow. However, changing the inclination leads to increase in the surface deformation. We often

ignore the interface motion while studying the motion of bulk Newtonian fluid flow, where the interface motion (or fluctuation) is zero or negligible. We often use the boundary conditions of continuity of stresses at the interface between the phases. However, whenever the Brownian or non-Brownian particles are present in the system, these boundary conditions are not valid in general. In such case, the motion of interface influences the other properties of flow. For example interface motion is associated with the free surface deformation or surface corrugation in suspension flow. Interface instability can also be induced by particle size, particle concentration gradients, suspending fluid viscosity, gradients of surface tension of suspending fluid, temperature gradients, etc. Nikolov *et al*. (1985) proposed a method for thermodynamic definition of the film and line tension effects on the attachment of particles to an interface. They described a differential interferometric method for experimental determination of the shapes of the bubble cap and the external meniscus. The prescription of the free interface configuration in gas-liquid, solid-liquid, solid-gas and liquid-liquid systems is of importance in a variety of processes. Brauner *et al*. (1996) employed energy consideration to predict the interface configuration. The effect of the fluid physical properties, in tube dimension, wall adhesion and gravitation on the characteristic interface curvature was explored. Their prediction of interface curvature provides the closer relation between tube dimension, wall adhesion and gravitation.

Kumar *et al*. (1998) investigated the free-surface turbulence in channel flow. They conducted the experiments in a horizontal channel of large aspect ratio in the (depth based) Reynolds number range of 2800-8800. The result indicates that the persistent structures on the free surface can be classified as upwellings, downdrafts, and spiral eddies. Upwellings are shown to be related to the bursts originating in the sheared region at the channel bottom and the eddies are seen to be generated at the edge of the upwellings. The resulting data show that the physical parameters characterizing the structures at interface scale with a mix of inner (wall shear stress and viscosity) and other variables. They measured the streamwise and spanwise velocities at the free surface by particle image velocimetry technique (PIV) and surface normal velocity near the free surface estimated by continuity. The free surface motion for a mixture of fluid and solid particles with high sediment concentration was studied by Federico (1997). He described the non-Newtonian rheological yield stress, viscous stress and turbulent-dispersiveness of hyperconcentrations and their dependence on sediment concentration. The velocity profile of uniform motion of sediment was also computed. The results showed that more gravity currents are possible for sediment than Newtonian fluid.

Law *et al*. (1998) measured the free surface motion in the vicinity of the air-water interface of a submerged confined jet. They have used a PIV based technique which allowed the interface movement and the velocity field immediately beneath, to be measured simultaneously. They obtained a detailed turbulence structure near the free surface region. Kiger and Pan (2000) developed a PIV technique which can be employed to study the simultaneous measurement of dilute two-phase flows. The main principle of the technique was to utilize a two-dimensional medium filter to generate separate images for the two phases, thus eliminating the errors induced by the distinct motion of the dispersed components. A variation of the digital particle image velocimetry (DPIV) technique was developed for the measurement of velocity at a free surface for low Froude number flows by Hirsa *et al*. (2001). It involves a two step process; first determining the location of the free surface in the digital images of the seeded flow using the fast Fourier transform-based method of surface elevation mapping (SEM). This method takes the advantage of total internal reflection at the interface. Next, a boundary-fitted DPIV code positions the interrogation windows below the computed location of the interface to allow for extrapolation of interfacial velocities. They designed this technique specifically to handle large surface-parallel vorticity which can occur when the Reynolds number is large and surface-active materials are present. Dabiri and Gharib (2001) have developed a non-intrusive approach for measuring simultaneous free-surface deformation and near-surface velocity. The method is based on digital particle image velocimetry (DPIV) and the reflective mode of the free surface gradient detector (FSGD). The interfacial process at gas-liquid interfaces for open, microfluidic flow cell was studied by Hoang *et al*. (2006). They seeded the free surface with florescent particles and studied the interface behavior from the reflected light scattering from the surface. Cherlo *et al*. (2010) studied the interaction between kinetics and mass-transfer effects for two-phase flow behavior in rectangular micro channels using the PIV technique.

Though there are a number of studies on free surface flow of single phase fluids, there are no reported studies on characterizing the surface fluctuations in case of concentrated suspensions. The past studies on surface corrugation using the power spectral analysis of the refracted light from the free surface provides only an indirect estimate of surface roughness (Loimer *et al*., 2002; Timberlake and Morris, 2005; Singh *et al*., 2006). Several applications involving free surface flow of concentrated suspension it is desired to have a proper estimate of the free surface deformation since this can significantly change the surface area which can influence the heat and mass transfer at the interface. Therefore, we have studied the free

surface motion in the velocity-vorticity plane during the open channel flow of concentrated suspension. This allowed us to measure average height of free surface deformation which can be related to the increase in the interfacial area. The effect of particle size, particle concentration and viscosity of suspending fluid on free surface deformation was studied.

2.4 AXIAL SEGREGATION IN ROTATING CYLINDER

Rotating cylinder is a common device which is employed in various processes handling granular materials, viscous fluids and suspensions. In the recent years there have been several studies on the pattern formation in horizontally rotating cylinder containing partially filled granular mixture and fluid-particle suspensions. The dynamic patterns depends on the free surface availability, angular speed of the rotation, particle size, particle shape, particle density, viscosity, density and surface tension of suspending fluid. Sanders *et al*. (1981) in an experimental study with pure Newtonian fluid observed that the liquid form as cells while rotating in the cylinder. They concluded that availability of free surface causes the instability even in the absence of gravity force. Thoroddsen and Mahadevan (1997) observed various phenomena in the partially filled rotating cylinder of Newtonian fluid. They suggested various forces acting on the flow as prime reasons for the occurrence of instability. The instability was attained at higher angular velocity, where the viscous fluid forms like shark teeth pattern. An experiment was conducted by Tirumkudulu *et al*. (1999) in a partially filled suspension in a horizontal Couette device. They found a new kind of instability during the flow of suspensions containing mono-dispersed neutrally buoyant particles in a high viscous Newtonian fluid, where the suspension under shear segregates into regions of high and low particle concentration along the length of the cylinder. After a year Tirumkudulu *et al*. (2000) conducted similar experiments but in a different geometry (horizontal cylinder) which was partially filled with the similar suspension and rotated about it horizontal axis. They found that within certain range of parameter space, the initially uniform suspension divided into cylindrical bands of high particle concentration separated by regions of pure liquid. They suggested that this instability is initiated by particle concentration fluctuation that affects the local viscosity of the suspension. Subsequent to the experimental investigation of this interesting phenomenon, there have been a few theoretical analyses to explain the instability mechanism which leads to particle accumulation in bands along the axis of the rotation.

A theoretical investigation of this observation was given by Govindarajan *et al*. (2003). They proposed an instability mechanism which leads to particle accumulation in bands along the axis of the rotation. Brady and Carpen (2002) argue that there is an instability mechanism in

non-Newtonian fluids when a jump in normal stress is present between the two fluids. By using stability analysis they have shown that the fluids with a negative second normal stress difference can be unstable with respect to transverse and span wise perturbations. Krasnapool'skaya (2003) experimentally studied fluid and granulated flow inside a horizontally rotating cylinder. They observed many phenomena such as segregation of particles different in dimensions, surface properties, and densities, which are observed in granulated media. The various patterns that were experimentally studied by them are – vortex-like patterns, deformation of the trailing and leading edges of the layer, shark-teeth patterns, fish-like patterns, formation of rotating layers, ring-like patterns and cellular patterns.

To investigate further the pattern formation in suspensions flow, Timberlake and Morris (2002) conducted further experiments in a partially filled inclined concentric cylinder or Couette device. They examined the dynamics of band formation and subsequent band motions for a range of fill fractions of the annular region and angle of inclination of the Couette device relative to the horizontal. In another interesting study Breu *et al*. (2003) conducted experiments with non-neutrally buoyant suspension in a partially filled rotating cylinder at high rotating speed. At such high speed the centrifugal force dominated the particles and segregation was observed. They observed the pattern formation and proposed that the instability occurs when the fluid and particles are of different density even though the cylinder was fully filled. However, they reported that no segregation in fully filled cylinder with neutrally buoyant concentrated suspension. Pan *et al.* (2007) numerically investigated the pattern formation in a rotating suspension of non-Brownian settling particles in incompressible Newtonian viscous fluids. These phenomena are modeled by the Navier-stoke equations coupled to the Euler-Newton equations, describing the motions of particles.

The industrial processes involving flow of suspension and granular mixture in rotating cylinders often involve presence of different sized particles. Though there are several studies with bi-dispersed granular particles, there are no reported studies with bi-dispersed particles suspended in viscous fluid. Experimental measurements of binary mixtures of granular media in a horizontal cylinder were reported by Hill and Kakalios (1994). The traditional axial segregation causes granular media to separate into bands of relatively pure single concentrations along the axis of rotation. In special cases the homogeneous mixed state could be restored simply by decreasing the speed of rotation. It is called reversible axial segregation of binary mixtures of granular materials. They classified the granular mixture segregation in

rotating drum as reversible segregation mixture, irreversible segregation mixture, and no segregation mixture. Hill *et al*. (1997) used CCD camera to capture images of particles dynamics and analyzed using image processing technique. They proposed that the axial segregation occurs due to the different dynamic angle of repose between the particles. Khakhar *et al*. (1996) obtained the transverse segregation pattern for binary particles rotating in a cylinder. The flow is divided into two regions: a rapid flow region of the cascading layer at the free surface and a fixed bed of particles rotating at the angular speed of the cylinder. Stevans (1998) have presented a review paper for powders mixtures partially filled in a horizontal, slowly rotating cylinders and explained their segregation patterns, segregation patterns in different model of cylinder such as plane cylinder, periodic modulated cylinder, and helical modulated cylinder.

A rotating suspension of non-buoyant particles can develop striking inhomogeneities in particle concentration, with regular band of high and low concentration along the symmetry axis. An order parameter, based on the average angular velocity of the particles, characterizes two distinct phases: a low-frequency segregated phase and a high-frequency dispersed phase. The axial band structure develops during the transition between these two phases (Lee and Ladd, 2005). Gans and Zupanski (1998) described a system in which vortices are shed from a cylindrical free surface approximately centered in a rotating flow. They examined the flow in a horizontal, rapidly rotating, partially filled cylinder. While rotating rapidly the liquid in the vortical state is largely confined to an annulus surrounding a cylindrical core. There was a periodic shedding of vortices from the neighborhood of the air-liquid interface. The vortices remove negative relative vorticity from the neighborhood of the interface. The frequency of shedding increases as one moves deeper into the vortical region of parameter space, until the process is continuous. Jain *et al*. (2001) reported alternate band formation in wet granular media or slurries as well as for dry granular mixtures. They found that particle segregation in dry granular mixture is significantly faster compared to that in suspensions in liquid media.

Matson *et al*. (2005) reported a systematic experimental study of concentration and velocity pattern formed in a horizontal rotating cylinder filled completely with mono-dispersed suspension of non-Brownian settling particles. Their system showed a series of concentration and velocity patterns, or phases, with varying rotation rate and solvent viscosity. They studied the individual phases using both side and cross-sectional imaging to examine the detailed flow structures. The overall phase diagram of the system is mapped out as a function of the rotation rate and solvent viscosity. They made attempts to analyze the functional form of the

phase boundaries in order to understand the transition mechanism between phases. Subsequent work of Matson *et al*. (2006) studied a suspension of non-Brownian settling particles in a completely filled horizontal rotating cylinder which demonstrated a rich array of concentration and velocity patterns. Individual flow states or phases were studied using both side and cross-sectional imaging to examine the detailed flow structures.

Kalyankar *et al*. (2008) examined the concentration and velocity patterns observed in a horizontal rotating cylinder completely filled with a mono-dispersed suspension of non-Brownian buoyant particles. The unique patterns or phases are mapped by varying both the rotation rate and the solvent viscosity. Individual phases are identified using both frontal (θ-z plane) and axial (r-θ plane) views. Phase boundaries were compared to those obtained for suspensions of non-buoyant particles. Expressing the boundaries in terms of dimensionless parameters unifies the data for several samples at low rotation rates. Joseph *et al*. (2003) observed that the both lighter- and hydrophobic heavier-than-liquid particles will float on liquid–air surfaces. Capillary forces cause the particles to cluster. This kind of clustering causes particles to segregate into islands and bands of high concentrations in thin liquid films rimming the inside of a slowly rotating cylinder partially filled with liquid. A second regime of particle segregation, driven by secondary motions induced by off-centre gas bubbles in a more rapidly rotating cylinder at higher filling levels, was identified. A third regime of segregation of bi-dispersed suspensions was found in which two layers of heavier-than-liquid particles that stratify when there was no rotation, segregate into alternate bands of particles under rotation.

CHAPTER 3

APPARENT WALL SLIP VELOCITY MEASUREMENTS IN FREE SURFACE FLOW OF CONCENTRATED SUSPENSIONS

3.1 INTRODUCTION

Suspensions of solid particles in viscous fluids are often encountered in various applications such as paints, polymer, pharmaceuticals products, drilling mud, and food products. Suspensions are also prevalent in a number of natural settings such as debris flow, lava flow, and flood waves carrying extremely high concentration of sediments. At dilute concentrations, the suspensions of solid rigid particles in Newtonian fluid are often modeled as effective Newtonian fluid having a concentration dependent viscosity. However, at moderate and high particle concentrations the hydrodynamic interactions significantly alter the flow characteristics and we often observe many interesting phenomena, which are not seen in the flow of a Newtonian homogeneous fluid under similar boundary conditions. Apparent wall slip of particles is one such phenomenon and this has attracted large number of studies (Yoshimura and Prud'homme, 1988; Yilmazer and Kalyon, 1989; Kalyon *et al*., 1993; Aral and Kalyon, 1994; Jana *et al*., 1995; Ekere *et al*., 2001; Kalyon, 2005; Nickerson and Kornfield, 2005; Lam *et al*., 2007; Ahuja and Singh, 2009). Though the phenomenon of wall slip is quite old but it still attracts significant attention due to its practical importance. Moreover, the nature of wall slip under various flow conditions is far from understood. The wall slip phenomenon is basically the occurrence of apparent relative velocity between the wall and the fluid at the wall. However, since the fluid is continuum, even in concentrated suspensions there is no 'true slip'. It is in reality an 'apparent slip' created by a region of high velocity gradient close to the wall compared to the bulk. This appears as an apparent slippage of the suspension through a thin liquid- rich layer (slip layer) of thickness δ at the wall (Vand, 1948). The slip layer is depleted of suspended particles compared to the adjacent regions of

bulk suspension. As a result, if the rheological measurements are carried out with smooth geometries, the measured viscosity (also called as apparent viscosity) is much lower than the true viscosity of suspensions. The wall slip effects are generally observed in the flow of highly viscous two-phase materials in rheometers, pipe, or any channel with smooth wall. Near the smooth, solid boundary, the local microstructure is depleted because the suspended particles cannot penetrate the solid walls. This particle deficient layer can also be observed even if there was no flow. This is known as static geometric depletion effect which could result from steric, hydrodynamic, viscoelastic, chemical and gravitational forces acting on the solid particles adjacent to the wall (Barnes, 1995). In some situations, the walls can also repel adjacent particles because of electrostatic forces arising between the particles and the walls. During the bulk flow, the resulting hydrodynamic and entropic forces can move the particles further away from the walls. The presence of large particles as disperse phase, smooth walls, low speeds or flow rates and, wall and particles carrying electrostatic charges are some of the reasons which enhance the slip effects. Shear induced migration (Leighton and Acrivos, 1987b) can also cause depletion of particles near the wall and enhance the wall slip.

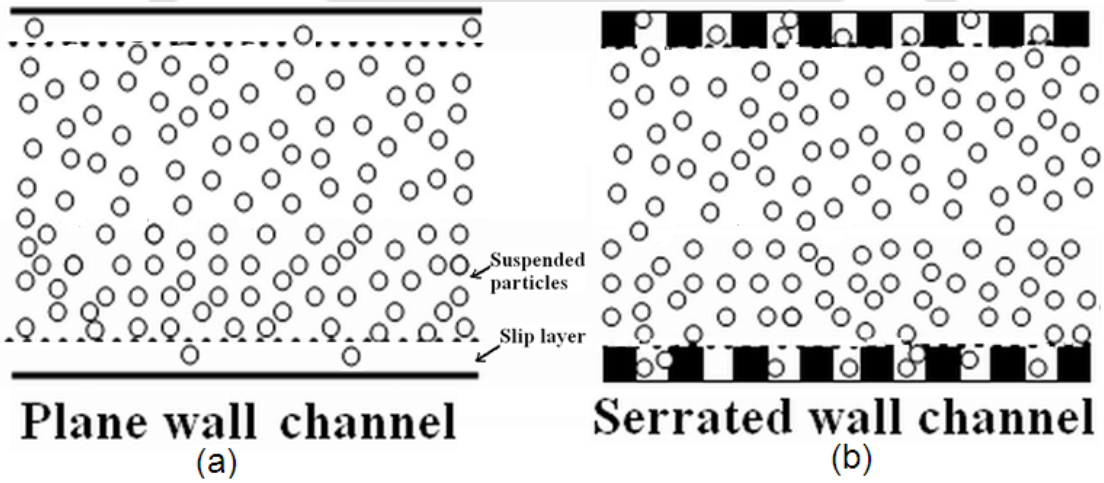

Figure 3.1: Schematic diagram showing (a) the formation of slip layer at the plane wall and (b) prevention of slip layer with the rough wall.

It is now well known that to prevent slip at the wall, roughened and serrated wall surfaces can be used (Barnes, 1995). If the slip layer thickness is comparable with the height of surface irregularities, then slip would not develop (Soltani and Yilmazer, 1998). Figure 3.1 shows the role played by the surface roughness in the suppression of wall slip effects. Near the plane wall there is a thin liquid- rich layer (slip layer) which is responsible for apparent wall slip. However, in case of rough wall, the particles can move inside the groove of the serrations and hence the whole suspension can be treated as continuum as there is no-slip layer. Therefore,

if one carries out velocity profile measurements for the flow geometry with rough wall, both true and apparent velocity profiles will be the same. On the other hand, measurements in smooth wall geometry will show a different apparent velocity profile due to wall slip.

The motivation of the present work comes from the above mentioned studies as well as some recent experiments on surface corrugation in free surface flow of concentrated suspensions (Loimer *et al*., 2002; Timberlake and Morris, 2005). In a recent experiment Singh et al. (2006) observed that the free surface velocity profile in a gravity driven open channel flow is blunted. The deviation of velocity profile from the Newtonian profile increased as the particle concentration was increased. In the past Karnis *et al*. (1966) and Sinton and Chow (1991) have also reported velocity blunting but no measurable non-uniformity of particle concentration. Koh *et al*. (1994) have measured the velocity and concentration profiles in pressure driven flow of concentrated suspension in a rectangular channel. Based on their measurements they speculate that there could be significant 'slip' between the particles and the suspending fluid which increases with increase in particle concentration and size. Blunted velocity profile was also reported in the experiments of Lyon and Leal (1998) when concentration profile showed no in-homogeneities. The motivation of our study on wall slip comes from these observations. It is also our objective to investigate further the work of Singh *et al*. (2006) and study the effect of apparent wall slip velocity on surface corrugation in the free surface flow of concentrated suspension in open channel. It is well known that non-colloidal concentrated suspensions have non-zero normal stress differences. Many polymeric fluids have large first normal stress difference. Under condition of no-slip, polymeric fluids with negative (extensional) first normal stress difference will behave like a stretched membrane. The non-colloidal suspensions are known to have positive (in the compression sense) first and second normal stress differences. Whether, the presence of wall slip causes the free surface to appear in the form of surface corrugation was the motivation behind studying the effect of wall slip on surface corrugation.

Jana *et al*. (1995) determined the apparent wall slip coefficient of concentrated suspensions of non-colloidal PMMA particles in a viscous Newtonian fluid in a narrow gap Couette device by measuring the velocity profile across the gap using a laser Doppler anemometer system and then extrapolating the results to the walls. The slip coefficients thereby obtained were found to be insensitive to the magnitude of the applied shear rate. However, their measurements could be influenced by lateral migration of particles initiated by the presence of the wall and non-uniform velocity gradients. The wall slip in concentrated suspension can

manifest even if there is no shear induced migration. Ahuja and Singh (2009) have studied wall slip in simple shear flow via Stokesian Dynamics simulation and demonstrated that apparent slip is present even in simple shear flow, where the shear induced particle migration is absent. During the flow of suspension the particles cannot cross the wall and physically cannot occupy the space very close to wall as efficiently as they can away from the wall. This wall depletion will always result into a thin layer of fluid called as apparent slip layer. Under the conditions of inhomogeneous shear flow, there can be migration near the wall which can increase the depletion of particles resulting into enhanced slip. However, the method we adapt to measure slip velocity is to compare the velocity profiles from rough wall channel as well as smooth wall channel at the same axial locations. Thus, the extent of migration is expected to be same in both the cases. The slip velocity which is difference of the near-wall velocity in these two cases will be the true measure of wall slip.

In this work, PIV technique was used to perform the measurements of velocity profiles at the free surface. Power spectral densities were computed from the intensities of the refracted light from the free surface. Section 3.2 describes the experimental facilities and procedures including the optical arrangements and PIV analysis method. The materials used and method of preparation is explained in Section 3.3. Section 3.4 presents the results from our measurements followed by the conclusion in Section 3.5.

3.2 EXPERIMENTAL FACILITIES AND PROCEDURES

3.2.1 Channel and flow apparatus

Fig.3.2a shows the schematic diagram and Fig.3.2b shows the photograph of our experimental setup. The channels used in this study were 43.6 cm long, 2.2 cm wide and 5.5 cm deep. The plane channel was made of 5 mm thick glass and the rough channel of Perspex material of same thickness. The roughness of the side walls were created by uniform serrations (as shown in Fig.3.1). The gap and height of asperities in the side walls of rough channel (henceforth, called as serrated channel) were 1 mm each. A screw pump with variable speed AC motor was used to circulate the suspension in the channel. In order to dampen the small fluctuations produced by the screw pump during the flow, the upstream and downstream sections of the channel were connected to reservoirs of dimensions (12.5 cm x 7 cm x 3.2 cm) and (12.5 cm x 3 cm x 3.2 cm) respectively. Besides, there were array of baffles in the upstream reservoir to provide uniform mixing and remove any unsteadiness in the flow before it enters the open channel. In the Fig.3.2a, x is the span-wise direction, y is the flow

direction, and *z* is the direction of gravity. The two ends of the reservoir were connected to the screw pump via circular tubes of inside diameter 2 cm which circulated the suspension in the channel. The screw pump was specifically designed to handle suspensions of large particles. The speed of the pump as well as inclination of the channel could be adjusted to get the desired flow. The optical arrangements to capture images for PIV analysis is also shown in the Fig.3.2 (a-b). An Argon ion continuous laser from Spectra Physics (actual power 1W, k = 514 nm) was used as light source. Two plane mirrors were used to reflect the beam and a cylindrical lens was used to generate a horizontal light sheet illuminated from the downstream side of the channel (shown by the shaded region in the x–y plane of the Fig.3.2a). The images were captured using a 1360 x 1024 pixel CCD camera (PixFly HiRes from PCO) in conjugation with a macro zoom lens (Navitar). The camera can either operate in fixed mode (video mode) or in double shutter mode to capture images. In our experiments the camera was operated in fixed mode which captured images at the rate of 19 frames/s. At this recording speed the time duration between subsequent images was 52 ms. The maximum (centerline) velocity in the channel varied from 0.5 cm/s to 2.2 cm/s. The maximum wall shear rate reached in these experiments was less than 10 s^{-1}. The Reynolds number based on particle size and suspending fluid viscosity was $O(10^{-3})$ and even smaller if effective viscosity of suspension is considered.

3.2.2 Particle image velocimetry

Particle Image Velocimetry (PIV) is a non-intrusive, full field optical technique based on image processing of tracer particles dispersed in the flow domain. This technique is used for instantaneous measurements of the velocity field and it has been applied to a many kinds of flows. In any PIV experiments, the fluid of interest is seeded with neutrally buoyant tracer particles, which are illuminated by a light source (usually a laser sheet for better illumination of tracer particles). The images of these tracer particles at different times are recorded with a CCD camera. The instantaneous velocity field in the plane of visualization is obtained from the displacement of tracer particles between two successive images (Adrian *et al*., 1995). The details of PIV analysis can be found in our earlier work (Singh *et al*., 2006). The free surface was visualized by seeding the flow with hollow glass particles of diameter 10–25 μm supplied by ICI Limited. The amount of tracer particles added was very small compared to the volume of suspended particles (<0.01%). These tracer particles are hollow and hence simply float on the surface without influencing the flow behavior of suspended particles which are below the interface.

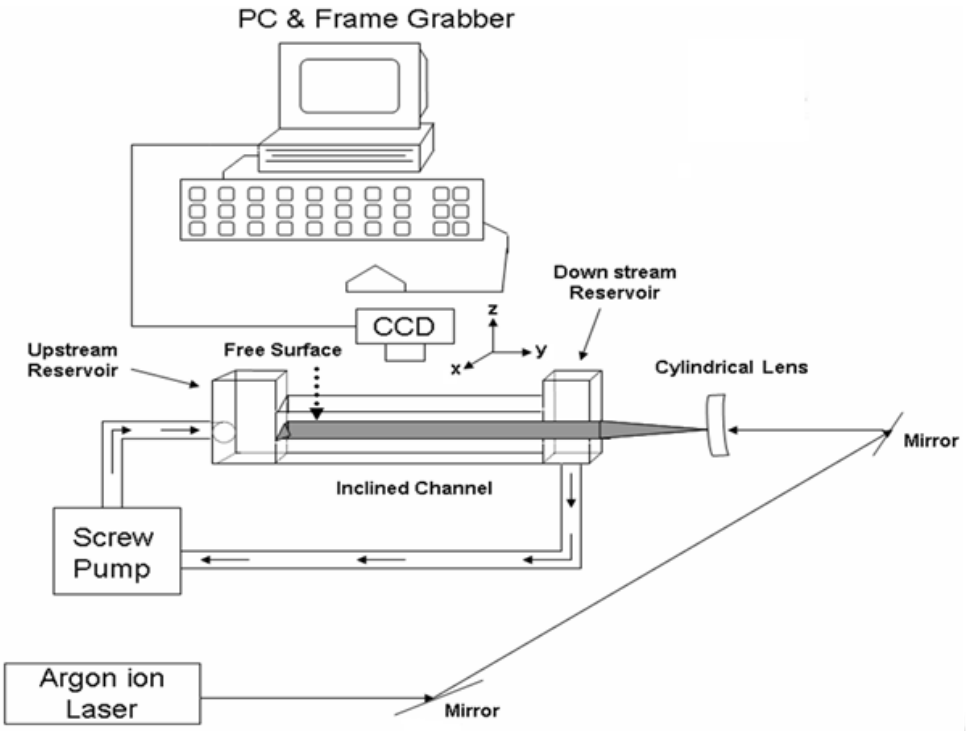

(a)

(b)

Figure 3.2: (a) Schematic diagram of the experimental setup and optical arrangements for PIV study. (b) Photograph of experimental setup and optical arrangements.

Figure 3.3a shows a representative PIV photograph of the image of tracer particles at the free surface in *x–y* plane and respective vector map of velocity field is shown in Fig.3.3b. With the lens operating at magnification of 0.7 the captured view of the flow field was 15.5 mm x 11.5 mm. These images were saved in 680 x 512 pixel, 12 bits format gray scale images on a computer via frame grabber. To calculate the velocity vectors from pair of images we have used the PIV analysis software PIV SLEUTH (Christensen *et al*., 2000). The image pairs were interrogated using two frame cross-correlation technique of Adrian *et al*. (1995). The spot size for the flow field interrogation was 128 x 128 pixels with 75% overlap between the interrogation windows. Thus the size of the interrogation window was approximately 2.9 mm x 2.9 mm and the distance between two adjacent interrogation windows was about 729 m. The correct size of interrogation window was estimated by processing the images with the window sizes varying from 32 x 32 pixels to 256 x 256 pixels and choosing the size that resulted minimum spurious vectors. The image interrogation with window size of 128 x 128 pixels resulted 13 rows and 14 columns of vectors for each image. The good quality of images insured that very few wrong vectors were computed. The vectors with low signal to noise ratio were removed and replaced with the interpolated vectors from the nearest points.

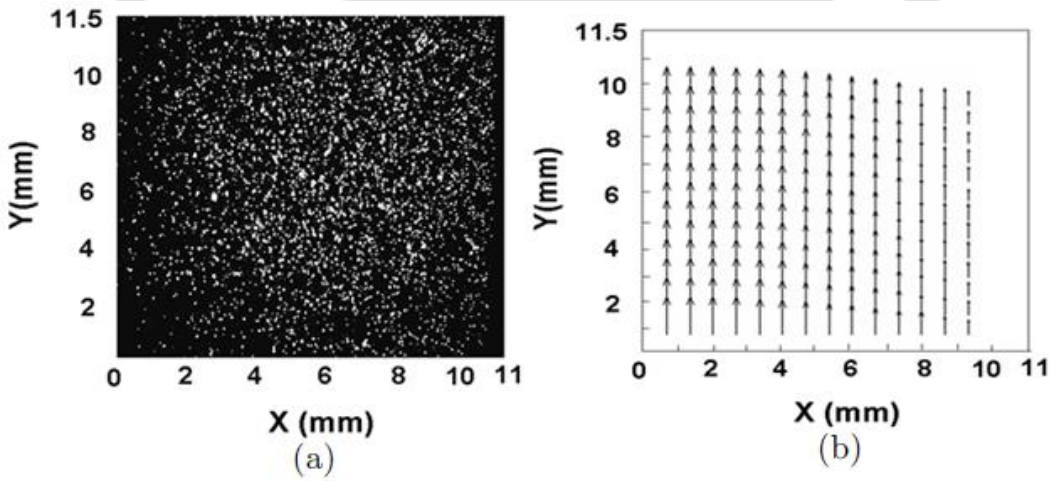

Figure 3.3: (a) A sample PIV image of tracer particles at the free surface of the channel (b) vector map of velocity field.

3.3 PREPARATION OF SUSPENSION

All the experiments were carried out with neutrally buoyant suspension which required density matching of fluid and particles. Four different sizes with two different densities of particles and four different viscosities of suspending fluids were used to prepare various suspensions in this study. To study the effect of particle size the suspension of polystyrene

spheres (density of 1.05 g/cc) with mean diameter of 80 µm, 250 µm and 500 µm dispersed in glycerol-water mixture were prepared separately. In another study suspension of PMMA spheres of mean diameter 200 µm was dispersed in glycerol–water mixture. To study the effect of suspending fluid viscosity on wall slip 500 µm polystyrene spheres were dispersed in 98 cP of Ucon oil and 204 cP of Triton-X-100. To achieve density matching with PMMA particles of density 1.18 g/cc, the suspending fluid was prepared by mixing of 74% glycerol and 26% water (volume%). This fluid had viscosity of 19.5 cP and its surface tension was 60.4 mN/m at 24 °C. The other particles used in our study were polystyrene spheres of density 1.05 g/cc. The suspending fluid for this case was 25% glycerol and 75% water (volume %). The viscosity and surface tension of this fluid was 2.05 cP and 48.4 mN/m respectively. The suspension of 500 µm polystyrene particles in 98 cP of Ucon oil was prepared by direct mixing since its density was nearly equal to polystyrene density 1.05 g/cc. The suspension of polystyrene particles in pure Triton-X-100 was also nearly neutrally buoyant since its density (1.07 g/cc) is very close to the particle density (1.05 g/cc). The surface tension of the Ucon oil and Triton-X-100 was 39.4 mN/m and 30 mN/m respectively at 24 °C. Approximately 1000 ml of suspension was needed to fill the flow apparatus. To prepare the suspension required amount of particles and appropriate liquid were added in a beaker and stirred vigorously to achieve homogeneous mixing and dispersion. However, during the mixing small air bubbles were formed which needed to be removed. This was achieved by keeping the suspension under vacuum for overnight, allowing the bubbles to rise up. Suspension cleared of air bubbles was then gently transferred into the channel. The particle size distribution of polystyrene spheres of mean diameters 80 µm, 250 µm, and 500 µm is shown in Fig.3.4. The corresponding curve for 200 µm PMMA particles is shown in the Fig.3.5. The particle's size distributions were analyzed using a particle size analyzer (Malvern Instruments).

For the rheological characterization of the suspending fluid mixture, the HAKKE RS1 rheometer was used. Experiments were performed in a wide gap concentric cylinder or couette device. Figure 3.6 shows the schematic of a typical wide gap coquette device showing the inner rotating part and outer stationary cup. The fluid is confined between the two concentric cylinders with inner cylinder rotating at an angular speed. The flow was steady, laminar and isothermal with symmetry in θ direction. The shear rate at the inner cylinder for wide gap geometry is given by

$$\dot{\gamma} = \frac{2\Omega}{1-k^2} \tag{3.1}$$

where, $k = \frac{R_i}{R_a}$ is the ratio of the radius of inner cylinder to that of the outer cylinder. For our Couette geometry k was 0.876.

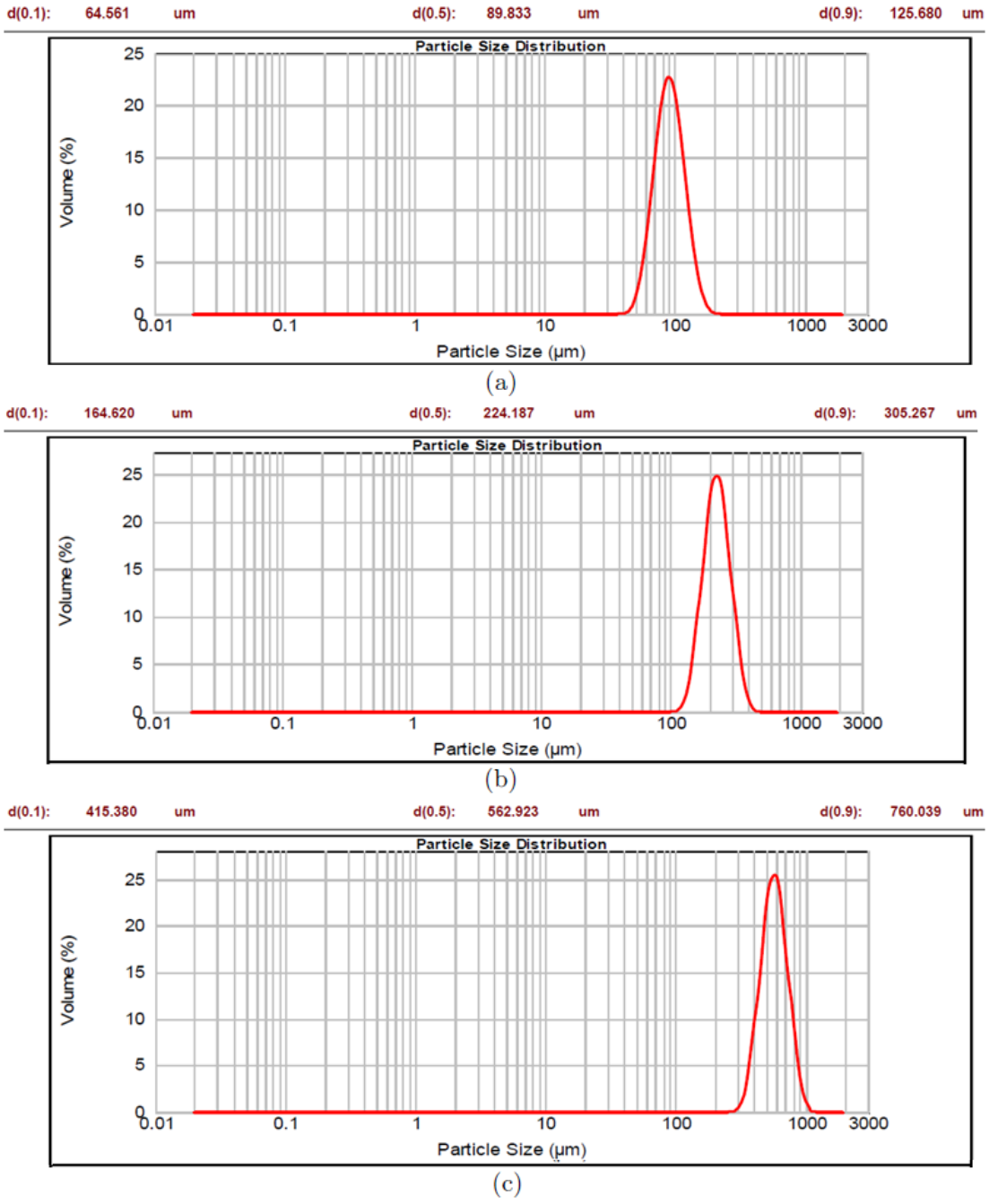

Figure 3.4: Particle size distribution of polystyrene particles for different sizes: (a) 80 µm (b) 250 µm and (c) 500 µm.

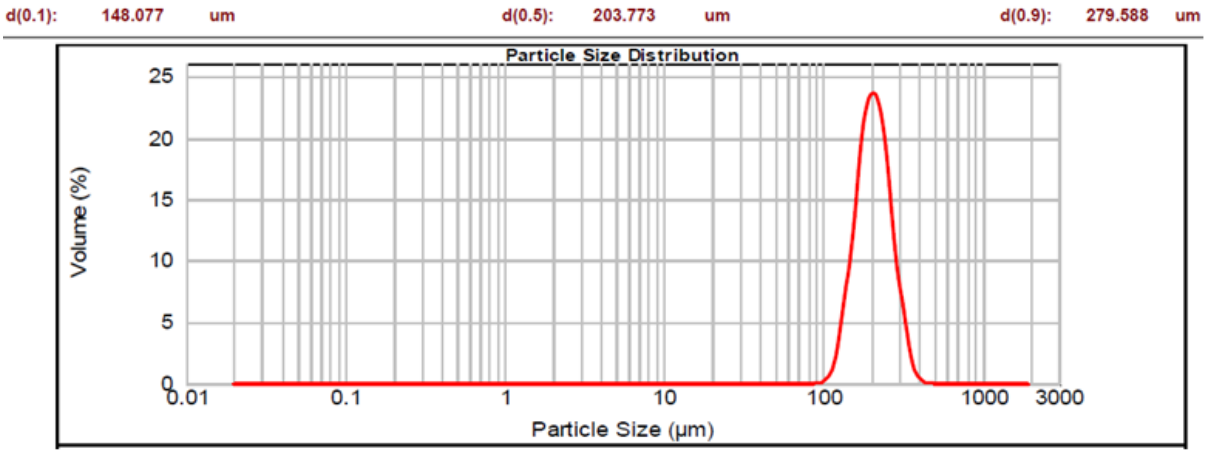

Figure 3.5: Particle size distribution of PMMA particles of mean diameter 200 µm.

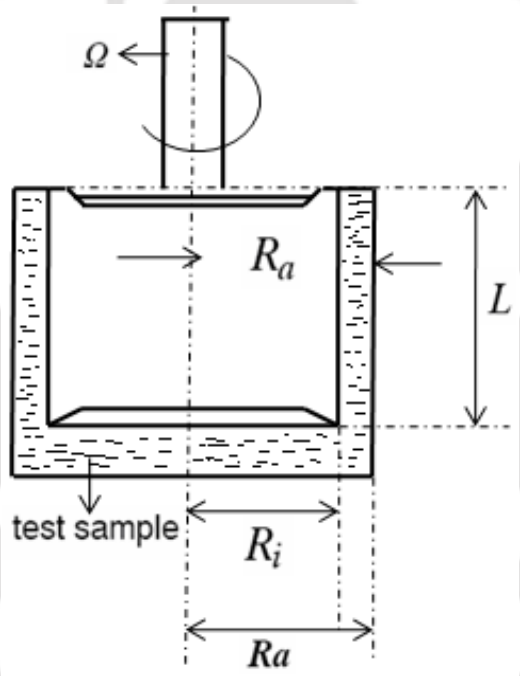

Figure 3.6: Standard HAAKE design of a coaxial concentric cylinder geometry.

Both serrated and plane types of Couette geometries were available in our lab. The radius of the outer cup is 21.7 mm and radius of the inner rotor is 20.71 mm which makes the annular gap to be 0.99 mm. The surface tensions of all suspending fluids have been measured by Wilhelmy plate method using a tensiometer from GBX advanced technology instrumentation. The results of viscosity measurements for various suspending fluids are shown in Fig.3.7. Measurements were carried out at three different fixed shear rates (100 s^{-1}, 200 s^{-1}, 300 s^{-1}) but the results are shown at 300 s^{-1} only. The viscosity did not change much with shear rate.

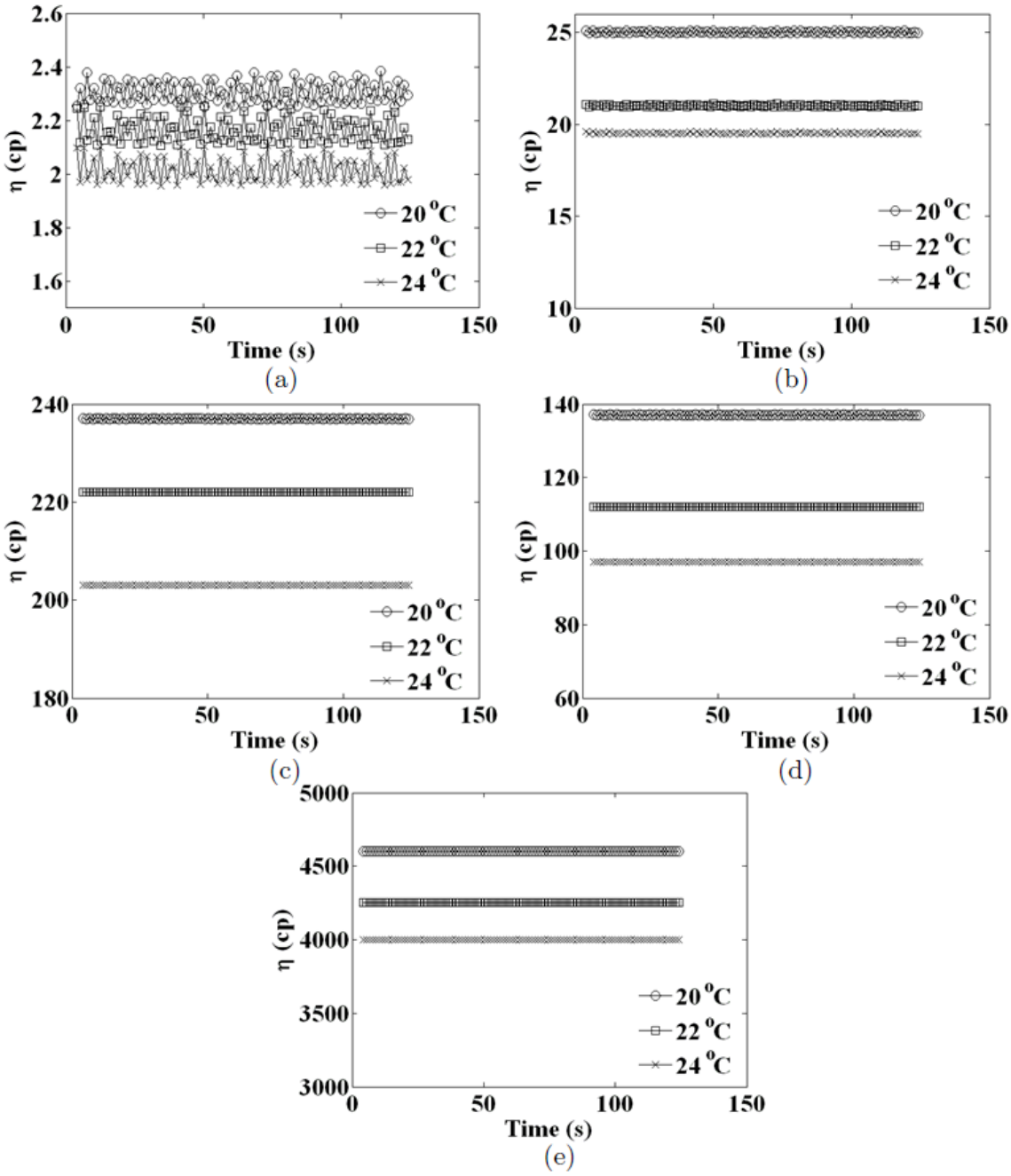

Figure 3.7: Viscosity of various suspending fluids at different temperature (a) 25% glycerol and 26% water mixture (b) 74% glycerol and 26% water mixture (c) Triton-X-100, (d) Ucon oil, (e) 76% Triton-X-100, 16% $Zncl_2$ and 8% water mixture. The results shown are at fixed shear rate of 300 s^{-1}.

3.4 RESULTS AND DISCUSSION

3.4.1 Free surface velocity profile for suspending fluid

Figure 3.8 shows the results of free surface velocity profiles for various suspending fluids with the plane wall channel. The profiles determined with the serrated wall channel are shown in the Fig.3.9. The comparative plots for some fluids are presented in the Fig. 3.10. It can be easily observed that the velocity profiles are parabolic with both the channels and it matches closely with the analytical profile for a Newtonian fluid. These results confirm the accuracy of PIV measurements and it also ascertains that the serrations at the walls do not change the velocity profile for suspending fluid. In the next section, we present similar profiles for concentrated suspensions and observe that wall slip can change the velocity profiles.

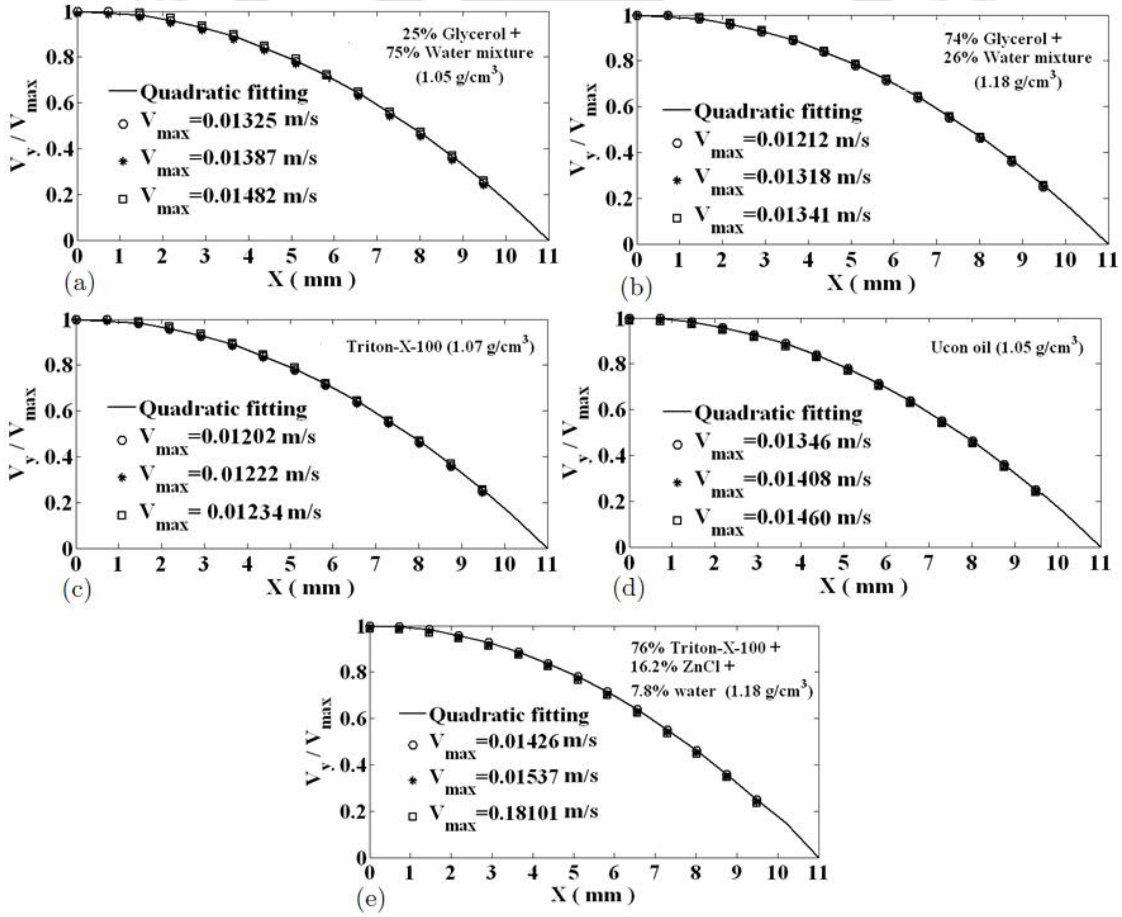

Figure 3.8: Free surface velocity profiles for various suspending fluids (Newtonian fluids) measured for the plane channel (a) 25% glycerol and 26% water mixture (1.05 g/cc), (b) 74% glycerol and 26% water mixture (1.18 g/cc), (c) pure Triton-X-100 (1.07 g/cc), (d) Ucon oil (1.05 g/cc), (e) 76% Triton-X-100, 16% $Zncl_2$ and 8% water mixture (1.18 g/cc).

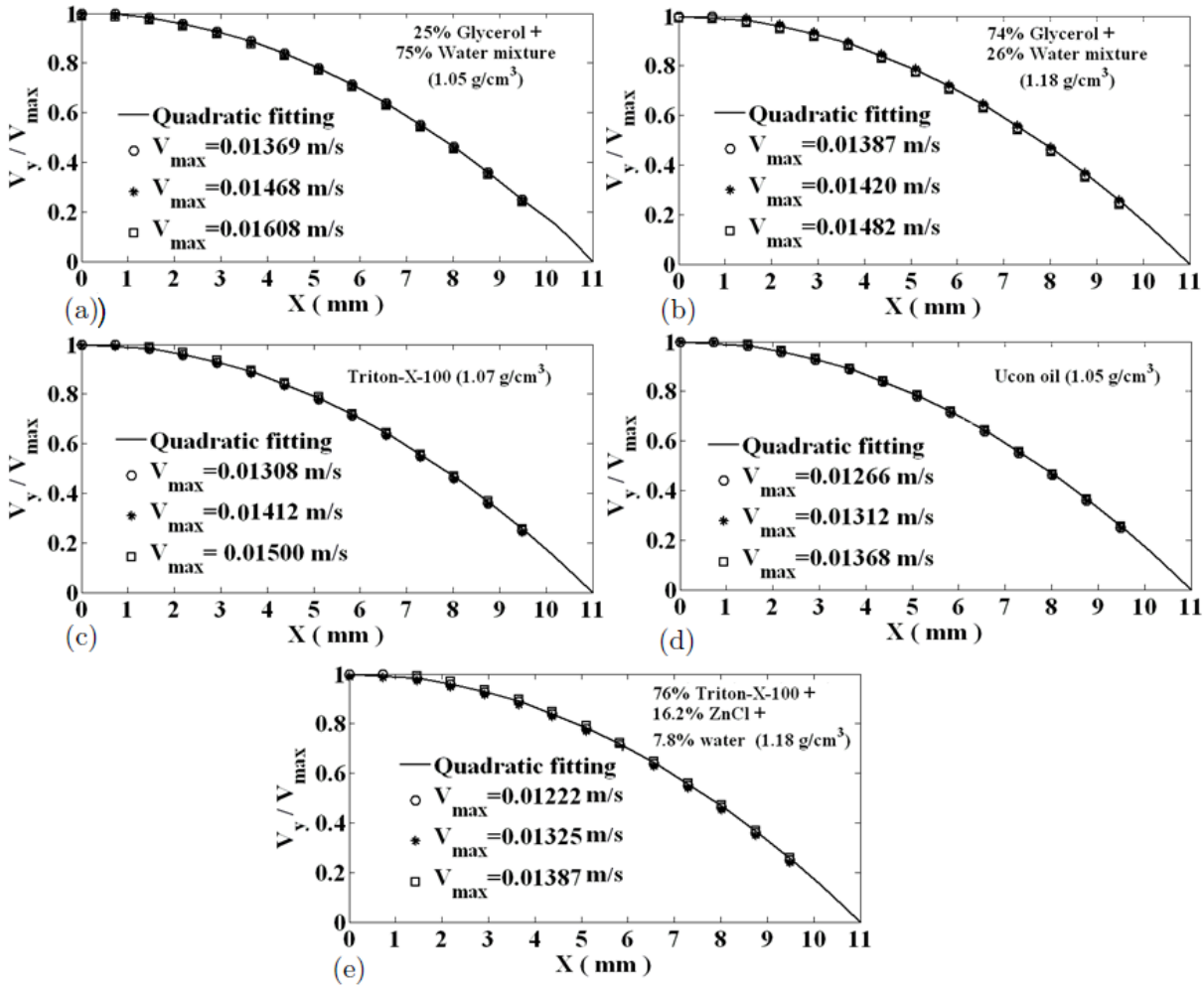

Figure 3.9: Free surface velocity profiles for various suspending fluids (Newtonian fluids) measured for the serrated channel (a) 25% glycerol and 75% water mixture (1.05 g/cc), (b) 74% glycerol and 26% water mixture (1.18 g/cc), (c) pure Triton-X-100 (1.07 g/cc), (d) Ucon oil (1.05 g/cc), (e) 76% Triton-X-100, 16% $Zncl_2$ and 8% water mixture (1.18 g/cc).

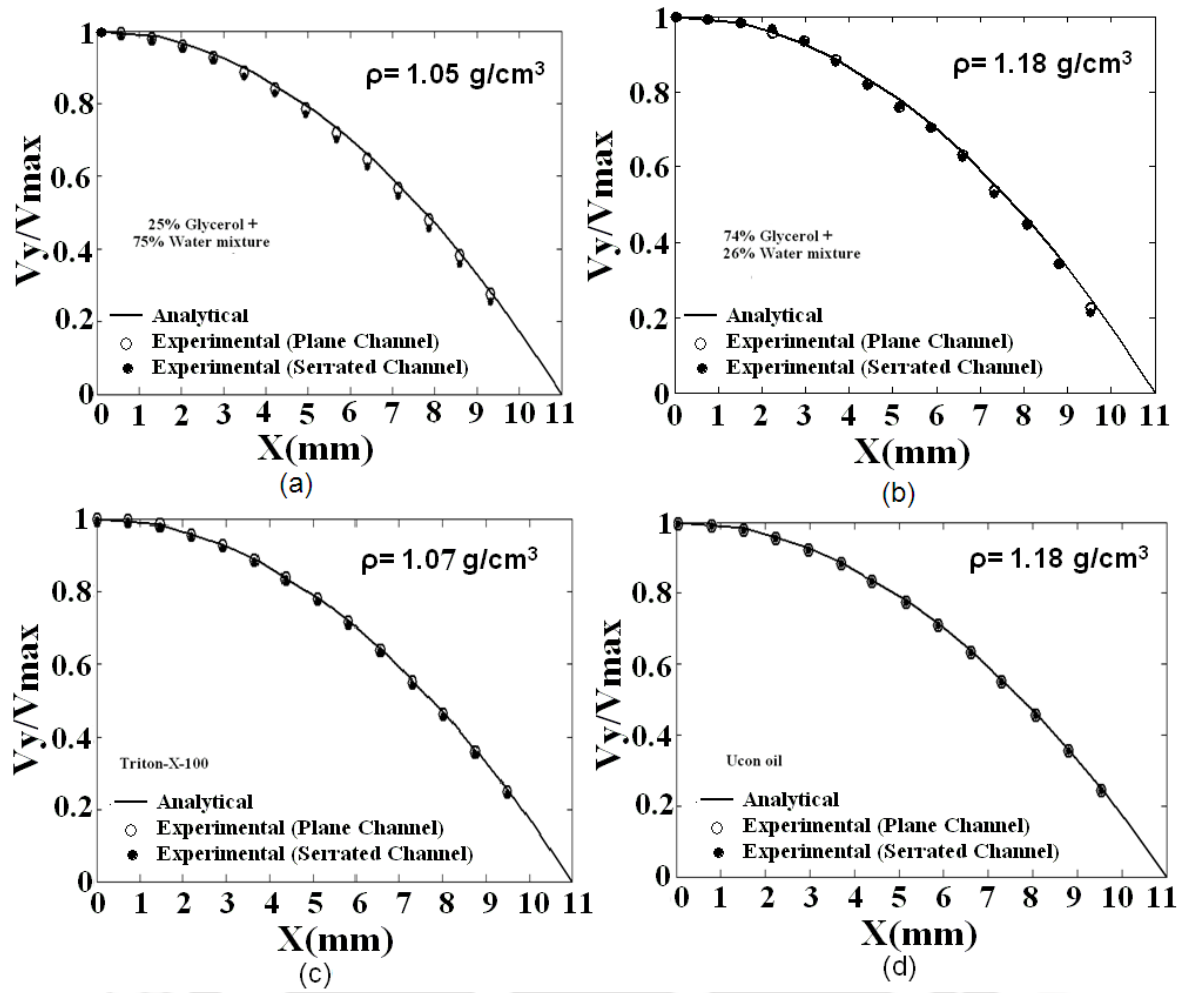

Figure 3.10: Mean y-velocity profile for pure suspending fluid for both plane and serrated channel (a) mixture of 25% glycerol and 75% water (1.05 g/cc), (b) mixture of 74% glycerol and 26% water mixture (1.18 g/cc), (c) Triton-X-100 (1.07 g/cc), (d) Ucon oil (1.05 g/cc).

3.4.2 Free surface velocity profile for concentrated suspension

This section provides measurements of velocity profile for concentrated suspensions and compares it for the plane and serrated wall channel. To get the mean velocity profiles, an average over 100 velocity vectors obtained by cross-correlation analysis of 100 consecutive pairs of images was performed. A reasonably good agreement is observed which confirms that image interrogation at the present concentration of tracer particles produced very few erroneous velocity vectors. To find out the location, where the velocity profile was fully developed beyond the entrance effects we have measured the profiles at different locations for both plane and rough channels. Figure 3.11 shows the velocity profiles at various axial locations for suspensions of 500 µm particles. It can be observed that the profiles beyond 27.3 cm are all similar. This indicates that the velocity profile is indeed fully developed at

this location and further downstream. Almost all suspensions attained fully developed profile at the axial location of 27.3 cm. Therefore, all the velocity measurements were carried out at the axial location of 27.3 cm from the entrance of the channel. Fig.3.12 through Fig.3.15 show the y-velocity (scaled with the centerline velocity) at various centerline velocity (V_m) for suspension 200 µm (PMMA) and 80 µm, 250 µm, 500 µm (polystyrene) particles respectively. The volume concentration of particles was 40% in all the cases. It can be observed that the scaled velocity profiles are similar for different flow rates. This is true for the both plane and serrated channels. This observation also confirms that the measured velocity profiles at the above mentioned location were fully developed. We obtained similar behavior for higher concentration of particles. It is to be noted that the velocity profile for suspension flow in serrated channel closely matches with the Newtonian profile, whereas there is significant blunting in case of the smooth channel.

The blunting in velocity profile was also observed in the studies of Singh *et al*. (2006) with smooth channel. In many situations the shear induced migration will cause migration of particles from the wall to the centre of the channel. This causes inhomogeneous concentration profile across the channel and blunting of the velocity profile. However, the blunting of velocity profile in situations, where we do not expect significant bulk migration is interesting and requires careful attention. In the present experiments we expected that continuous mixing of suspension in the screw pump, and the small length of the channel would have prevented significant lateral migration of particles across the channel. To verify this, we had conducted one experiment in which a small fraction of the suspending PMMA particles were dyed in black color. The image of these particles showed uniform concentration across the whole channel width. This indicates that there may not be appreciable bulk migration in the *x*–*y* plane for which we report the velocity profiles. It is true that particle migration starts rapidly but the time scale to reach developed profile is much larger. Many experiments on shear induced migration (Graham *et al*., 1991; Phillips *et al*., 1992; Corbett *et al*., 1995) have observed that migration phenomena in suspensions of volume fraction up to 55% is rather slow in agreement with its diffusive origin.

It is to be noted that our experiments were performed in such a way that the total strain which is the quantity that controls the extent of migration is nearly same in both serrated and smooth wall case. Therefore, the apparent slip velocity is expected to be not influenced by the bulk migration. However, we do not discount the effect of particle migration close to the wall on the depletion layer which gives rise to wall slip. Leighton and Acrivos (1987a) argue that due

to shear induced diffusion the average distance traveled by the particles of radius a, perpendicular to the flow direction, y, in time t would be $y \approx 2(Dt)^{1/2}$, where D is the shear induced diffusivity, and $D = d(\phi)\dot{\gamma}a^2$. The value of d(ϕ) can be estimated from the measurements of self diffusivity (Leighton and Acrivos, 1987a; Breedveld *et al.*, 2002) which is found to be ~ 10^{-1} for concentrated suspensions (ϕ >0.3). This value should be much smaller if collective diffusivity of particles is considered as opposed to the self diffusivity. The shear rate ($\dot{\gamma}$) at the wall achieved in most of our experiments was ~1s^{-1} and the average velocity in the channel was ~1 cm s^{-1}. The velocity measurements used in the analysis of wall slip were performed at 27 cm downstream of the channel. Thus, it can be easily calculated that during the average flow path of suspension (from the inlet to the measurement location), a particle near the wall can migrate 1-2 particle diameter. On the other hand, based on the scaling arguments of Leighton and Acrivos (1987a), Nott and Brady (1994) have estimated that the characteristic length scale (L) to reach steady state migration profile in a channel of width, H would be given as $\frac{L}{H} = \frac{1}{d(\phi)}\left(\frac{H}{a}\right)^2$. This suggests that the channel length in our investigation is several orders of magnitude smaller to achieve significant bulk migration.

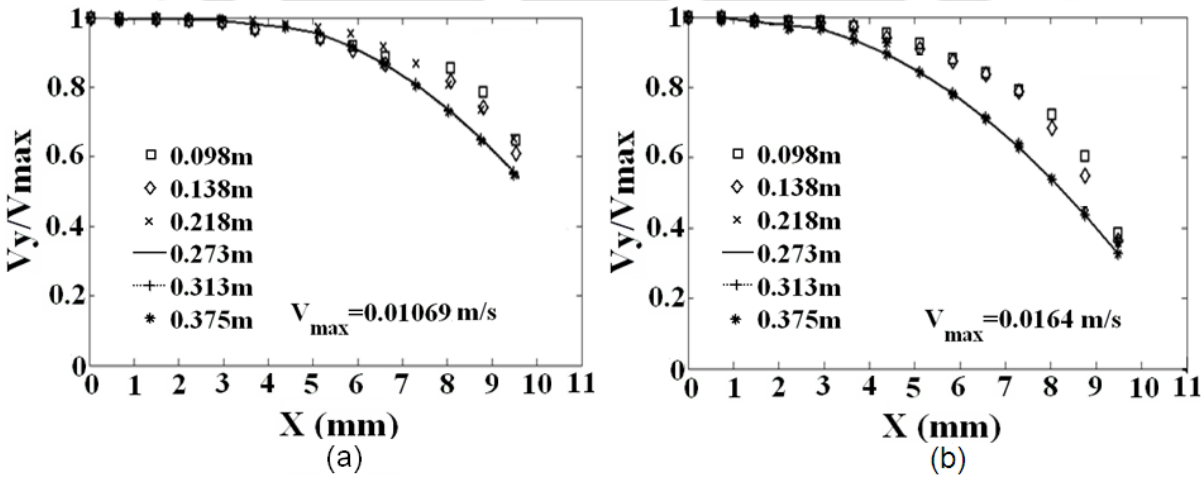

Figure 3.11: Mean y-velocity profile for concentrated suspension at different axial locations for (a) plane and (b) serrated channel. The particle volume concentration of suspension of 500 μm particles was 40%

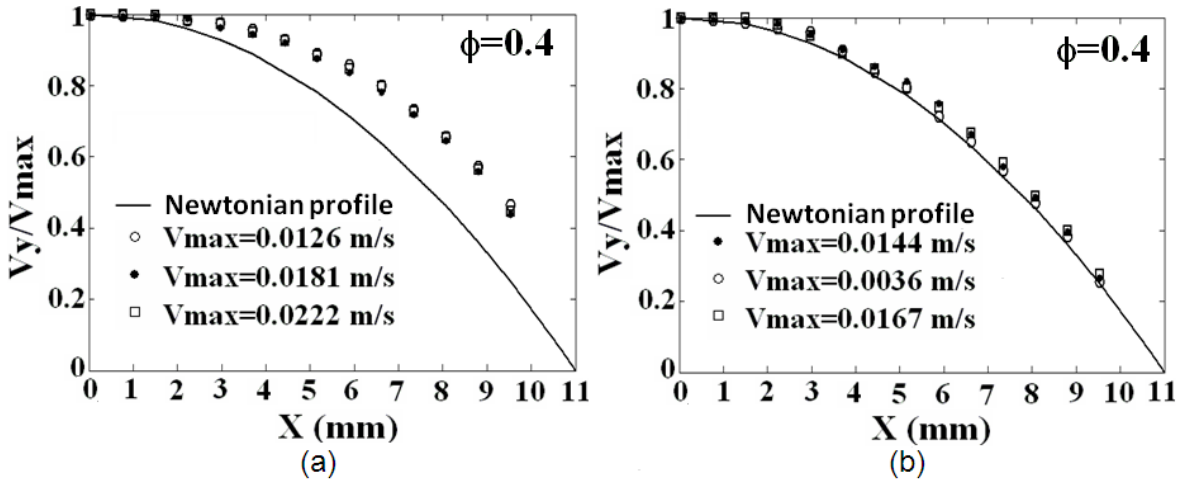

Figure 3.12: Mean y-velocity profile across the channel at various centerline velocities for suspension of 200 µm PMMA particles in 19 cP of suspending fluid at 40% concentration for (a) plane channel and (b) serrated channel.

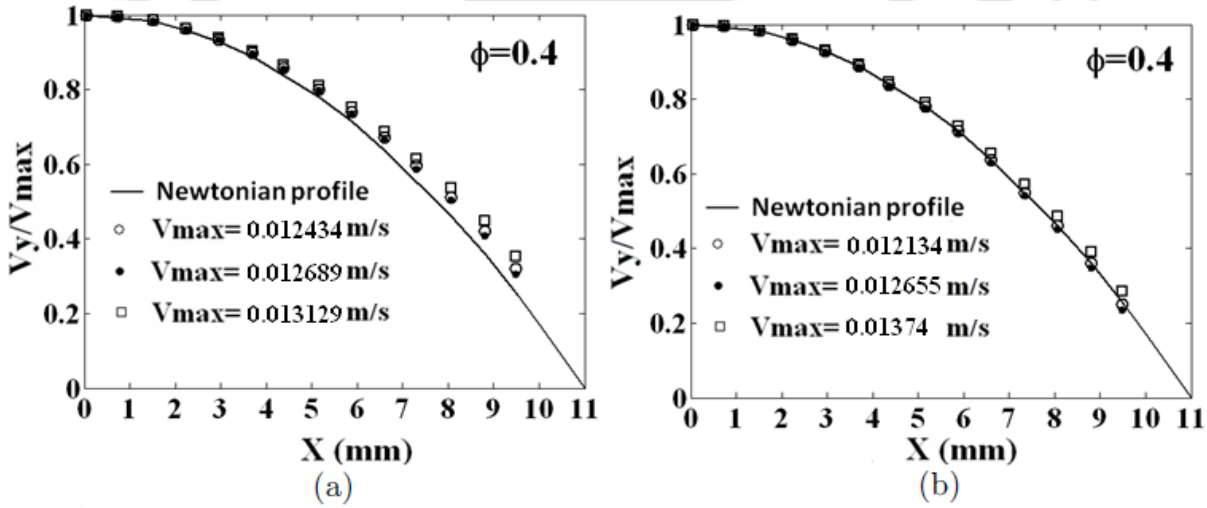

Figure 3.13: Mean y-velocity profile across the channel at various centerline velocities for suspension of 80 µm, polystyrene particles in 2.05 cP of suspending fluid at 40% concentration for (a) Plane channel (b) Serrated channel.

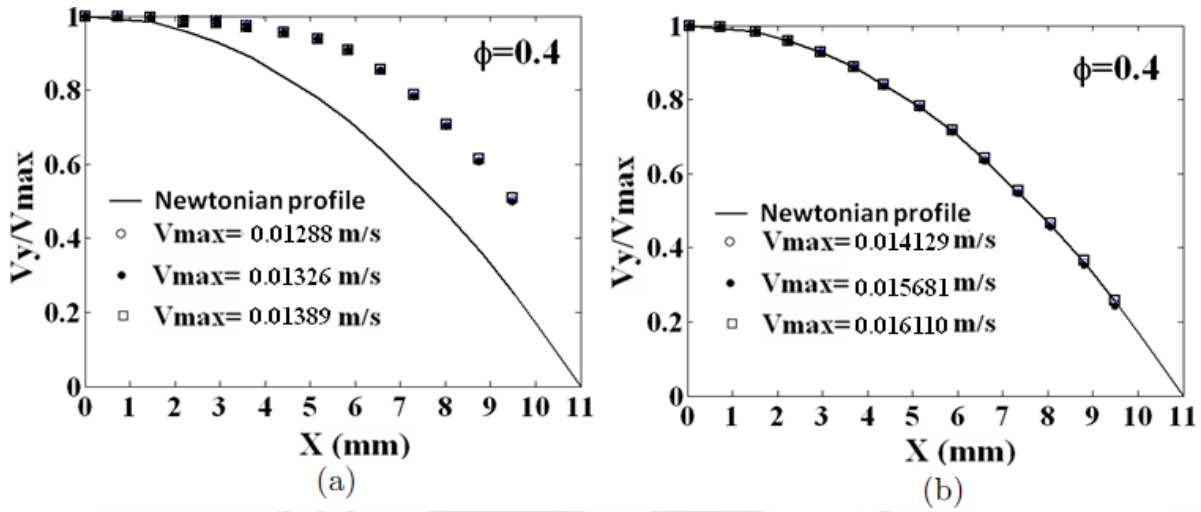

Figure 3.14: Mean y-velocity profile across the channel at various centerline velocities for suspension of 250 µm, polystyrene particles in 2.05 cP of suspending fluid at 40% concentration for (a) Plane channel (b) Serrated channel.

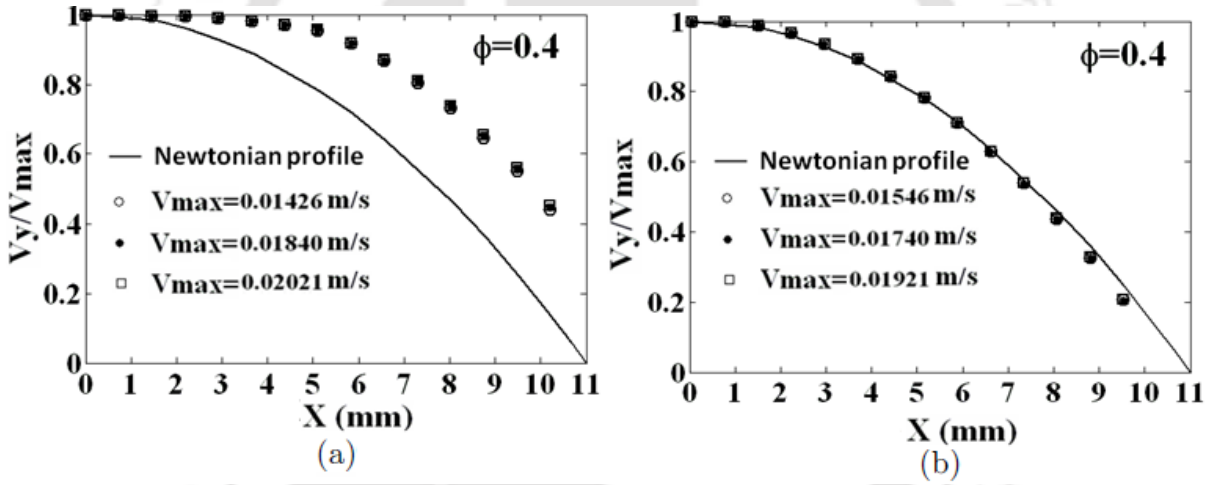

Figure 3.15: Mean y-velocity profile across the channel at various centerline velocities for suspension of 500 µm, polystyrene particles in 2.05 cP of suspending fluid at 40% concentration for (a) Plane channel (b) Serrated channel.

3.4.3. Wall slip coefficients

To study the effect of particle size and viscosity of suspending fluid on the wall slip, the velocity profiles for the suspensions of 200 µm PMMA particles in 19 cP suspending fluid and 500 µm polystyrene particles in 2.05 cP suspending fluid was considered at various particle fractions (ϕ =0.4, 0.45, 0.48 and 0.50). Figure 3.16 presents the comparison of velocity profiles for the plane and serrated channels at various concentrations for the suspension of 200 µm particles. The corresponding profile for the suspension of 500 µm particles is shown in Fig.3.19. It is to be noted that we were unable to evaluate the velocity

vectors very close to the channel wall due to the large size of the interrogation windows. Besides this, due to curvature effect the tracer particles close to the wall were not illuminated properly by the laser sheet (see Fig.3.3). When small interrogation window size (32 x 32 pixels) was chosen for PIV analysis we obtained erroneous velocity vectors. The correct velocity vectors were obtained for the interrogation window size of 128 x 128 pixels. Therefore, the first point at which we obtained velocity measurement was about 1.4 mm from the wall. To obtain the velocity value at the wall, we extrapolated the measurement points by curve fitting. For each concentration the experiment was conducted for three different flow rates. The wall velocity was obtained by extrapolation with three different curves fits of the data (quadratic, cubic and fourth degree polynomial) and error estimation was performed. When the curve for serrated channel is extrapolated to the wall, it gives velocity at the wall close to zero, matching with the Newtonian profile. However, for plane channel this value is positive. The difference between the two curves (plane and serrated channel) gives the wall slip velocities for that particular concentration of suspension. One can argue the justification behind the choice of this curve fitting when the velocity profile is not parabolic for the smooth channel. Though, analytical nature of the blunted velocity profile is not available, the present choice of curve fit closely matches with the experimental measurements. It can be also observed that there is significant difference between the velocity values for plane and serrated channel for the first measurement location close to the wall. This difference is close to the difference between the extrapolated values at the wall. Any deviation will not change the results qualitatively. Therefore, it is expected that the value of apparent wall slip velocity measured by this analysis is appropriate. It is clear that the wall slip velocity increases as the particle concentration is increased and the slip velocity is higher for 500 μm particles compared to 200 μm particles at the same concentration.

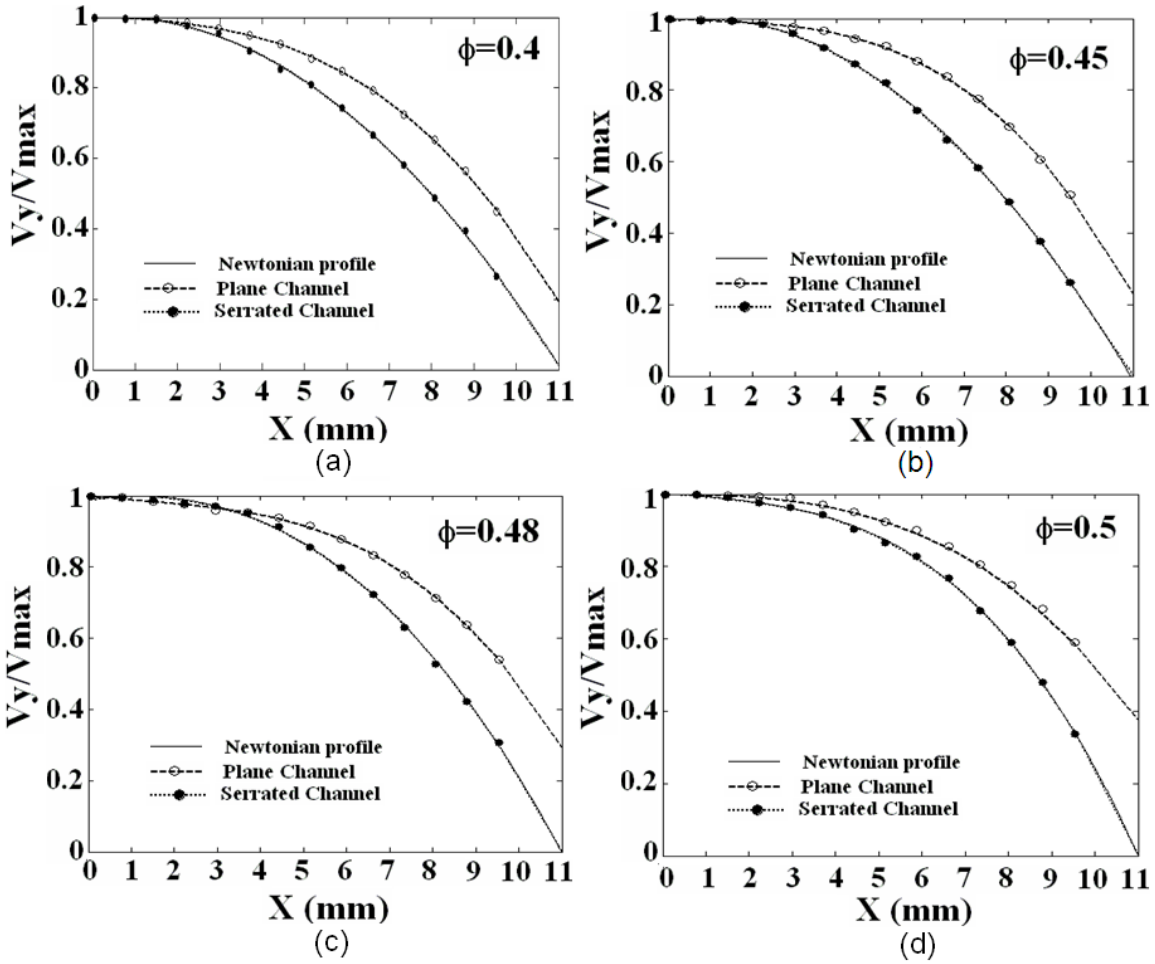

Figure 3.16: Mean y-velocity profile across plane and serrated channel at various concentrations (ϕ) of 200 µm particles present in 19 cP of viscous fluid. (a) ϕ=0.40, (b) ϕ=0.45, (c) ϕ=0.48, and (d) ϕ=0.50. The dashed lines are cubic spline fit of the experimental data and the solid lines are parabolic profile for Newtonian fluid.

In order to study the effect of particle size alone on the wall slip, we have taken suspensions of 80 µm, 250 µm and 500 µm particles. Each size of particles was dispersed in the glycerol water mixer of viscosity 2.05 cp (at 24°C). Figure 3.17 presents the comparison of velocity profiles for plane and serrated wall channels at various concentration for the suspension of 80 µm particles. The corresponding profiles for the suspensions of 250 µm and 500 µm are shown in Fig.3.18 and Fig.3.19 respectively. The wall slip velocity increases as the particle concentration is increased and the slip velocity is higher for 500 µm particles compared to 250 µm and 80 µm particles at the same concentration. Blunting of velocity profiles also increased with the increase of particle size in case of the plane wall channel.

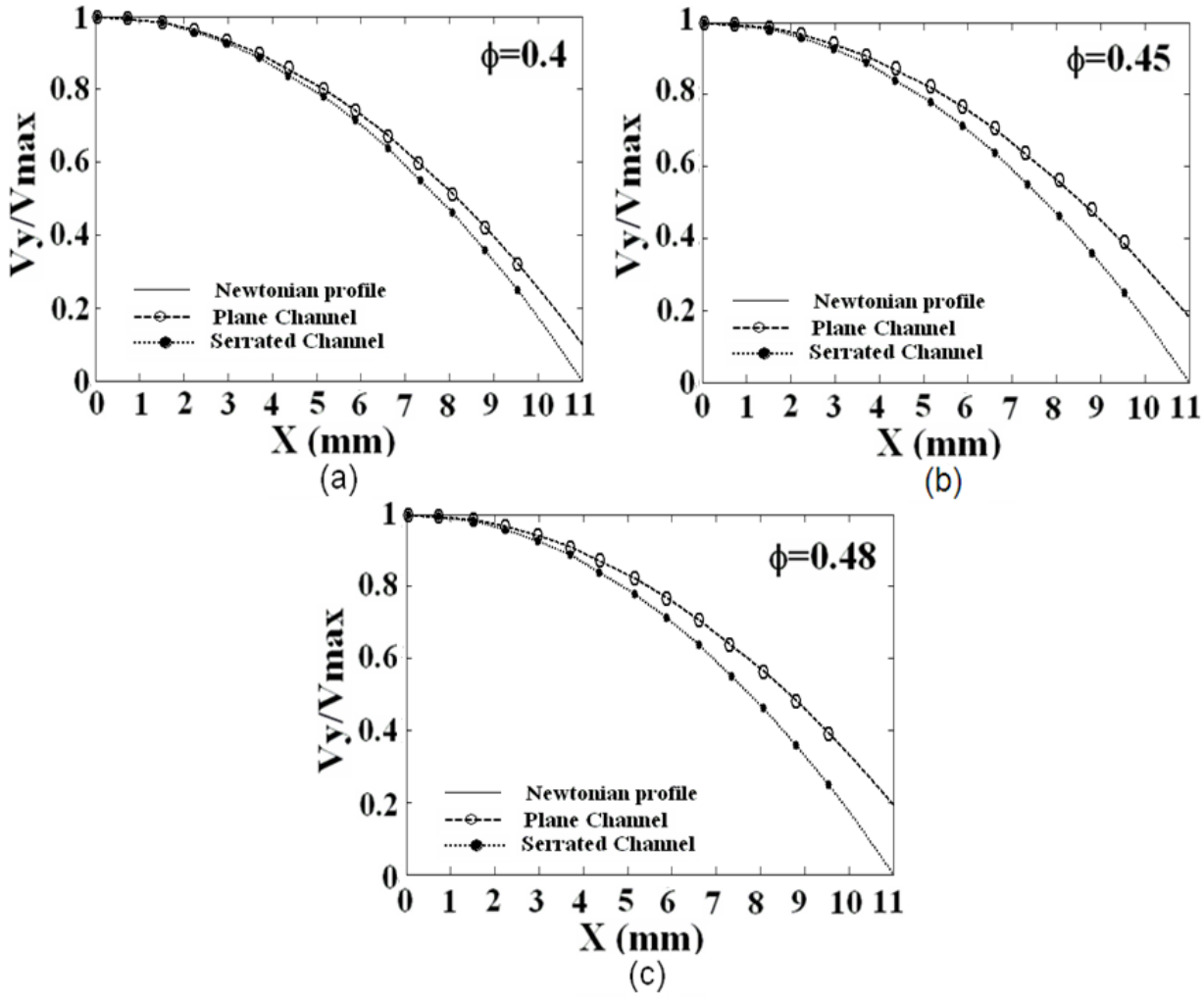

Figure 3.17: Mean y-velocity profile across plane and serrated channel at various concentrations (ϕ) of 80 µm particles in suspending fluid of viscosity 2.05 cP. (a) ϕ=0.40, (b) ϕ=0.45, and (c) ϕ=0.48. The dashed lines are cubic spline fit of the experimental data and the solid lines are parabolic profile for Newtonian fluid.

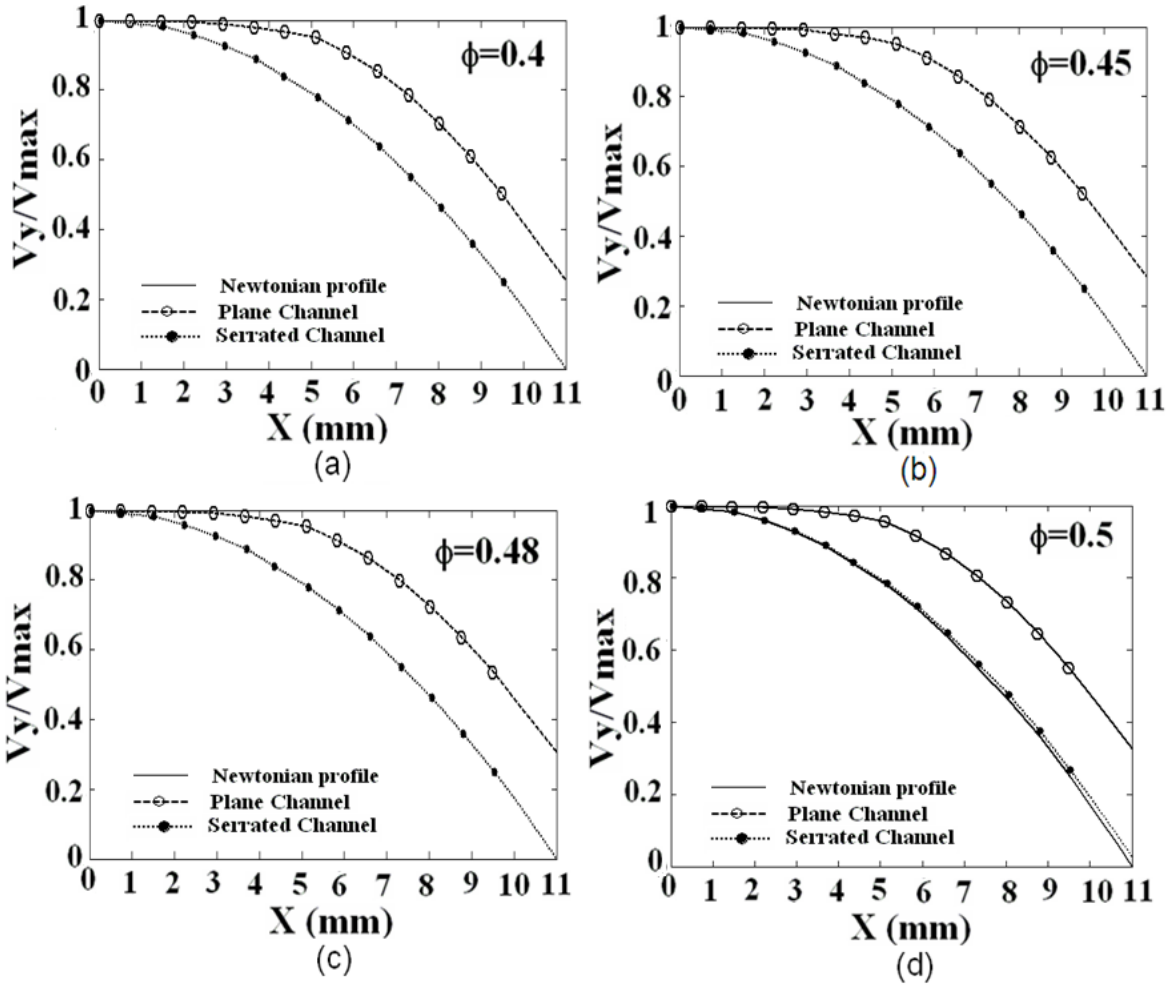

Figure 3.18: Mean y-velocity profile across plane and serrated channel at various concentrations (ϕ) of 250 μm particles in suspending fluid of viscosity 2.05 cP. (a) ϕ=0.40, (b) ϕ=0.45, (c) ϕ=0.48, and (d) ϕ=0.50. The dashed lines are cubic spline fit of the experimental data and the solid lines are parabolic profile for Newtonian fluid.

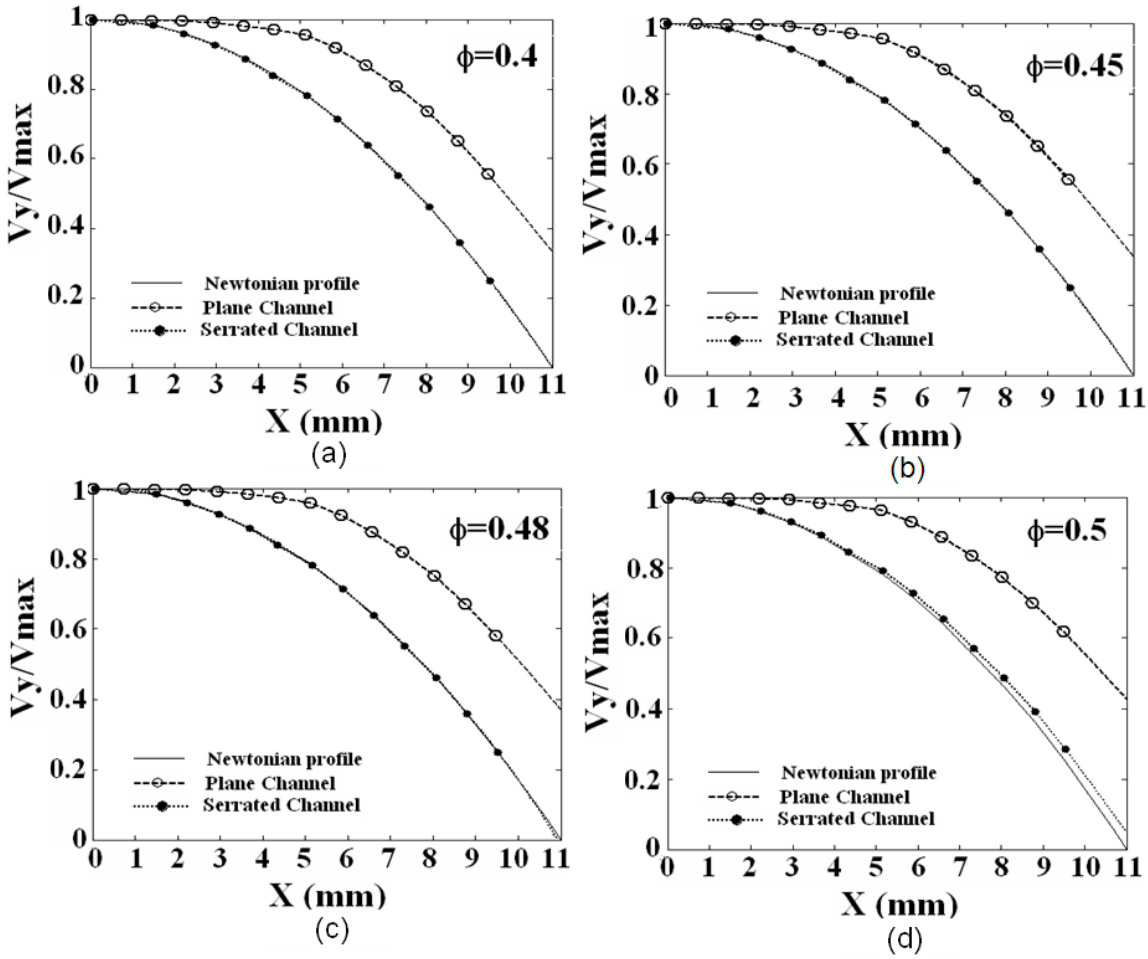

Figure 3.19: Mean y-velocity profile across plane and serrated channel at various concentrations (ϕ) of 500 µm particles in suspending fluid of viscosity 2.05 cP. (a) ϕ=0.40, (b) ϕ=0.45, (c) ϕ=0.48, and (d) ϕ=0.50. The dashed lines are cubic spline fit of the experimental data and the solid lines are parabolic profile for Newtonian fluid.

In order to study the effect of suspending fluid viscosity alone on the wall slip, we have taken suspensions of 500 µm particles dispersed in different fluids of viscosity 2.05 cP, 98 cP and 204 cP. Figure 3.19 presents the comparison of velocity profiles for plane and serrated wall channels at various concentrations for the suspension of 500 µm particles present in 2.05 cP of suspending fluid. The corresponding profiles for the suspensions of 500 µm particles present in 98 cP and 204 cP are shown in Fig.3.20 and Fig.3.21 respectively. The PIV analysis and velocity profile calculations were similar to the previous cases. It can be observed the wall slip velocity increases as the suspending fluid viscosity is decreased.

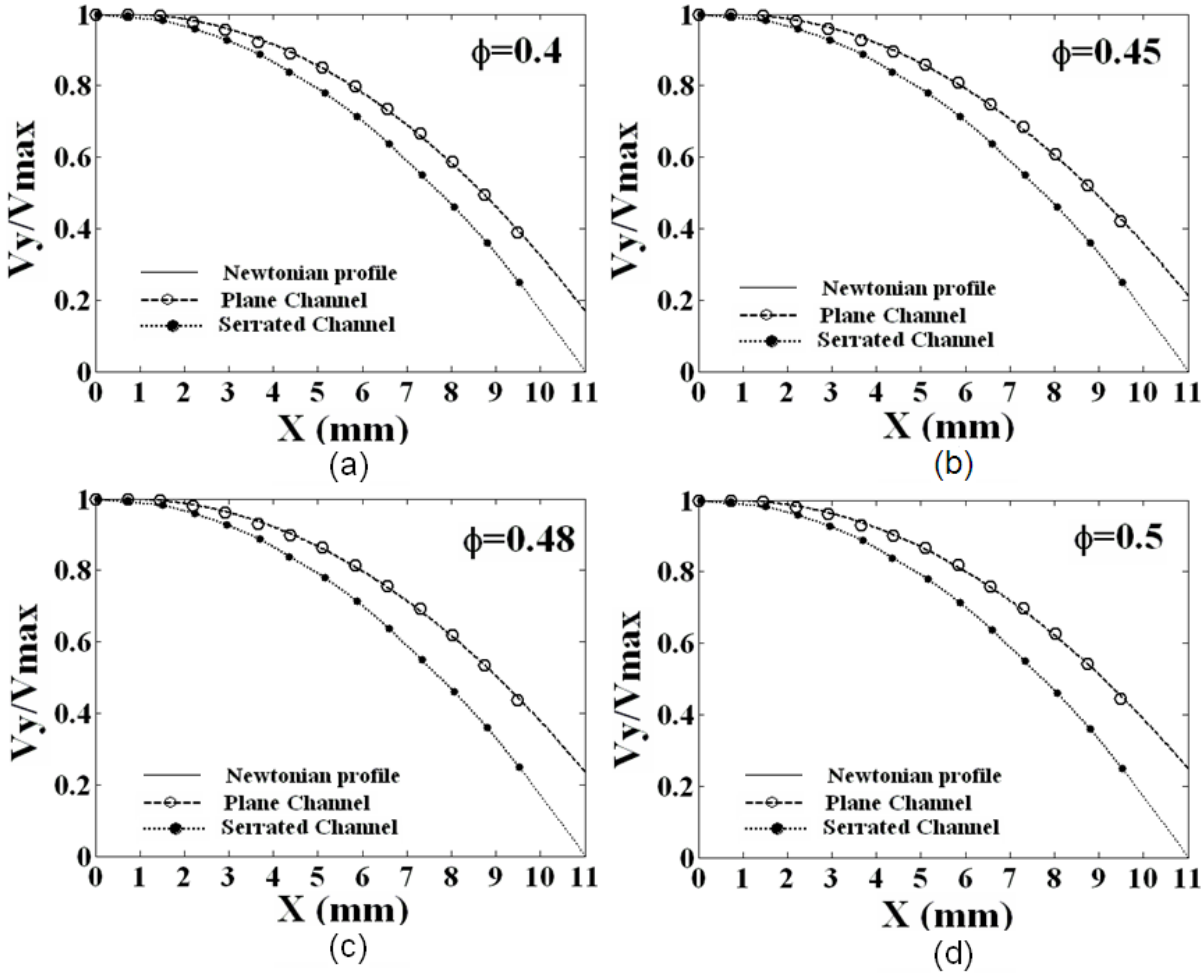

Figure 3.20: Mean y-velocity profile across plane and serrated channel at various concentrations (ϕ) of 500 µm particles in suspending fluid of viscosity 98 cP. (a) ϕ=0.40, (b) ϕ=0.45, (c) ϕ=0.48, and (d) ϕ=0.50. The dashed lines are cubic spline fit of the experimental data and the solid lines are parabolic profile for Newtonian fluid.

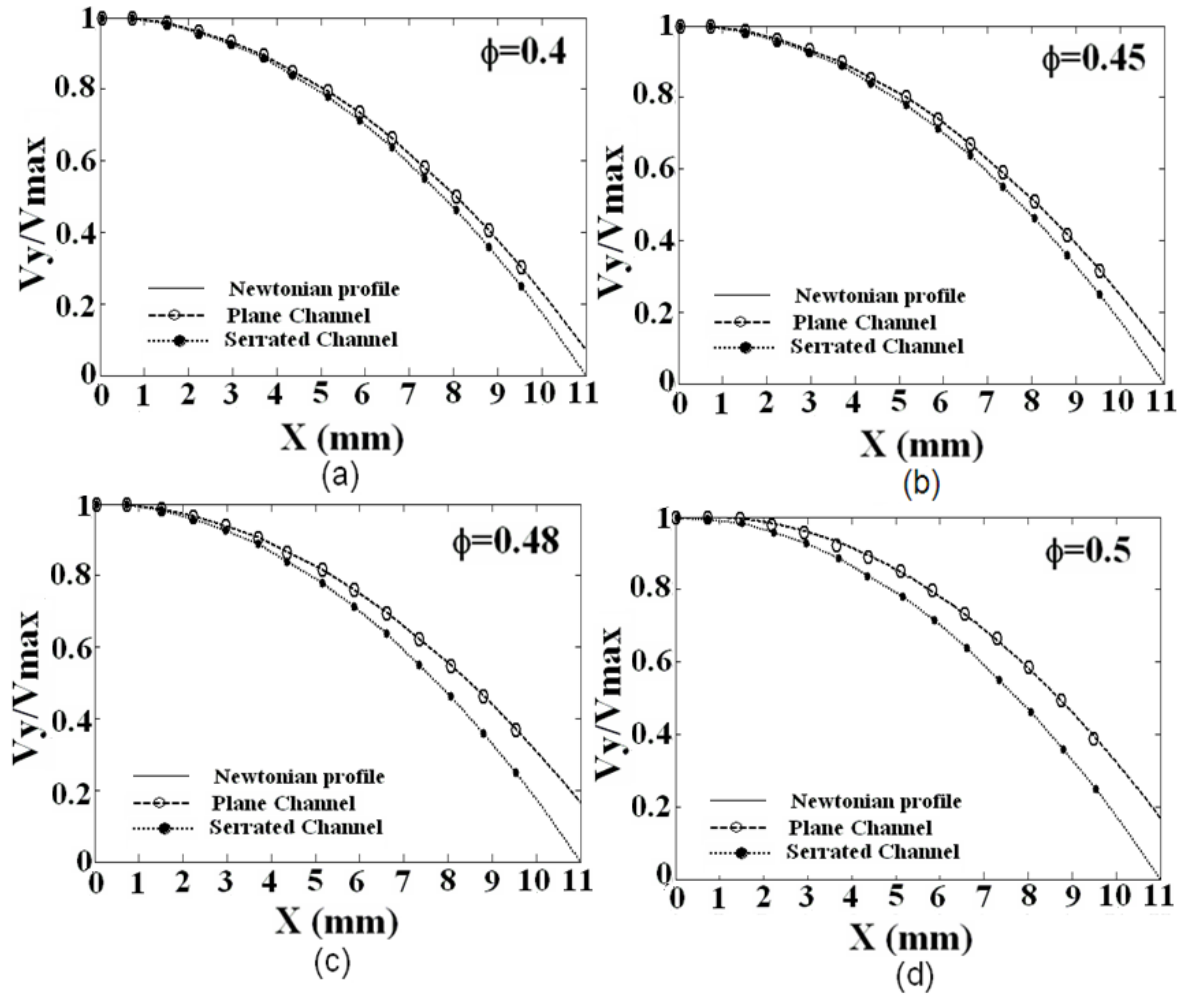

Figure 3.21: Mean y-velocity profile across plane and serrated channel at various concentrations (ϕ) of 500 μm particles in suspending fluid of viscosity 204 cP. (a) ϕ=0.40, (b) ϕ=0.45, (c) ϕ=0.48, and (d) ϕ=0.50. The dashed lines are cubic spline fit of the experimental data and the solid lines are parabolic profile for Newtonian fluid.

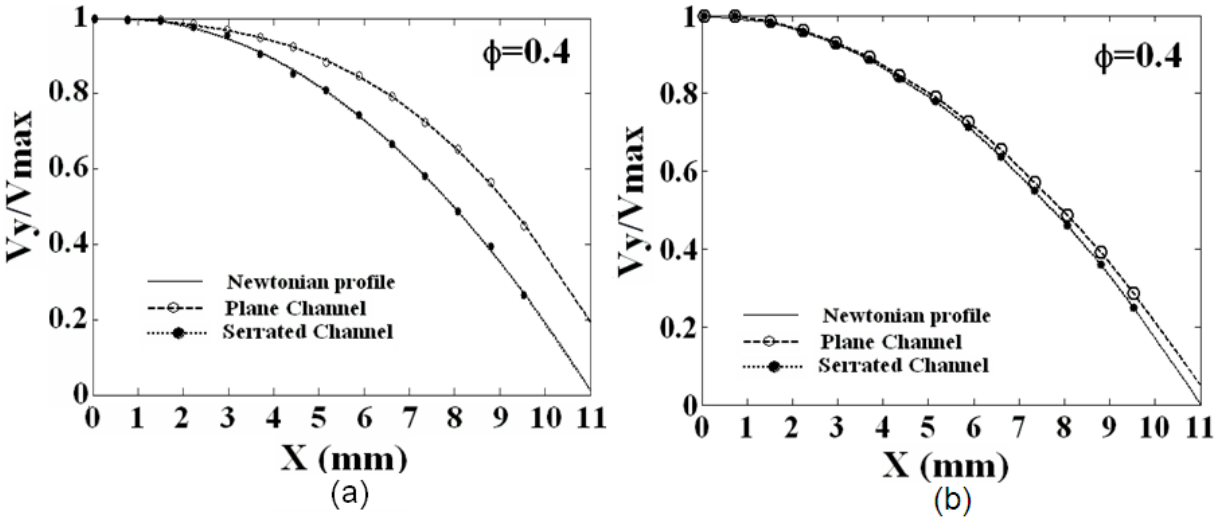

Figure 3.22: Mean y-velocity profile across plane and serrated channel at ϕ=0.40 for (a) 200 µm particles in suspending fluid of viscosity 19 cP (b) 200 µm particles in suspending fluid of viscosity 4000 cP. The dashed lines are cubic spline fit of the experimental data and the solid lines are parabolic profile for Newtonian fluid.

Figure 3.22 presents the comparison of velocity profiles for plane and serrated wall channels at ϕ=0.4 for the suspension of 200 µm particles present in 19 cP and 200 µm particles present in 4000 cP of suspending fluid. The wall slip is clearly much higher for suspending fluid of viscosity 19 cP. The wall slip coefficients (β) were determined from the following expression given by Jana et al. (1995),

$$\beta = \frac{u_s}{a\dot{\gamma}}, \tag{3.2}$$

where, u_s is the apparent wall slip velocity, $\dot{\gamma}$ is the apparent wall shear rate (determined from the slope of velocity profile of the plane channel) and a is the radius of particles. In the Fig.3.23a we have shown the slip velocity scaled by the centerline velocity plotted against the shear rate for various cases. Linearity of slip velocity in shear rate is established for all the cases. Fig.3.23b shows the plot of slip velocity against particle concentration. As expected the slip velocity increases with particle concentration. Wall slip is higher for suspension of 500 µm particles compared to that of 200 µm particles. Figure 3.24a shows comparative plot of dependence of apparent slip coefficient on particle concentration with the experimental measurements of Jana *et al*. (1995). There is qualitative agreement between the two measurements. However, the slip coefficients from our experiments are consistently higher than Jana *et al*. (1995). There could be several reasons for this observation. The PMMA

particles in the experiments of Jana et al. were much smaller compared to ours. The viscosity of suspending fluid in our experiments was also lower. It is well known that the viscosity of the suspending fluid affects the slip behavior of the suspension and a smaller viscosity gives rise to a greater wall slip velocity (Ahuja and Singh, 2009). Aral and Kalyon (1994) have studied the effect of temperature on apparent slip velocity of concentrated suspensions in torsional flow. They observed that the viscosity of the suspending fluid significantly affects the slip behavior of suspension and a smaller suspending fluid viscosity gives rise to a greater slip velocity. Assuming that the slip layer consists of solely of the suspending fluid of viscosity η_s, Yilmazer and Kalyon (1989) have determined the relationship between slip layer thickness δ and slip velocity (u_s) at a given shear stress τ_R as $\delta = \frac{u_s \eta_s}{\tau_R}$. Since the slip layer thickness for a given concentration only depends on particle size (Kalyon, 2005), it is clear that slip velocity will be inversely proportional to the suspending fluid viscosity. Our results are in qualitative agreement with this scaling. In Fig.3.24b, it can be easily noticed that when ($\beta a \eta_s$) is plotted against particle concentration these curves are indeed similar. It is to be noted that the suspension used in the study of Jana *et al.* (1995) was not neutrally buoyant due to mismatch between fluid and particle densities and this could be one of the reason for small quantitative difference.

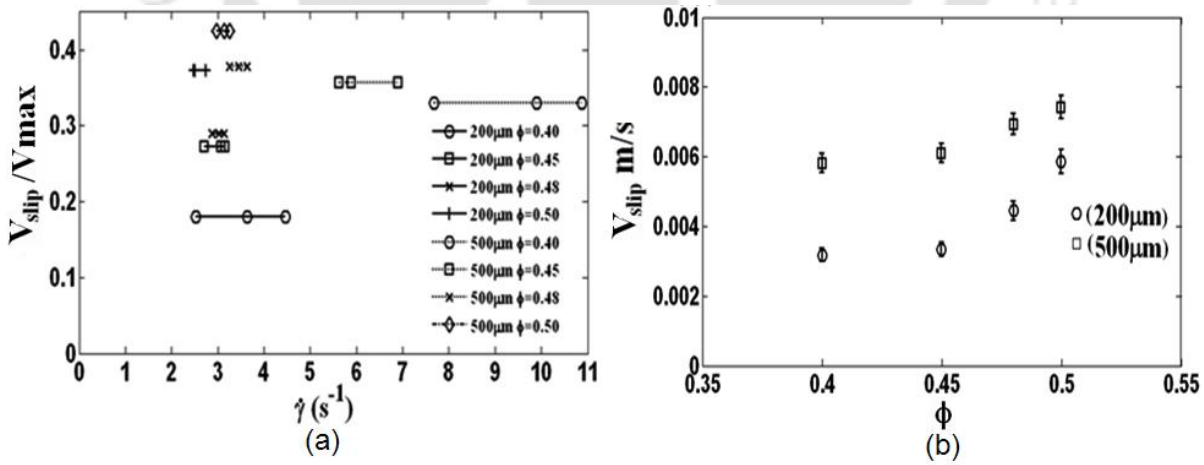

Figure 3.23: (a) Plot of slip velocity scaled with maximum centerline velocity against shear rate for the suspensions of 200 μm particles in 19 cP of suspending fluid and 500 μm particles in 2.05 cP of suspending fluid at various concentrations and (b) Plot of wall slip velocity against particle concentration.

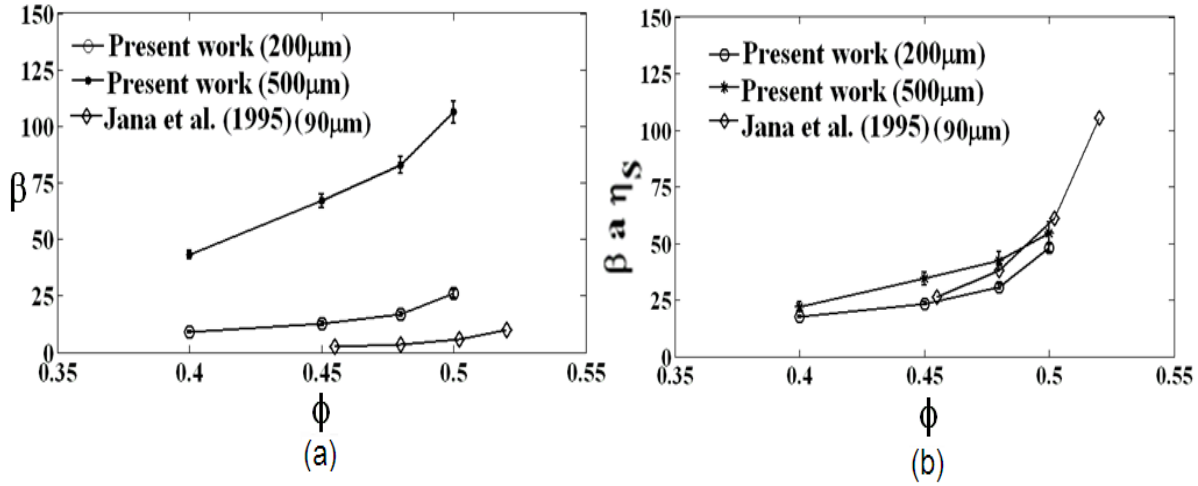

Figure 3.24: (a) Plot of apparent wall slip coefficient (β) with particle concentration and (b) comparison of slip coefficient after taking account the particle size, a, and viscosity of suspending fluid η_s (200 μm in 19 cP and 500 μm in 2.05 cP).

In Fig.3.25a we have shown the slip velocity scaled by the centerline velocity plotted against the shear rate for suspending fluid of viscosity of 80 μm, 250 μm, and 500 μm particles in 2.05 cP of suspending fluid at 24°C. Figure 3.25b shows the plot of slip velocity against particle concentration for this case. As expected the slip velocity increases with particle concentration in this case as well. Wall slip is higher for suspension of 500 μm particles compared to that of 250 μm and 80 μm particles. The results for 80 μm particles are shown up to the particle fraction of 0.48, since we were unable to get good PIV images for higher concentrations. Figure 3.26a shows comparative plot of dependence of apparent slip coefficient on particle concentration with the experimental measurements of Jana et al. (1995). There is qualitative agreement between the two measurements. For smaller particles, there is significant deviation which was due to erroneous vector resulting from large mismatch in refractive index of this fluid and the particles. For larger sized of the particles, it was possible to capture clear images.

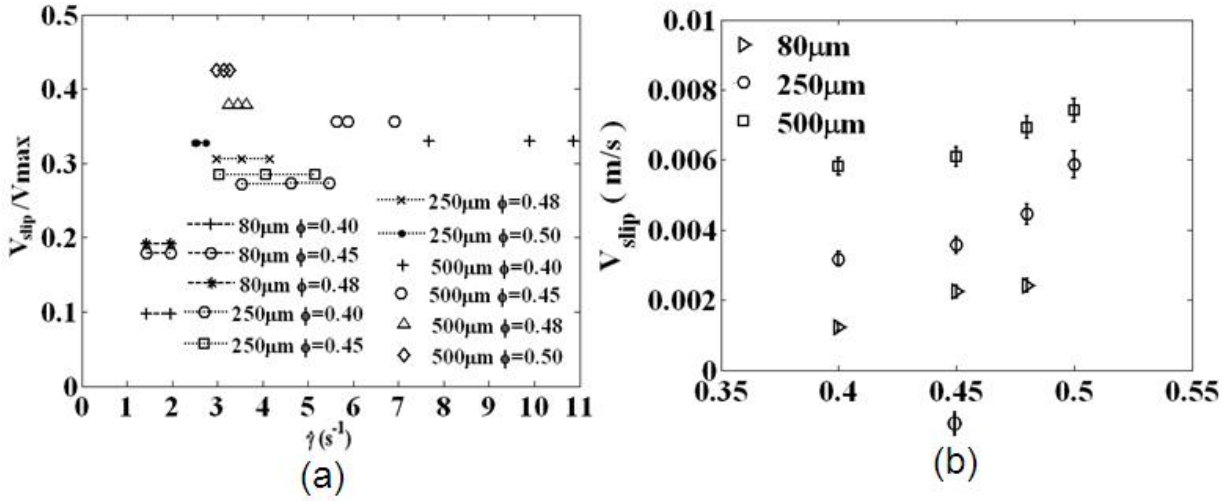

Figure 3.25: (a) Plot of slip velocity scaled with maximum centerline velocity against shear rate for the suspensions of 80 μm, 250 μm, and 500 μm particles present in 2.05 cP of suspending fluid at various concentrations and (b) Plot of wall slip velocity against particle concentration.

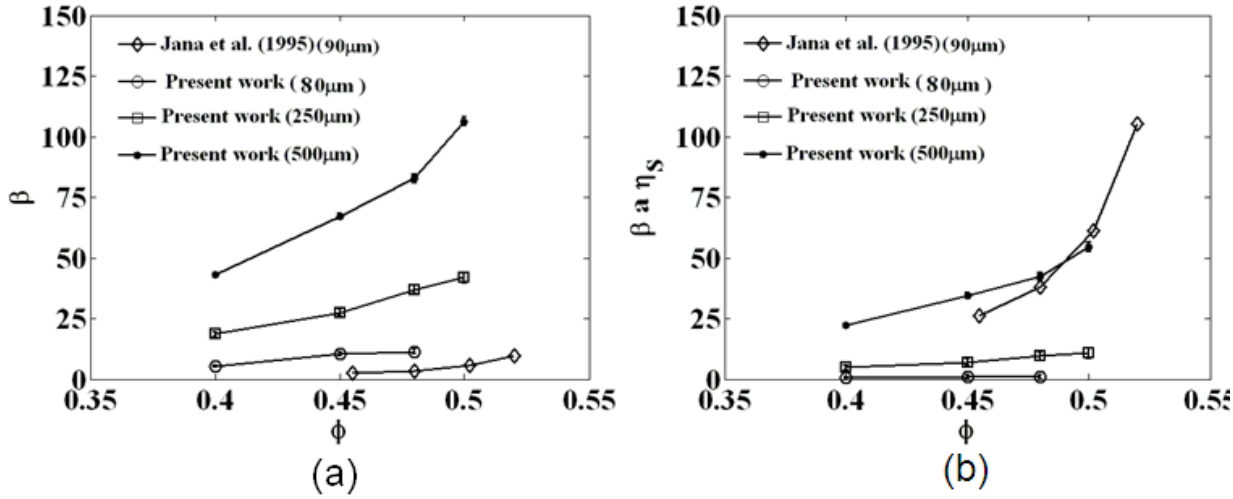

Figure 3.26: (a) Plot of apparent wall slip coefficient (β) with particle concentration and (b) comparison of slip coefficient after taking account the particle size, a a, and viscosity of suspending fluid η_s (80 μm, 250 μm and 500 μm particles in 2.05 cP).

In Fig.3.27a, we have shown the slip velocity scaled by the centerline velocity plotted against the shear rate for suspension of different suspending fluids but the same particle size. Figure 3.27b shows the corresponding plot of slip velocity against particle concentration. As expected the slip velocity increases with particle concentration. Wall slip is higher for suspension with 2.05 cP of suspending fluid compared to that of 98 cP and 204 cP (at 24°C) of suspending fluids. Figure 3.28a shows the comparative plot of dependence of apparent slip coefficient on particle concentration with the experimental measurements of Jana *et al.*

(1995). There is again good qualitative agreement between the two measurements when we compare the plot of ($\beta a \eta_s$) against particle concentration in the Fig. 3.28b.

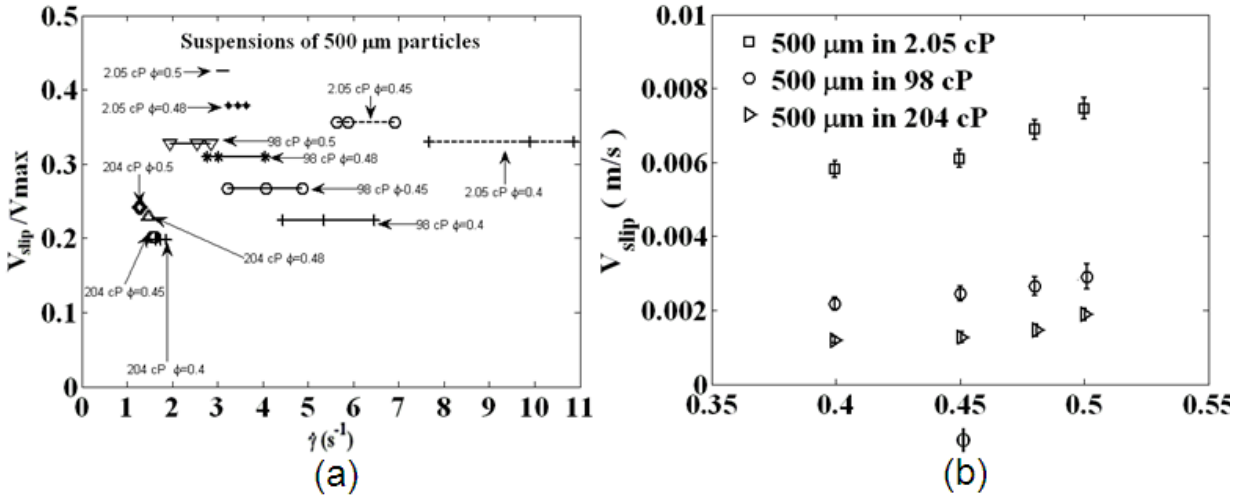

Figure 3.27: (a) Plot of slip velocity scaled with maximum centerline velocity against shear rate for the suspension of 500 μm particles in suspending fluids of viscosity 2.05 cP, 98 cP, and 204 cP. (b) Plot of wall slip velocity against particle concentration.

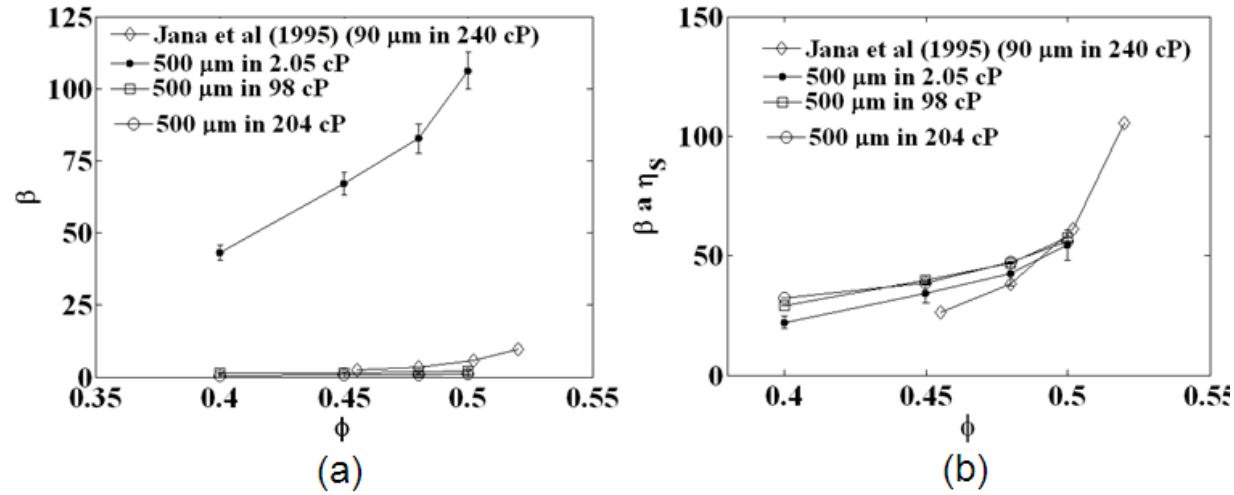

Figure 3.28: (a) Plot of apparent wall slip coefficient (β) with particle concentration and (b) comparison of slip coefficient after taking account the viscosity of suspending fluid η_s (2.05 cP, 98 cP and 204 cP at 24°C. The particle size in all the cases of our measurement was 500 μm.

3.5 CONCLUSION

In this chapter, we have carried out measurement of apparent wall slip velocity at various concentrations for suspension with different sized particles as well as different suspending fluids. We have conducted experiment on two channels one with plane surface and other with serrated surface. The various suspensions were prepared towards study of the effect of

particle size, volume fraction of particles and the viscosity of suspending fluids. The images were captured using a 1360 x 1024 pixel CCD camera (PixFly HiRes from PCO) in conjugation with a macro zoom lens. The camera was operated with frame rate of 19 frames/s and the duration between subsequent images was 52 ms. The captured images were used for the velocity profile measurement using the tool of Particle Image Velocimetry (PIV). To find out the accuracy of PIV measurements, we performed the comparison of experimentally determined mean y – velocity profile for both the channels (plane and serrated) with the analytical value (parabolic profile) for the Newtonian suspending fluids. To get the mean velocity profiles, an average of 100 velocity vectors was taken which were obtained by cross – correlation analysis of 100 consecutive pairs of images. All the velocity measurements were carried out at the axial location of fully developed from the channel entrance. It was observed that the scaled velocity profiles are similar at different flow rates. This is true for both plane and serrated channel. In the present experiments, no significant particle migration was expected. Moreover, the mixing of suspension in the screw pump and the small length of channel ensured that lateral migration of particles across the channel remained minimal. The wall slip coefficients (β) were determined. Linearity of slip velocity in shear rate was observed. The plot of slip velocity against particle concentration was also shown. As expected, the slip velocity increases with particle concentration and particle size but decreases with increase in the viscosity of suspending fluid. Comparative plot of dependence of apparent slip co-efficient on particle concentration with the experimental measurements of Jana *et al*. (1995) was presented. The results are in reasonably good agreement.

CHAPTER 4

FREE SURFACE CORRUGATION IN OPEN CHANNEL FLOW

4.1 INTRODUCTION

Even at low Reynolds number, the free surface flow of concentrated suspensions of non-colloidal particles exhibits surface corrugation. It is also well known that non-colloidal concentrated suspensions have non-zero normal stress differences. Many polymeric fluids have large first normal stress difference. Under condition of no-slip polymeric fluids with negative (extensional) first normal stress difference will behave like a stretched membrane. The non-colloidal suspensions are known to have positive (in the compression sense) first and second normal stress difference. Whether the presence of wall slip causes the free surface to exhibit shape (like when a stretched membrane is suddenly relaxed) in the form of surface corrugation was the motivation behind studying the effect of wall slip on surface corrugation. The corrugation structure depends on a number of factors such as particle concentration, shear rate, particle size and surface tension of the suspending fluid. By analyzing the power density of the refracted light from the free-surface, the surface roughness was characterized. Since the relative illumination intensity is associated with the local inclination of the surface, study of temporal and spatial intensity spectra provided valuable information about the wave amplitude and frequency of the surface deformation patterns. It was observed that the disturbances at the free surface span over wide range of frequency and wavelength. We have performed experiments to study whether wall slip affects the surface corrugation pattern or not. The surface images were taken by placing the camera above the surface and illuminating the free surface using cold light source (Thorlab). The light source was placed at an appropriate angle so that it reached the camera lens after refraction from the free surface. The corrugated surface refracted the light depending upon the local free surface orientation. Our objective is also to study the effect of plane walled and serrated walled channel. The setup

arrangement for plane walled channel is shown in Fig.4.1. Power spectral densities of image intensity for both temporal and spatial directions provide indirect estimate of surface corrugation since the exact relation between surface curvature and intensity of the image is not known (Loimer *et al*., 2002; Timberlake and Morris, 2005). The near surface particle fluctuation causes deformation of the interface. When the deformation relaxes, the energy contained within it is released back into the fluid. This may further affect the surface topography elsewhere. The experiments were studied towards the effect of suspended particle size, suspended particles fractions and suspending fluid viscosity. The power spectral density (PSD) of image intensity values was computed using fast Fourier transform similar to Singh et al. (2006). A total of 444 frames were taken to get the PSDs.

Figure 4.1: Photograph showing the experimental arrangements for capturing images of surface corrugation.

4.2 CHARECTERIZATION OF FREE SURFACE CORRUGATION

The recent studies on free surface flow of concentrated suspension (Loimer *et al*., 2002; Timberlake and Morris, 2005; Singh *et al*., 2006) have shown that surface corrugation patterns of many length scales are present. It was observed that the roughness of the surface disturbances depends on the particle size, particle concentration and on the surface tension of the suspending fluid. These studies have characterized the surface corrugation by the analysis of the spectra of the refracted light from the free surface. it was also observed that as the particle fraction increases the autocorrelation in flow direction declines faster until a critical fraction is reached, thereafter the autocorrelation in flow direction declines faster until a

critical fraction is reached, thereafter the autocorrelation functions decays slowly. The auto-correlation function represents how the flow structure at a location is correlated with that at some downstream location. Faster decay of auto-correlation with spatial dimension indicates larger fluctuation at the free-surface. On the other, hand if the interface region is largely moving with the mean flow this would result into slow decay of auto-correlation function. Singh *et al*. (2006) had also observed that as the concentration increases the blunting of velocity profiles across the channel increases. Now, it is clear that in the absence of significant particle migration the velocity profile indicates the presence of slip between the fluid and particle velocities near the wall of the channel. Therefore, we have performed experiments to study whether wall slip affects the surface corrugation pattern or not. The surface images were taken by placing the camera above the surface and illuminating the free surface using cold light source (Thorlab). The light source was placed at an appropriate angle so that it reached the camera lens after refraction from the free surface. The corrugated surface refracted the light depending upon the local free surface orientation. Power spectral densities of image intensity for both temporal and spatial directions provide indirect estimate on surface corrugation since the exact relation between surface curvature and intensity of the image is not known (Loimer *et al*., 2002; Timberlake and Morris, 2005). The near surface particle fluctuation causes deformation of the interface. When the deformation relaxes, the energy contained within it is released back into the fluid. This may further affect the surface topography elsewhere. Figure 4.2 shows the sample image which is taken for PSD analysis for surface corrugation.

Figure 4.2: A sample image for PSD analysis to charecterize the surface corrugation. The sample image was taken for suspension of 250 μm polystyrene particles in the suspending fluid of viscosity 2.05 cP. The volume fraction of the suspension was 0.3.

4.3 RESULTS AND DISCUSSION

By analyzing PSD results at different concentration in both channels, we try to investigate corrugation structure at the free surface in shear flow of concentrated suspension. Our objective is also to study the effect of concentration, effect of particle size, and effect of suspending fluid viscosity on the surface roughness of fluctuations near the free surface which is required to characterize the flow structures in free surface flow of suspensions. Moreover apparent wall slip co-efficient measurement is of fundamental importance to application to material processing as the surface effect is particularly manifest at the interface where the transport of mass, momentum and energy are affected. We present here the comparison of power spectral densities of image intensity for both temporal and spatial directions in both plane and serrated channels. Though the exact relation between the surface curvature and intensity of the image is not known, such spectra do provide a qualitative estimate of the length and time scale of the surface roughness. Such analysis along with the PIV data can increase the understanding of the free-surface flow, its scales and the nature of the flow structures. The near surface particle fluctuation causes deformation of the interface. When the deformation relaxes, the energy contained within it is released back into the fluid. This may further affect the surface topography elsewhere. The length scale associated with the flow structures can be estimated by using Taylor hypothesis, i.e. multiplying the time scale with the local average velocity at that position (Taylor, 1938). In the turbulence literature, this energy cascade is revealed by the turbulent kinetic energy spectra. However the correct analysis of the kinetic energy spectra requires continues velocity measurements at small time intervals. Since this was not possible from our velocity measurements, we have studied the spectra of the image intensity. For temporal measurements photographs were taken at a frame rate of 19 frames/s. The power spectrum densities (PSD) of image intensity values were computed using the fast Fourier transform similar to Singh et al. (2006). A total of 444 frames were taken to get the PSD. To study the effect of particle size we have prepared suspension with different particle sizes (80 µm, 250 µm and 500 µm mean diameter). The viscosity of the suspending fluid was 2.05 cP for all the three suspensions. The corresponding power spectra for these suspensions are shown in Fig. 4.3 through Fig.4.5. To study the effect of viscosity of suspending fluid, we have prepared suspensions with 500 µm particles mixed in three different suspending fluids of viscosity 2.05 cP, 98 cP, and 204 cP. The corresponding spectra for these cases are shown in the Fig.4.5 through Fig.4.7. Figure 4.8 shows the power spectra for suspension of 200 µm particles in suspending fluid of

viscosity 19 cP. All these plots show large peaks at regular intervals indicating the presence of flow structures at multiples time scale. The frequencies of the peaks are nearly same for both plane and serrated channels. In addition to this, the nature of the plots are same for both channels at all concentrations that we studied. There is no marked difference in the spectral distribution for all particle size and suspending fluid viscosity. This could be due to the fact that spectra were studied in the plane of free surface and it is possible that the spread of corrugation structure in the plane of free surface is similar for all the suspensions. However, it is desired to study the corrugation in velocity-vorticity plane (perpendicular to the plane of free surface) to quantify the corrugation and its dependence on particle size and viscosity of the suspending fluid. This is done in the next chapter. For a given suspension, the comparison of spectra from plane channel and rough channel gives an idea about the effect of wall slip on surface corrugation. In all the cases it was observed that the natures of these plots are nearly same. This indicates that wall slip may not have any apparent effect on the surface corrugations due to particle size, suspending fluid viscosity, particle fractions and plane or serrated wall.

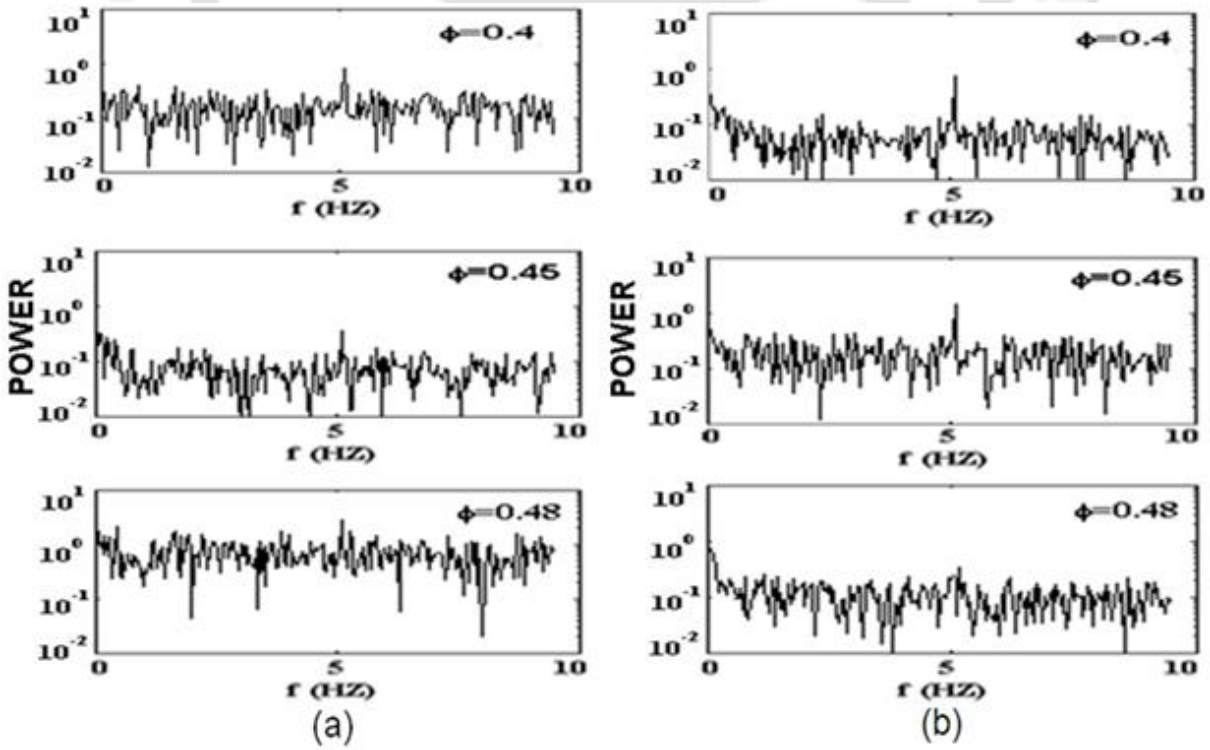

Figure 4.3: Temporal PSD at different particle concentrations for (a) plane and (b) serrated channel. The particle size was 80 μm and the viscosity of suspending fluid was 2.04 cP.

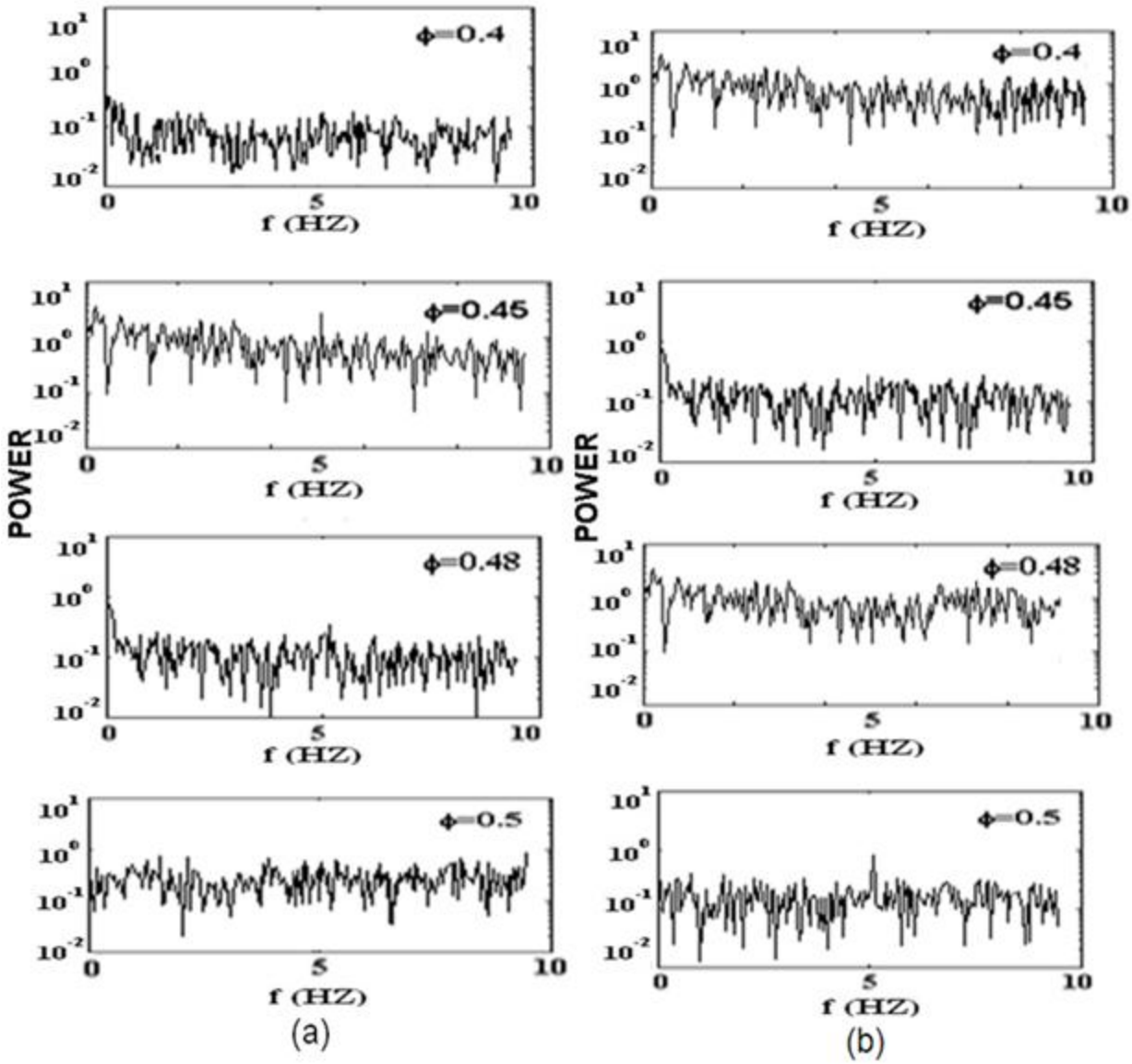

Figure 4.4: Temporal PSD at different particle concentrations for (a) plane and (b) serrated channel. The particle size was 250 μm in this case. The suspending fluid was same as in fig. 4.3.

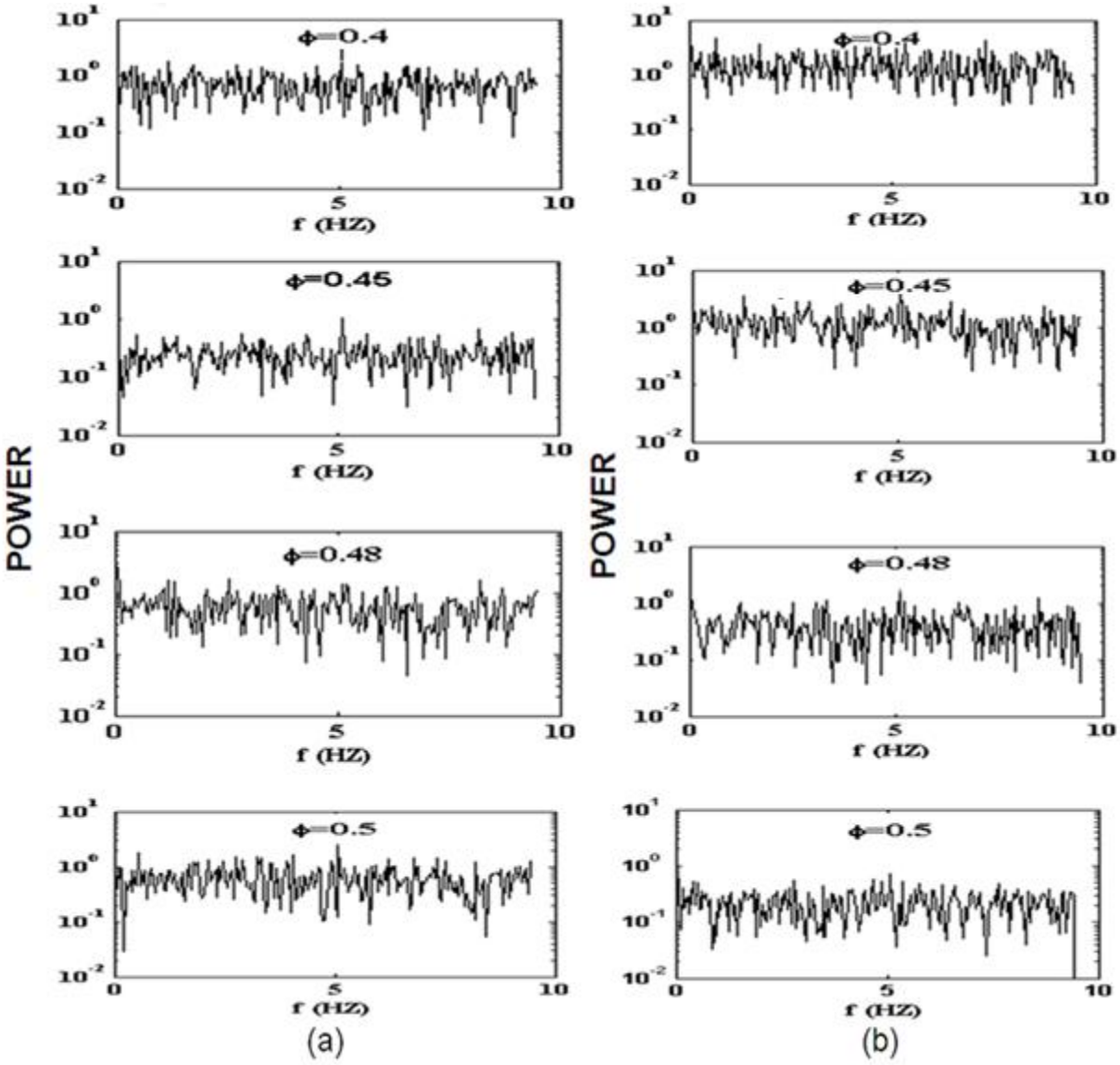

Figure 4.5: Temporal PSD at different particle concentrations for (a) plane and (b) serrated channel. The particle size was 500 μm in this case. The suspending fluid was same as in fig. 4.3.

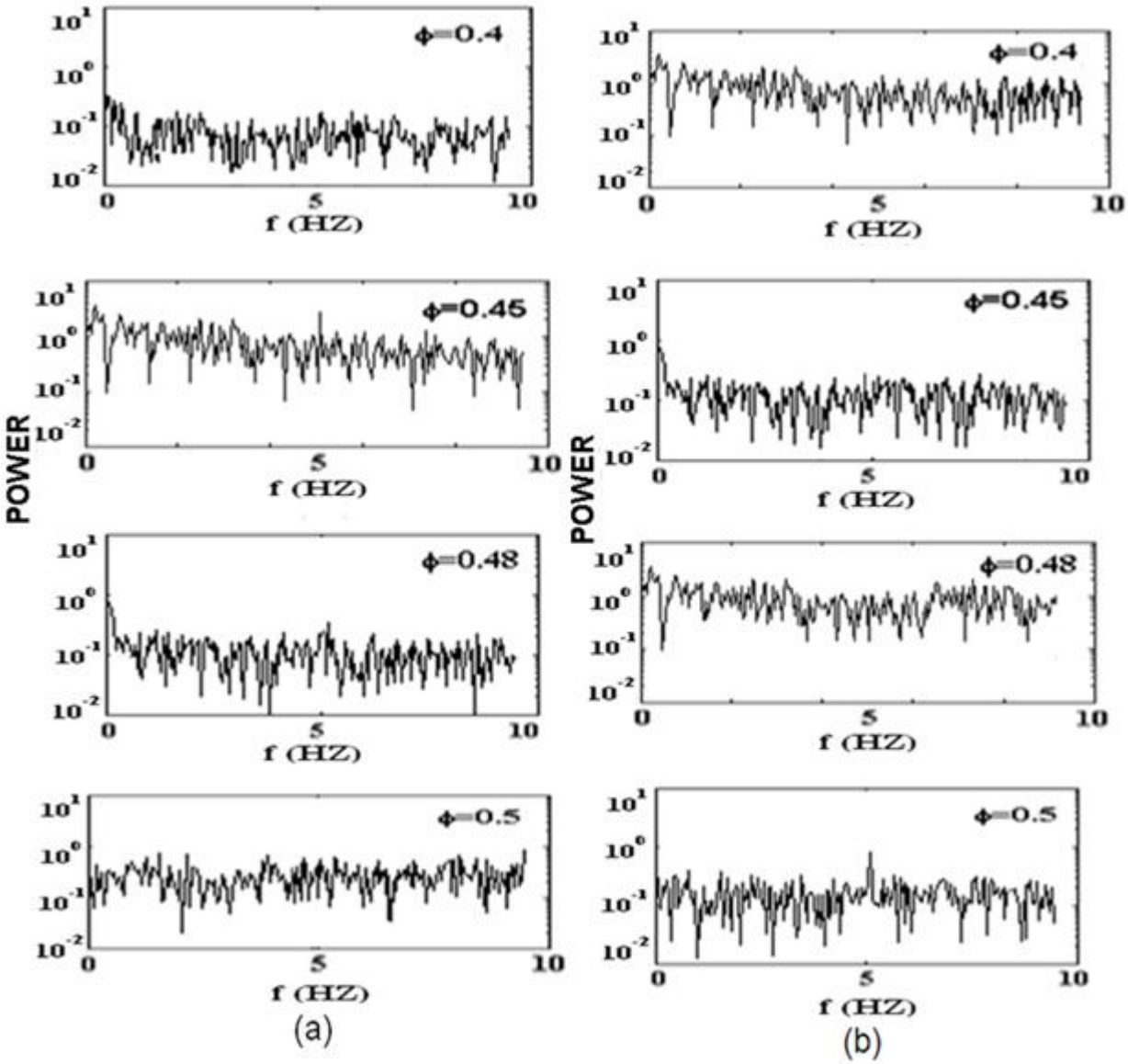

Figure 4.6: Temporal PSD at different particle concentrations for (a) plane and (b) serrated channel. The particle size was 500 μm and the viscosity of suspending fluid was 98 cP.

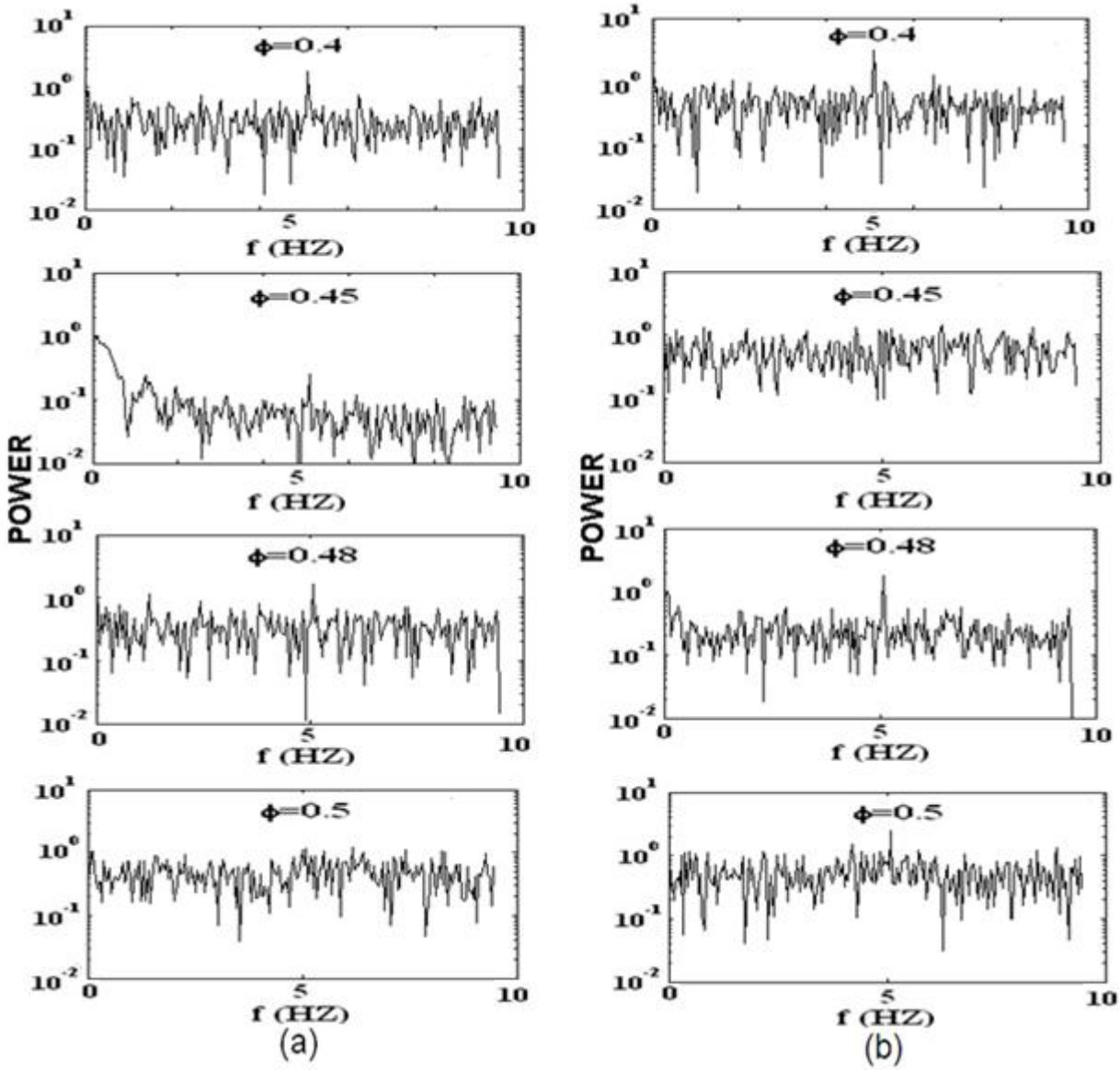

Figure 4.7: Temporal PSD at different particle concentrations for (a) plane and (b) serrated channel. The particle size was 500 μm and the fluid viscosity was 204 cP in this case.

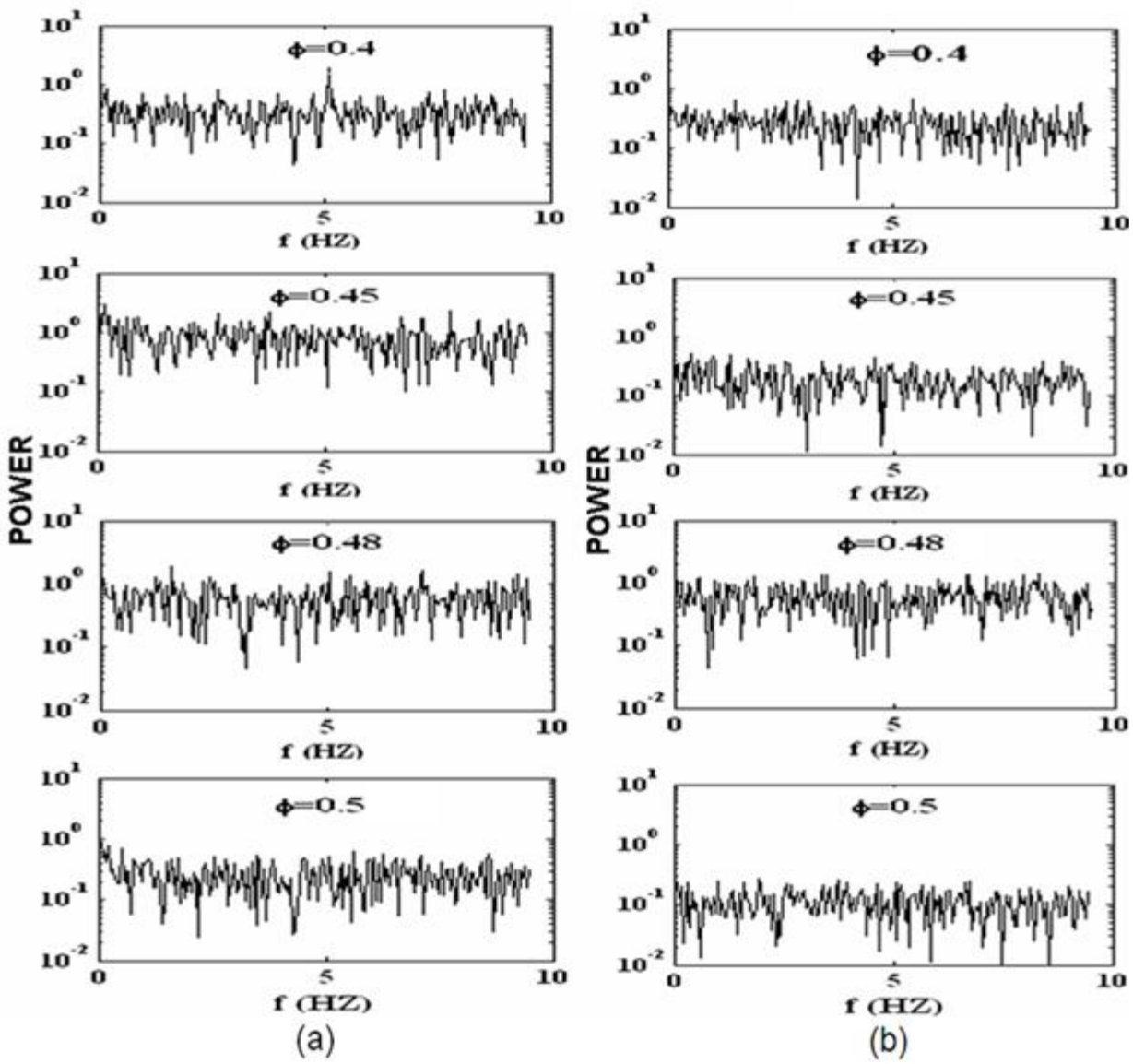

Figure 4.8: Temporal PSD at different particle concentrations for (a) plane and (b) serrated channel. The particle size was 200 µm and the fluid viscosity was 19 cP.

As mentioned previously, the autocorrelation function represents how the flow structure at a particular location is correlated with that at the neighboring downstream locations. A faster decay of autocorrelation with spatial dimension indicates larger fluctuation at the free-surface. On the other hand, if the flow structure at the interface is largely moving with the mean flow this would result into a slower decay of autocorrelation function. In Fig.4.9 through Fig.4.14, we have compared spatial autocorrelation in *x* and *y* directions for suspensions of various particle size (80 µm, 250 µm and 500 µm) in 2.05 cP of suspending fluid at various particle fraction. The similar plots for various suspension of 500 µm particles in different suspending fluids are shown in Fig.4.15 through Fig.4.18. Figures. 4.19 and 4.20 are for suspension of 200 µm particles in suspending fluid of viscosity 19 cP. A common observation in all the plots is that after sharp decay the curve flattens for all the concentrations. The mean level of the plateau portion of the curve is expected to have no relation to corrugation estimation. It could be that the overall intensity of the cold light source in the experiments for plane and serrated channel was not same. The plots for different concentrations reveal that the flow structures uncorrelated faster for particle concentration of 0.40 and 0.45 (it can be observed from the rate of decay of autocorrelation function in the inset of the plots). However, with particle concentration of 0.50, we observe that the autocorrelation decay is relatively slow. The behavior is similar for both plane and serrated channels and the initial rate of decay was found to be nearly equal. The results are similar for all suspensions irrespective of the size and viscosity of suspending fluid. This observation is in agreement with the earlier findings of Loimer *et al*. (2002) and Singh *et al*. (2006) who reported maximum disorder at particle concentrations between 0.40 and 0.45. The rate of decay of autocorrelation function is related to the flow structures. At low concentration, the particle fluctuations are not strong enough and the flow structures convect with the mean flow. On the other extreme, i.e., when the particle concentration approaches to maximum flowing fraction, the particles again follow ordered motion due to crowding effect (Ackerson, 1990; Ovarlez *et al*., 2006). There exists a critical particle fraction value when the fluctuations are strong enough to produce wide spectrum of uncorrelated flow structures. Therefore, our study shows that wall slip does not change the nature of surface corrugation patterns observed during free surface flow of concentrated suspensions.

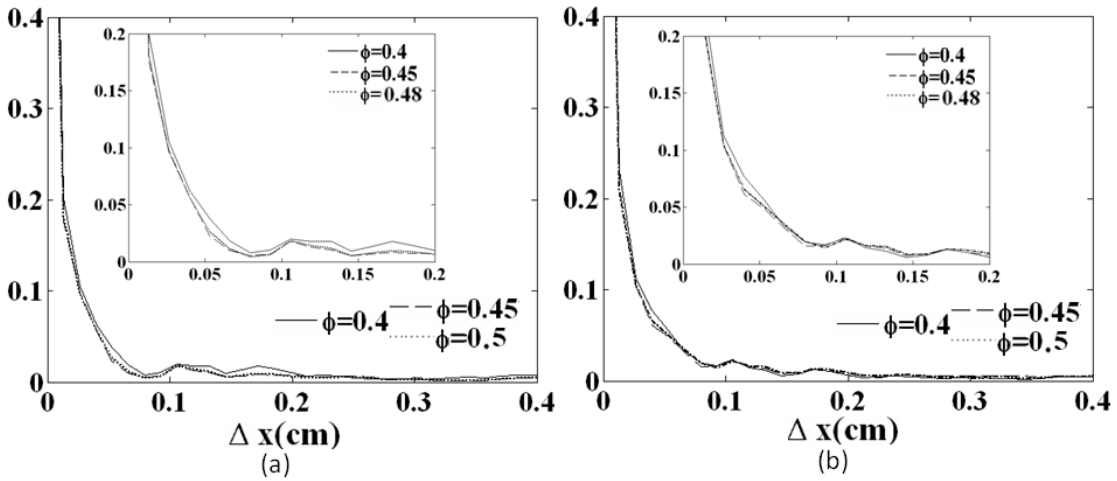

Figure 4.9: Normalized spatial auto-correlation in x (spanwise) direction for suspension of 80 µm particles in fluid of viscosity 2.05 cP. (a) plane and (b) serrated channel.

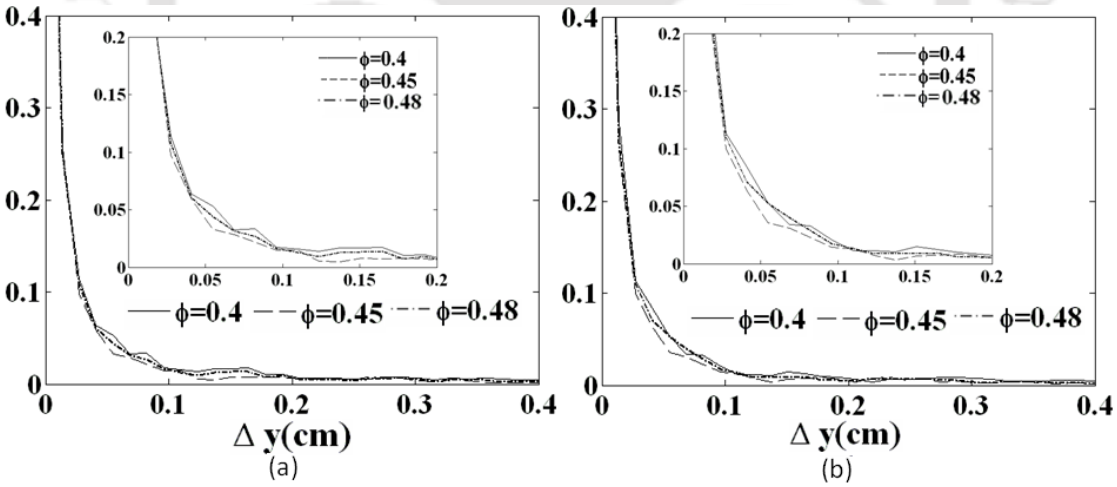

Figure 4.10: Normalized spatial auto-correlation in y (flow) direction for suspension of 80 µm particles in fluid of viscosity 2.05 cP. (a) plane and (b) serrated channel.

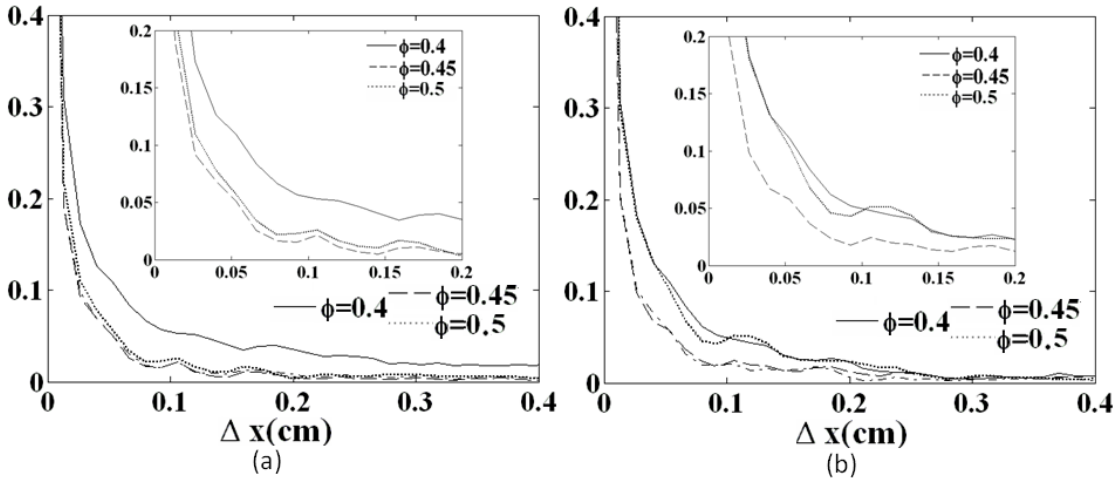

Figure 4.11: Normalized spatial auto-correlation in x (spanwise) direction for suspension of 250 µm particles in fluid of viscosity 2.05 cP. (a) plane and (b) serrated channel.

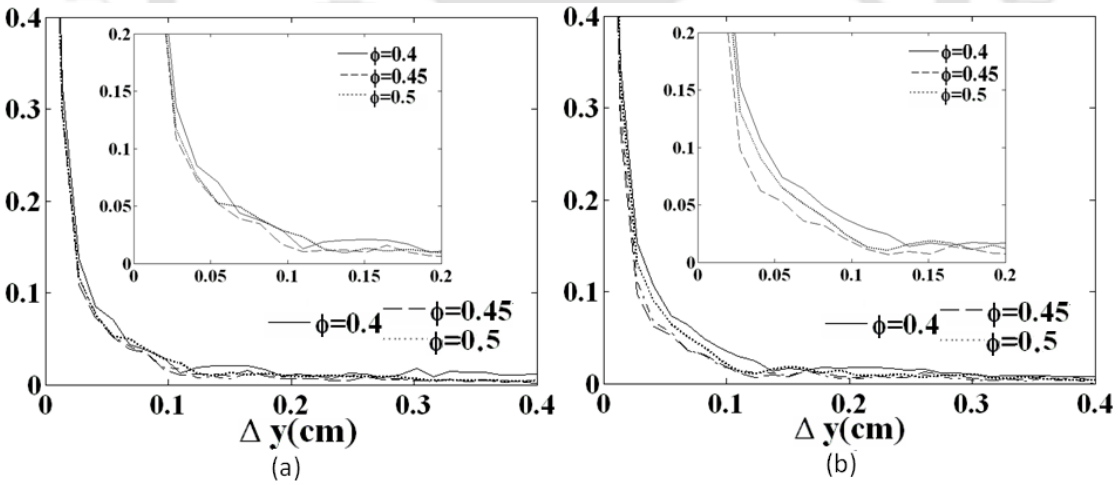

Figure 4.12: Normalized spatial auto-correlation in y (flow) direction for suspension of 250 µm particles in fluid of viscosity 2.05 cP. (a) plane and (b) serrated channel.

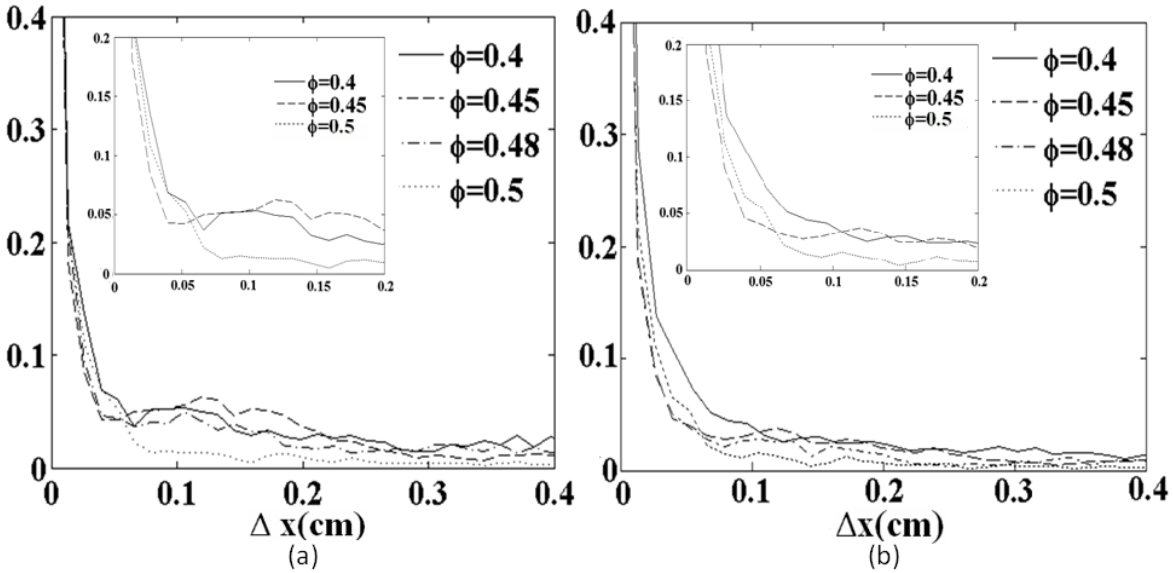

Figure 4.13: Normalized spatial auto-correlation in x (spanwise) direction for suspension of 500 µm particles in fluid of viscosity 2.05 cP. (a) plane and (b) serrated channel.

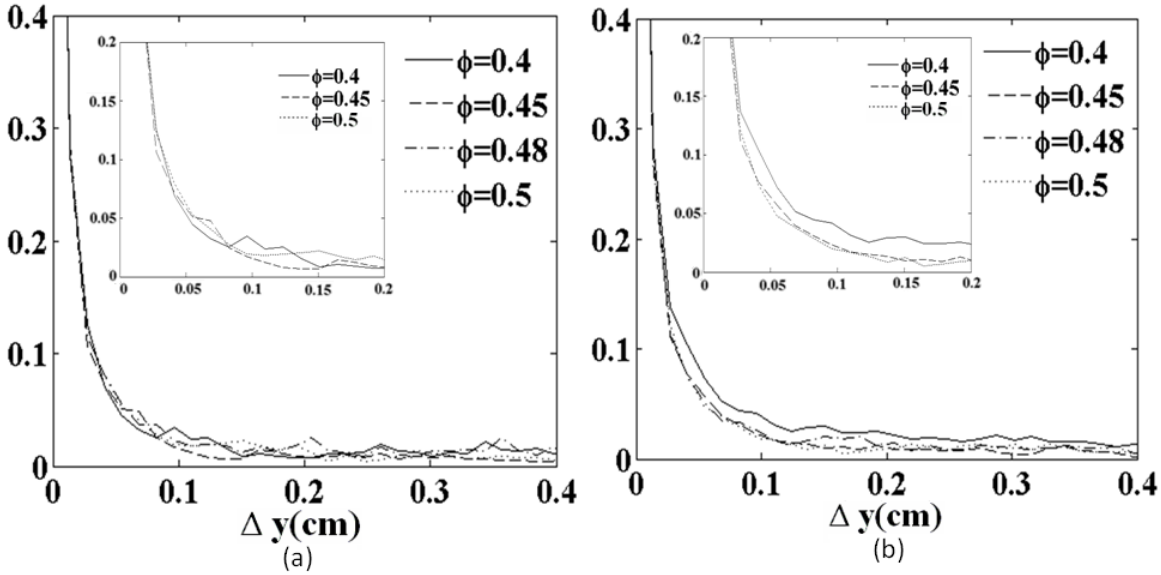

Figure 4.14: Normalized spatial auto-correlation in y (flow) direction for suspension of 500 µm particles in fluid of viscosity 2.05 cP. (a) plane and (b) serrated channel.

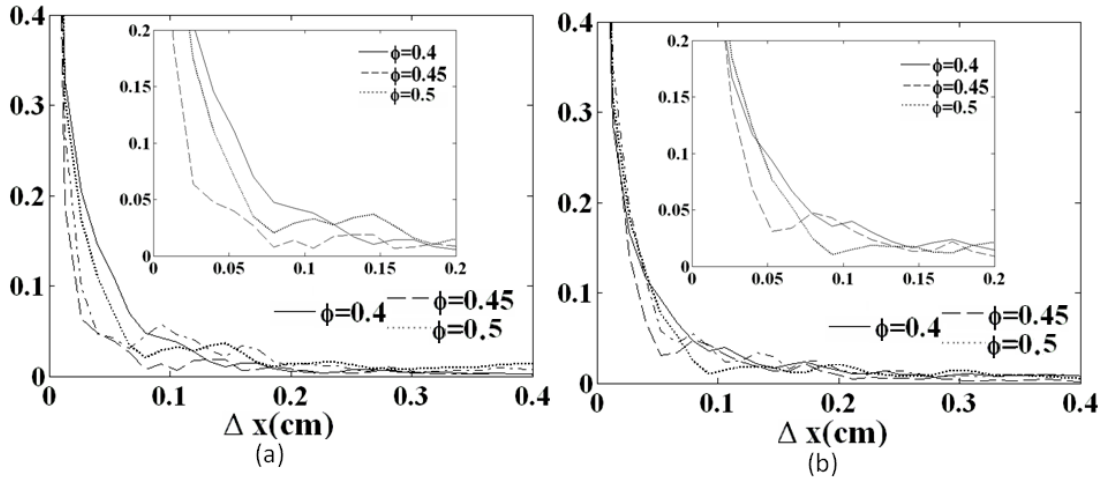

Figure 4.15: Normalized spatial auto-correlation in x (spanwise) direction for suspension of 500 µm particles in fluid of viscosity 98 cP. (a) plane and (b) serrated channel.

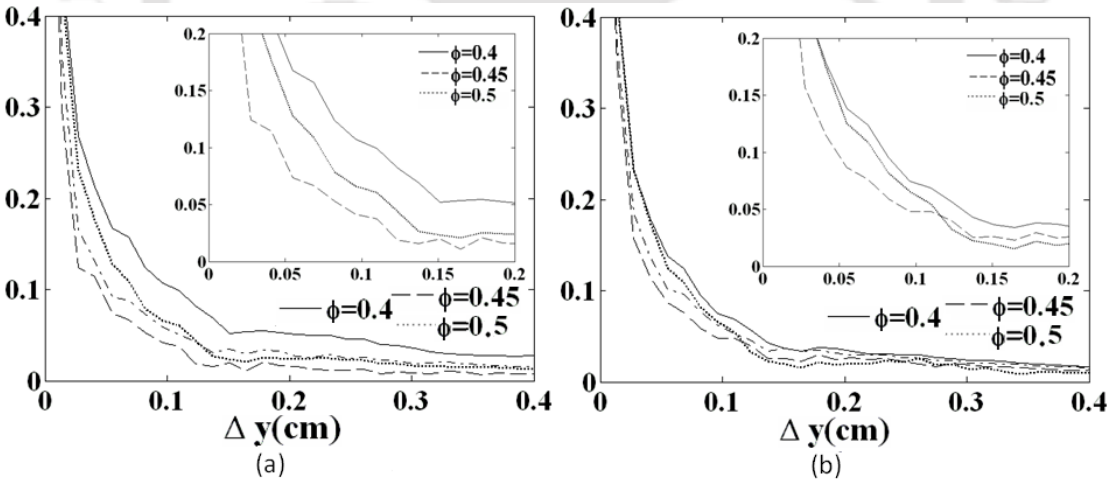

Figure 4.16: Normalized spatial auto-correlation in y (flow) direction for suspension of 500 µm particles in suspending fluid of viscosity 98 cP. (a) plane and (b) serrated channel.

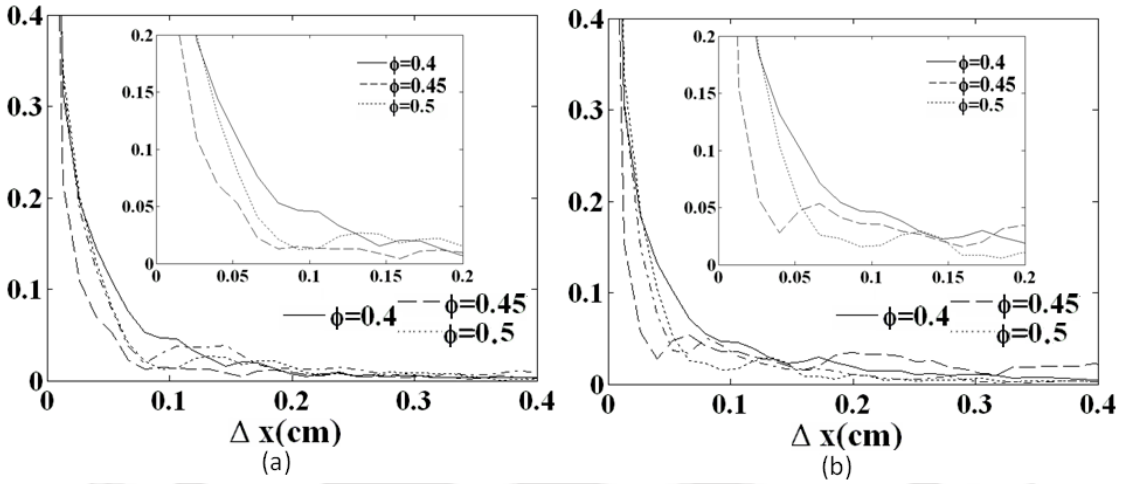

Figure 4.17: Normalized spatial auto-correlation in x (spanwise) direction for suspension of 500 µm particles in suspending fluid of viscosity 204 cP. (a) plane and (b) serrated channel.

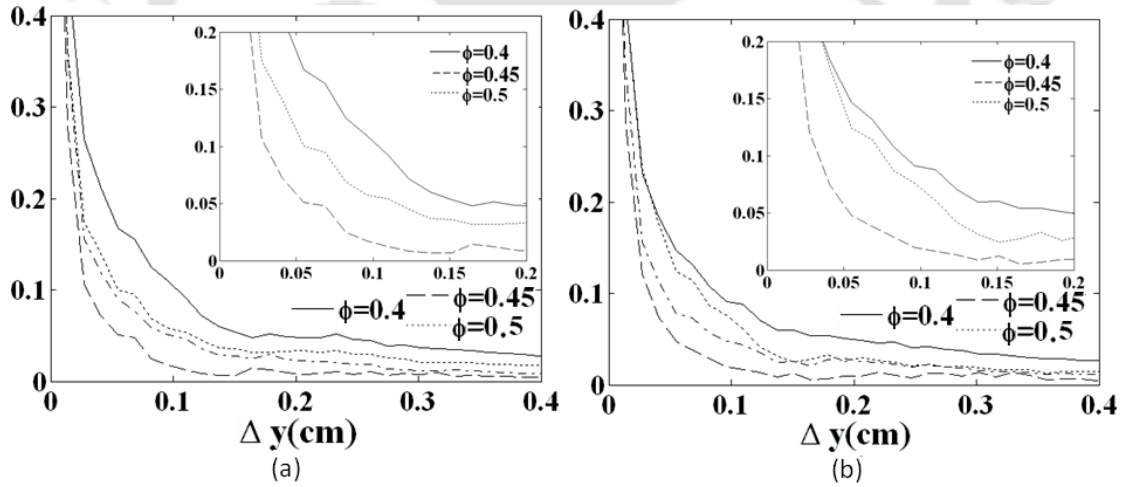

Figure 4.18: Normalized spatial auto-correlation in y (flow) direction for suspension of 500 µm particles in suspending fluid of viscosity 204 cP. (a) plane and (b) serrated channel.

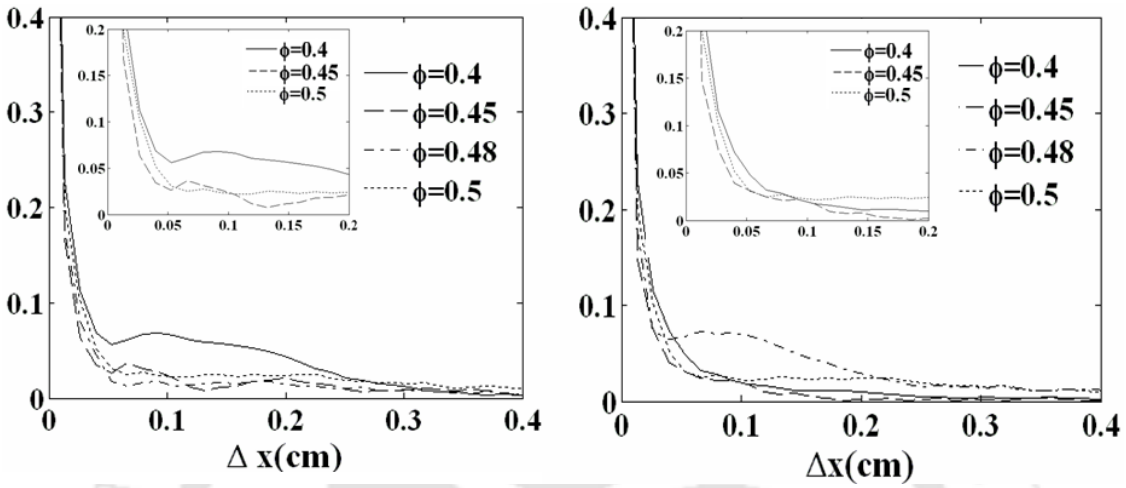

Figure 4.19: Normalized spatial auto-correlation in x (spanwise) direction for suspension of 200 µm particles in fluid of viscosity 19 cP. (a) plane and (b) serrated channel.

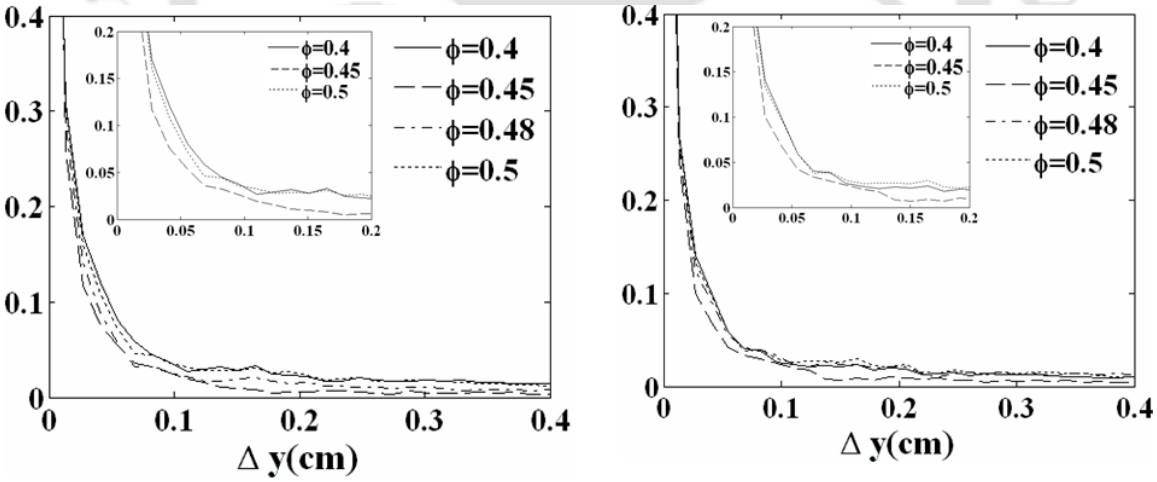

Figure 4.20: Normalized spatial auto-correlation in y (flow) direction for suspension of 200 µm particles in fluid of viscosity 19 cP. (a) plane and (b) serrated channel.

4.4 CONCLUSION

The effect of slip velocity on surface corrugation was studied by analyzing the spectra of refracted light from the free surface. It was found that the normalized spatial and temporal spectra are similar for both plane wall and serrated wall channels. The spatial autocorrelation in flow and span-wise directions shows that there is an optimum concentration at which the surface corrugation is the largest. The rate of decay of auto correlation functions was found to be similar for both plane and serrated channels. Therefore, it appears that the slip affects the velocity profile across the channel but this has no apparent effect on the surface corrugation patterns. Thus, our study concludes that wall slip does not appear to change the nature of surface corrugation patterns observed during free flow of concentrated suspensions. Our study showed that the wall slip only changes the velocity profile and it has no apparent effect on the surface corrugation. Therefore, our achievement in this aspect was to confirm that the surface corrugation is actually a bulk response and cannot originate from boundary problem (such as development of slip layer). This is because the slip layer affects are confined near the wall, the bulk shape of the surface remains unchanged. Based on the indirect analysis of power spectra and autocorrelation of refracted light from the free surface, we speculate that wall slip may not be influencing the surface corrugation profile. The quantitative measurement of free surface perturbations is presented in the next chapter.

CHAPTER 5

MEASUREMENT OF INTERFACE LOCATION IN OPEN CHANNEL FLOW

5.1 INTRODUCTION

An interface is a common boundary between two different phases, such two immiscible liquids or a liquid and an insoluble gas. Our system consists of air and suspension. Determination of the air liquid interface is important in many engineering applications. During the flow of concentrated suspensions, the interaction near the interface between the air and suspension plays main role in several phenomena. As we know, even at low Reynolds number, the free surface flow of concentrated suspension exhibits the corrugation at free surface which depends on the factors like particle concentration, particle size, suspending fluid viscosity, surface tension etc. (Loimer *et al*., 2002). This corrugation structure is associated with the interface fluctuation. Hence it is significant to determine the interface location and study the perturbation of air-suspension interface in free surface flow of concentrated suspension. The proximity of particles to the interface causes the film and line tension effect over the interface which can influence surface fluctuations. Hence, it is important to determine the free surface fluctuations as well as velocity measurements (Nikolov *et al*., 1985). Nonintrusive measurement techniques were developed to obtain the surfactant concentration and the velocity field by Hirsa *et al*., (2001). Kumar *et al*., (1998) carried out experiments to investigate the characteristic of free-surface turbulence in channel flow. When the particles are present in Newtonian fluid, the concentration of particles plays an important role, which modifies the flow field pattern as reported by Federico (1999). Law *et al*., (1999) suggested a PIV based technique to perform flow measurements in the vicinity of the air-water interface. The location of the interface was determined by using an edge detection routine method. In the theoretical study of velocity fluctuations near an interface between a turbulent region and stably stratified layer shows that eddies with frequency of the

same order as the buoyancy frequency of the stratified layer. The mean squared vertical velocity is zero at infinite buoyancy frequency and greatest at interface (Carruthers and Hunt, 1985). Kirgsmann *et al*., (1998) investigated the effect of pressure disturbance moving at a constant velocity along the interface of a thin viscous film flowing down an inclined plate. Form their study, the pressure driven disturbance depends upon the depth of the film thickness and inclination angle of the plate. Free surface instability in single and multilayer flows, in the limit of long wave disturbances, arises due to the perturbation in shear stresses at the free surface.

Direct measurements of instability of interface have been limited due to experimental difficulties. There are several studies on the PIV technique to determine the velocity field but not many on the determination of interface location. The interface position was validated using PIV (Tsue and Savas, 2002) and a digital particle image velocimetry (DPIV) method was developed for free-surface boundary layer measurements (Hirsa *et al*., (2001). Dabri and Gharib (2001) used DPIV technique for simultaneous free surface deformation and near-surface velocity measurements. Only few works have been reported for free surface study with PIV technique (Wasterweel *et al*., 1997; Hirsa *et al*., 1997; Kumar *et al*., 1998; Kiger *et al*., 2000). The interface location can also be characterized from the analysis of light reflection (Bingman, 1996) and this has been used in some natural settings such as sea and river water. The surface radiation at sea level enters the water at air-water interface. Some of it gets reflected back (depending on the angle of incidence and the refractive index of water). The angle of incidence varies throughout the day as sun moves across the sky. Here, the sun light reflection depend the surface properties of the water. Reflectivity-area isotherm of arachidic acid on pure water has been characterized between the interface of air and acid on the water surface with constant angle of incidence, where the formation of a monolayer on the water surface modifies the Brewster angle condition and light reflection is observed. Areas of different brightness due to different molecular density or refractive index in the monolayer was recorded and analyzed by Honig and Mobius, (1991). The experiment of Rashidi *et al*., (1992) provided a measurement technique for wave-turbulence interaction in free-surface channel flows using micro bubbles tracer and visualization. The mechanism of free surface instability of non-Newtonian laminar flows was studied theoretically and experimentally by Wang (2002). Du *et al*., (2007) determined that the interface velocity is proportional to the interface stiffness, mobility and curvature. Interface also plays a predominant role in the biological and micro fluidic processes, such as interfacial properties

for processes of peripheral proteins and lipid molecules, where in a biological membrane gas-liquid interface allow independent control of parameters in micro flow cell (Hoang *et al.*, 2006). Cherlo *et al.*, (2010) carried out the experimental and numerical investigation of two phase flow behavior in rectangular micro-channel. They have used PIV technique to study the interface in micro rectangular channel.

Though there are some studies on air-liquid interface during flow situations, there are no reported works on air-suspension to the best of our knowledge. As we have discussed earlier that the corrugation has many length scales above and below particle size and it appears in the form of waves traveling with the local surface fluid speed. The surface deformation reflects a balance between surface tension and viscous forces (Loimer *et al.*, 2002). In the free surface flow of suspension the near surface particle fluctuation causes deformation of the interface. No detailed investigation has been reported on that transport rate and quantitative structure for the air-suspension interface under specific flow conditions due to the lack of basic understanding of the interfacial fluctuations (Law *et al.*, 1999. There are no experimental measurements to quantify the air-suspension interface perturbation associated to the surface corrugation, where the air-suspension interface greatly influences the free surface corrugation structure. Figure 5.1a explains that the interface has no fluctuation in Newtonian fluid flow, however, when the non-colloidal particles are introduced in Newtonian fluid, the interface would start to fluctuate due to the hydrodynamic interaction between the particles (Fig. 5.1b).

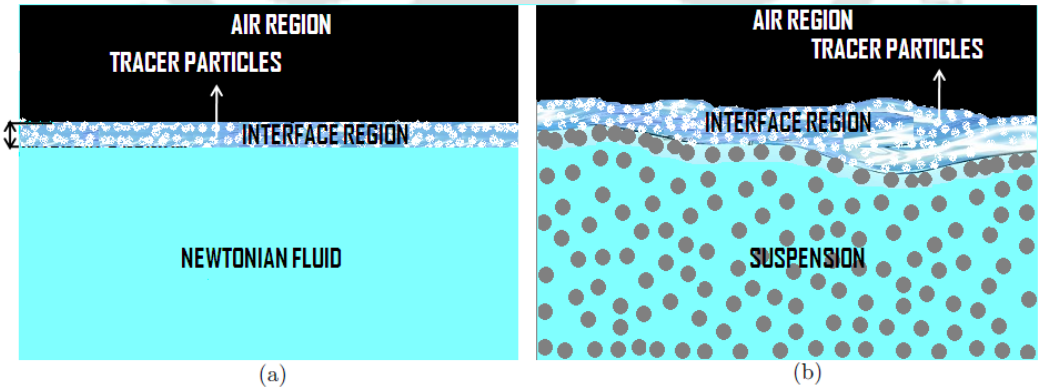

Figure 5.1: (a) Zero interface fluctuation at Newtonia fluid flow, (b) Interface fluctuation at suspension flow.

In this work, we have reported the quantitative study of the interface in the velocity-vorticity plane during the free surface flow of concentrated suspension. PIV technique was used to perform the measurement of velocity profile below the free surface. The location of the

interface for air-suspension is determined using an edge detection routine method. The fluctuation and perturbation of interface is calculated in terms of mean squared fluctuation and mean squared vertical velocity at the interface.

5.2 EXPERIMENTAL DETAILS

5.2.1 Channel and flow apparatus

The schematic of experimental setup and photograph of experimental arrangements are shown in Fig. 5.2(a-c). It consists of a horizontal channel of 43.6 cm length, 2.2 cm width and 5.5 cm depth. The channel was made of 5 mm thick glass. In the upstream and downstream of the channel there was one reservoir each of volume (12.5 cm x 7 cm X 3.2 cm) and (12.5 cm x 3 cm x 3.2 cm) respectively. As reported earlier the purpose of the upstream reservoir was to make the suspension flow gentle before it enters through the main channel. To further reduce the velocity fluctuation produced by screw pump, we made some baffle like arrangement in the upstream reservoir of the channel. In the Fig. 5.2a, x is the span wise direction, y is the flow direction and z is the gravitational direction. The two ends of the reservoir were connected via circular tubes of diameter 2 cm to a screw pump, which re-circulated the suspension in the channel. The screw pump was specifically designed to handle suspension of large particles. The clearance between the screw and barrel of the pump was 0.5 cm. The speed of the screw pump could be adjusted to get the desired flow. The suspension in the channel was filled to a level such that the free-surface in the x-y plane was always above the inlet and outlet regions. The optical arrangements (described in the next section) imaged the interface in a downstream location of the channel which was 27 cm from the inlet section. The location was chosen, where the free surface velocity profile was fully developed.

5.2.2 Optics for interface location and PIV images

The optical arrangements for capturing the interface location and free surface vertical velocity were similar to the one described in chapter 3. However, the laser light sheet plane was in velocity-vorticity plane. To locate the interface, CCD camera was placed on one side of the channel. To get a clear view of the interface, the camera was inclined to a small angle as shown in Fig. 5.3. The camera angle position was calibrated with number of different angles and found $\alpha = 30.2°$ was given the better view of interface.

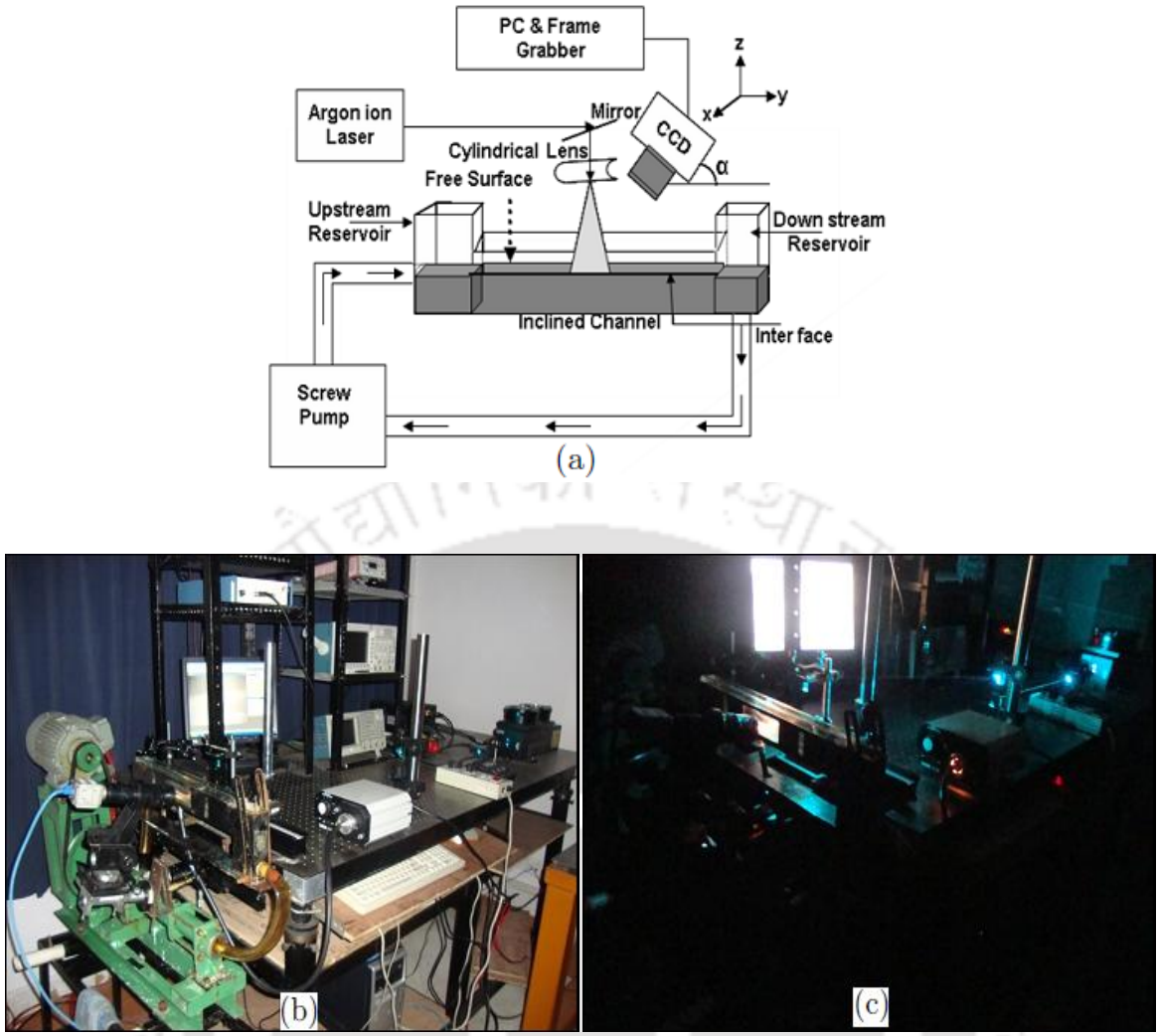

Figure 5.2: (a) Schematic diagram of the experimental setup and optical arrangements for PIV study. (b) (c) Photographs of experimental setup and optical arrangements.

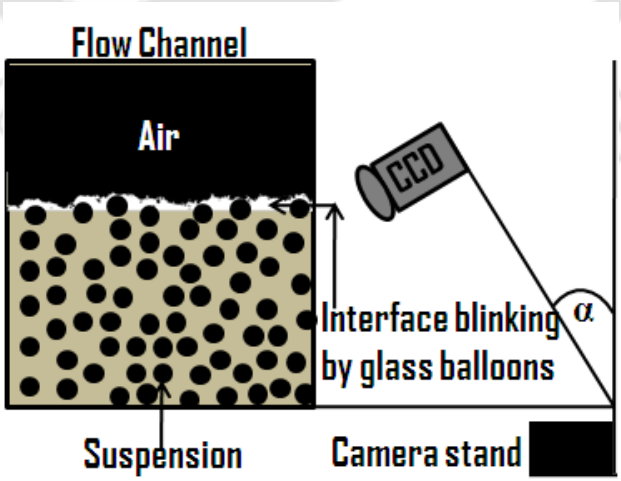

Figure 5.3: CCD camera viewing angle position for interface tracking.

5.2.3 Preparation of suspensions

It was our objective to study of the effect of suspended particle size, effect of particle fractions and suspending fluid viscosity on free surface fluctuations. Hence, we have prepared five different kind of suspension as explained below.

Effect of size: To study the effect of size, the particles used in preparing suspensions were polystyrene spheres of mean diameters 80 μm, 250 μm and 500 μm. Each size of polystyrene particles was suspended in a mixture of 24% glycerol and 76% of water. This combination of suspending fluid was neutrally buoyant with polystyrene particles of density 1.05 g/cm^3. The suspending liquid had a viscosity of 2.05 cp and its surface tension was measured to be 48.4 mN/m at 26 °C.

Effect of suspending fluid viscosity: To study the effect of suspending fluid viscosity, 200 μm PMMA particles were suspended in 75% glycerol and 25% water mixture. This mixture was also neutrally buoyant with PMMA particles of density 1.18 g/cm^3. The suspending fluid viscosity was 19.5 cp and surface tension was measured to be 60.4 mN/m at 24 °C. To prepare the another suspension, 200 μm of PMMA particles were suspended in mixture of 76% Triton-X-100 (t-Octylphenoxypoly-ethoxy-ethonal) 16.2% zinc chloride (ZnCl), and 7.8% water, with percentage based on mass. This mixture was having the density of 1.18 g/cm^3, viscosity of 4000 cp and surface tension of 34.2 mN/m at 24 °C.

Approximately 1000 ml of suspension was prepared to fill the flow apparatus. However, during the mixing small air bubbles were formed which needed to be removed. This was achieved by keeping the suspension under vacuum for 1 day, allowing the bubbles to rise up. Suspension cleared of air bubbles was transferred into the channel very slowly. Suspensions of 10%, 20%, 30%, 40%, 45%, 48%, and 50% volume fractions of particles were prepared to study the effect of concentration on interface fluctuations. To get clear insight for number of suspensions used in this work, we have presented them in Table 5.1.

Table. 5.1. Suspensions used for studies in the interface fluctuation.

S.NO	Kind of Study	Suspensions	Properties at 24 °C
1	Effect of suspended particle size: (Polystyrene particles suspended in 24% glycerol and 76% water mixture.)	Suspension 1	Particle size: **80 µm** Particle density: 1.05 g/cm^3 Suspending fluid density: 1.05 g/cm^3 Suspending fluid viscosity: 2.05 cP Suspending fluid surface tension: 48.4 mN/m
		Suspension 2	Particle size: **250 µm** Particle density: 1.05 g/cm^3 Suspending fluid density: 1.05 g/cm^3 Suspending fluid viscosity: 2.05 cP Suspending fluid surface tension: 48.4 mN/m
		Suspension 3	Particle size: **500 µm** Particle density: 1.05 g/cm^3 Suspending fluid density: 1.05 g/cm^3 Suspending fluid viscosity: 2.05 cP Suspending fluid surface tension: 48.4 mN/m
2	Effect of suspending fluid viscosity for 1.18 g/cm^3 of PMMA particles	Suspension 4 (PMMA particles suspended in 75% glycerol and 25% water mixture.)	Particle size: 200 µm Particle density: 1.18 g/cm^3 Suspending fluid density: 1.18 g/cm^3 Suspending fluid viscosity: **19.5 cP** Suspending fluid surface tension: **60.4 mN/m**
		Suspension 5 (PMMA particles suspended in mixture of 76% Triton-X-100, 16.2% ZnCl and 7.8% water.)	Particle size: 200 µm Particle density: 1.18 g/cm^3 Suspending fluid density: 1.18 g/cm^3 Suspending fluid viscosity: **4000 cP** Suspending fluid surface tension: **34.2 mN/m**
3	Effect of suspending fluid viscosity for 1.05 g/cm^3 of polystyrene particles	Suspension 6 (Polystyrene particles suspended in ucon oil)	Particle size: 500 µm Particle density: 1.05 g/cm^3 Suspending fluid density: 1.05 g/cm^3 Suspending fluid viscosity: **98 cP** Suspending fluid surface tension: **39.5 mN/m**
		Suspension 7 (Polystyrene particles suspended in Triton-X-100)	Particle size: 500 µm Particle density: 1.05 g/cm^3 Suspending fluid density: 1.068 g/cm^3 Suspending fluid viscosity: **204 cP** Suspending fluid surface tension: **30 mN/m**

5.3 RESULTS AND DISCUSSION

The contrast between the suspension and air which indicates the location of the interface was determined using an edge detection method. As mentioned earlier, the interface was visualized by illuminating the tracer particles over the free surface. When the camera was placed normal to the side of the channel wall, the concave shape of the meniscus obstructed the clear view of the interface. Therefore, the camera was placed at some inclination and it was calibrated for this position. At this angle the interface was clearly visible. The CCD camera was fixed in that particular inclination (Fig. 5.3). A set of 444 images were captured for the analysis of the interface location. The experiments were conducted for pure suspending fluids and various suspensions. Each experiment was conducted for three different flow rates.

5.3.1 Interrogation of PIV images and bulk vertical velocity

The captured images were saved in 680 x 512 pixels, 12 bits format gray scale images on a computer via frame grabber. The hollow tracer particles get mostly concentrated at the interface due to buoyancy. For measuring the bulk velocity beneath the interface we dispersed polystyrene particles (10 μm) as tracers which had the same density as that of the dispersed polystyrene particles. For suspensions of PMMA particles the tracer particles to measure the bulk velocity profile was also the same.

To calculate the bulk vertical velocity from pair of images, we have used the PIV analysis software PIV SLEUTH (Christension et al., 2001). The procedure was similar to the one described in chapter 3. Figure 5.4 shows a vector map of the velocity field. Figure 5.5 through 5.12 shows the bulk velocity profile in the y-z plane for various suspensions at various flow rate and concentrations. It is observed that the velocity is zero near the wall but increases towards the interface where it has maximum velocity. This experiment was conducted for all prepared suspensions. All the velocity profiles are qualitatively similar. The results prove that there is no effect of particle sizes as well as suspending fluid viscosities on bulk vertical velocity in the free surface flow of suspensions. For certain suspensions, it could be noticed that the velocity vectors were erroneous at low flow speeds. This arises due to difficulty in finding correlation peaks when the displacement is very small. The velocity profiles at higher flow rates were captured with more confidence. We would also like to mention that at higher concentration of suspension we could not obtain clear images for all suspensions due to large mismatch in refractive index. To obtain velocity profiles at higher

concentrations we have carried out numerical simulations using the 'Diffusive-Flux Model' of Phillips *et al*. (1992).

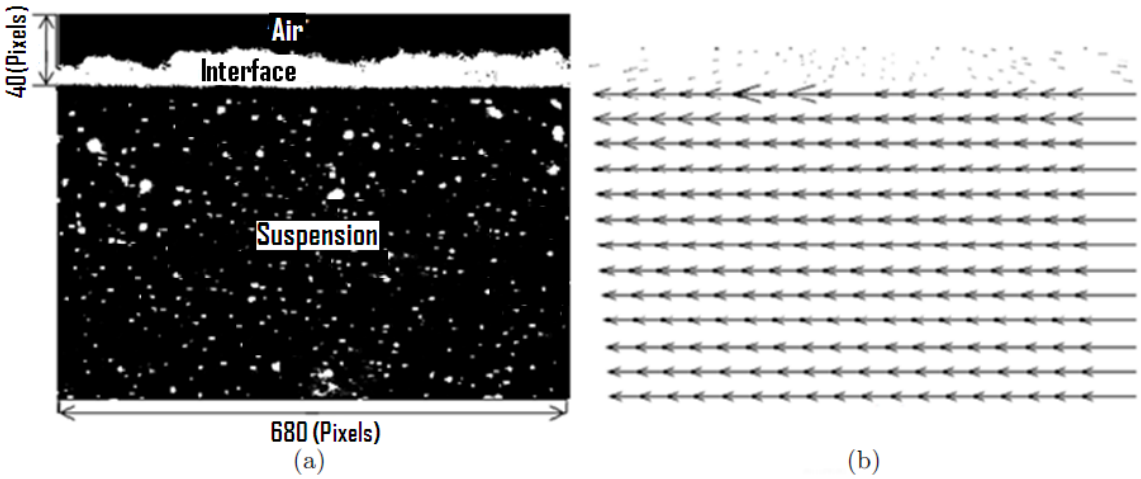

Figure 5.4: (a) A sample PIV image of tracer particles near the interface (b) Vector map of velocity field beneath the interface.

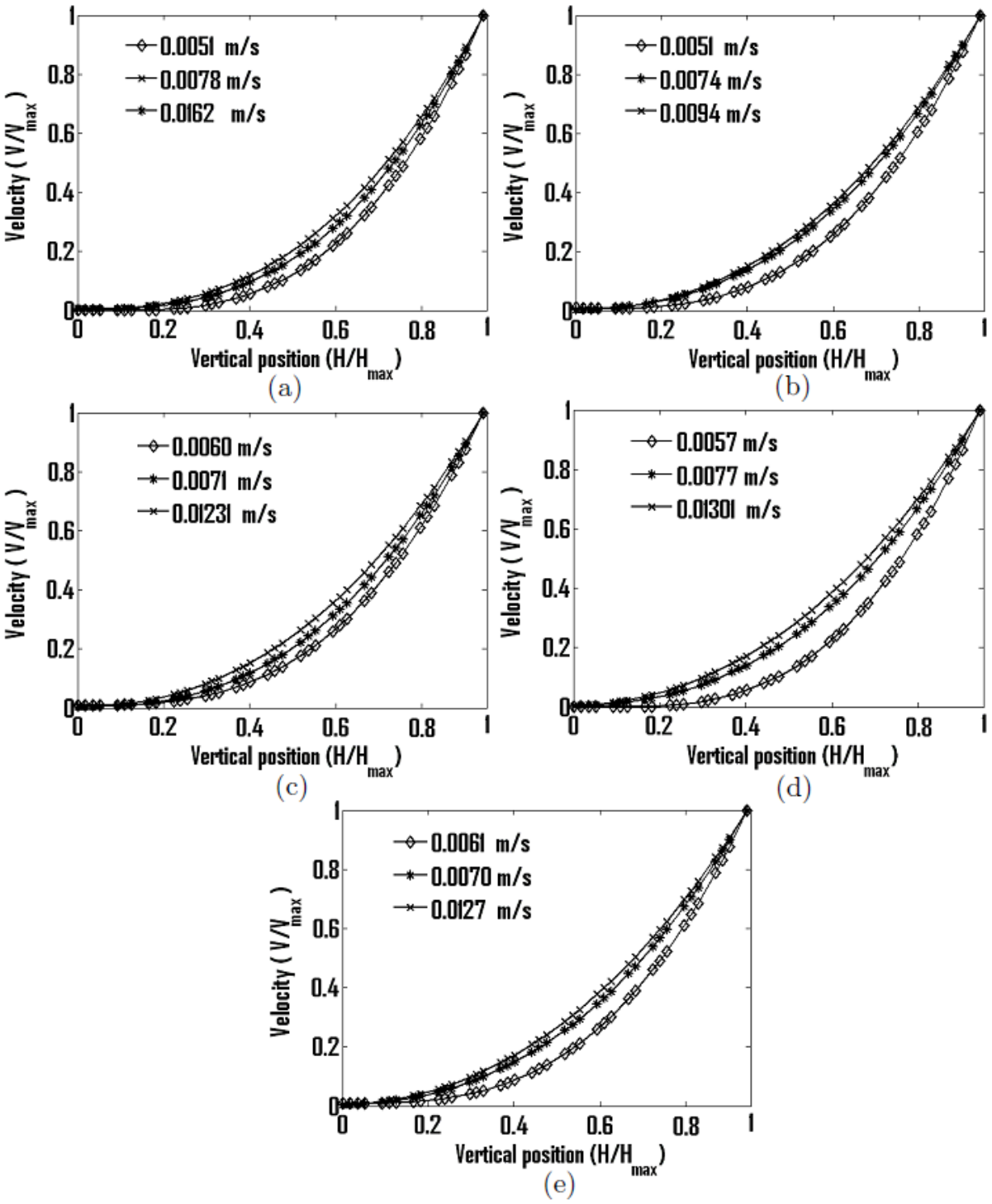

Figure 5.5: Bulk velocity profile beneath the interface for pure suspending fluid. The viscosity of these fluids were (a) 2.05 cP (b) 19 cP (c) 4000 cP (d) 98 cP (e) 204 cP measured at 24°C.

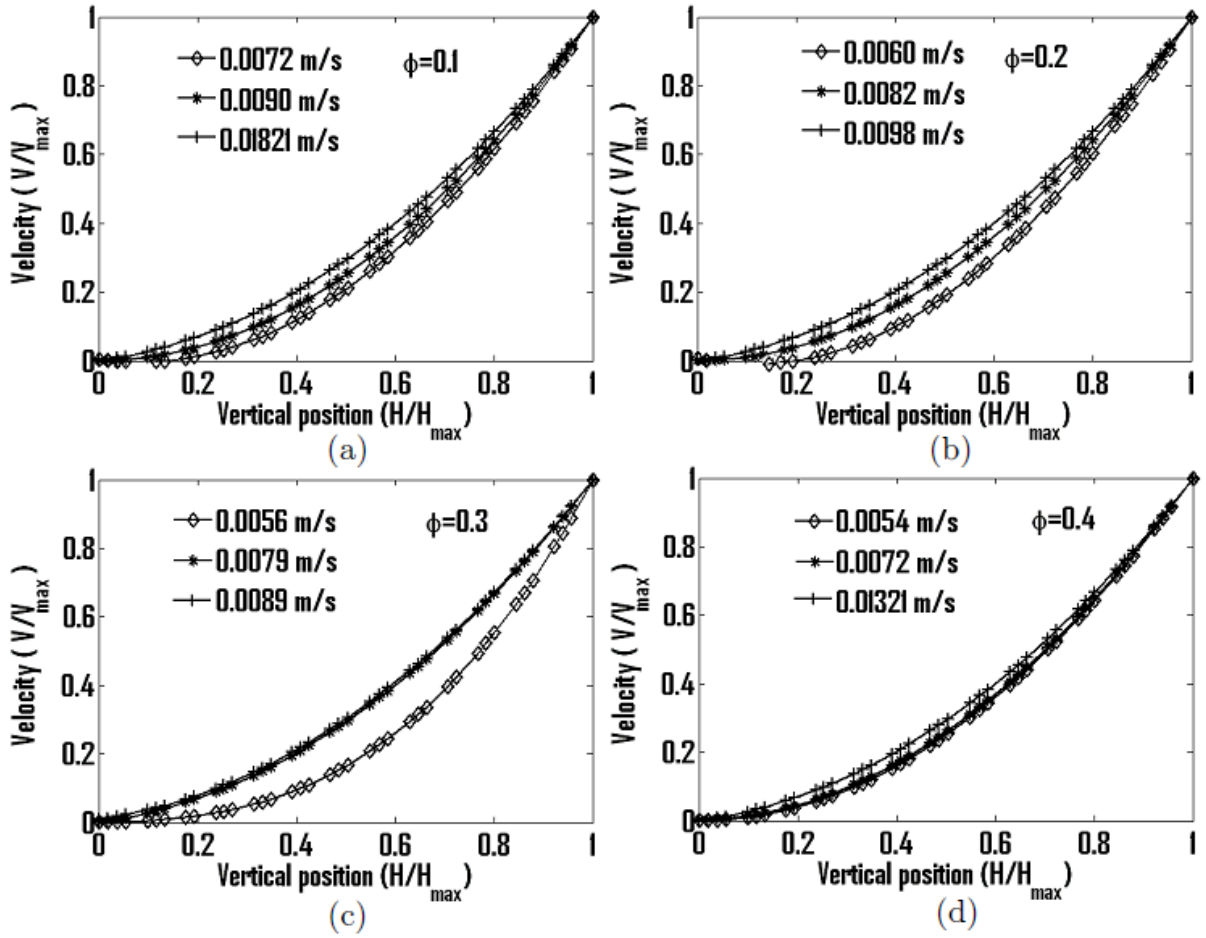

Figure 5.6: Bulk velocity profile beneath the interface for suspensions of various concentrations: (a) 10% (b) 20% (c) 30% (d) 40%. The suspensions were prepared with polystyrene particles of 80 μm present in 2.05 cP of density matched suspending fluid.

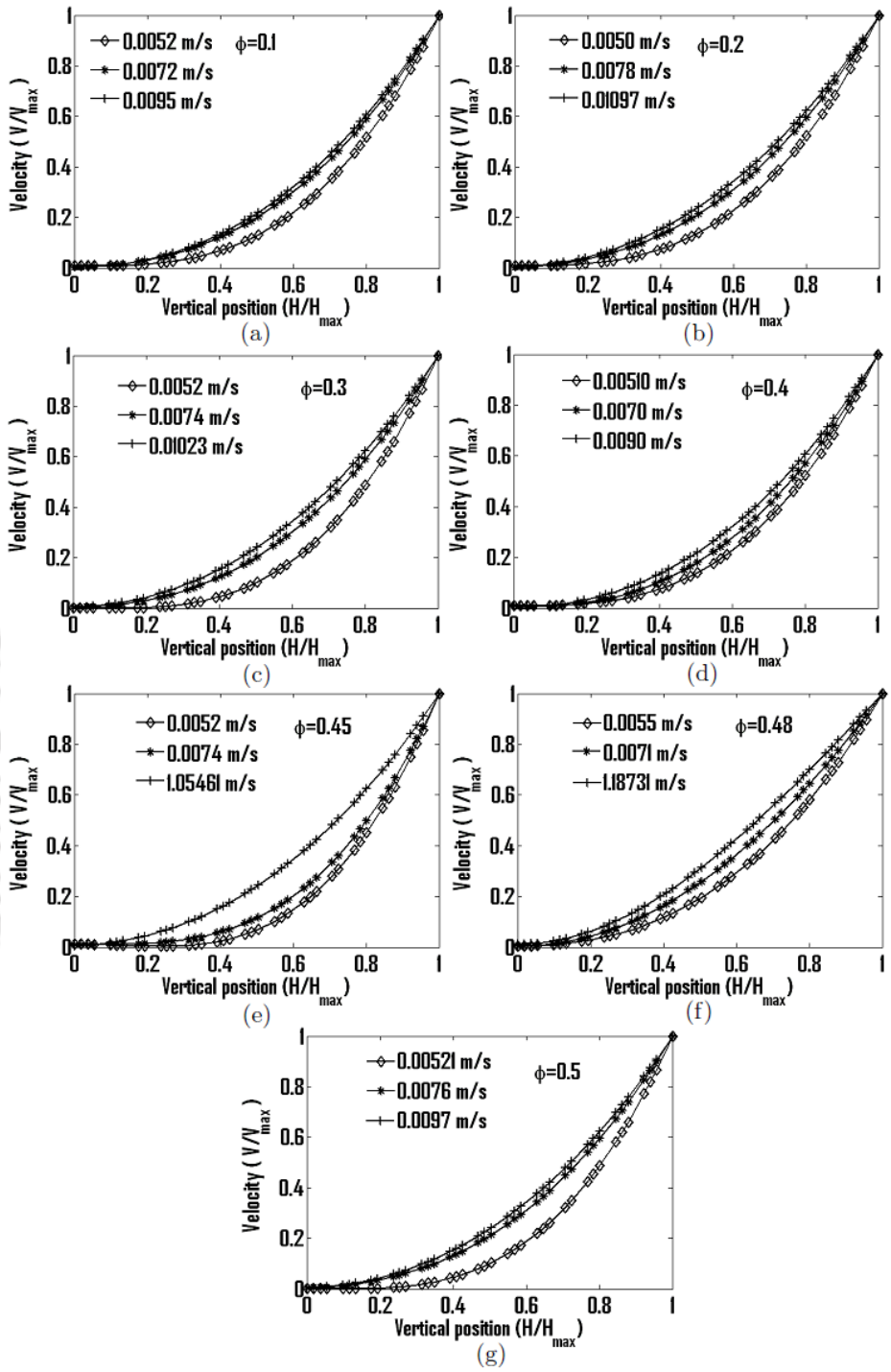

Figure 5.7: Effect of concentration on bulk velocity profiles. (a) 10% (b) 20% (c) 30% (d) 40% (e) 45% (f) 48% (g) 50%. The suspensions of various concentrations were prepared with 250 µm polystyrene particles in 2.05 cP of density matched suspending fluid.

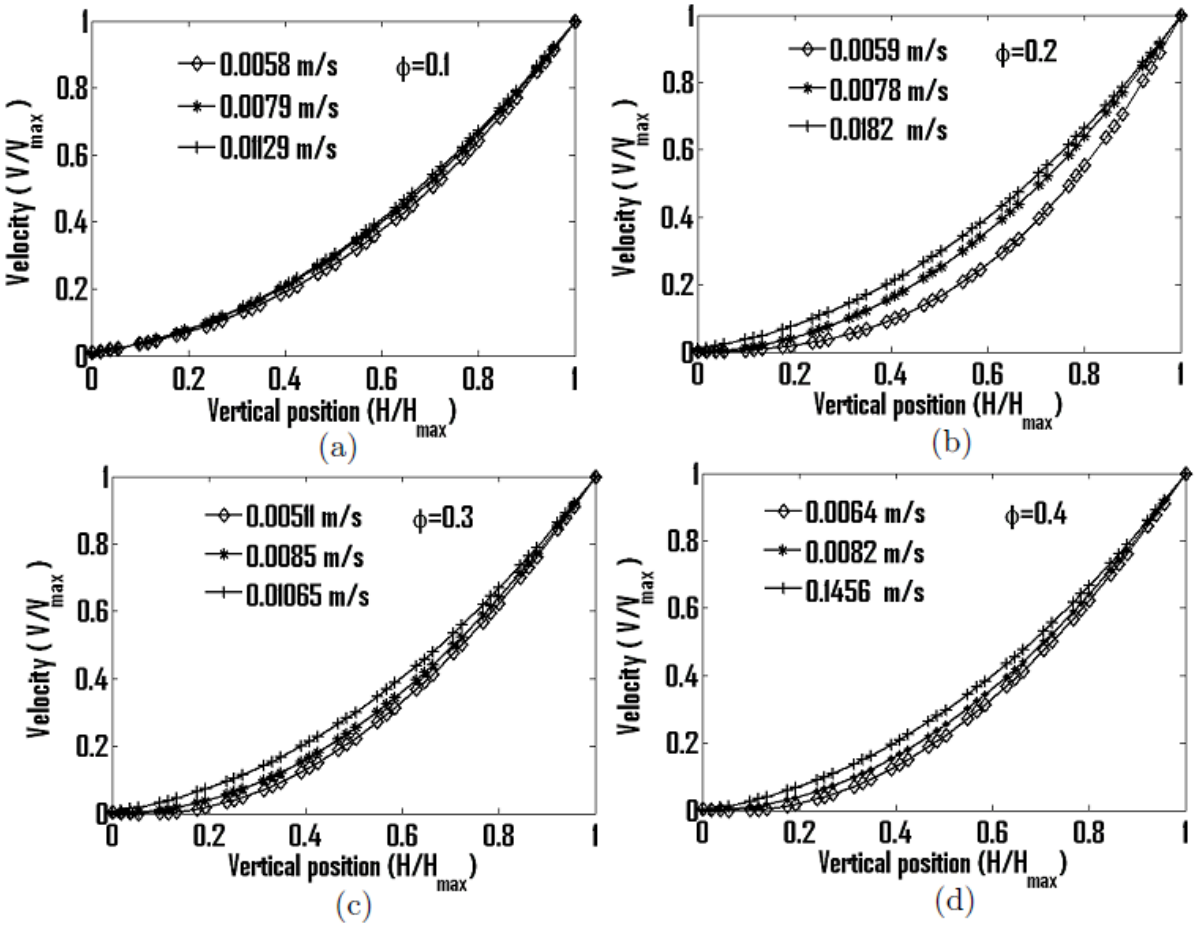

Figure 5.8: Effect of concentration on velocity profiles. (a) 10% (b) 20% (c) 30% (d) 40%. The suspensions of various concentrations were prepared with 500 μm polystyrene particles in 2.05 cP of density matched suspending fluid.

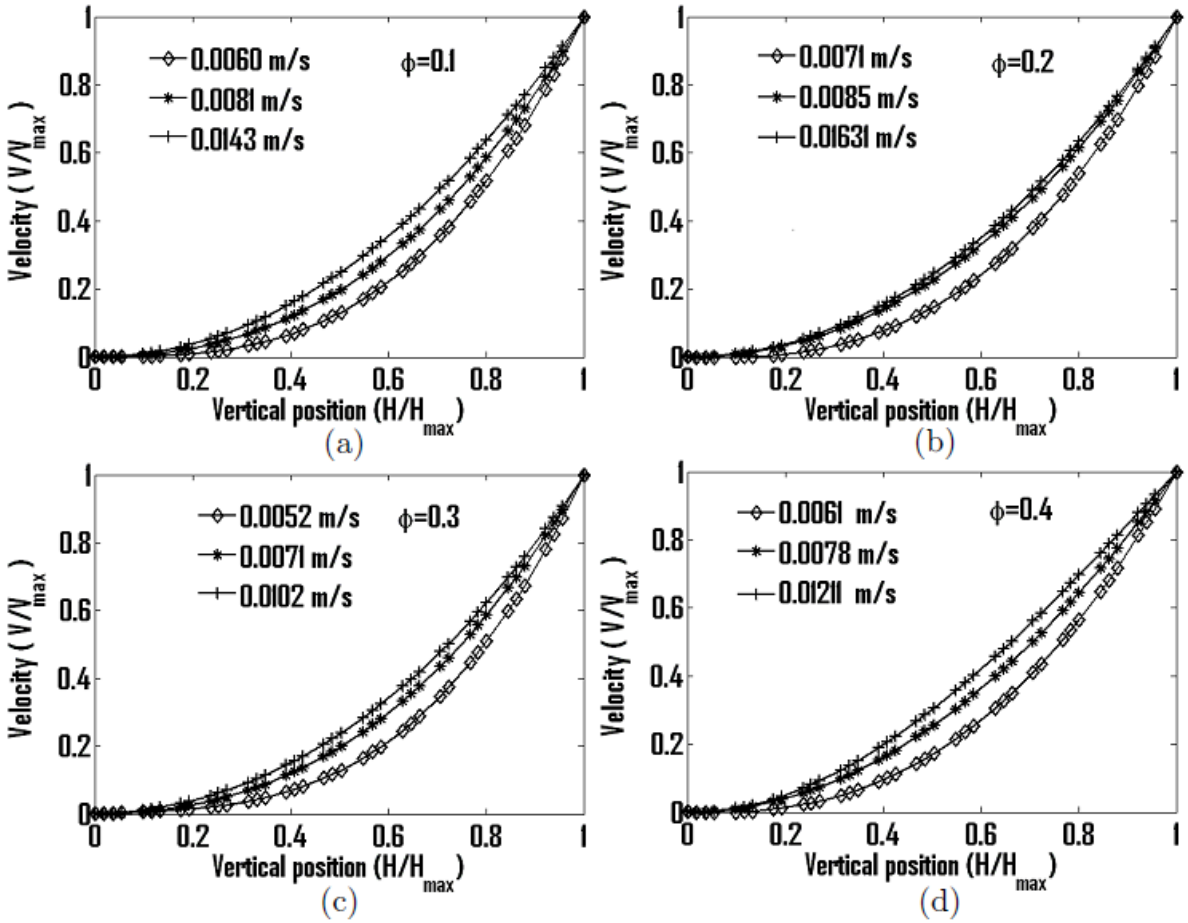

Figure 5.9: Effect of concentration on velocity profiles. (a) 10% (b) 20% (c) 30% (d) 40%. The suspensions of various concentrations were prepared by dispersing 200 µm PMMA particles indensity matched suspending fluid of viscosity 19 cP

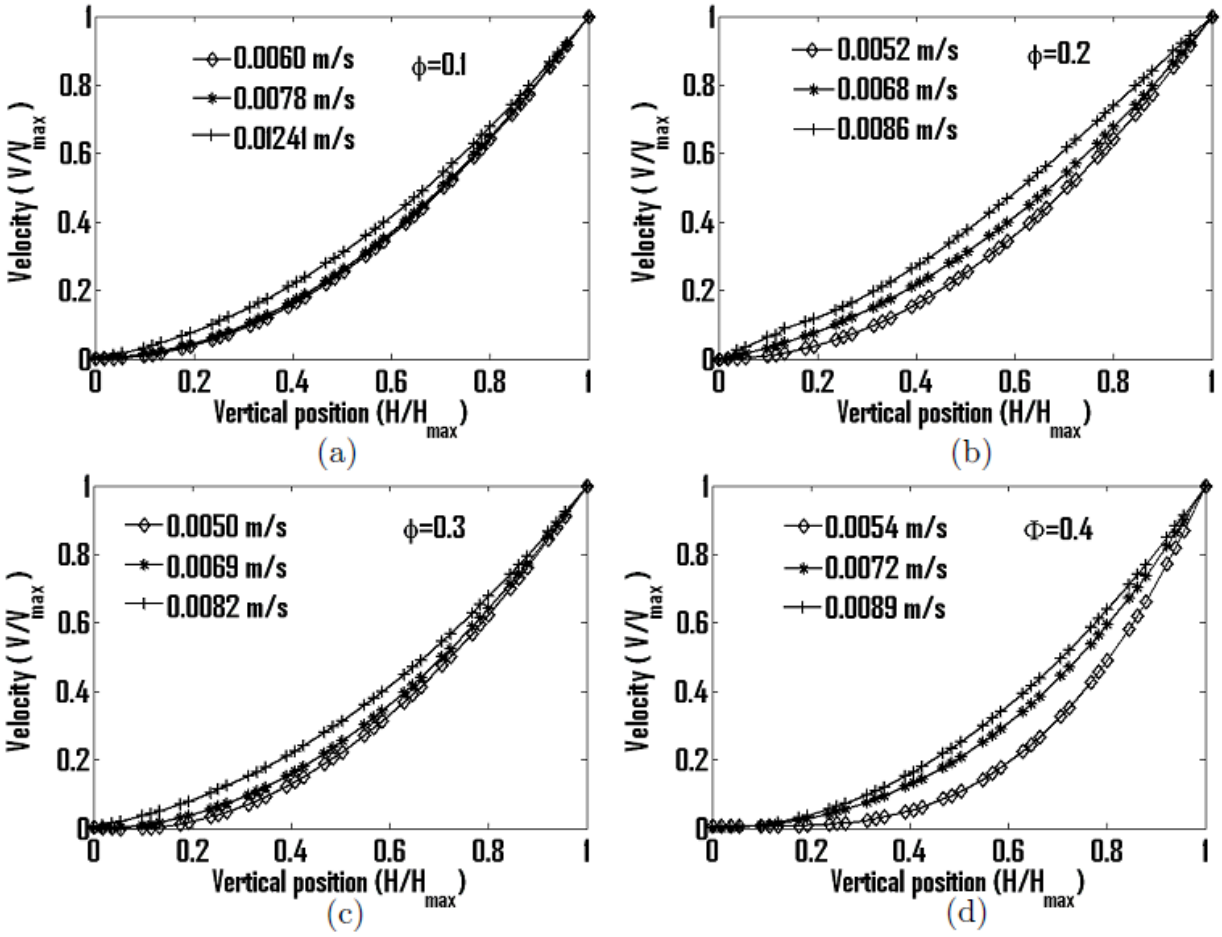

Figure 5.10: Effect of concentration on velocity profiles. (a) 10% (b) 20% (c) 30% (d) 40%. The suspensions of various concentrations were prepared by dispersing 200 μm PMMA particles in density matched suspending fluid of viscosity 4000 cP.

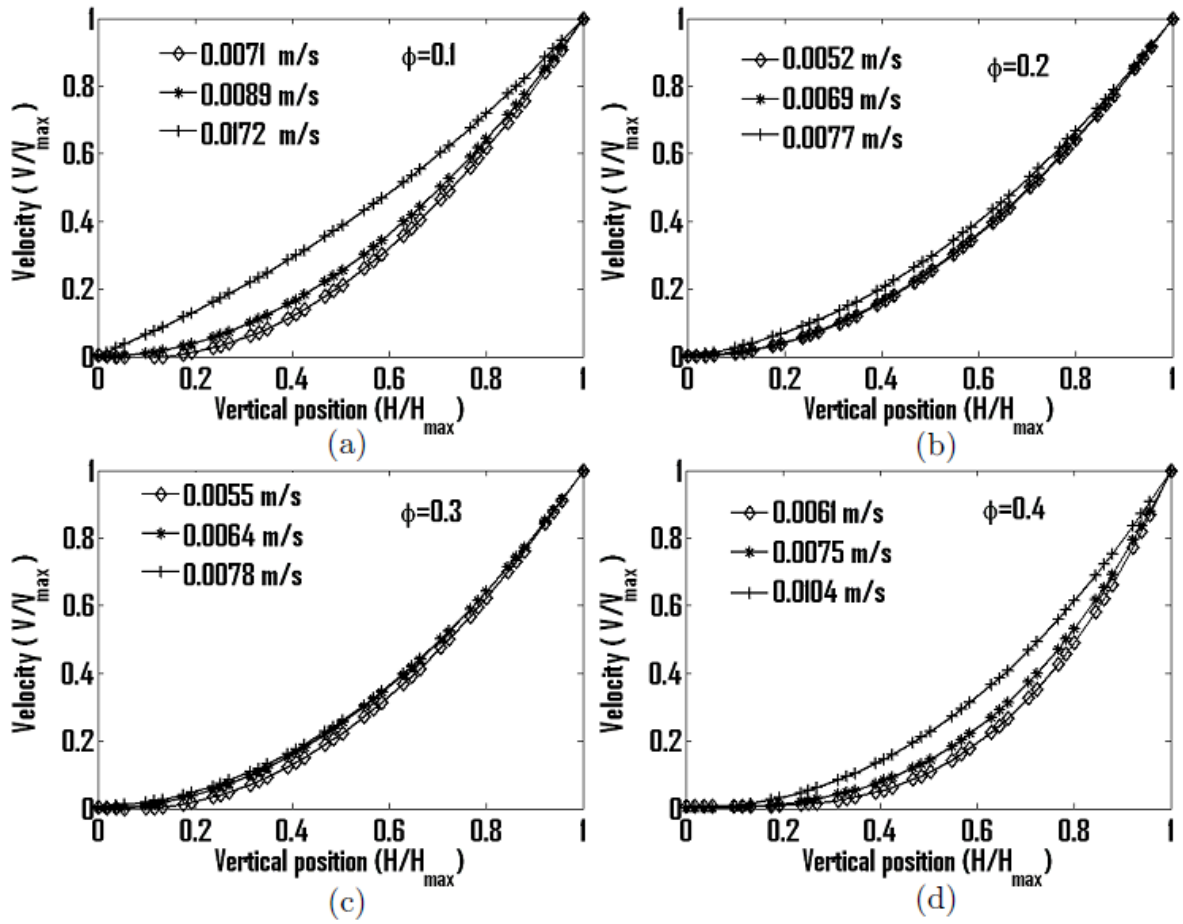

Figure 5.11. Effect of concentration on velocity profiles. (a) 10% (b) 20% (c) 30% (d) 40%. The suspensions of various concentrations were prepared with 500 µm polystyrene particles in density matched suspending fluid of viscosity 98 cP.

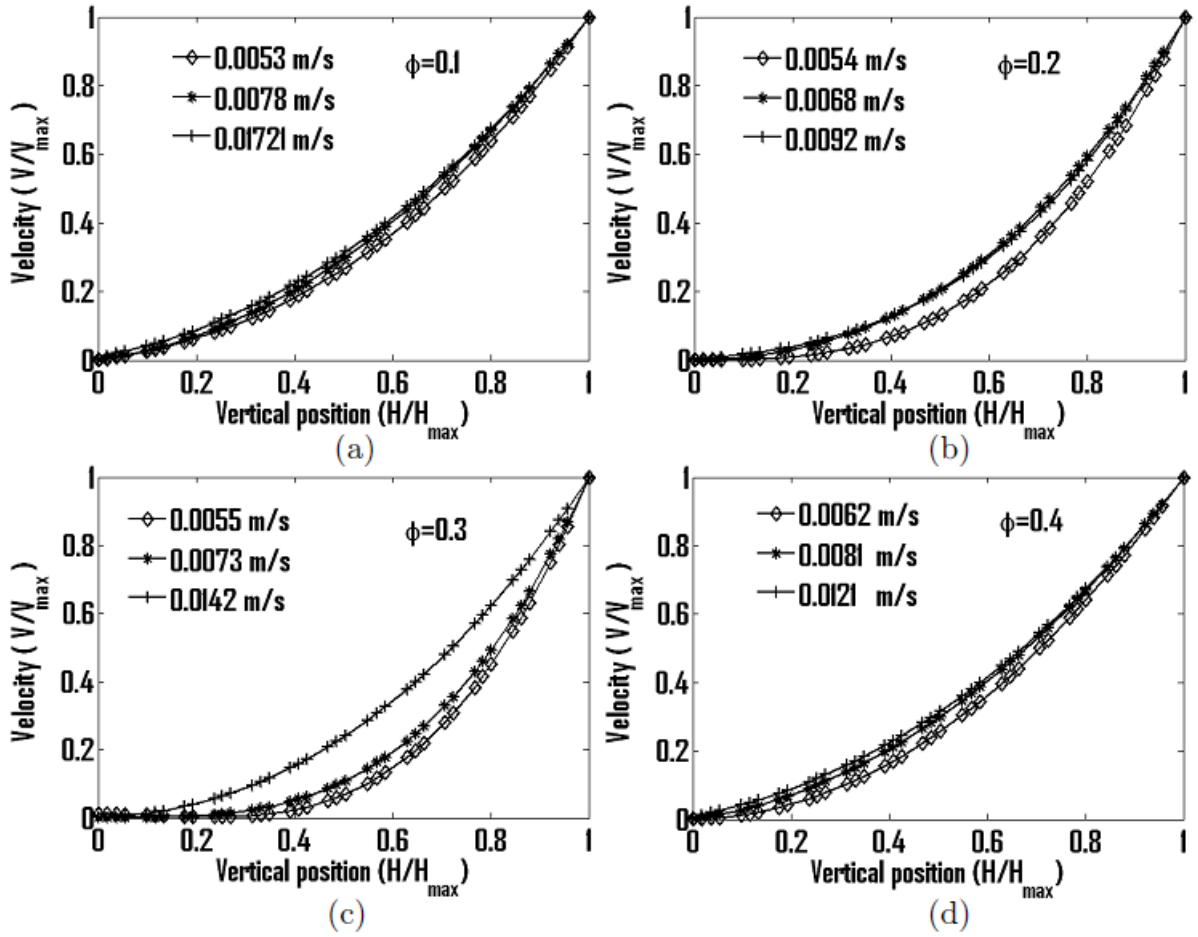

Figure 5.12. Effect of concentration on velocity profiles. (a) 10% (b) 20% (c) 30% (d) 40%. The suspensions of various concentrations were prepared with 500 μm polystyrene particles in density matched suspending fluid of viscosity 204 cP.

5.3.2 Diffusive flux model for suspension flow

It was observed during experiments that due to mismatch in the refractive index of particles and suspending fluid the velocity vectors were erroneous for some suspensions. Moreover for all type of suspensions, it was difficult to get good quality of PIV images beyond 40% concentration of particles. To evaluate the correctness of the velocity profiles in the experimental observations as well as to predict velocity profiles for suspension of higher concentrations, we have used Diffusive flux model (Phillips *et al*., 1992) which is briefly described below.

In the Diffusive flux model, the entire suspension is treated as a single phase and we solve the basic governing equations: continuity and momentum along with steady state mass

conservation for particles. These continuity and momentum equations are respectively described as,

$$\nabla \cdot u = 0 \tag{5.1}$$

$$\rho\left(\frac{\partial u}{\partial t} + u \cdot \nabla u\right) = -\nabla p + \nabla \cdot \tau \tag{5.2}$$

where, u denotes suspension velocity, ρ is for density of suspension, p is pressure and τ denotes the stress tensor which is given by

$$\tau = 2\eta(\phi)\dot{\gamma} \tag{5.3}$$

where, $\dot{\gamma} = \frac{\nabla u + \nabla u^t}{2}$ is the rate-of-strain tensor and $\eta(\phi)$ is suspension viscosity represented by Krieger model with,

$$\eta(\phi) = \eta_0(1 - \phi/\phi_m)^{-1.82} \tag{5.4}$$

where, η_0 is the viscosity of suspension media, ϕ is the particle volume fraction and ϕ_m is maximum packing fraction that is assumed to be equal to 0.68. The steady state mass conservation for particles is represented as,

$$\frac{\partial \phi}{\partial t} + u \cdot \nabla \phi = -\nabla \cdot N_t \tag{5.5}$$

where, N_t is total diffusive flux. The left hand side denotes the convective flux and right hand side stands for diffusive flux.

The particle flux due to spatially varying interacting frequency is given as,

$$N_c = -\rho K_c a^2(\phi^2 \nabla \dot{\gamma} + \phi \dot{\gamma} \nabla \phi) \tag{5.6}$$

The viscosity gradient-induced migration flux is given as,

$$N_\eta = -\rho K_\eta \dot{\gamma} \phi^2 \left(\frac{a^2}{\eta}\right) \frac{d\eta}{d\phi} \nabla \phi \tag{5.7}$$

The total diffusion flux is therefore can be written as,

$$N_t = N_c + N_\eta \tag{5.8}$$

Diffusion coefficients K_c and K_η are empirical constants determined experimentally. In our simulation, we use constant values for K_c and K_η as suggested by Philips *et al*. (1992) as 0.41 and 0.62 respectively. The implementation of Diffusive flux model in general frame work of CFD simulations is reported in Yezaz and Singh (2011). Here we have applied similar procedure but with free surface boundary condition at the interface. At the interface we set the shear stress to be zero. No-slip boundary conditions are provided at the channel walls. At the inlet velocity boundary condition is provided and at the channel outlet we set outflow boundary conditions. The geometry and grid used in the simulation with fluent 6.3 is shown in Fig.5.13.

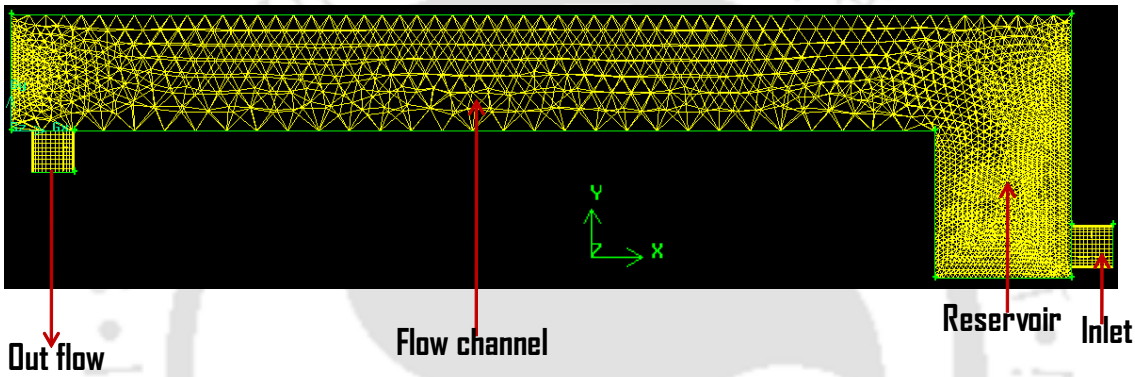

Figure 5.13: Geometry and typical Grid for simulation of suspension flow in 2D channel with Diffusive flux model.

The simulation results too provided the similar profile observed in experiments, where the velocity at bottom wall is zero and it attains maximum at interface. There is reasonably good match between the two results. The simulations at higher concentrations also produced similar profiles. It is to be noted that we did not observe any concentration gradient which shows that no significant shear induced migration occurred. This is expected for the short length of the channel.

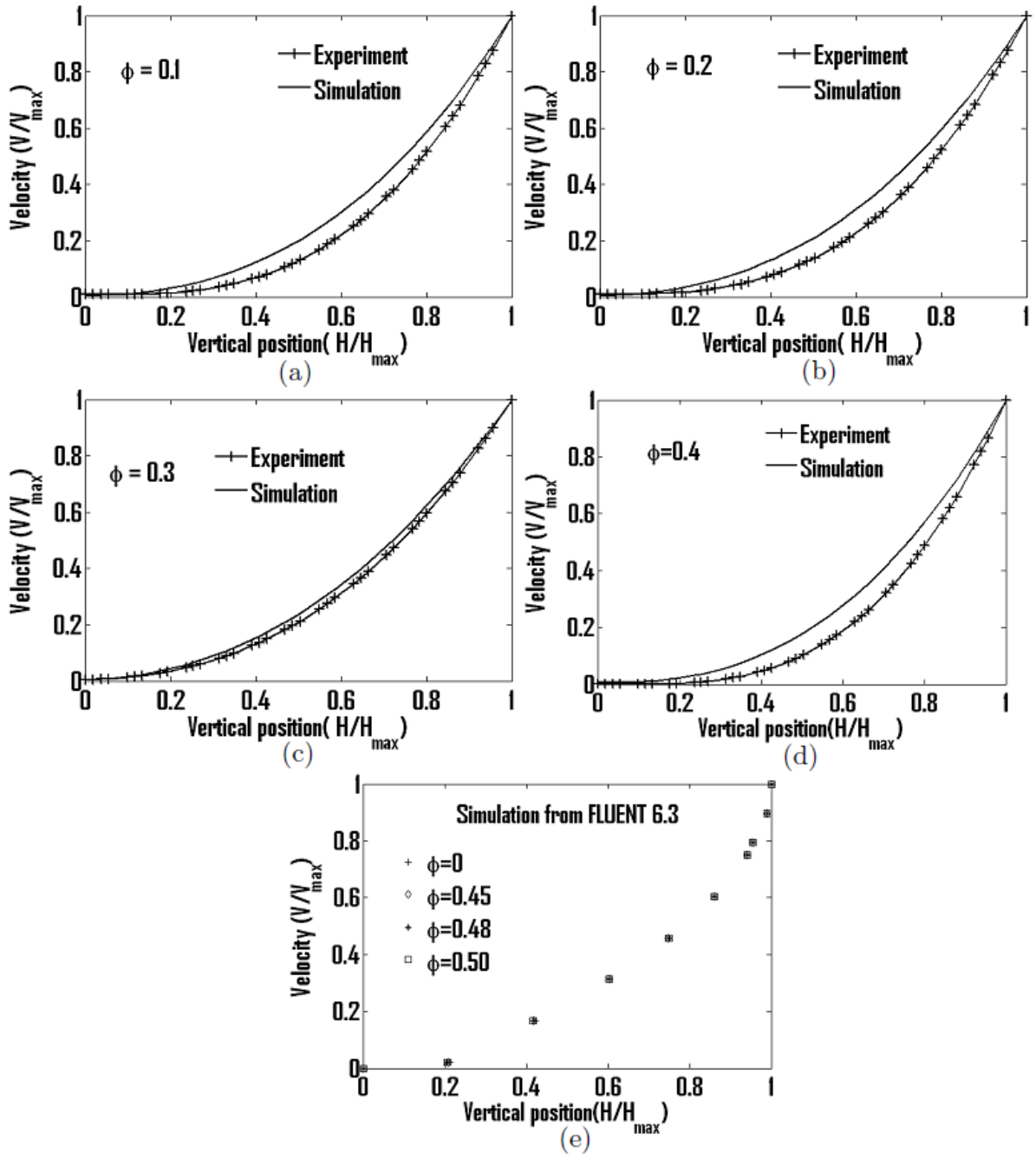

Figure 5.14: Simulation results compared with experimental values for bulk vertical velocity profile (beneath the interface) for suspension with (a) 10% (b) 20% (c) 30% (d) 40% of concentration of particles. (e) The simulation results for 45%, 48% and 50% concentration of particles which were not possible with PIV analysis. The suspensions were dispersion of 500 µm polystyrene particles in density matched suspending fluid of viscosity 2.05 cP

5.3.3 Determination of the interface location, interface vertical velocities and fluctuations

To determine the interface location and to measure the perturbation of free surface flow of concentrated suspension the flow visualization method has been used. In this work the interface is visualized by introducing tracer particles which accumulate near the free surface in open channel flow. When a vertical sheet of laser light illuminates the visualization plane, the region of the suspension produces a luminance which contrasts very sharply with the air side. The edge of this contrast is location of the interface. The advantage of this method is that the interface will always show up as a very distinctive and continuous edge. Since the screw pump was circulating the suspension continuously the tracer particle was well mixed with the suspension and it always being illuminated by the light sheet from free surface to bottom of the channel. Here the suspension side was bright due to illuminating tracer particles and air side was dark. Therefore interface can be located by determining the edge of the luminance contrast between the air and suspension. Fig.5.15 explains the interface fluctuation due to particles fluctuations near the free surface. In these figures Y_1, Y_2, Y_3 etc are interface locations at various positions along the length of the channel and Y_0 is the location of the un-perturbed interface. At a particular instant of time the root mean squared fluctuation of the interface can be give by,

$$Y_m(t_1) = (1/N[(Y_1-Y_0)^2 +(Y_2-Y_0)^2 + (Y_3-Y_0)^2 +\ldots..+ (Y_N-Y_0)^2])^{1/2} \quad (5.9)$$

Similarly we can evaluate root mean squared fluctuations at some other time instants given as,

$$Y_m(t_2)= (1/N[(Y_{11}-Y_0)^2+(Y_{12}-Y_0)^2 +(Y_{13}-Y_0)^2+\ldots..+(Y_{1N}-Y_0)^2])^{1/2} \quad (5.10)$$

$$Y_m(t_n) = (1/N[Y_{n1}-Y_0)^2+(Y_{n2}-Y_0)^2+(Y_{13}-Y_{0)}{}^2+\ldots\ldots+(Y_{nN}-Y_0)^2])^{1/2} \quad (5.11)$$

The mean of the above quantities gives the measure of time and space averaged fluctuation of the interface. In our experiments 444 images were recorded with the time interval of 52 µs.

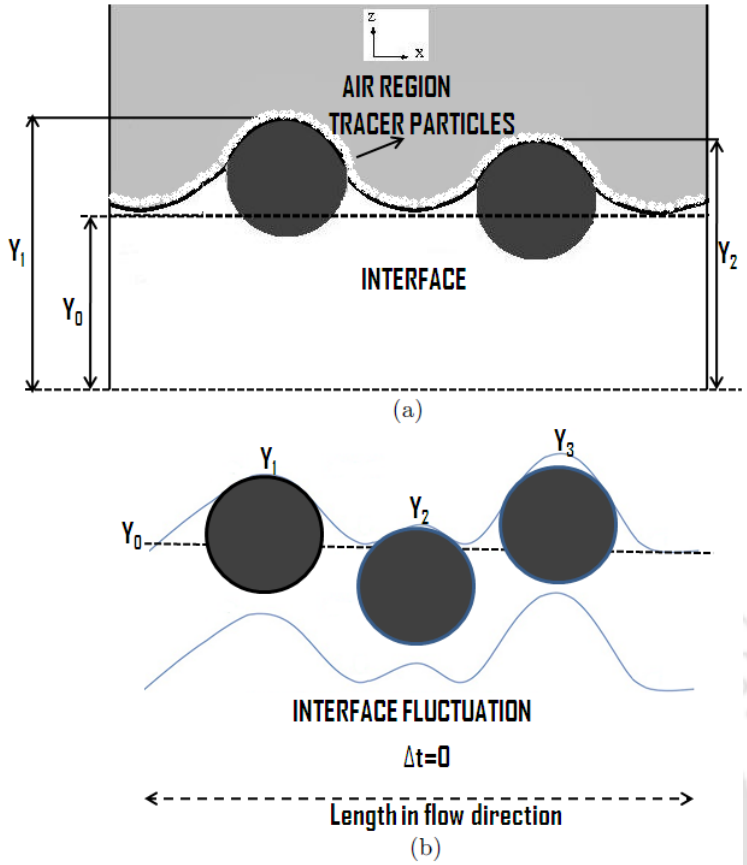

Figure 5.15: Schematic diagram explaining the origin of interface fluctuation due to suspended particles (a) and resulting contour of the instantaneous interface location (b).

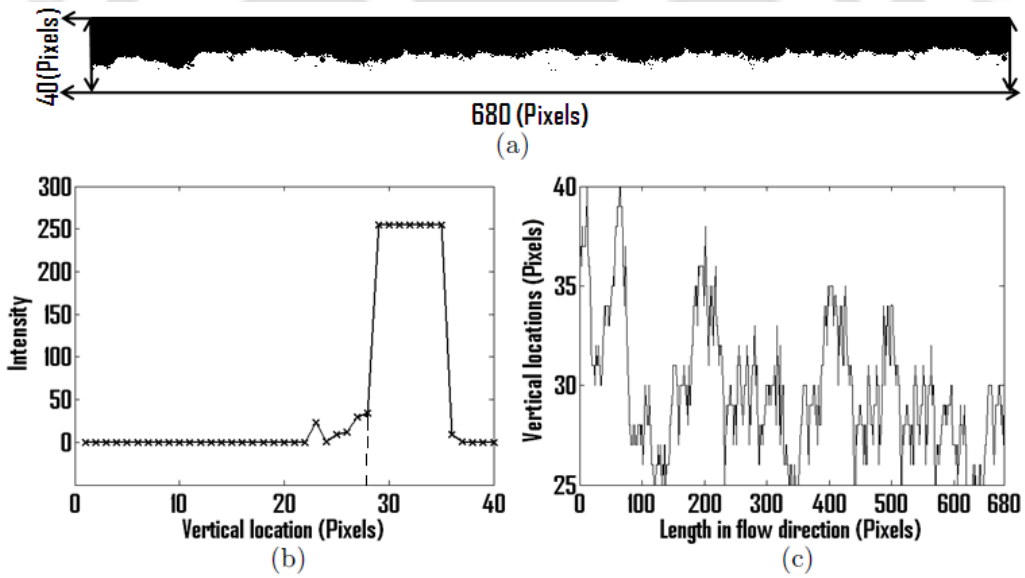

Figure 5.16: (a) A sample image of interface (b) Intensity variation in vertical direction at a given axial location (c) Location of the interface along the axial length at a given instant of time.

Figure 5.16a shows the sample image of interface region captured from the CCD camera. The captured gray scale images of interface have the intensity value between 0 (air region) and 255 (tracer particles at the interface). To determine the location of the interface the gradient

of intensity at every location was computed. The position of maximum gradient locates the interface as shown in Fig. 5.16b. The location of the interface at a particular instant of time is shown in Fig. 5.16(c). To measure the perturbation of the interface we have computed the root mean squared vertical position. Figure 5.17 through 5.24 shows the time trace of the root mean squared mean vertical position of the interface for Newtonian fluid and suspensions at various concentrations. In order to show the relative strength of these interface fluctuations we have set the Y-axis scale same in all the plots. It can be easily observed in Fig.5.17 that the pure suspending fluid has negligible interface fluctuations compared to the concentrated suspensions. We also notice that the perturbation of the interface is low at small flow speed but increase rapidly at higher flow rates.

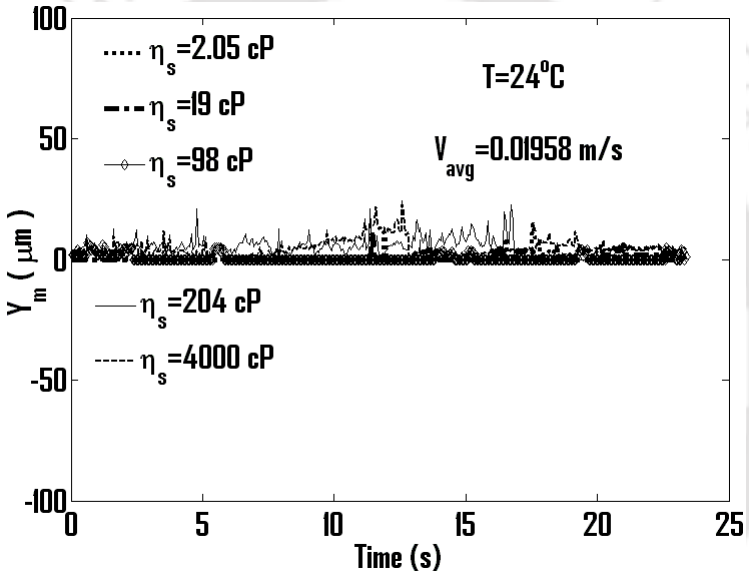

Figure 5.17: Mean squared interface fluctuation plotted with time for various pure suspending fluids which has the different viscosity.

The effect of particle concentration on interface fluctuations can be studied in the Fig.5.18 through Fig.5.24 which are plotted for various suspensions studied in this work. For all the concentrations, we observe that the fluctuation increases with the increase in the flow speed. It is interesting to note that for suspension of given concentration, as we decrease the viscosity of suspending fluid, the fluctuation is increased (Fig.5.21 through Fig.5.24). Figure 5.18 represents studies on suspension of 80 μm particles present in suspending fluid of viscosity 2.05 cP. The corresponding plots for 250 and 500 μm particles are shown in Figs. 5.19 and 5.20 respectively. These three figures illustrate the effect of particle size in the interface perturbation of suspension flow. It can be easily observed that the interface height fluctuation increases with increase in the particle size.

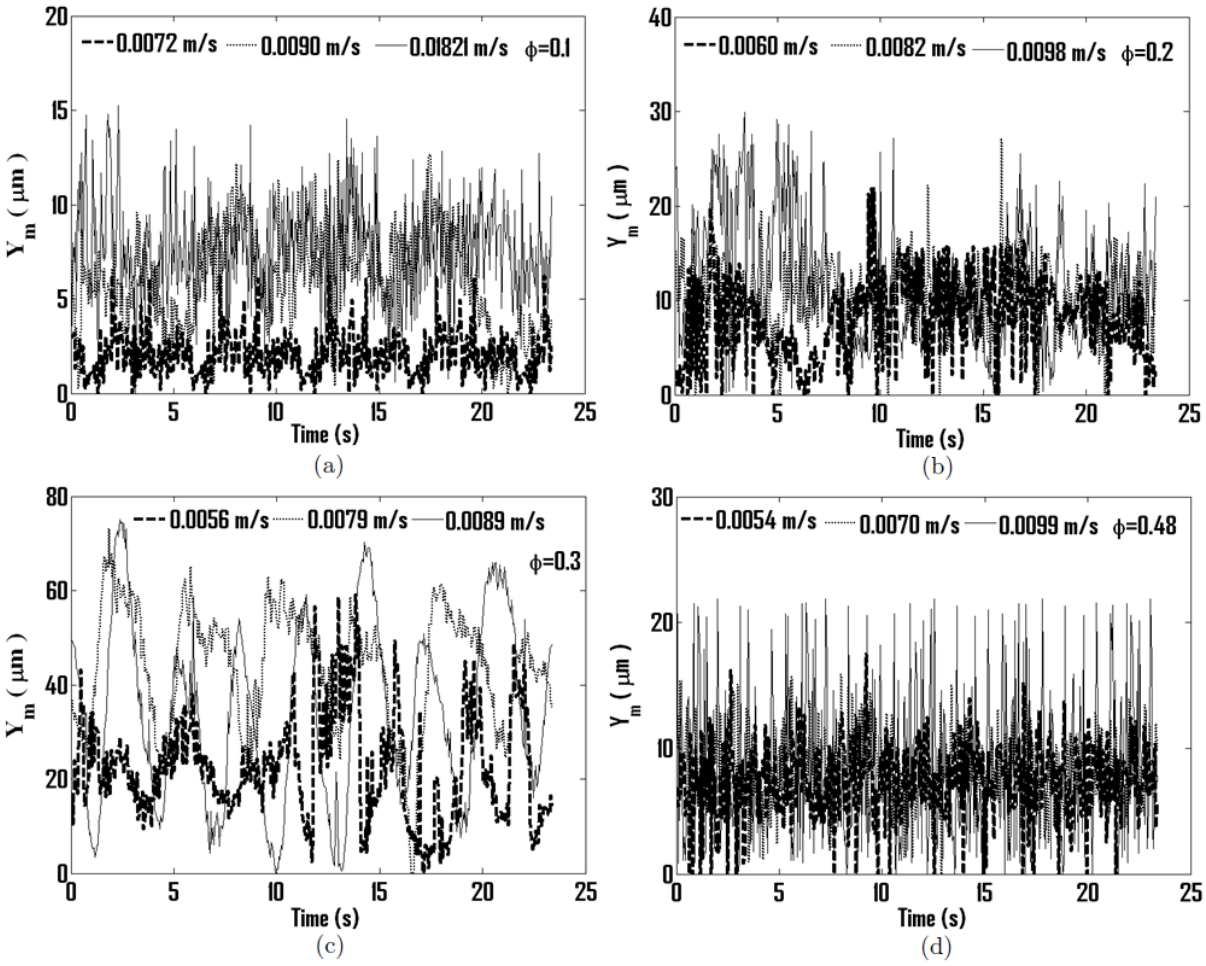

Figure 5.18: Mean squared interface fluctuation plotted with time for (a)10% (b)20% (c)30% (d)48% suspension of 80 μm particles present in suspending fluid of viscosity 2.05 cP.

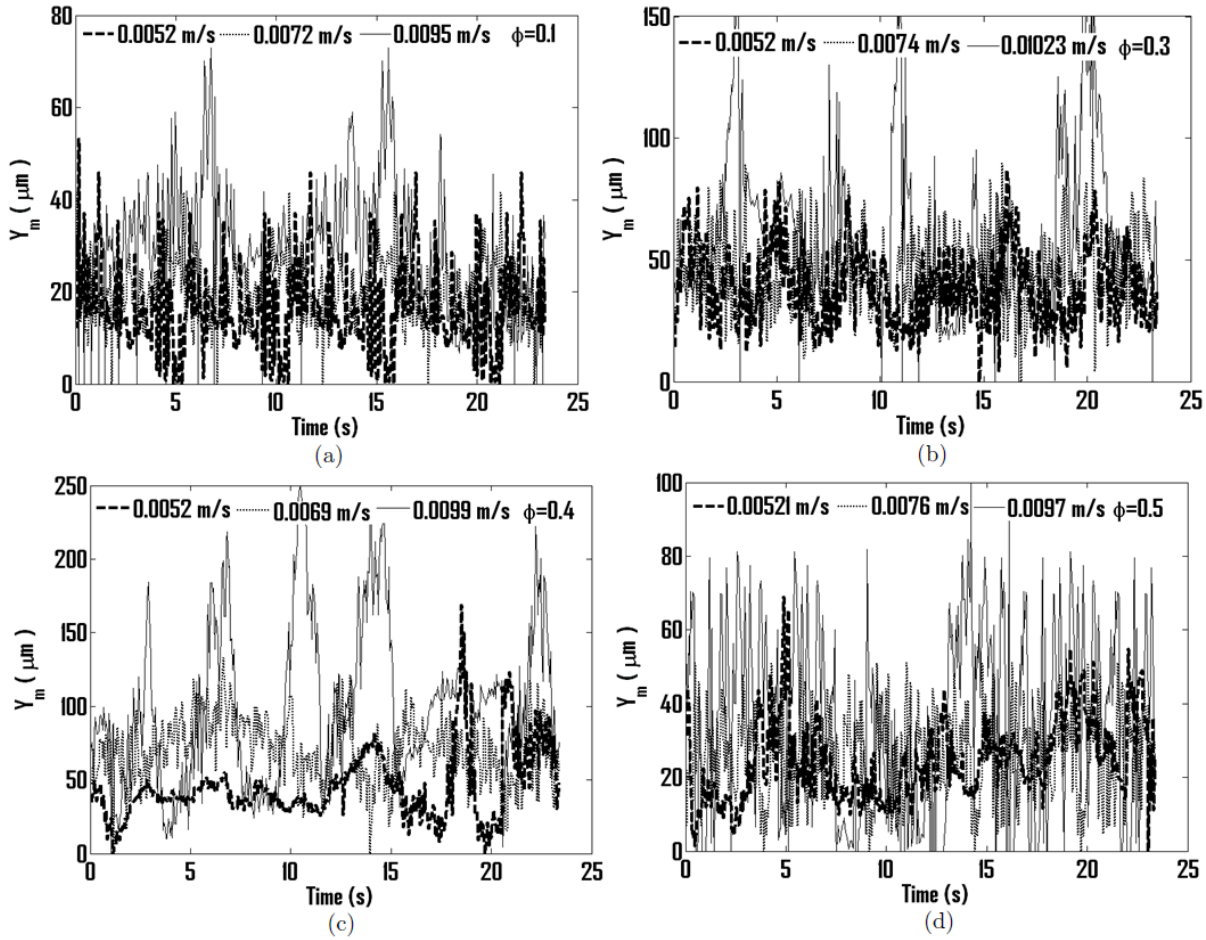

Figure 5.19: Mean squared interface fluctuation plotted with time for (a)10% (b)30% (c)40% (d)50% suspension of 250 μm particles in suspending fluid of viscosity 2.05 cP

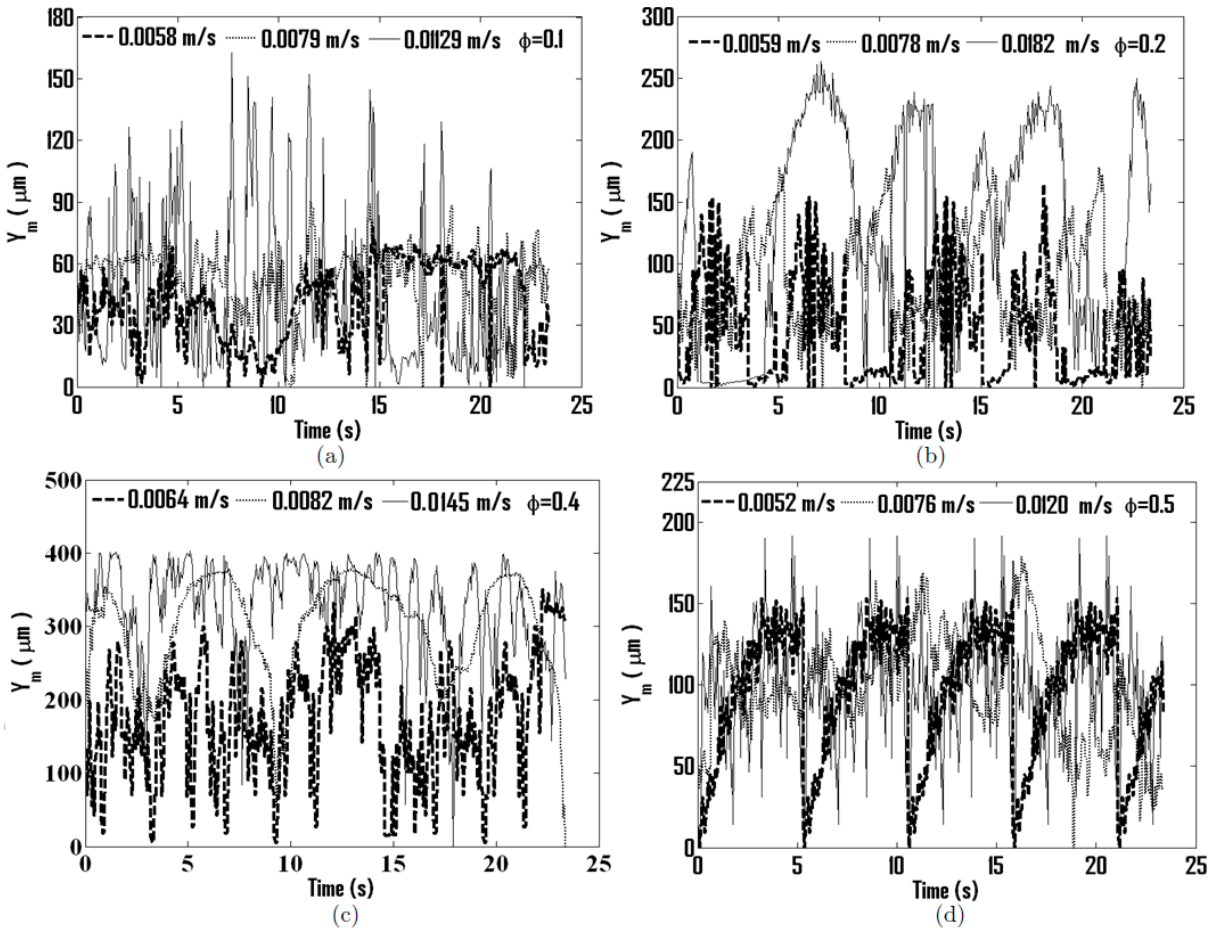

Figure 5.20: Mean squared interface fluctuation plotted with time for (a)10% (b)20% (c)40% (d)50% suspension of 500 μm particles in suspending fluid of viscosity 2.05 cP

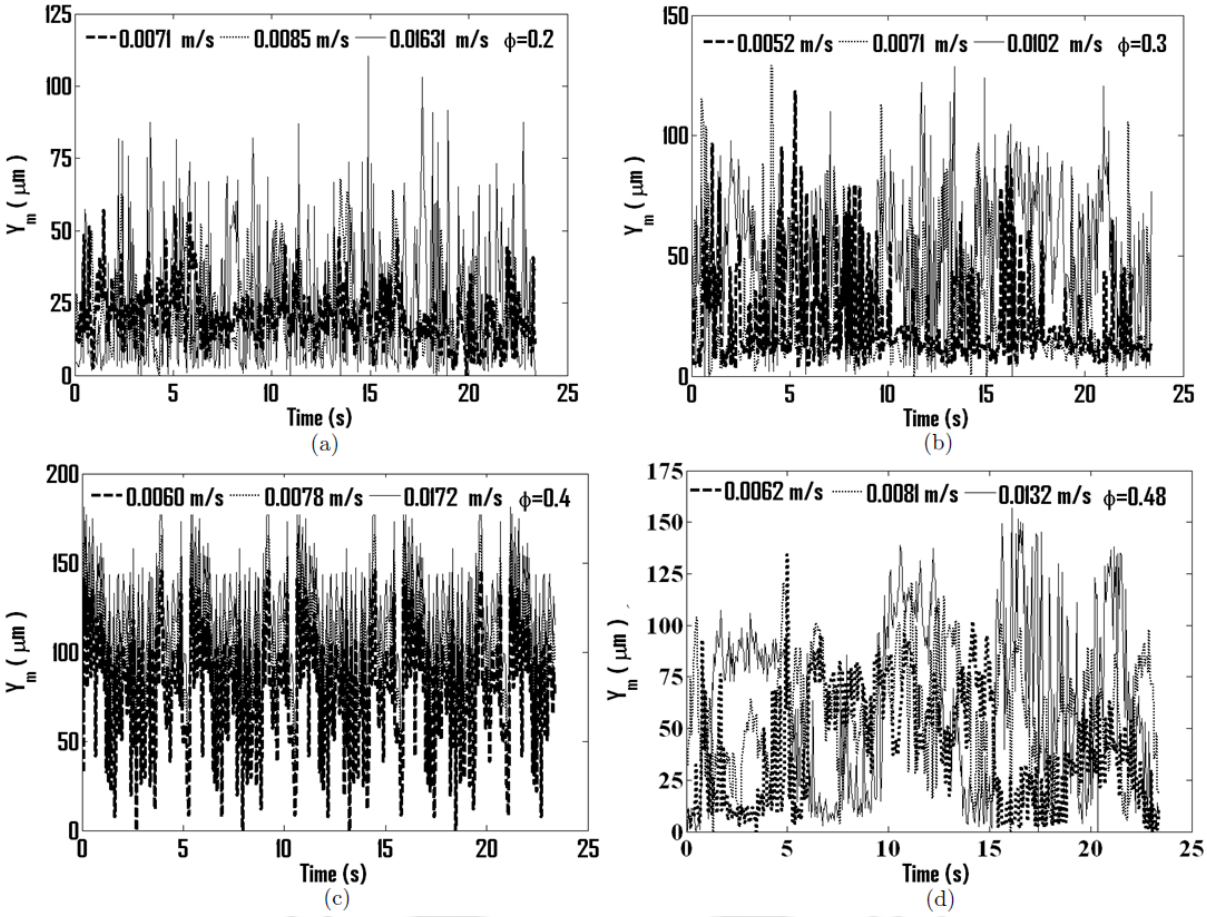

Figure 5.21: Mean squared interface fluctuation plotted with time for (a)20% (b)30% (c)40% (d)48% suspension of 200 μm particles present in suspending fluid of viscosity 19 cP

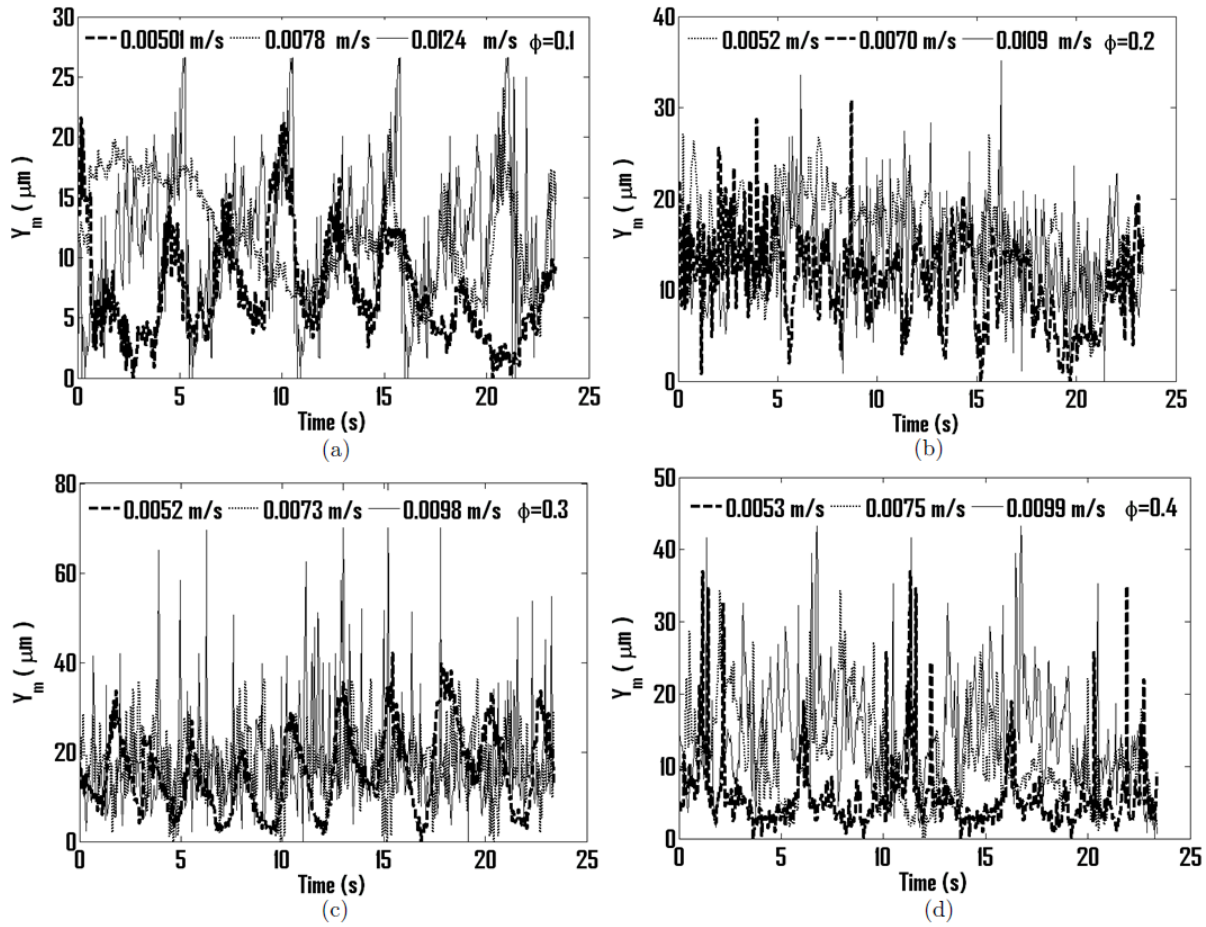

Figure 5.22: Mean squared interface fluctuation plotted with time for (a)10% (b)20% (c)30% (d)40%. suspension of 200 μm particles in suspending fluid of viscosity 4000 cP.

Figure 5.21 through 5.24 illustrates the effect of suspending fluid viscosity on interface fluctuations. Figures 5.21 and 5.22 for the suspension of 200 μm PMMA particles in suspending fluid of viscosity 19 cP and 4000 cP respectively. Figure 5.23 shows the interface fluctuation for 500 μm polystyrene particles suspended in fluid of viscosity 98 cP whereas Fig.5.24 for 500 μm polystyrene particles in suspending fluid of viscosity 204 cP.

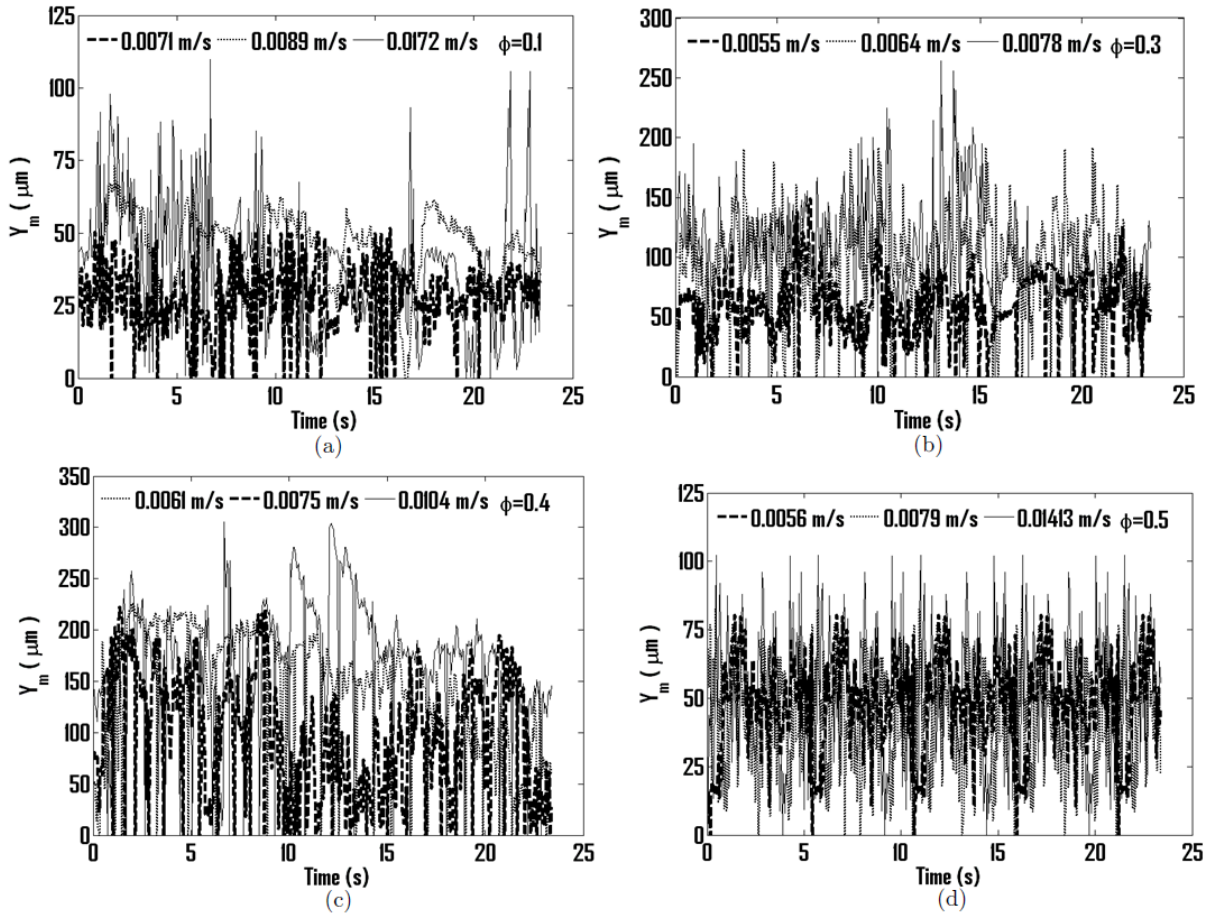

Figure 5.23: Mean squared interface fluctuation plotted with time for (a)10% (b)30% (c)40% (d)50% suspension of 500 μm polystyrene particles in suspending fluid of viscosity 98 cP

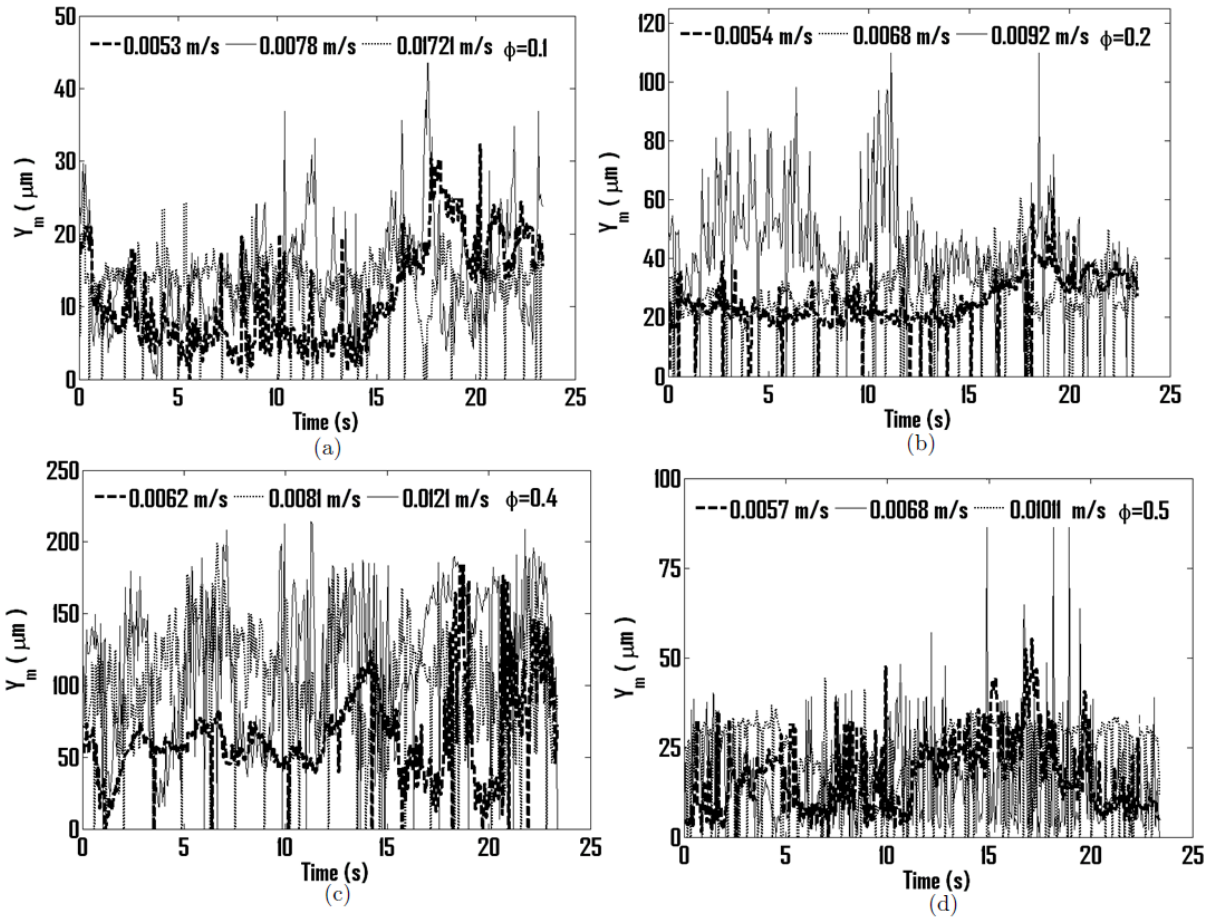

Figure 5.24: Mean squared interface fluctuation plotted with time for (a)10% (b)20% (c)40% (d)50% suspension of 500 μm particles in suspending fluid of viscosity 204 cP

A very significant observation is that the mean squared fluctuation first increases with particle concentration and then at certain optimum particle fraction it reaches maxima before decreasing further after the increase of concentration. This optimum particle concentration value which depends on the particle size and suspension viscosity lies in the range of 30 to 40%. For example, the suspension of 80 µm particles in the suspending fluid of viscosity 2.05 cP the maximum perturbation of the interface was observed for 30% whereas for 250 µm and 500 µm particles (in the same suspending fluid) the maxima was observed at close to 40 %. In the Fig.5.25 through Fig.5.27, we have plotted the time averaged root mean squared fluctuation of the interface at various maximum centerline velocities. It can be clearly observed that for a given concentration the time averaged fluctuation appears to increase linearly with flow rate. The growth of fluctuation is almost linear with the flow speed. It can be observed from the slope of the curve that it is less for lower concentration but increases as the particle concentration increases. The slope of the curve also increases till the optimum concentration is reached, thereafter both the slope and values of fluctuations decreases. As mentioned previously it can be noticed that the fluctuation increases with increase in the particle size but decreases with the increase in the viscosity of suspending fluid. These results can be summarized in Fig.5.28, where we have plotted the time averaged root mean squared fluctuation (scaled by the flow speed) against the particle concentration.

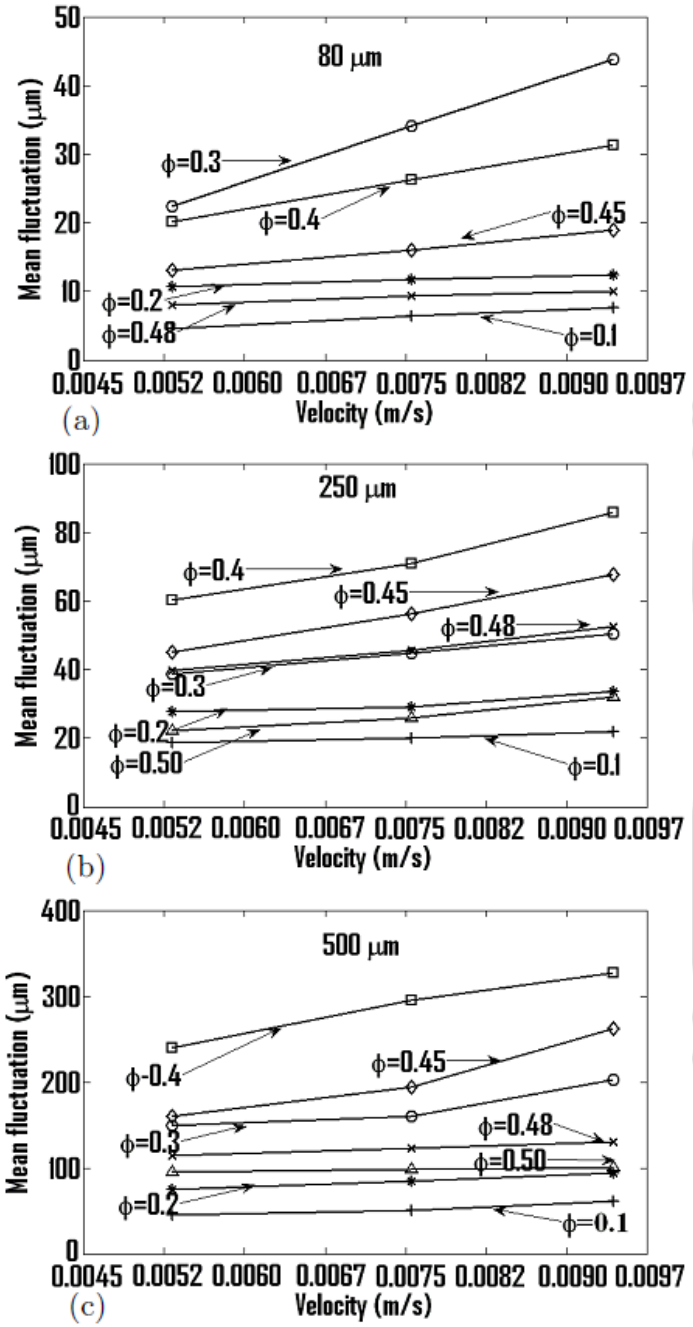

Figure 5.25: Time averaged mean squared fluctuation of the interface location plotted against flow rate in the channel for (a) 80 μm (b) 250 μm (c) 500 μm particle's suspension at various particle concentrations.

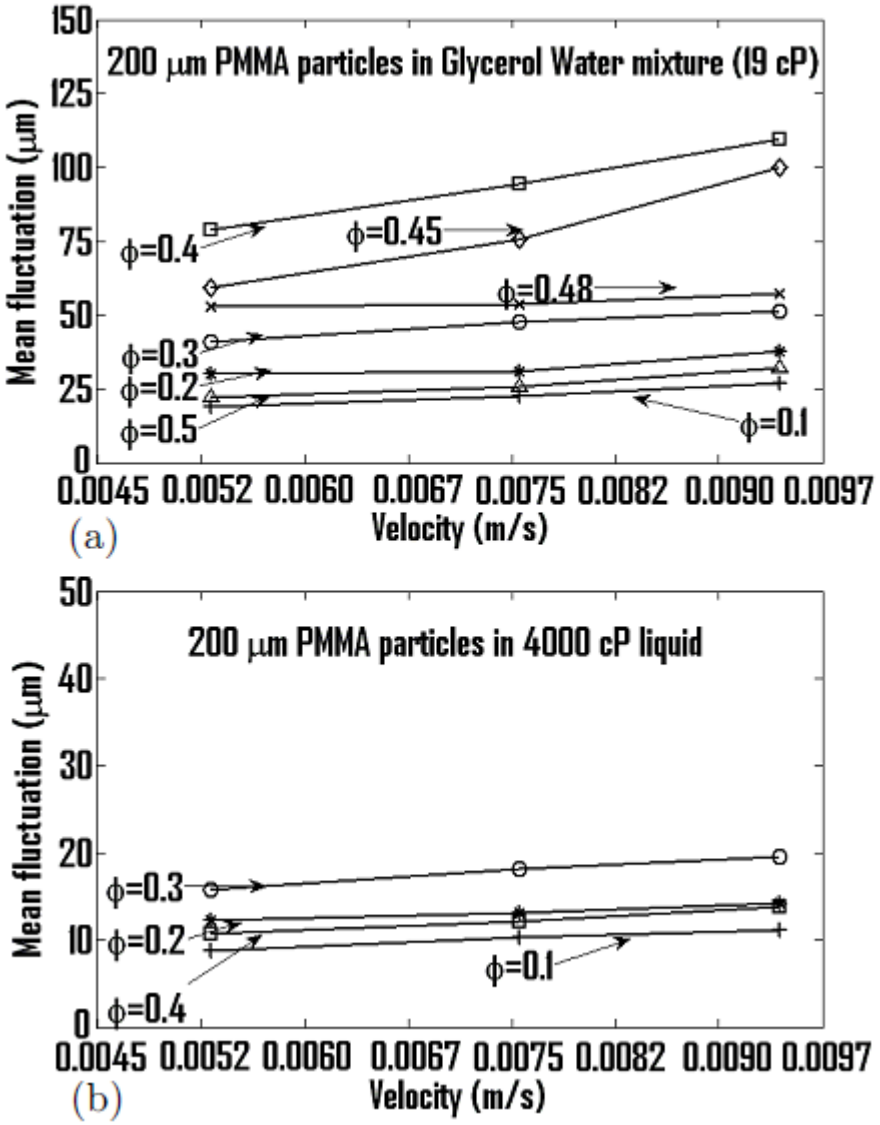

Figure 5.26: Time averaged mean squared fluctuation of the interface location plotted against flow speed in the channel for 200 μm particles present in (a) 19 cP of suspending fluid (b) 4000 cP of suspending fluid at various particle concentrations.

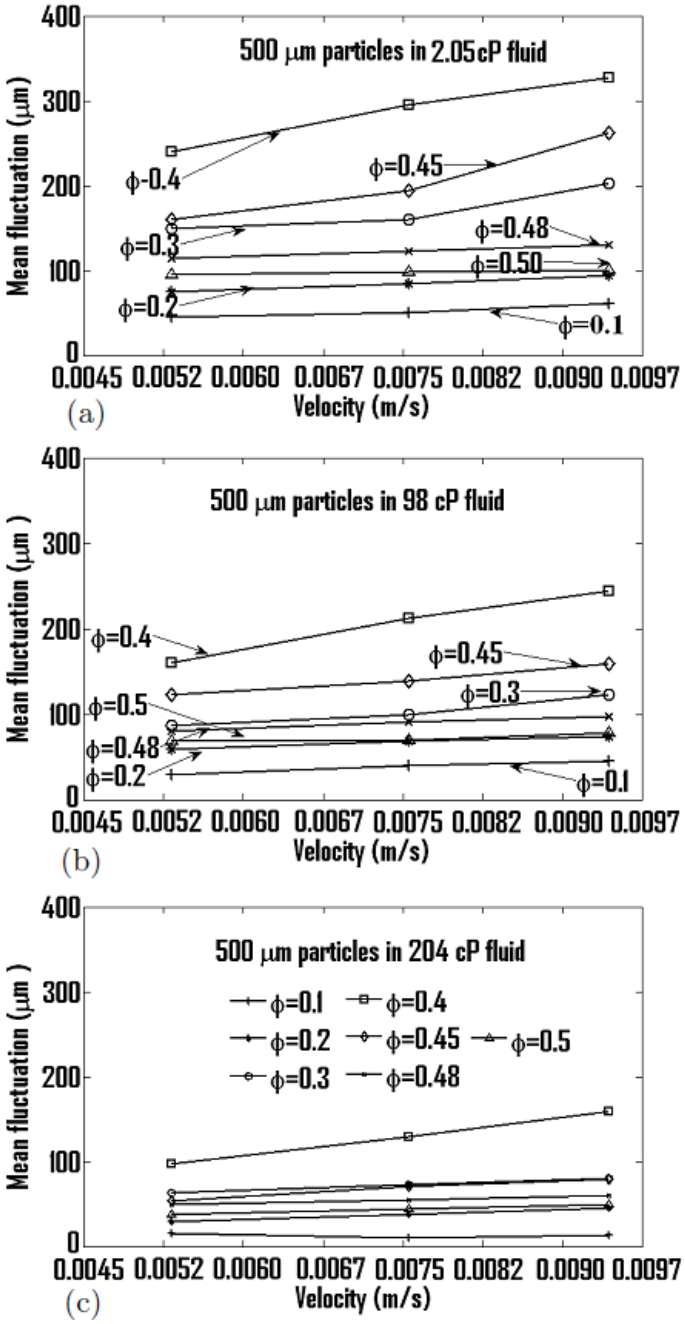

Figure 5.27: Time averaged mean squared fluctuation of the interface location plotted against flow speed in the channel for 500 μm particles present in (a) 98 cP of suspending fluid (b) 204 cP of suspending fluid at various particle concentrations.

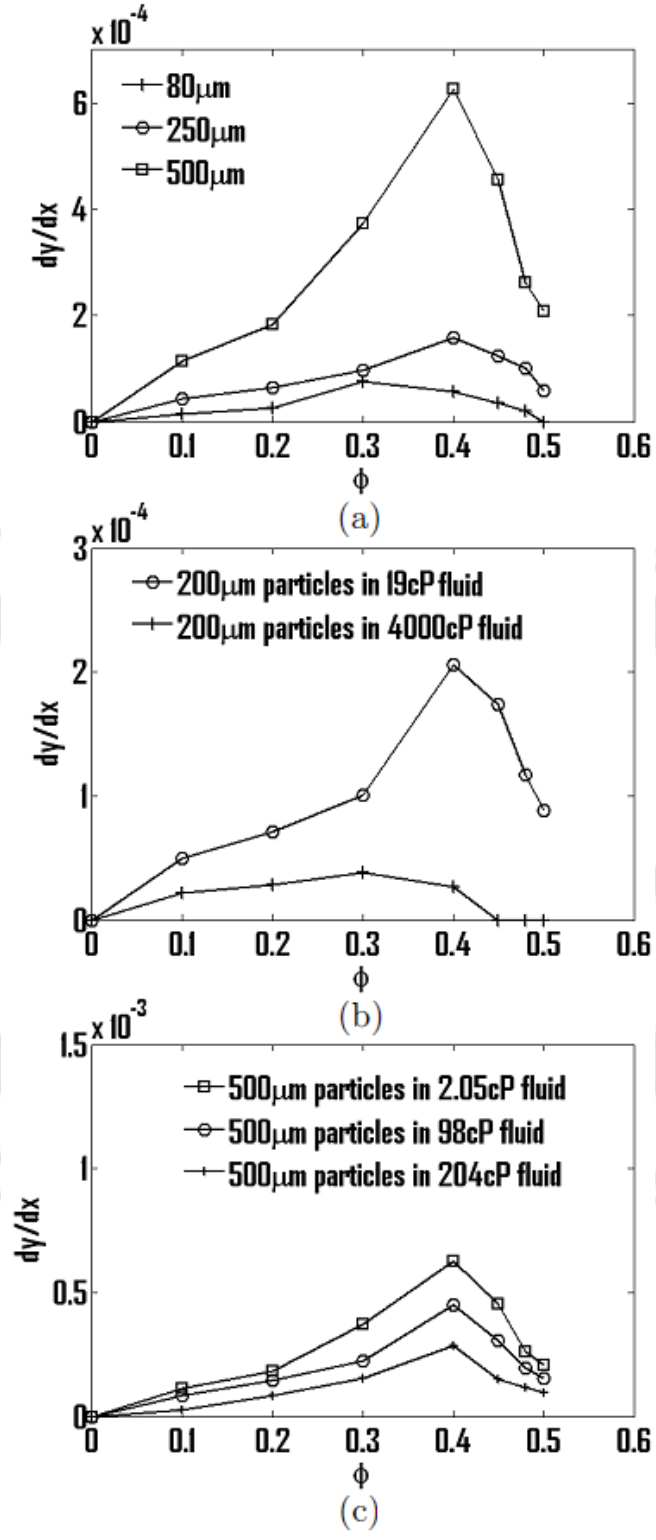

Figure 5.28: Slope of the mean fluctuation of the interface shows the variation with particle concentration towards (a) effect of particle size (b) effect of suspending fluid viscosity for 200 μm particles (c) Effect of suspending fluid viscosity for 500 μm particles.

From the evolution of interface location with time the vertical velocity of the interface was also computed and is shown in Fig.5.29 through Fig.5.38. Interface vertical velocity was calculated from the knowledge of vertical mean displacement of interface between two successive images. The interface vertical velocity (ω) can be calculated as: $\omega = (Ymt_1 - Ymt_2) / \Delta t$ (see Fig.5.15). It can be observed that the interface vertical velocity fluctuation also exhibits the same result as was the case in interface fluctuation discussed above. The vertical velocity of the interface for pure suspending fluid is almost zero. The interface vertical velocity also increases with particle concentration up to certain optimum concentration; thereafter it shows a decrease with concentration. Interface vertical velocity is found to increase with increase in flow rate. For the comparison point of view, Fig.5.29 and Fig.5.30 show the interface vertical velocity for pure suspending fluid and for suspension respectively. The vertical velocity of the interface for different suspending fluid is plotted in Fig. 5.31, and it does show that it is indeed small even for the fluid as viscous as 4000 cp. The effect of particle concentration on the interface vertical velocity is shown in the Figs.5.32 through 5.34. These results which show vertical velocity fluctuation have been studied for three different sizes of particles, i.e., 80 µm, 250 µm and 500 µm respectively. It is quite clear that with increase in particle, the vertical velocity of interface also increases. The effect of viscosity of suspending fluid on vertical velocity of the interface (for suspension of 200 µm particles) can be observed from Fig .5.35 and Fig.5.36. The same for the suspension of 500 µm particles is shown in Fig. 5.37 and Fig. 5.38.

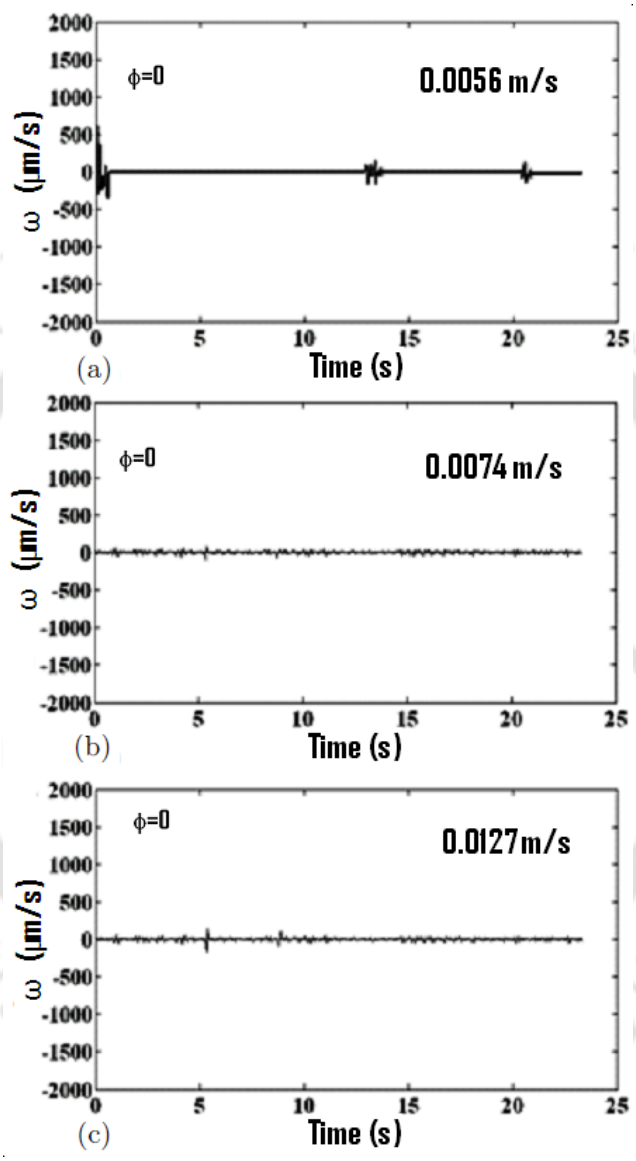

Figure 5.29: Time trace of vertical velocity of the interface for pure suspending fluid of viscosity 2.05 cP at different centerline velocities: (a) 0.0056 m/s (b) 0.0074 m/s (c) 0.0127 m/s.

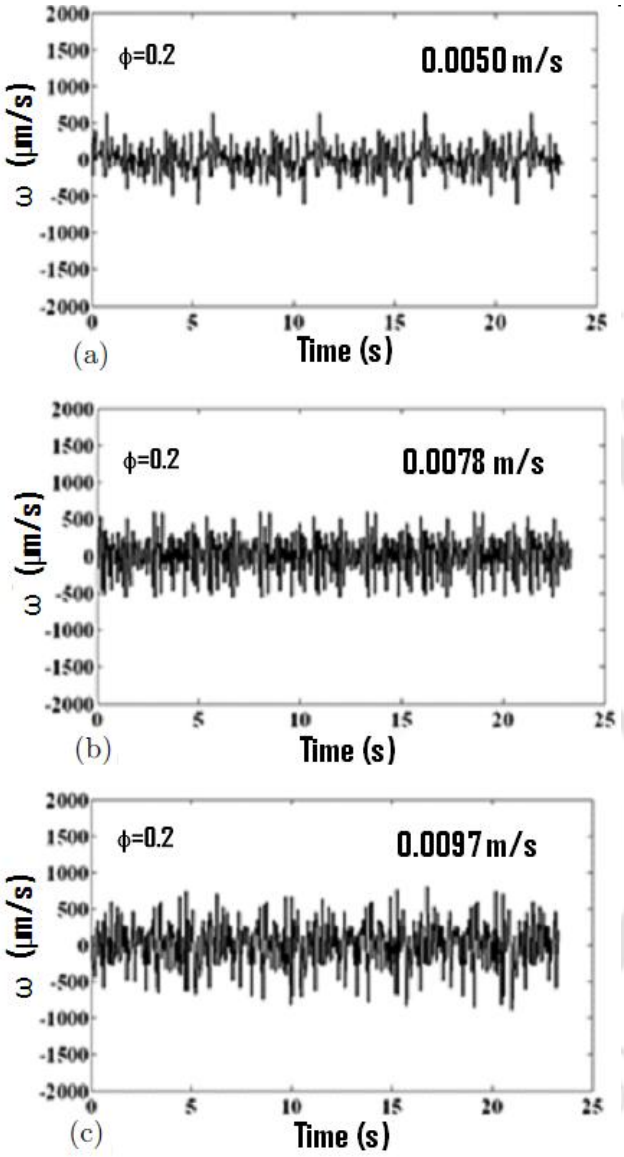

Figure 5.30: Time trace of vertical velocity of the interface for suspension of 500 μm of particles present in 2.05 cP of suspending fluid at different flow rate (a) 0.0050 m/s (b) 0.0078 m/s (c) 0.0097 m/s The particle fraction of suspension is 20%.

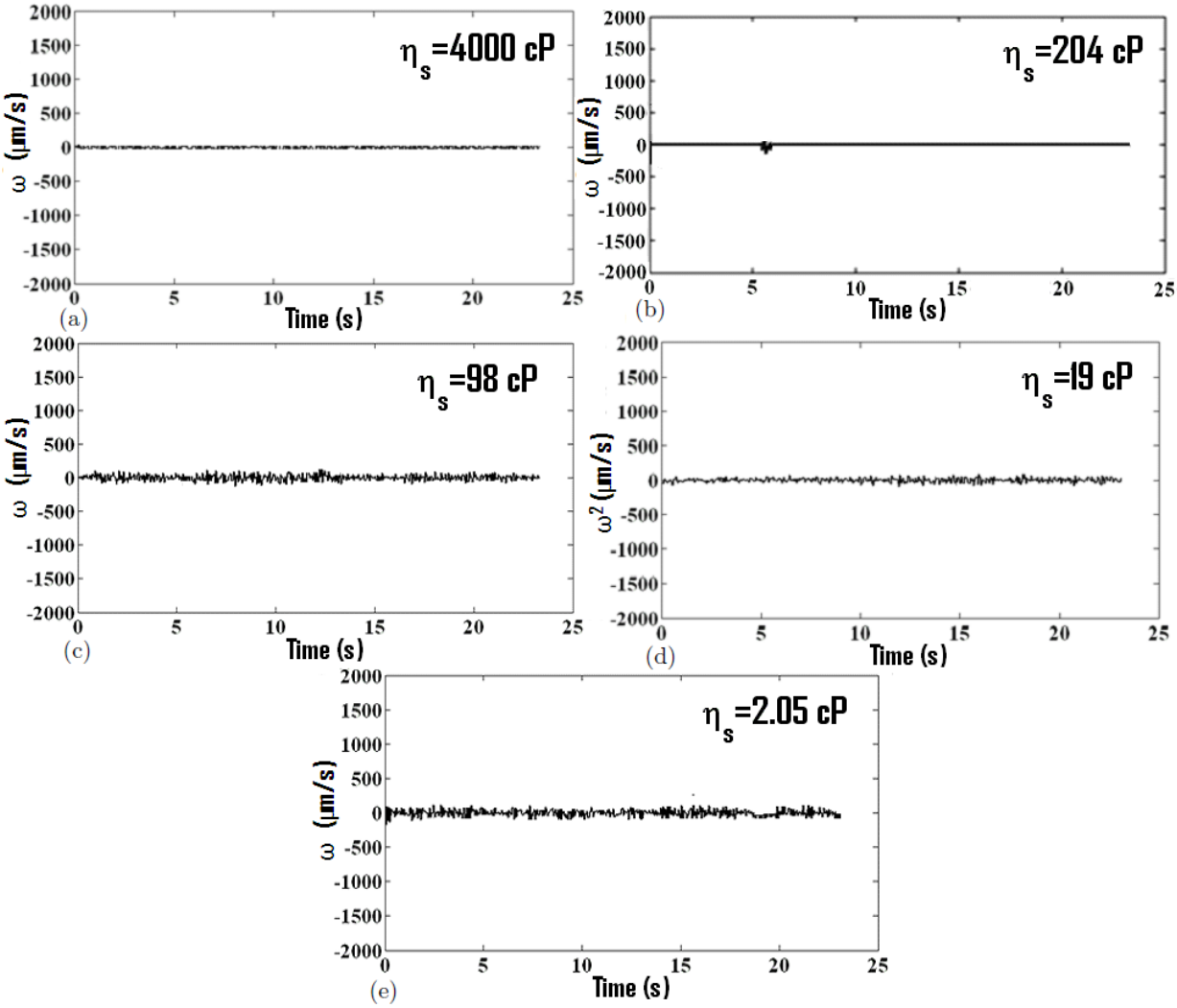

Figure 5.31: Time trace of vertical velocity of the interface for various pure suspending fluid for centerline velocity of 0.0076 m/s. The viscosity of suspending fluids in these cases were: (a) 4000 cP (Triton-X-100+ZnCl+water mixture) (b) 204 cP (Triton-X-100) (c) 98 cP (Ucon oil) (d) 19 cP (Glycerol water mixture) (e) 2.05 cP (Glycerol water mixture).

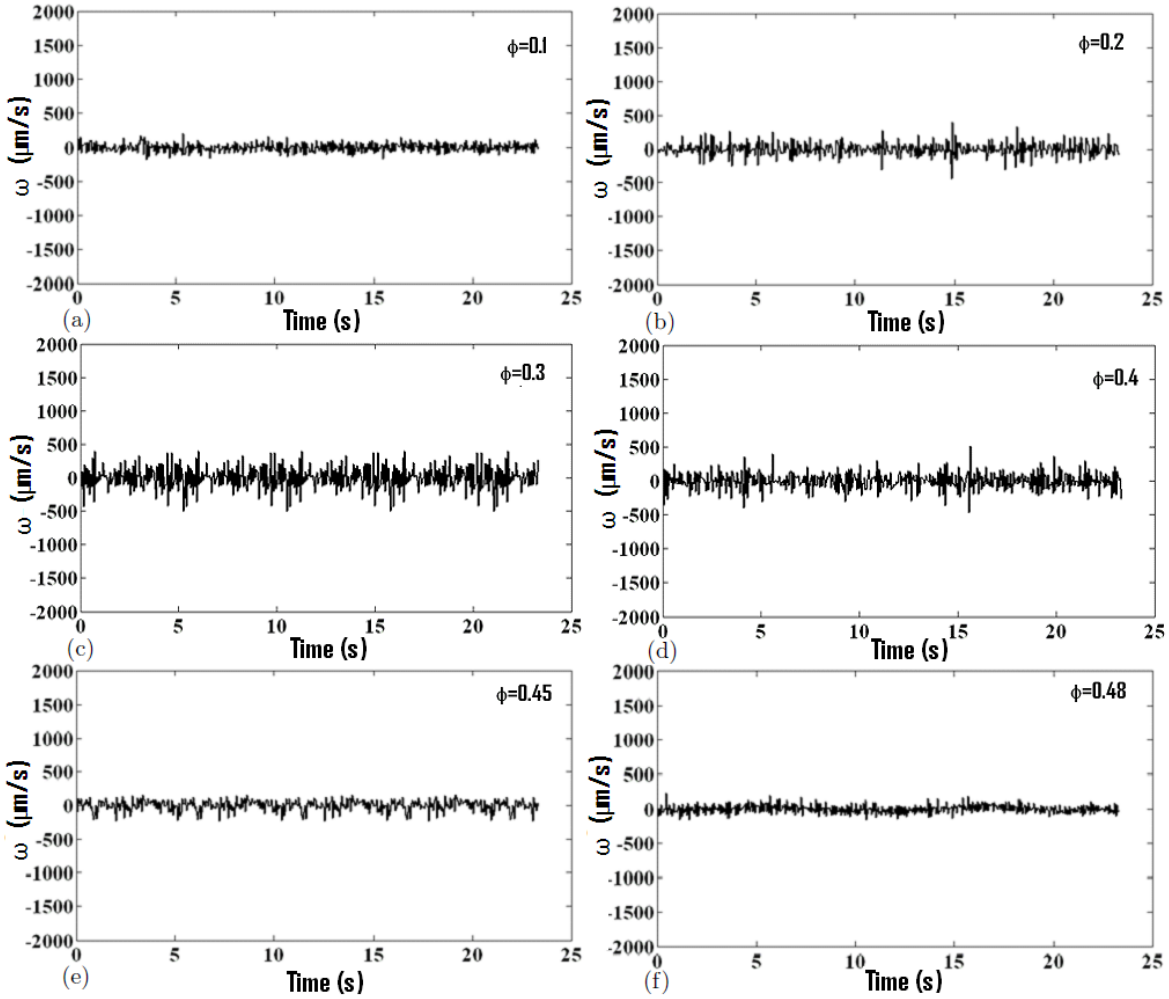

Figure 5.32: Time trace of vertical velocity of the interface for suspension of 80 μm particles present in 2.05 cP of suspending fluid for centerline velocity at range of 0.0076 m/s. The particle concentration for these studies was: (a) 10% (b) 20% (c) 30% (d) 40% (e) 45% (f) 48%.

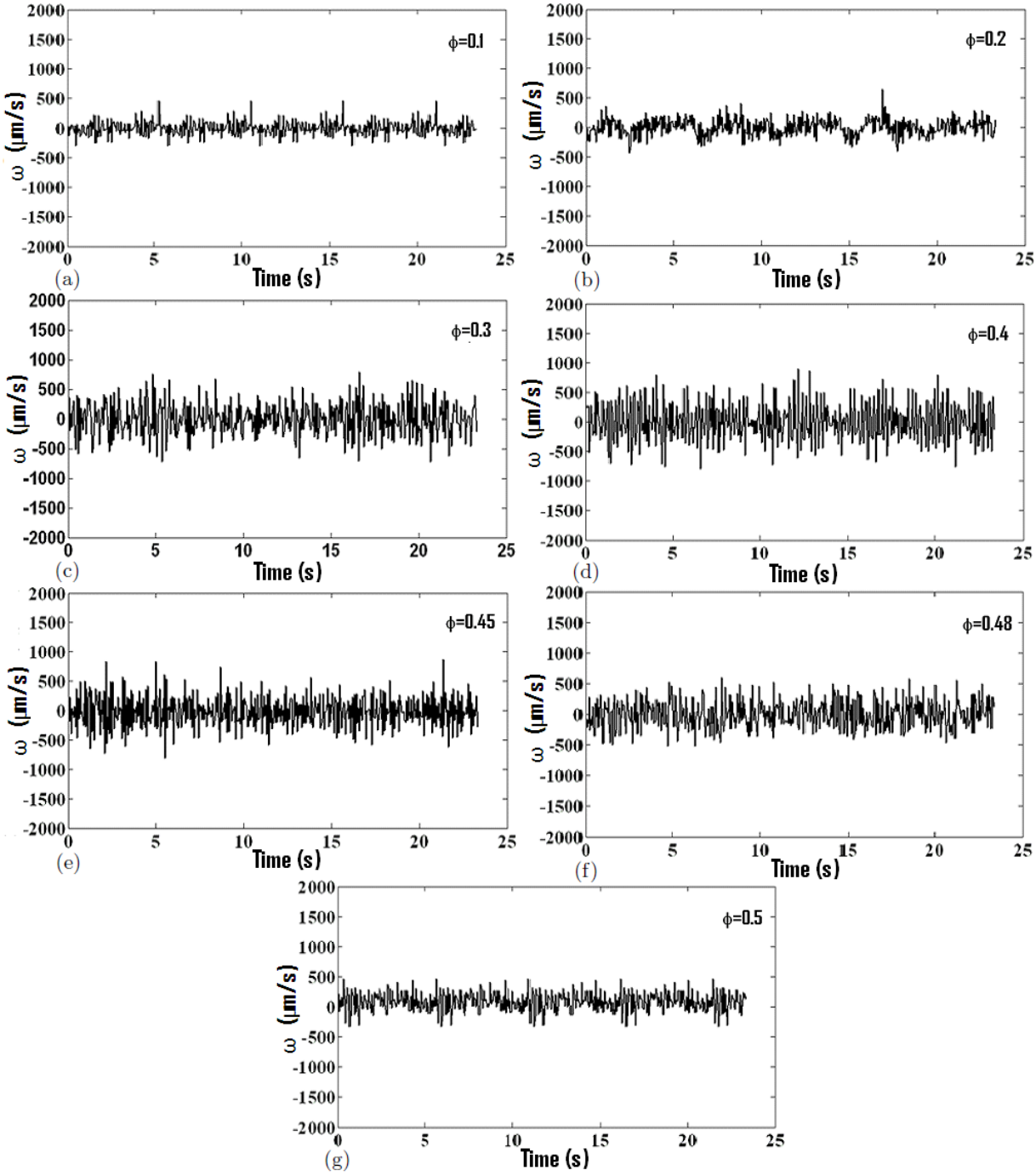

Figure 5.33: Time trace of vertical velocity of the interface for suspension of 250 μm particles present in 2.05 cP of suspending fluid for various particle concentrations: (a) 10% (b) 20% (c) 30% (d) 40% (e) 45% (f) 48% (g) 50%. The centerline velocity for all cases were at the range of 0.0073 m/s.

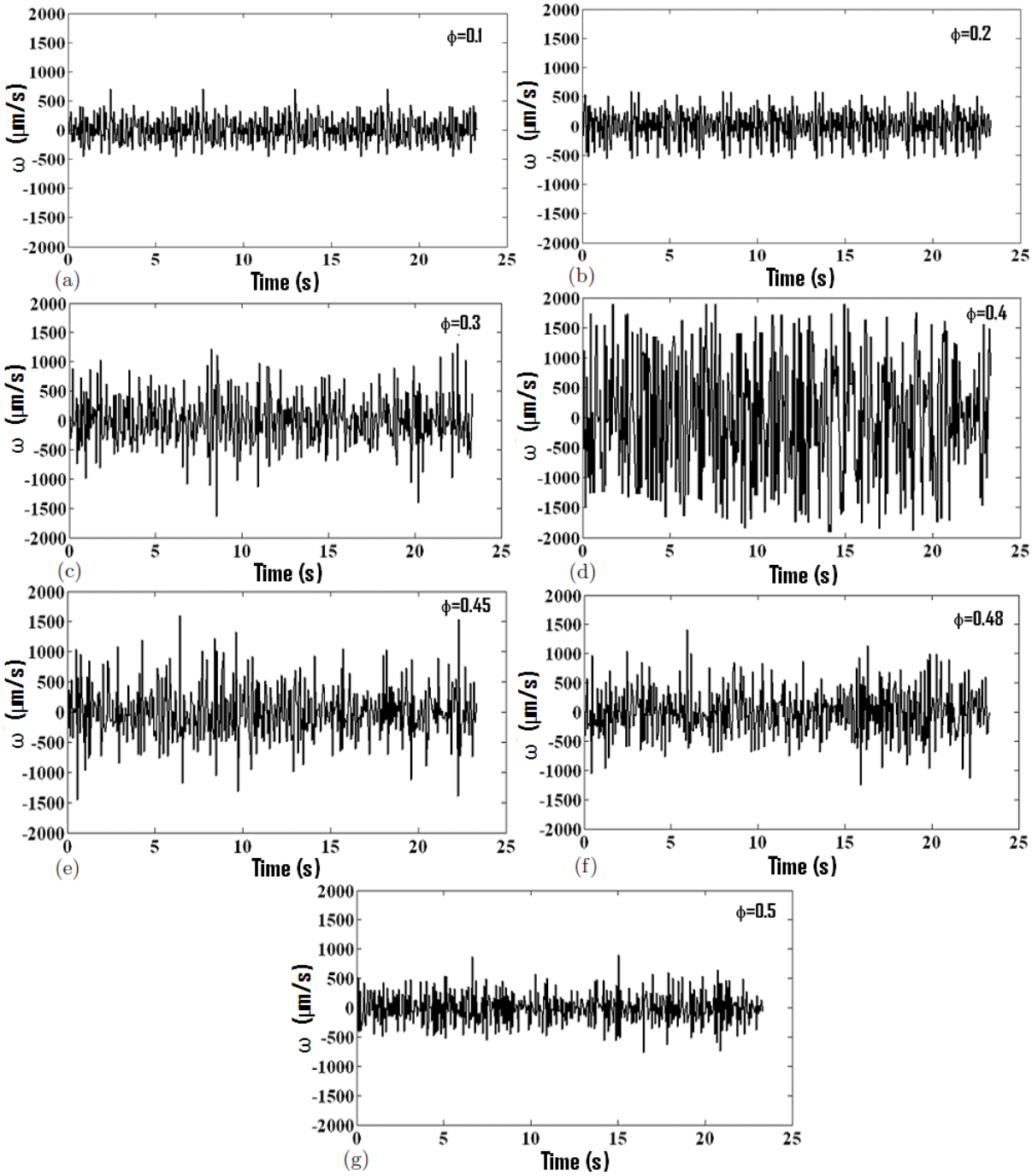

Figure 5.34: Time trace of vertical velocity of the interface for suspension of 500 μm particles in suspending fluid of viscosity 2.05 cP. The concentration of particles in these cases was: (a) 10% (b) 20% (c) 30% (d) 40% (e) 45% (f) 48% (g) 50%. The centerline velocity for all cases were at the range of 0.0071 m/s.

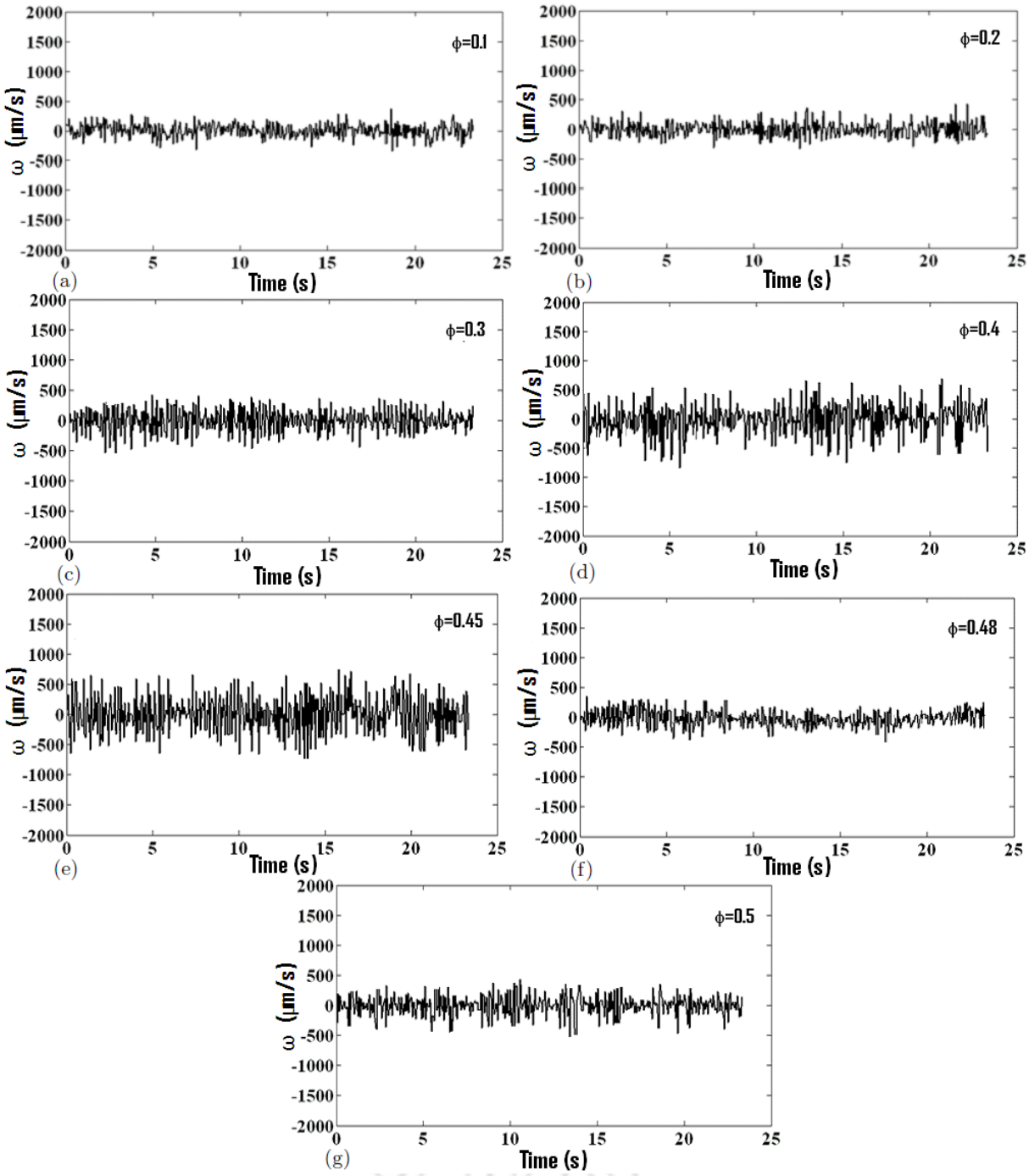

Figure 5.35: Time trace of vertical velocity of the interface for suspension of 200 μm particles in suspending fluid of viscosity 19 cP. The particle concentrations in these cases were: (a) 10% (b) 20% (c) 30% (d) 40% (e) 45% (f) 48% (g) 50%. The centerline velocity for all cases were at the range 0.0076 m/s.

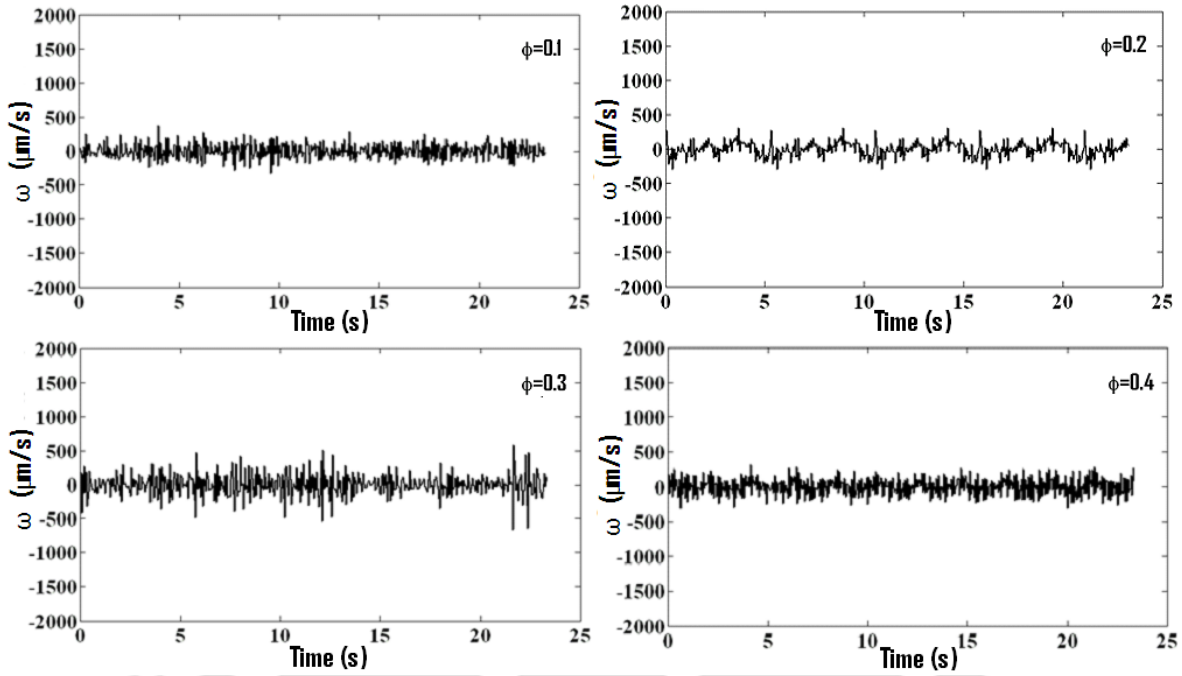

Figure 5.36: Time trace of vertical velocity of the interface for suspension of 200 μm particles in suspending fluid of viscosity 4000 cP. The particle concentrations in these cases were: (a) 10% (b) 20% (c) 30% (d) 40% and the centerline velocity for all cases at the range of 0.0074 m/s.

\

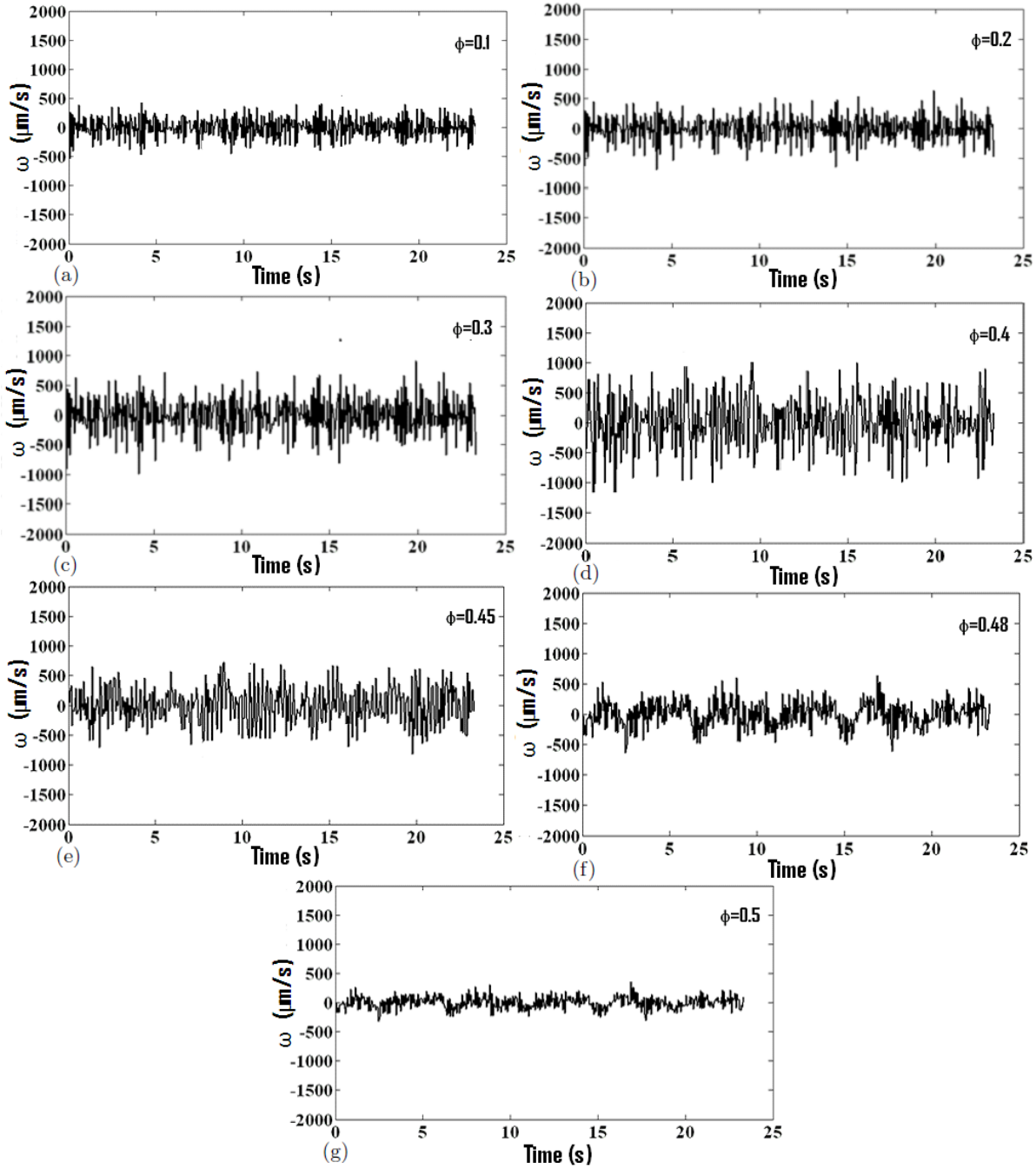

Figure 5.37: Time trace of vertical velocity of the interface for suspension of 500 μm particles in suspending fluid of viscosity 98 cP for the centerline velocity for all cases at the range of 0.0073 m/s. The particle concentrations in these cases were: (a) 10% (b) 20% (c) 30% (d) 40% (e) 45% (f) 48% (g) 50%.

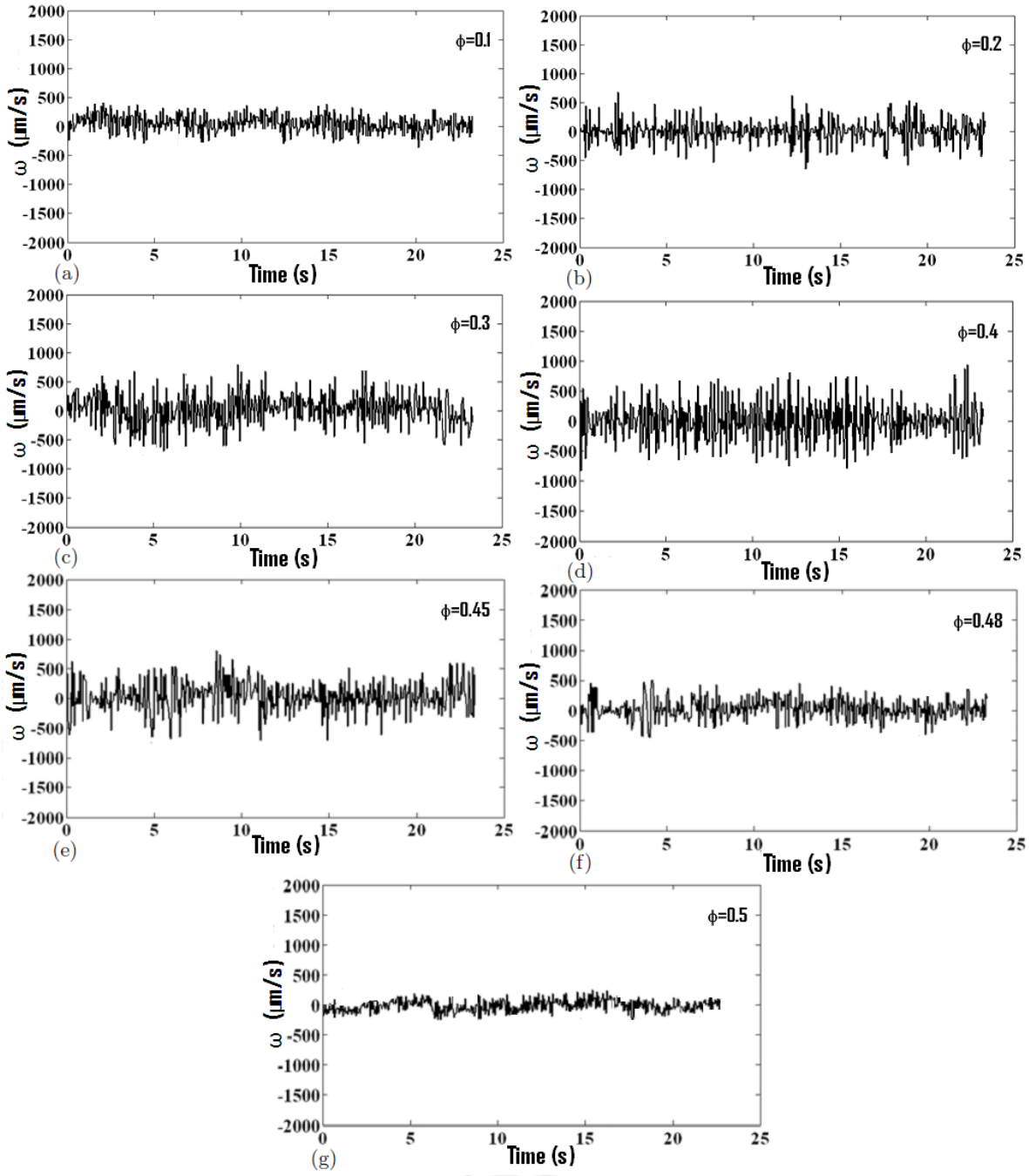

Figure 5.38: Time trace of vertical velocity of the interface for suspension of 500 μm particles in the suspending fluid of viscosity 204 cP for the centerline channel velocity for all cases at the range of 0.0073 m/s. The particle concentrations were (a) 10% (b) 20% (c) 30% (d) 40% (e) 45% (f) 48% (g) 50%.

As was the case for the interface height fluctuations, for a given concentration the root mean squared vertical velocity of the interface also appears to increase linearly with flow speed. This has been shown in Fig.5.39 through Fig.5.41. It is also clear that the suspension of larger particles exhibit larger velocity fluctuations at the interface. Similar was the case with the effect of viscosity of suspending fluid viscosity. A suspension with less viscosity produces larger vertical velocity fluctuations compared to that of higher viscosity. We would like to mention that it was desired to keep another parameter, i.e. surface tension of the suspending fluid same while studying the effect of viscosity. We were unable to get suspending fluids of same surface tension but different viscosities. However, the fluids which we have chosen have nearly similar surface tension values. The effect of viscosity is to dampen the fluctuations. When the particle concentration is small there were no significant particle-particle interaction and hence the fluctuations and surface perturbation is also small. As the particle concentration is increases particle-particle interactions produce a surface which is not only rough in topology but also executes rapid movement. At an optimum concentration the particle-particle interactions result into an interface which is having the highest corrugation (and hence the surface area). At much higher particle concentration the suspended particles are so close to each other that there free movement is restricted and they are bound to move with the bulk flow. This results into decreased surface corrugation and interface velocity in the vertical direction. From Fig.5.42, it can be clearly observed that the vertical velocity of interface is negligible for pure fluid but increases rapidly with particle concentration till optimum particle concentration is reached. These profiles are same for any particle size and any viscosity of suspending fluid. However, the surface corrugation is high for bigger particle size and low viscosity of suspending fluid as they are exhibiting the more interface perturbation. These results are of great significance in understanding the free surface area of the interface. It also suggests what particle fraction can produce maximum area so that the knowledge can be utilized in heat and mass transfer applications of concentrated suspensions. There are several applications in food processing and material processing industries where this knowledge is crucial. From the average height of the corrugated surface above the mean free surface, it can be easily estimated that an increase in interface area as high as 60% is possible.

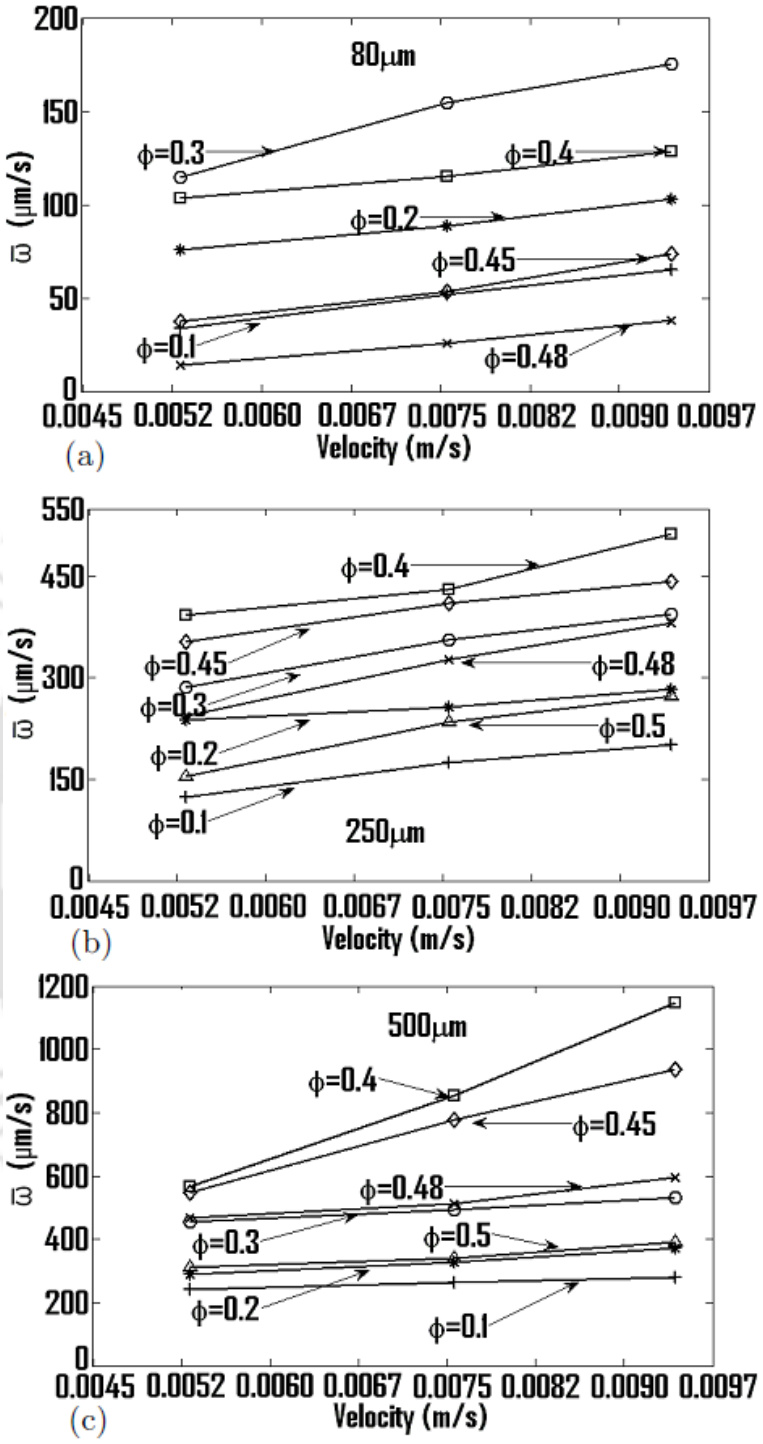

Figure 5.39: Time averaged vertical velocity of the interface at various flow speeds in the channel for various particle concentrations. The particle size in these cases were: (a) 80 μm (b) 250 μm (c) 500 μm.

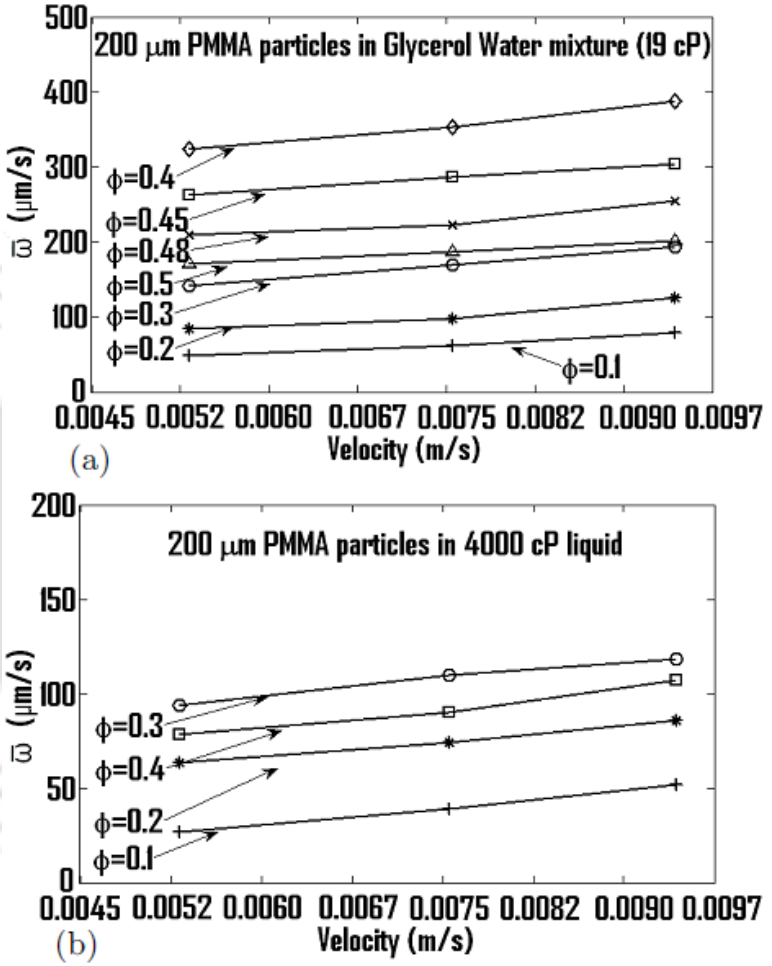

Figure 5.40: Time averaged vertical velocity of the interface at various flow speeds in the channel for suspension of 200 μm particles. The viscosities of suspending fluid in these cases were: (a) 19 cP (b) 4000 cP

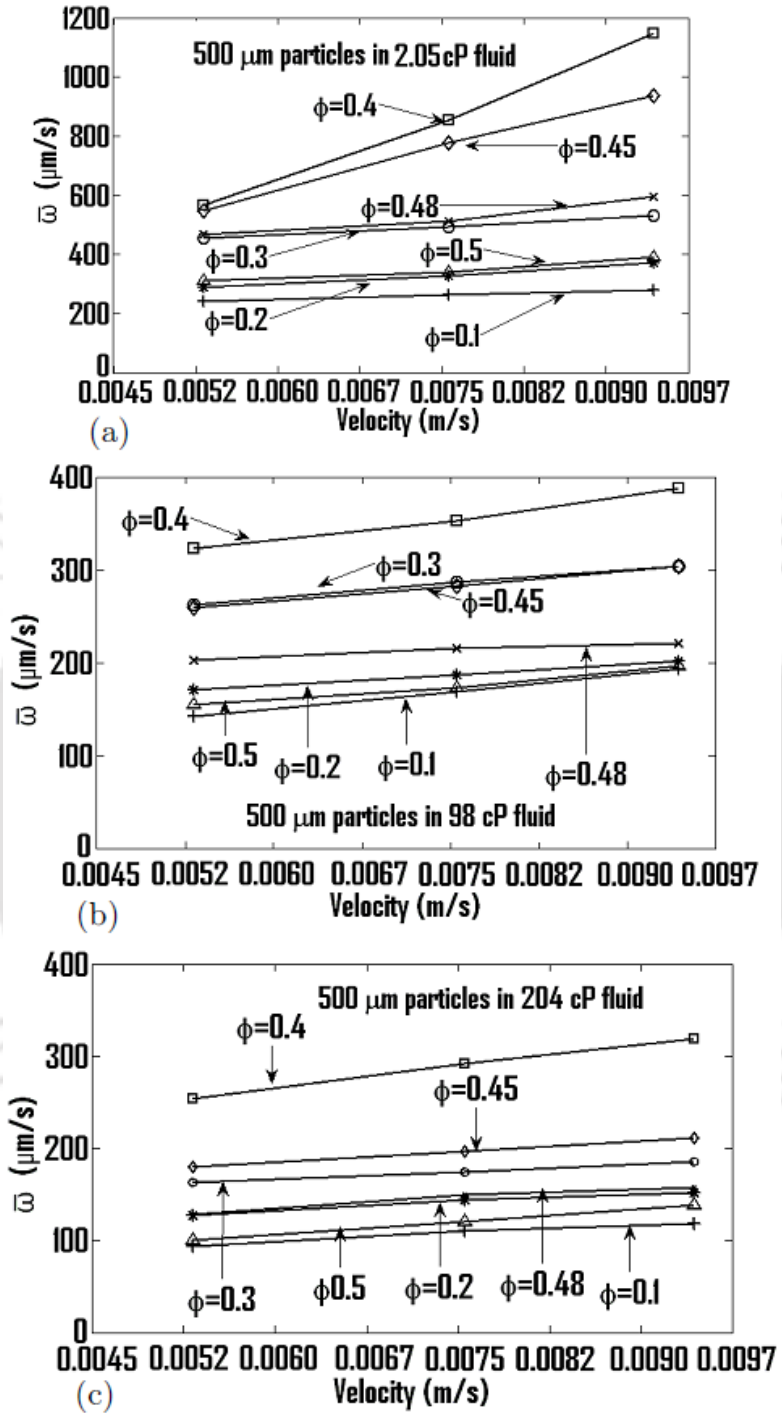

Figure 5.41: Time averaged vertical velocity of the interface plotted against flow speeds for various particle concentrations for suspension of 500 μm particles. The viscosities of suspending fluid were: (a) 2.05 cP (b) 98 cP (c) 204 cP

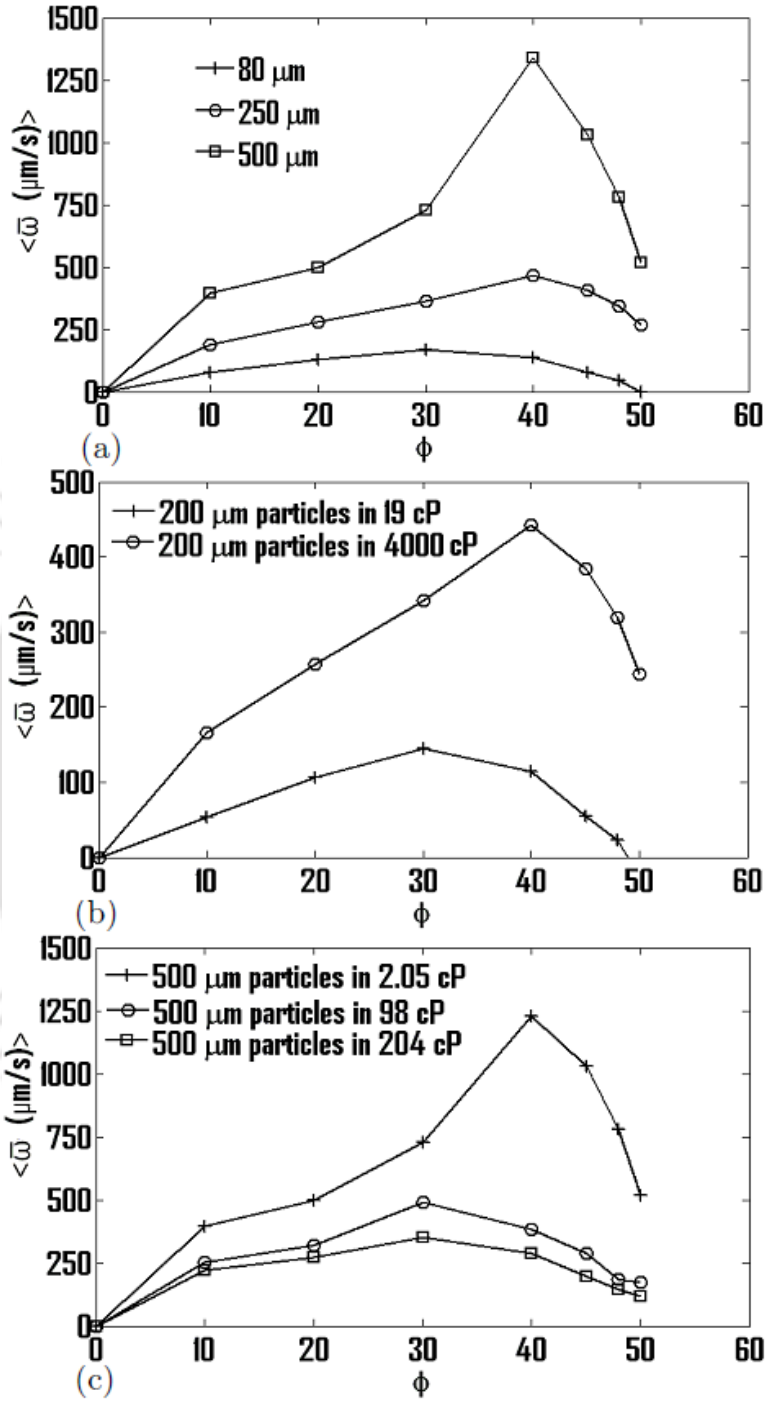

Figure 5.42: Variation of time averaged vertical velocity of the interface with particle concentration. (a) Effect of particle size (b) Effect of suspending fluid viscosity for 200 μm particles (c) Effect of suspending fluid viscosity for 500 μm particles.

5.4 CONCLUSION

The free surface flow of concentrated suspension in open channel was studied in this work. The location of the interface was determined from the gradient of image intensity of the tracer particles which floated on the free surface. The velocity in the bulk (beneath the free surface) was determined by PIV technique. The interface fluctuations are very small at low concentration of particles but increases with increase in particle concentration. There is an optimum particle concentration at which the interface fluctuation is the largest. Thereafter it decreases with increase in particle concentration. For a given concentration of particles the interface fluctuation increases linearly with the flow speed. The analysis of interface location and vertical velocity of the interface both showed the same trend. This indicates that during the free surface flow of concentrated suspensions the distortion of the interface develops resulting into corrugated surface. Due to this corrugation the interface area also changes. These phenomena is same for any of particle size and suspending fluid viscosity but the values are more for bigger particle size and low viscosity of suspending fluid suspension. The interface fluctuation or surface corrugation does not affect the bulk velocity profile beneath to the free surface (-*z* direction). The results from this study are very useful in predicting the interface are in such systems as in many applications it is the interface where heat and mass transfer plays an important role in material processing.

CHAPTER 6

FREE SURFACE FLOW OF BI-DISPERSED SUSPENSION IN ROTATING CYLINDER

6.1 INTRODUCTION

Suspension of solid rigid particles in viscous fluid present in rotating cylinder has many practical applications in chemical, metallurgical, plastics, pharmaceutical and food processing industries. For example, mixing of different sizes of particles dispersed in fluid medium is carried out in a rotating drum to prepare pastes for manufacture of composite membranes. Cement kilns also employ rotating drums for mixing of particles. Pan coater (which is a rotating tube device) is commonly used in pharmaceutical industries for coating different sizes of capsules and tablets. To improve the coating performance of such devices it is essential to understand the movement of particles and fluid inside the pan coater (Pandey and Tutron, 2005). In mixing operations it is desired that the particles remain homogeneously dispersed and do not segregate (Matson *et al*., 2005). On the other hand the phenomenon of particle segregation also provides an easy way of separating the particles by taking advantage of segregation caused by simply rotation of the cylinder. In some recent studies, it has been observed that suspension of mono-dispersed neutrally buoyant particles in a partially filled horizontally rotating cylinder segregates in to bands of particles that are separated by regions of pure fluid (Tirumkudulu *et al*., 1999; Tirumkudulu *et al*., 2000). In another experiment, Timberlake and Morris (2002) observed alternate bands of relatively concentrated and dilute particle fraction along the axis of a partially filled inclined concentric cylinder. The number of bands was found to increase with the rotation speed of the cylinder. In these studies, the fluid-air interface is thought to be important for axial segregation as no segregation was observed when the tube was fully filled with the neutrally buoyant particles. Subsequent to these experiments, Breu *et al*. (2003) studied the flow of non-neutrally buoyant suspension of mono-dispersed in a completely filled cylinder. They observed similar instabilities and

pattern formations at higher rotation speed where centrifugal forces on the particles dominated over other forces. The reason for this observation was thought to be the density difference between the fluid and particles. Matson *et al*. (2006) further demonstrated that a suspension of non-colloidal settling particles in a completely filled horizontal cylinder demonstrates a rich array of concentration and velocity patterns at various rotation rates. In case of non-neutrally buoyant, mono-dispersed suspension the particles approach in downward side and expel in upward side and the formation of clusters depends on the rotation speed (Pan *et al*., 2007). Kalyankar *et al*. (2008) have also observed unique concentration and velocity patterns in a horizontally rotating cylinder completely filled with a mono-dispersed suspension of non-Brownian particles. To our knowledge there are no reported studies on suspension of bi-dispersed non-neutrally buoyant particles in rotating cylinder. In most of the practical applications the suspensions often have particles of different sizes. This motivated us to study the segregation pattern for bi-dispersed system. The initial distribution of particles in bi-dispersed suspension of non-neutrally buoyant and neutrally buoyant present in a rotating cylinder is shown in Fig.6.1.

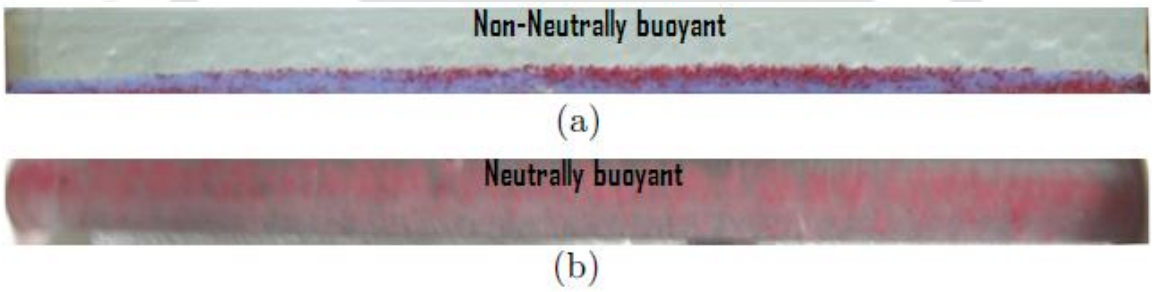

Figure 6.1: Photographs showing initial distribution of (a) Non-neutrally buoyant suspension (b) Neutrally buoyant suspension. The red color shows bigger particles and blue color that of smaller particles)

There are several studies on the axial segregation of bi-modal granular mixtures (Stevans, 1998; Khakhar *et al*., 1996) but not many on the particulate suspensions. Hill and Kakalios (1994) reported on the segregation of binary mixture of glass beads into sharp bands of alternating large and small particles along the axis of rotation. They have shown that the segregation bands were visible at higher angular speed which disappeared when the angular speed was decreased. They also noted that if the granular particles have different dynamic angle of repose, then a drift current will develop along the axis of rotation which tends to separate them into the two sizes. The particles with various bi-diversity were classified based

on their segregation behavior as per the following three categories; no segregation at any rotation speed, non-reversible axial segregation and reversible axial segregation (Hill and Kakalios, 1995; Hill *et al*., 1997). In our work, on particulate suspensions, the bi-dispersed particles were chosen which comes under the first category i.e., no segregation at any rotating speed under dry granular rotation. Jain *et al*. (2001) reported alternate band formation in wet granular media or slurries as well as for dry granular mixtures. They found that particle segregation in dry granular mixture is significantly faster compared to that in suspensions in liquid media. These works have shown that for bi-dispersed mixture of granular particles the axial and radial segregation of small and large particles occurs when the static angle of repose of these particles is unequal. The particles undergo a solid body rotation about the cylinder axis. The particles experience convective motion due to the shear flow and a random motion resulting from particle-particle collisions. The mechanism of pattern and size segregation in suspensions can be quite different as the hydrodynamic forces play an important role here which are absent in granular mixtures.

Gans and Zupanski (1998) have described a system for generation of vortices in rapidly rotating cylinder partially filled with water. They performed experiments in a regime dominated by inertial forces and obtained results which are independent of viscosity and surface tension of the fluid. Krasnopol *et al*. (2003) have shown eight different flow patterns in pure fluid as well as granular materials rotating in a partially filled horizontally rotating cylinder. It has been shown in the above mentioned studies that the viscous drag, gravitational and centrifugal forces play a vital role in segregation. Lee and Ladd (2005) have performed numerical simulations of non-neutrally buoyant particles in rotating cylinders and observed regular bands of high and low concentration along the symmetric axis as observed in the experiments (Matson *et al*., 2003; Thomas *et al*., 2001). Despite their industrial importance there are no reported studies on the size segregation of bi-dispersed suspensions in horizontally rotating cylinder. There are several factors which contribute to the initially of suspension in rotating cylinder and this instability leads to axial segregation of smaller and bigger particles forming a number of alternate bands.

6.2 DETAILS OF EXPERIMENTAL SETUP

The experimental setup used in this study is shown in Fig.6.2. It consists of a 20.7 cm long horizontally aligned transparent acrylic tube with inner diameter of 1.2 cm. Both ends of the tube are closed with rubber plugs and mounted on the two ends by precision bearings for

smooth rotation. One end of the cylinder is connected to DC servo motor through flexible coupling. The rotational speed of the motor can be varied using a variable DC power supply. To capture the particle motion and their spatial distribution along the axis of the tube, we used CCD camera (PCO Pixelfly), which was placed on the top of the rotating cylinder. A cold light source (Thorlab) was used to illuminate the suspension in the tube. To show the qualitative results good moving come still camera was used. Both neutrally-buoyant and non neutrally-buoyant suspension's studies were conducted in the same experimental setup only.

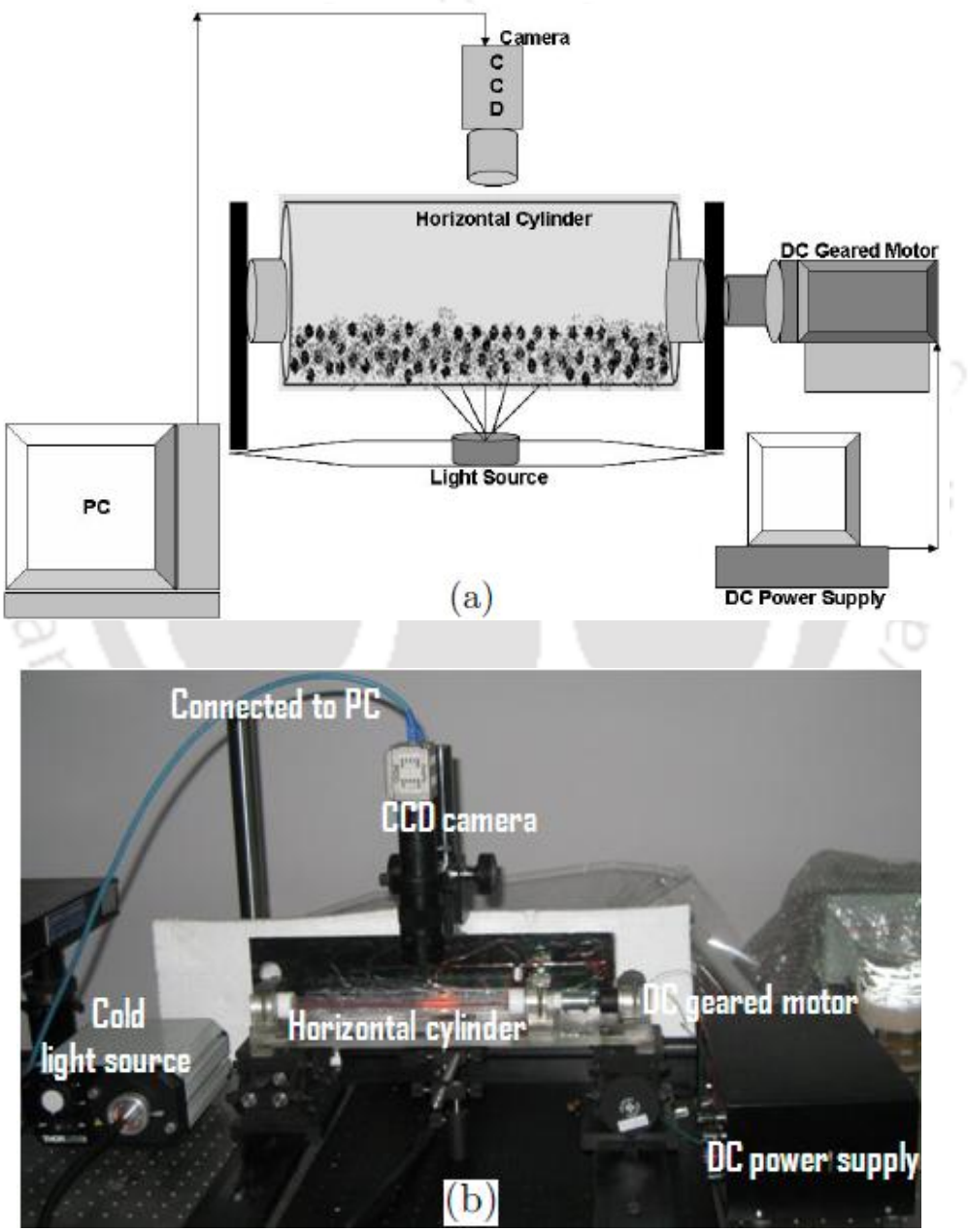

Figure 6.2: (a) Schematic diagram of the experimental setup of horizontally rotating cylinder, (b) Photograph of the experimental arrangement.

6.3 NON-NEUTRALLY BUOYANT SUSPENSION IN ROTATING CYLINDER

Non-neutrally buoyant suspension of bi-dispersed non-colloidal particles in viscous fluid rotating in a horizontal cylinder displays in-homogeneities in particle distribution with alternate bands of high and low particle concentrations along the symmetric axis of the cylinder. Experiments were carried out to characterize the axial segregation in bi-dispersed suspension at various filling fraction and rotation speed of cylinder. The mixture of same particles in absence of any suspending fluid did not show any segregation. However, in case of particles suspended in water it was observed that the rate of segregation increases with increase in filling fraction. Once the particles get segregated along the full length of the cylinder, these bands start to migrate along the tube axis finally merging to give wider bands. For a given filling fraction the rate of segregation increases with the angular speed of the rotating cylinder. When the tube is partially filled the particle segregation is observed at higher angular speed, whereas in fully filled case the segregation starts at much lower rotation speed for the same concentration of particles. The segregation pattern changes as the rotation speed is increased. At higher speed, the centrifugal force dominates over gravitational and viscous drag forces and this result into completely different segregation patterns. We have also analyzed the evolution of concentration profile from the image analysis of the particles. The suspension was prepared by dispersing spherical PMMA particles (Polysciences) in water. In our studies on bi-dispersed suspensions, the spherical particles comprised of equal volume percentage of small and large particles. The mean diameter of smaller particles (a_1) was 203 µm and that of larger particles (a_2) was 580 µm. Thus the ratio between the particle diameters (d_p) was found to be 2.8. The particle density was 1.18 g/cc and suspending fluid density (ρ_s) was 0.9982 g/cc at 25°C. The density difference between the particle and suspension ($\Delta\rho$) was found to be 0.1818 g/cc. The viscosity of the suspending fluid (η) was measured to be 1 cP at 25 °C. The particle size distribution for both bigger and smaller particles is shown in Fig.6.3.

The Reynolds numbers for this system can be defined in four different ways. These are based on 1) particle radius (a) and the settling velocity, 2) particle radius and angular speed of rotation (Ω), 3) cylinder radius (R) and the settling velocity and 4) cylinder radius and angular speed of rotation. As our system has two different sizes of particles (therefore different settling velocities), the Reynolds number based on the angular speed of rotation and

cylindrical radius is the most appropriate to classify the flow regimes. The segregation pattern is dependent on the fill fraction and size of particle and hence, there is more than one length scale present in our system to define the Reynolds number. However, to study the effect of rotation speed on particle segregation we chose to define the Reynolds number based on the cylinder radius and angular speed of rotation and is defined as $R_{ew} = R^2\Omega\rho_s/\eta$. Experiments were conducted for dry particles (in absence of suspending fluid), partially filled and fully filled suspension in the horizontally rotating cylinder. Each experiment was run for 24 hr to observe the continuous change in the segregation pattern of particles along the axis of the tube. To examine the role of free surface on the segregation, the experiments were conducted for both fully filled and partially filled tube. The filling fractions studied were 25%, 50%, 75% and 100% respectively. The experiments were conducted from very low rotation speeds to a maximum of 219.2 rpm at which the Reynolds numbers (R_{ew}) varied from 0 to 905.6. At low Reynolds number, gravity dominates over other forces whereas at high Reynolds number the centrifugal forces dominated on the particles. Between these two extremes, we observed a number of flow patterns, particle distribution and band formation. To characterize the segregation behavior, we have conveniently divided the experiments into three separate regimes. The definitions of these regimes are purely based on the observation of particle dynamics and segregation patterns. For our system of settling particles in water it was observed that due to viscous drag the particles move up along the tube wall and then fall back due to gravity. Since the particles are heavier than fluid, the resultant of gravity and buoyancy force will always be downward. If the fluid was very viscous, it is expected that the particles would have been carried along with the fluid in full rotation. Therefore, we felt appropriate to call this as gravity dominated regime to differentiate it from high speed flows where centrifugal forces spun the particle along the tube wall in full circle. For the rotation rate $N <$ 40 rpm, the particles motion is confined in the bottom of the cylinder without rising up along the tube wall. For 40 rpm $<N <$ 120 rpm which we conveniently call partially centrifugal force dominated regime the particles were observed to move up to the top of the tube along the tube wall and then fall back. The partial rise of the particles is due to centrifugal forces acting on it. Near the top of the tube, gravity overcomes the viscous drag and centrifugal force and as a result the particles fall back to the bottom of the tube. For $N > 120$ rpm, both smaller and larger particles were spun in full circle along the tube wall. In this regime, the centrifugal force dominates over viscous drag and gravity.

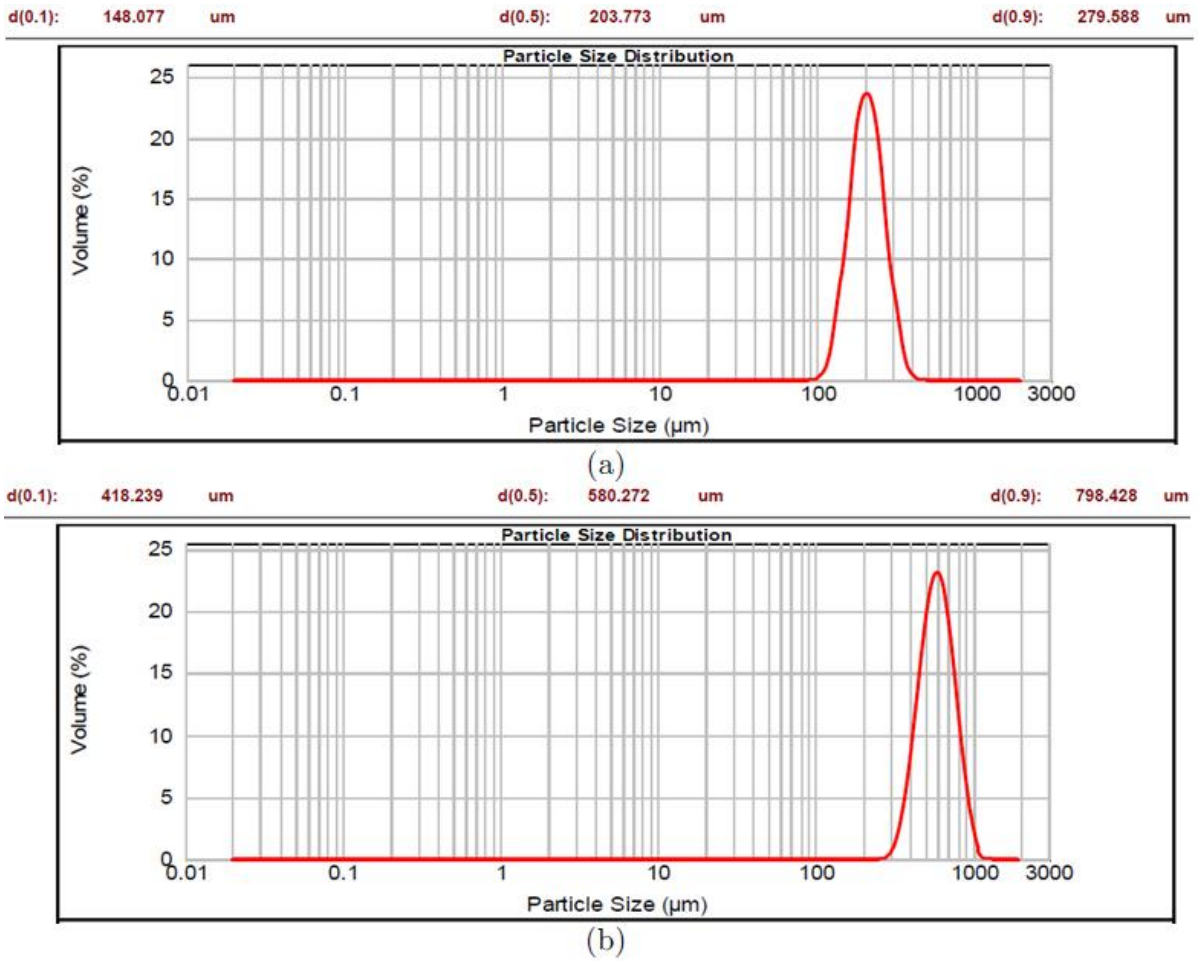

Figure 6.3: Particle size distribution of PMMA particles for (a) 203 μm (b) 580 μm.

6.3.1 Results and discussion

We first conducted experiments with the bi-dispersed mixture of dry granular PMMA particles to see if these type of particles exhibit size segregation. In general, the granular mixture segregates into bands when small differences in size, density or shape of particles exist. Other factors such as surface roughness of the particles or friction between the wall and the particles may also influence the segregation behavior. Hill and Kakalios (1994) claimed that segregation does not occur when smaller and larger particles obey equality in dynamic angle of repose. If the two different sized particles have different dynamic angle of repose, then a drift current will develop along the axis of rotation which tends to separate the particles according to their sizes. The drift flux is expressed as $J_d = \beta_1 \partial C_1/\partial z$. Here C_1 is the concentration of larger particles, β is a function of the height variation along the rotating axis (z), and can be expressed as a monotonic function of the difference between the dynamic angle of repose ($\Delta\psi$). For equal angle of repose of the two types of particles the value of β_1

will be zero, which predicts no segregation (Hill and Kakalios, 1997). The PMMA particles used in our study were spherical (sphericity = 0.97) and smooth. Though the sizes of particles were different, the density and angle of repose was expected to be identical. As expected we did not observe any size segregation even after 24 hours of continuous rotation. Though, the friction between the particles and cylinder wall may also be a reason for segregation. However, it appears in our system there was no sufficient friction between the smooth spherical particles and smooth rotating cylinder. In the following section, we present results for suspension of bi-dispersed PMMA particles in water. As explained above, we have divided our study into three different regimes based on the observation of segregation patterns.

6.3.1.1 Axial segregation in gravity dominated regime (N < 40)

A. *Fully filled cylinder*

The suspension was prepared by mixing equal volume percentage of smaller and larger particles. The larger particles were colored in black dye whereas the smaller particles are left in its natural transparent white color. After mixing the particles in water the suspension was quickly transferred to the tube. The volume percentage of particles in the tube was 8.08 %. The cylinder was rotated at constant speed and the evolution of particle concentration was monitored for 24 hours. The experiments were carried out for various rotation speed of the cylinder (1 to 40 rpm). The corresponding Reynolds number in this regime varied from 5.37 to 157.48. At low rotation rates, it was observed that both smaller and larger particles tumble up and down in the bottom of the cylinder. In this regime, the viscous drag force moves up the particles and then under action of gravity the particles fall downward. Soon after the start of rotation the larger particles form band at both end of the tube. After sometime, such bands of both larger and smaller particles start appearing in the whole tube along the horizontal axis at the bottom of the cylinder. The few color photographs of segregation patterns at various rotation rates of gravity dominated regime is shown in Fig.6.4 to show a clear view of segregation pattern. The photographs of segregation patterns for over all gravity dominated axial rotations are shown in Fig.6.5. Figure 6.5a shows the initial distribution of particles in the tube. At low rotation (N < 3 rpm), there was no segregation even after 3 days of continuous rotation (Fig.6.5b). At slightly higher speed (N = 4.1 rpm), segregation patterns were clearly visible in the cylinder (Fig.6.5c). The segregation patterns were more distinct for higher rotation rates (N > 4.1 rpm) which can be seen in the Fig.6.5 (d-n). The particles in a

rotating suspension experience viscous drag, gravity and buoyancy forces. At low Reynolds number, the viscous drag is proportional to particle radius (a) and the balance of gravity and buoyancy force is equal to $\frac{4}{3}\pi a^3 \Delta\rho g$. At minimum fluidization, the viscous drag overcomes this net force due to gravity and buoyancy. Since the density difference is same for both larger and smaller particles, the smaller particles will travel larger distance along the tube compared to the larger particles. This relative movement of larger and smaller particles leads to instability and size segregation similar to one observed in binary mixture of dry granular particles. In dry granular mixtures in rotating drums, this instability is caused by the difference in frictional forces on larger and smaller particles due to difference in dynamic angle of repose (Hill and Kakalios, 1995). When we compare the number of bands at various rotation rates after 24 hours of observation an interesting fact is clearly visible. The number of bands decrease as the rotation speed is increased and as a result the band widths are larger. This is due to merging of adjacent bands and we describe this phenomenon in section C. At 38.1 rpm (Fig.6.5o) the number of bands reduced to just two (one small and one large). However, when the rotation was continued further the bigger and smaller particles again started dispersing. As noted above the larger particles always occupy the end position of the tube. In Figure 6.6 we have shown the images at one end of the cylinder at different times. The band growth with time is clearly visible in this photograph.

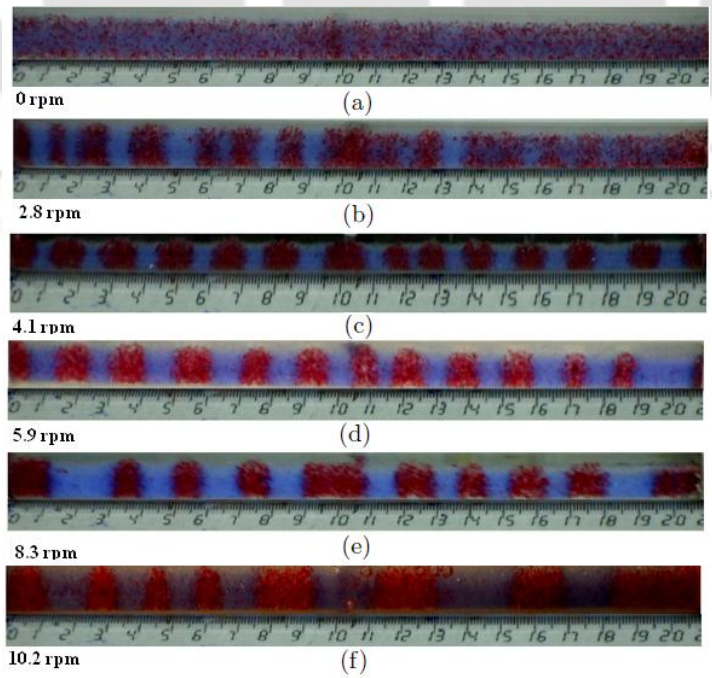

Figure 6.4: Few segregation pattern in fully filled horizontally rotating cylinder in the gravity dominated regime. Red regions show bigger particles and blue regions smaller particles.

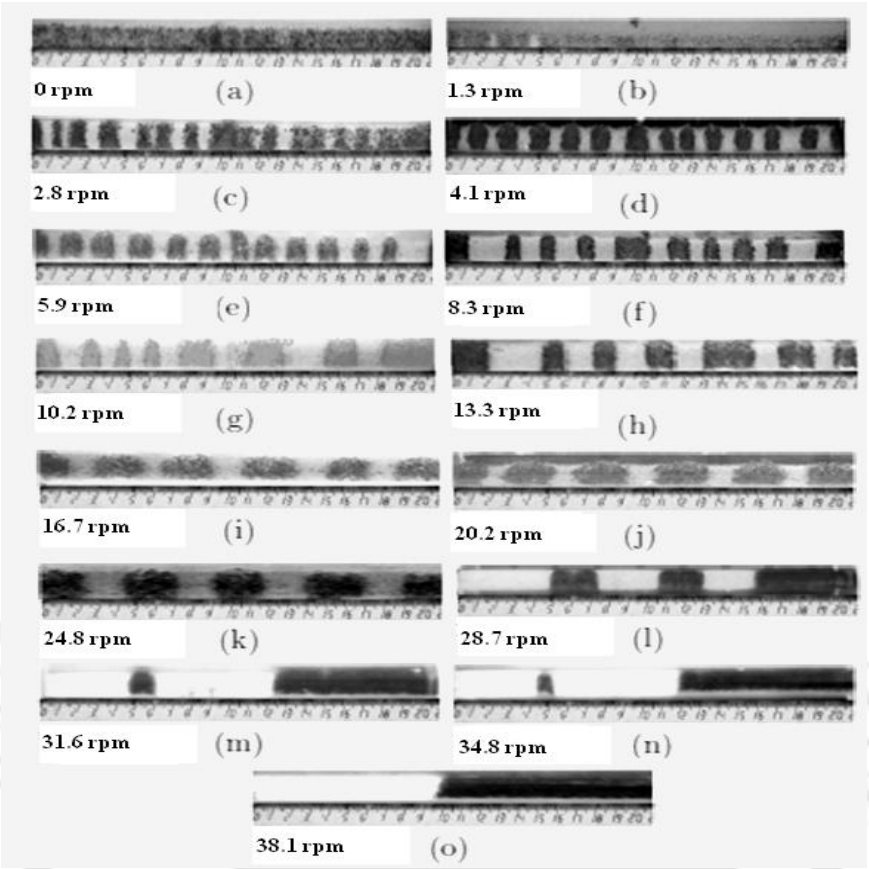

Figure 6.5: Complete segregation pattern in fully filled horizontally rotating cylinder in the gravity dominated regime. Black regions show bigger particles and white regions smaller particles.

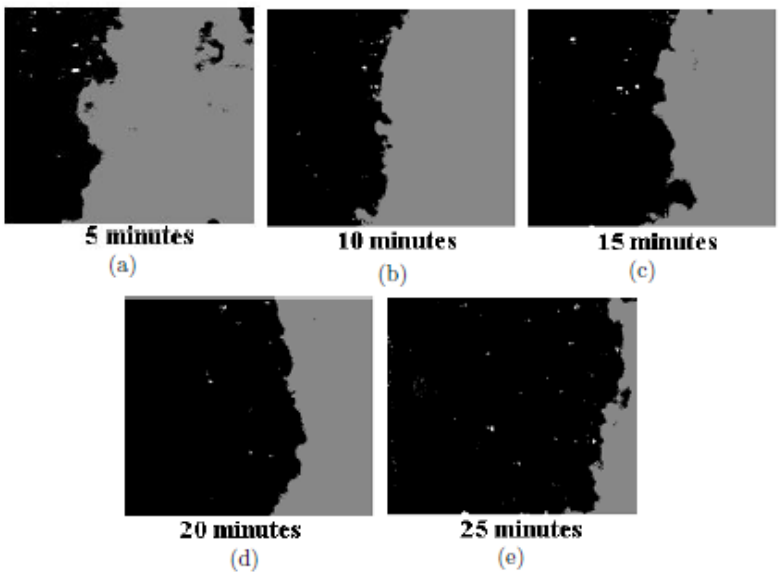

Figure 6.6: The growth of band of larger particles at various stage of rotation. The angular speed of rotation was 4.1 rpm at which the Reynolds number was 16.94.

B. *Partially filled cylinder*

In order to explain the effect of free surface on the axial segregation, we have carried out the studies for three different filling fractions, 25%, 50% and 75%. For all the three fill fractions, the volume concentration of particles in the suspension was maintained at 8.08%. This was the same concentration in the case of fully filled cylinder. It is observed that the segregation rate for partially filled case is significantly lower than the fully filled case. At 75% filling fraction the complete segregation was observed at 5.9 rpm which is shown in Fig.6.7a. However, it took longer time (nearly 5 hours after the start of rotation) whereas for the completely filled tube the complete segregation of bands was observed within an hour at the same rotation rate. At lower filling fraction (50 %), the complete segregation was obtained after 10 hours (Fig.6.7b) whereas for 25% fill fraction the complete segregation was not achieved even after 24 hours of observation as shown in Fig.6.7c. As explained in the earlier section, the net forces on the bigger and smaller particles are different as a result these particles undergo relative separation which grows continuously until clear bands are formed. In case of partially filled case, the relative separation in each revolution of the cylinder is smaller compared to the fully filled case. It was observed that for low rotation rates the particles remain below the air-water interface and the maximum distance a particle travels is from the bottom of the tube to the upper level of water. As we reduce the fill fraction the height of the water level also reduces. This is why we observe that the segregation rate decreases as the fill fraction is decreased. As observed in the case of fully filled cylinder, the rate of segregation increases with the rotation rate for partially filled case also. For 75 % fill fraction, we noticed that when the rotation speed of the tube was increased further (N = 13.3 rpm) some of the smaller particles (in a thin film at the cylinder wall) move along the wall of the tube completing full rotation and during downward plunge to the bulk water dispersed the clusters of bigger particles. Due to this action no clear band was observed. The same action is attained at lower rotation speed (N = 10.2 rpm) for 50 % fill fraction. For 25% filling fraction this behavior was observed at even lower speed (N = 8.3 rpm).

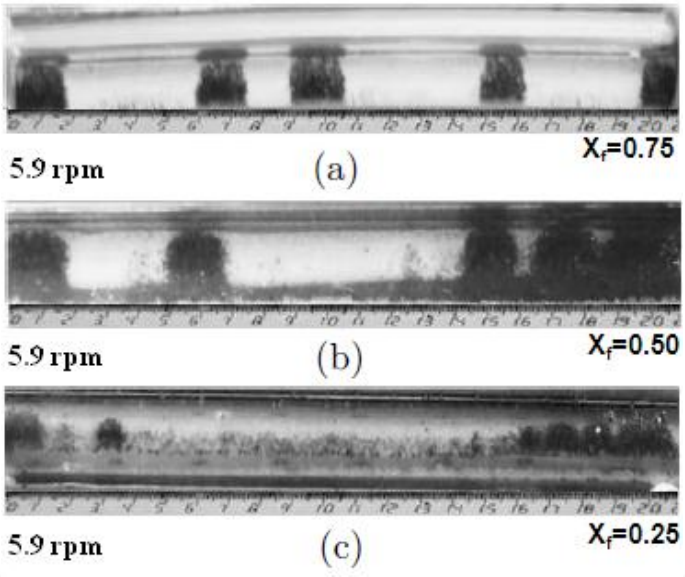

Figure 6.7: Band formation in partially filled horizontally rotating cylinder in the gravity dominated regime. (a) Segregation pattern at 75% filling fraction. (b) Segregation pattern at 50% filling fraction, (c) segregation pattern at 25% filling fraction. The rotation rate for all the three cases were 5.9 rpm at which the Reynolds number was 24.386.

C. *Particle concentration and band migration*

Digital image analysis is used to study the particle concentration distribution along the axis of the tube by placing a CCD camera on the top. The cold light source which was placed on the bottom easily passed though the smaller (transparent) PMMA particles whereas the bigger particles which were dyed black obstructed the light. The digitized image consisted of white and black pixels whose intensity varied between 0 and 255. This allowed us to correlate the particle distribution from the intensity profile of the images. Figure 6.8 shows the intensity variation along the axis of the tube normalized by the average intensity value (I_0) at the start of rotation. The peaks indicate the smaller particles whereas valleys are representative of larger particles. The initial distribution is homogeneous and we observe nearly uniform distribution (Figure 6.8a). At finite rotation rate (Fig.6.8b), we observe that the mean intensity values are higher. This is due to relatively higher concentration of smaller particles at the top. The bigger particles remain below the smaller ones. As the rotation rate is increased we observe clear peaks and valleys corresponding to the bands of smaller and bigger particles respectively (Fig.6.8c-j). These observations are similar to the photographs in Fig.6.5. The corresponding intensity profile for partially filled case is shown in Fig.6.9.

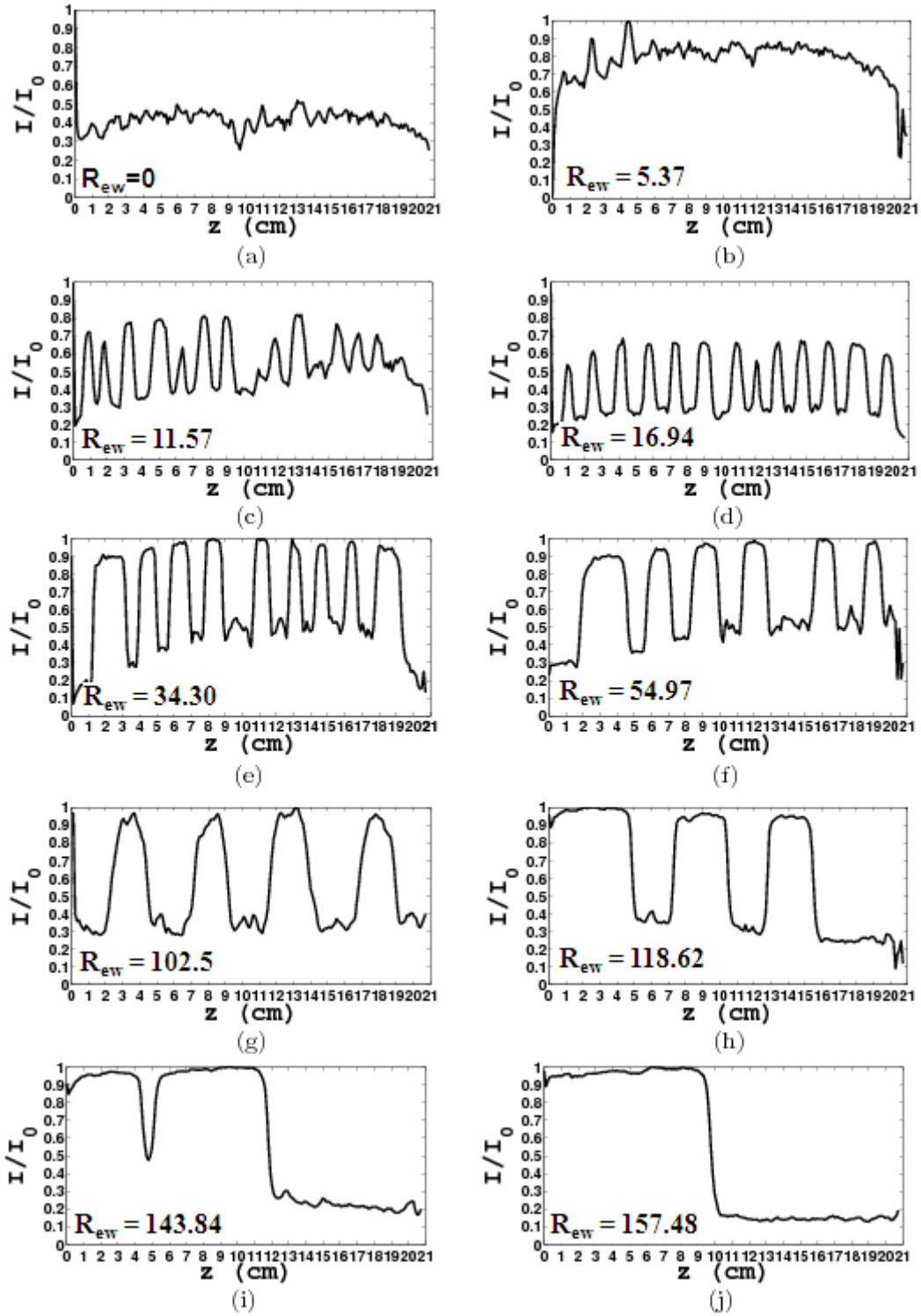

Figure 6.8: Normalized intensity profiles along the axis of the fully filled cylinder in gravity dominated regime. The peaks correspond to presence of smaller particles and the valleys for bigger particles.

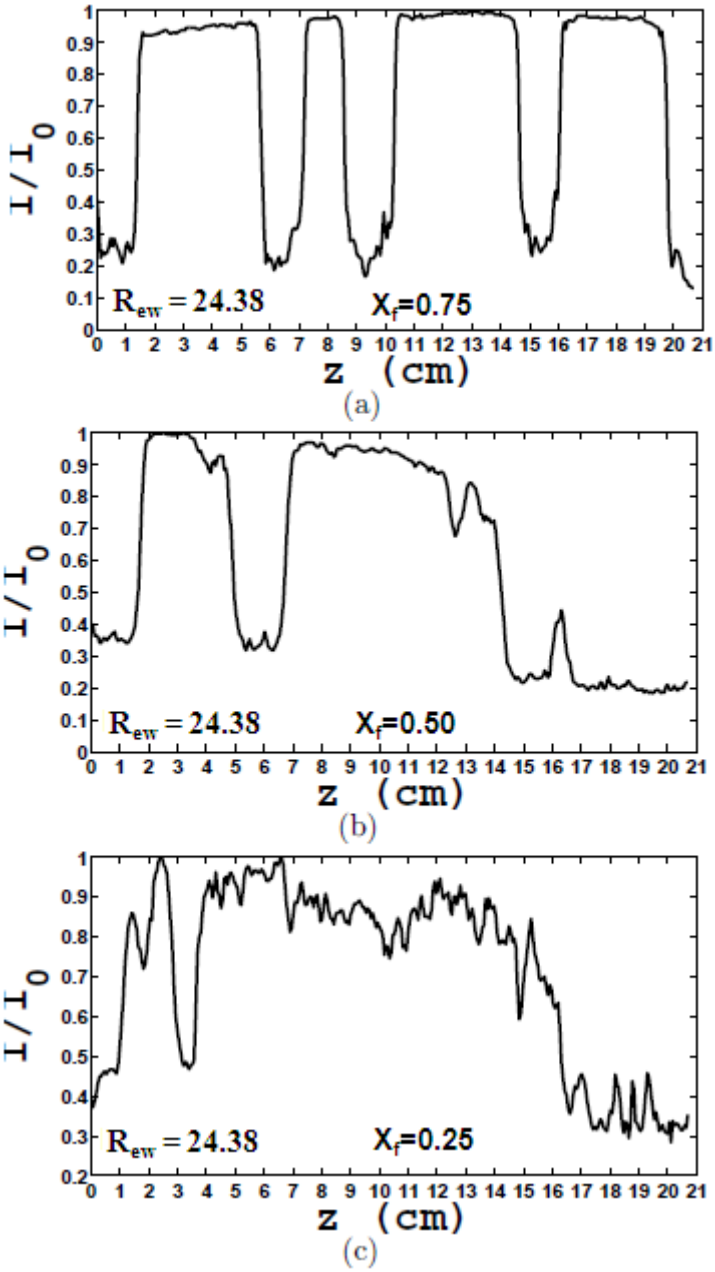

Figure 6.9: Normalized intensity profiles along the axis of the partially filled cylinder in gravity dominated regime. (a) 75% filling fraction. (b) 50% filling fraction. (c) 25% filling fraction. The rotation rate for all the three cases were 5.9 rpm.

When the cylinder is subjected to rotation, two stages are observed during the segregation process. In the first stage, both bigger and smaller particles started the formation of band at the two end of cylinder. Once the whole length of the cylinder got segregated into bands of smaller and bigger particles, in the second stage these bands started to migrate towards each other, i.e. bigger particles from one band moved to adjacent band of bigger particles. Similarly, the smaller particles from adjacent bands also joined together and formed a single band of larger width. Hence, the final number of segregated bands decreased but width of the bands increased. In Fig.6.10 we have shown images at different time intervals to show the dynamic nature of the band migration. It can be clearly observed that the central band of bigger particles slowly moves towards the right to the adjacent bands of bigger particles. After some time, this band completely merges with the adjacent bands and due to enrichment of particles the band width increases. It can be observed from Fig.6.11a that band formation process starts as soon as the rotation starts. After some time the alternate bands of bigger and smaller particles are formed along the full length of the tube. The dynamics thereafter is dependent on the rotation speed. For low rotation speeds the steady state persists for longer time during which we did not observe any change in number of bands. However, at higher speeds it was observed that the bands start moving axially. These bands of bigger and smaller particles join to form larger bands. As a result, we observe decrease in number of bands. Table 5.1 summarizes the evolution of band formation at various rotation rates. In Fig.6.11(b) we show the evolution of band with time for different fill fractions. The average intensity of the band closest to the end of the cylinder (normalized by the initial average intensity value at the start of rotation) is an indirect measure of particle concentration in a band. It is observed that that the rate of segregation as well as band migration increases with increase in filling fraction. When the tube is fully filled, the segregation is achieved quickly but the decay in band width due to migration is also quicker compared to the partially filled cases. Fig.6.12a shows that the number of bands at steady state (after band migration is complete) decreases with increase in the rotation speed of the cylinder. At higher rotation rate, the bands are formed more quickly but soon they join to form bands of larger widths. The similar behavior is also observed for partially filled cylinder but at relatively higher rotation speeds. The plot of average band width versus angular speed of rotation of the fully filled cylinder is shown in Fig.6.12b. The band widths of both bigger and smaller particles increase with rotation speed due to band migration. At higher speed, the band width increases but total number of bands decrease. We have earlier observed that two ends of the cylinder are always occupied by the

band of larger particles. In Fig.6.13 we have displayed the width of the band of larger particles at various filling fractions. The rotation speed in all the cases was same (N = 4.1 rpm). It was observed that as the filling fraction increases the band width decreases. The high segregation rate in fully filled case resulted into more number of bands. However, their band width was also smaller. Whereas, in partially filled case the segregation takes longer time, and the band width is also large. Figure.6.14a shows the growth of band width with time for different filling fractions. For lower filling fraction the time taken for complete segregation is long but end-band width is larger compared to that of higher filling fraction as shown in Fig.6.14b. The decrease in the band width is almost linear with filling fraction.

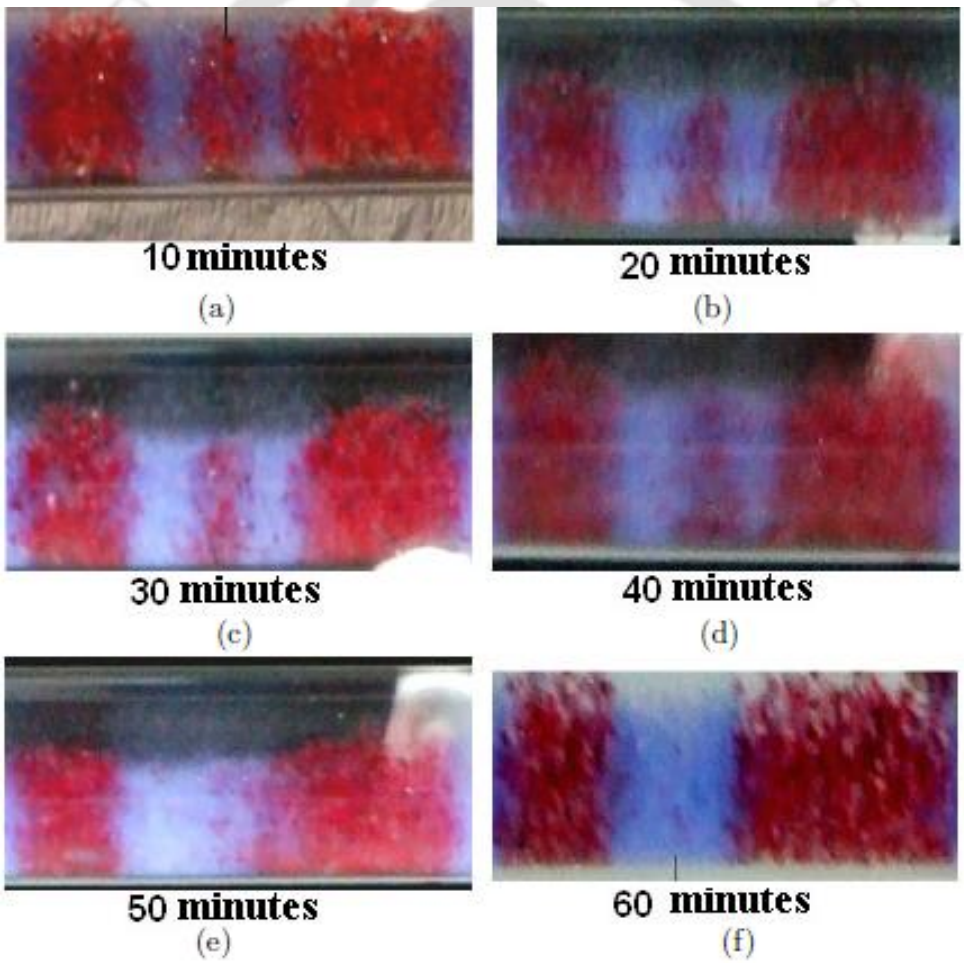

Figure 6.10: Band migration in axial direction shown at various stages of rotation. The smaller band (blue) of larger particles (red) in the center slowly moves to the right to join adjacent band. The angular speed and Reynolds number was same as in Fig. 6.6.

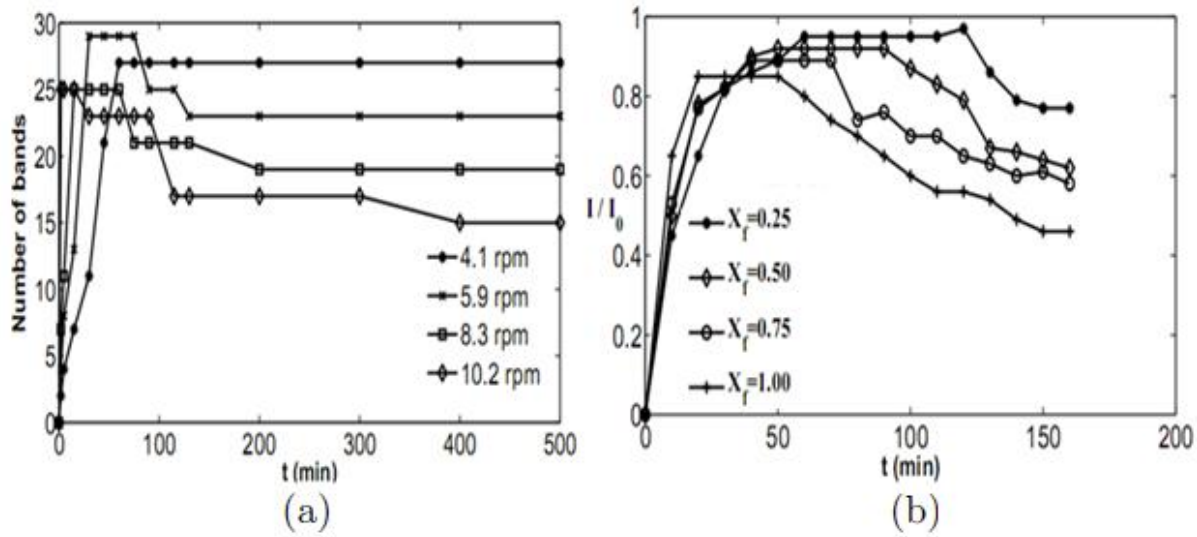

Figure 6.11: (a) Growth rate of band formation at various rotation speeds for fully filled cylinder (b) Growth of particle concentration (evaluated from the intensity of images) at different filling fractions. The angular speed and Reynolds number was same as in figure 6.2.

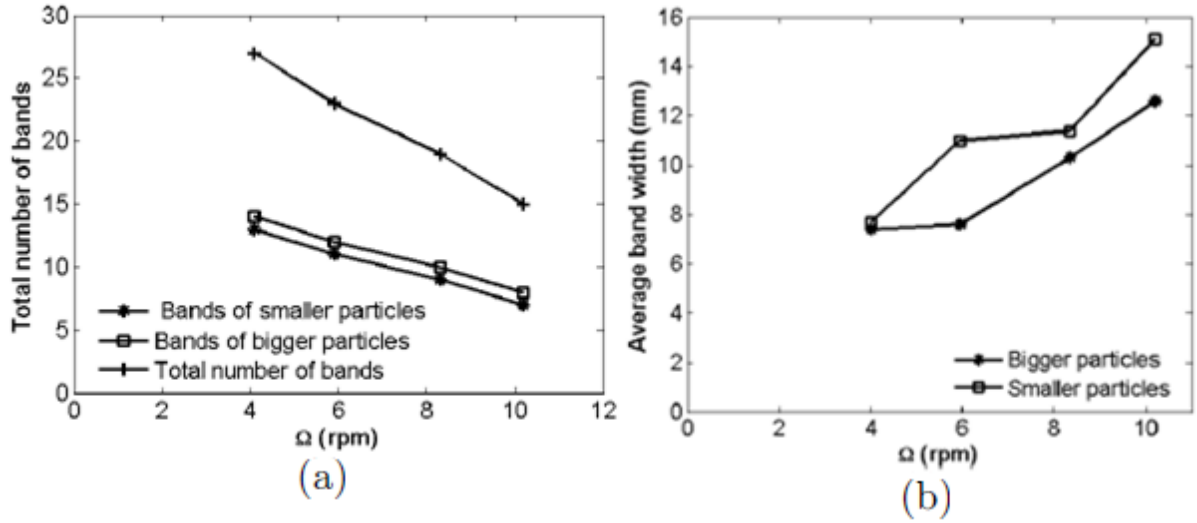

Figure 6.12: (a) Plot of total number of bands Vs rotation speed for fully filled cylinder (b) Growth of average band width with rotational speed of the cylinder.

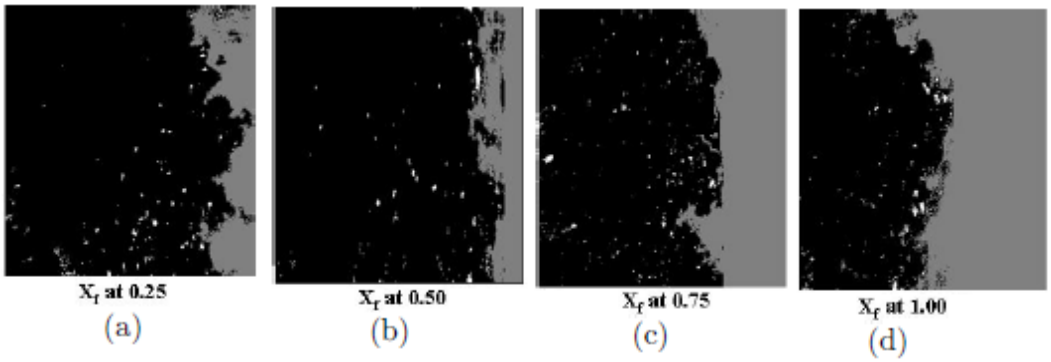

Figure 6.13: Photograph showing the band width of larger particles for various filling fractions (a) 25% (b) 50 % (c) 75% (d) 100%. The images at one end of the cylinder were taken after the complete segregation of particles. The rotational speed of cylinder was 4.1 rpm in all the cases.

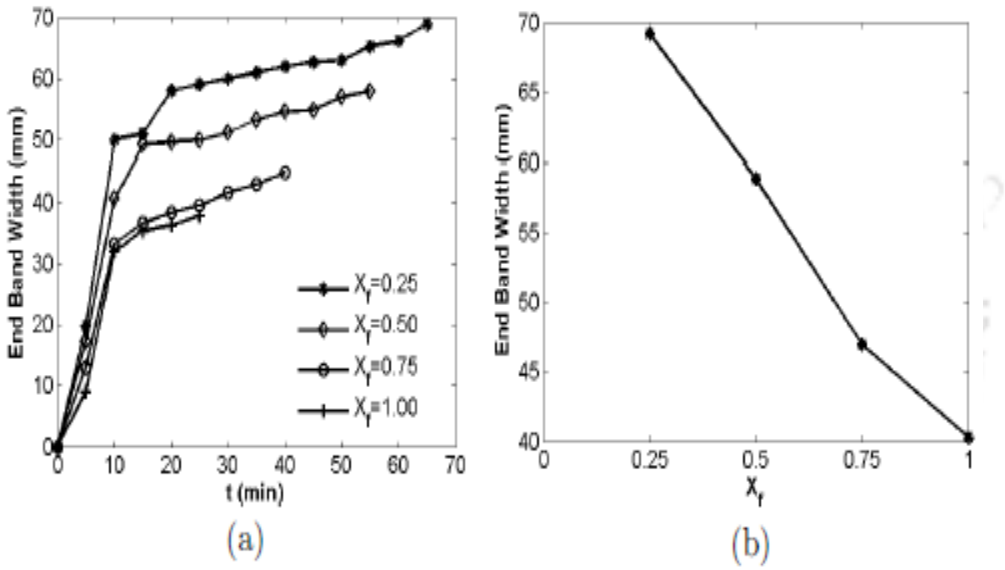

Figure 6.14: (a) Growth of band width at the tube end with time for various filling fractions. (b) Plot of fully developed band width at the tube end against filling fraction.

We have also studied the nature of particle motion during their rotation by taking the side view image. The camera was placed horizontally and the illumination was from the opposite end. Figure.6.15a shows the particle motion in fully filled cylinder rotating at low speed (gravity dominated regime). The larger particles moves near the bottom wall in a closed bracket "( )" fashion while the smaller particles in an open bracket ") (" fashion. The band of larger particles is found to expand when they approach to the top of the cylinder but converge during their downward motion. On the other hand, the band of smaller particles is found to contract during their upward motion and expand during their downward motion. We observed different pattern of motion in the experiments with partially filled cylinder. Figure.6.15b

shows the side view images of particles for 50% fill fraction at 4.1 rpm. Here, the bigger particles are found to converge during their upward motion and expand during the downward motion. While for the smaller particles the band expands during the upward motion and contract during downward motion in the bottom region. The experiments with 75% fill fraction displayed the behavior almost similar to that of the fully filled cylinder. We do not have a definite explanation to this observation but speculate that interplay between gravity, buoyancy and viscous drag forces is responsible for this. Statistics of segregation bands for completely filled tube in the gravity dominated regime given in Table 6.1.

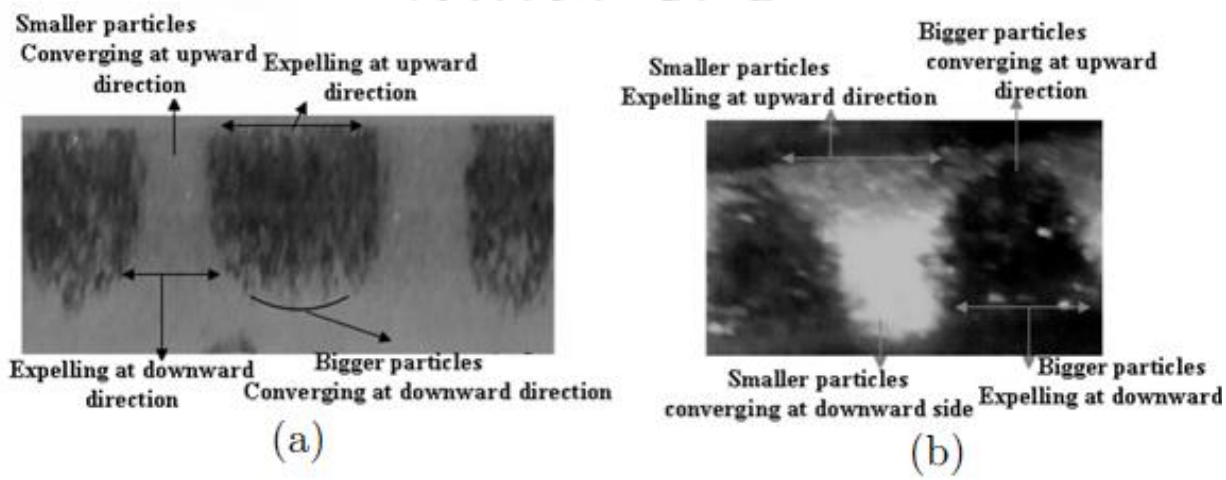

Figure 6.15: (a) Photograph of the band shape in dynamic condition for (a) completely filled tube. (b) 50 % filling fraction.

In the gravity dominated regime for the partially filled cylinder, the pattern of particle's bed movement is different from that of the fully filled cylinder. At static condition, the particles are present at the bottom wall of the cylinder. When the cylinder is subjected to rotation in the fully filled case both the larger and smaller particles rotate near the bottom of the cylinder as shown in Fig.6.16a. This is because at lower speed there is no significant centrifugal force to completely lift the particles to the top. However, for partially filled case at the same rotational speed it was observed that the bed of particles is dragged up to the free surface as can be seen in Fig.6.16b. The drag and sliding motion continues at this angle until it is under the dynamic equilibrium. This behavior is common for all filling fractions.

Table 6.1: Statistics of bands for completely filled tube in gravity dominated regime

S.No	Rotation speed of the tube (rpm)	Wall Reynolds number R_{ew}	Time taken for complete segregation (min)	Maximum number of bands	Total no. of bands after migration	No. of bands of bigger particles	No. of bands of smaller particles
01	1.3	5.37	1440	No complete segregation	-	-	-
02	2.11	11.57	170	Partial segregation	11	5	6
03	4.1	16.946	60	27	27	14	13
04	5.9	24.386	49	29	23	12	11
05	8.3	34.306	30	25	19	10	09
06	10.2	42.159	15	25	15	08	07
07	13.3	54.972	13	27	13	06	07
08	16.7	69.025	11	27	11	06	05
09	20.2	83.491	07	29	11	06	05
10	24.8	102.5	04	29	09	05	04
11	28.7	118.62	02	31	6	03	03
12	31.6	130.61	1.53	29	4	02	02
13	34.8	143.84	1.12	29	4	02	02
14	38.1	157.48	0.9	31	2	01	01
15	40.6	167.81	Start of partially centrifugal force dominated regime at which bands were not stable.				

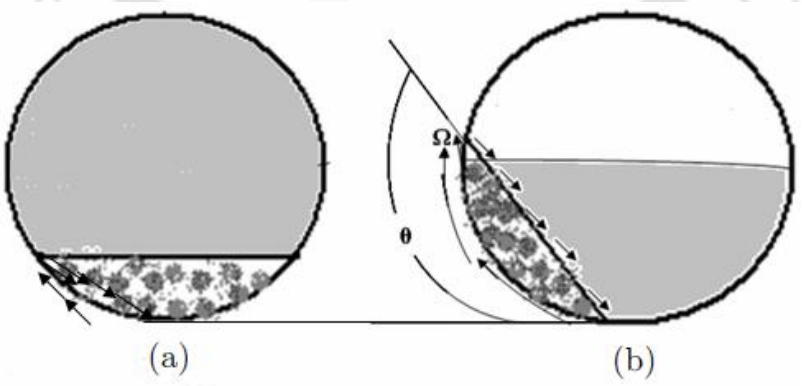

Figure 6.16: Schematic of the bi-dispersed particle's movement shown in r-θ view of (a) fully filled cylinder (b) partially filled cylinder.

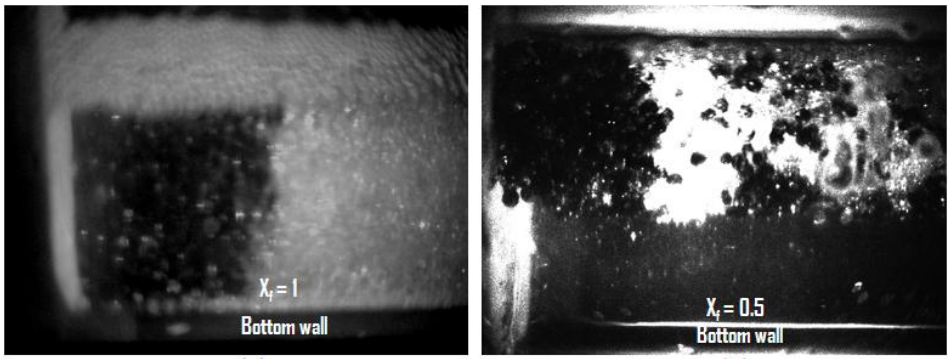

(a) (b)

Figure 6.17: Photographs of the bi-dispersed particle's movements shown in r-z plane of (a) fully filled cylinder (b) partially filled cylinder at 50% filling fraction. The rotation speed in both the cases were at 4.1 rpm.

6.3.1.2 Partially centrifugal force dominated regime (40 < N < 120)

When the rotation rate is further increased, the centrifugal force acting on the particles becomes significant and we get different segregation patterns. The larger particles will experience greater centrifugal force compared to the smaller particles. It was observed that at 40.6 rpm the smaller particles remain suspended in the fluid and are homogeneously dispersed. Whereas the larger particles rise up along the tube wall and near the top they fall back vertically downward as shown in Fig.6.18a. During the upward motion the viscous drag and vertical component of the centrifugal force opposes the downward gravitational force (Roberts *et al*., 1991). The net force on the particle is such that it is pulled up to the top of the cylinder. However, during the downstream motion the viscous drag and gravity forces are both in the downward direction. The vertical component of the centrifugal force is not strong enough to keep the particles rotating along the wall. As a result the bigger particles fall back vertically downwards. When the rotation rate is increased further (N=71.42 rpm) the smaller particles are forming a number of thin rings, while the larger particles are rising along the wall up to the top of the tube and then fall back downwards. This downward fall of larger particles disturbed the rings formed by smaller particles as shown in Fig.6.18b. Upon further increasing the rate of rotation (N) to 82.19 rpm, the bigger particles experience large centrifugal force and are found to complete full revolution and form unstable bands. These bands are also observed to move axially. This action disturbs the band of smaller particles as shown in the Fig.6.18c. Thus no stable segregation pattern was observed for $40 < N \leq 82$. For $82 < N \leq 120$ the smaller particles are completely dispersed in the suspending fluid while the larger particles form thin bands which are stable as can be observed in Fig.6.18 (d) and (e).

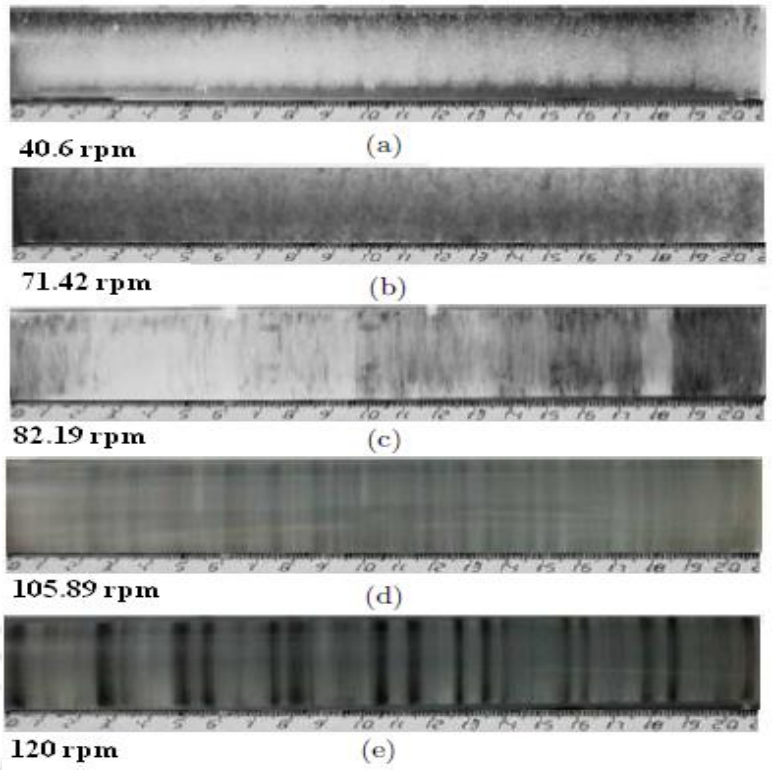

Figure 6.18: Segregation patterns in fully filled horizontally rotating cylinder in the partially centrifugal force dominated regime. Black regions show bigger particles and white regions smaller particles. The rotation rate for various cases is shown in the respective images.

6.3.1.3 Complete centrifugal force dominated regime (N > 120)

Upon further increase in the rotation rate (N > 120 rpm), we observed another pattern for bi-dispersed suspension in a completely filled horizontally rotating cylinder. In this regime, the centrifugal force on both smaller and larger particles is sufficient enough to move them along the wall of the cylinder in full circle. A number of concentration bands of particles separated by clear fluid are observed. Each band has bigger and smaller particles which are lying side by side (Fig.6.15). The number of bands was found to increase with the rotation speed of the cylinder (Fig.6.16). Even though the bigger and smaller particles spun with rotating wall due to centrifugal force, some of particles are ejected from the band, mostly the bigger ones. They again reach to the nearby band of same size particles by spiraling outwards about the axis of rotation in a helical path. Roberts *et al.* (1991) have given the detailed analysis of single particle motion in a fully filled rotating cylinder. We could not carry out the trajectory analysis of the particle motion at high rotation rates due to lower frame rate of the camera used in our study. Such analysis can be performed using a high speed camera.

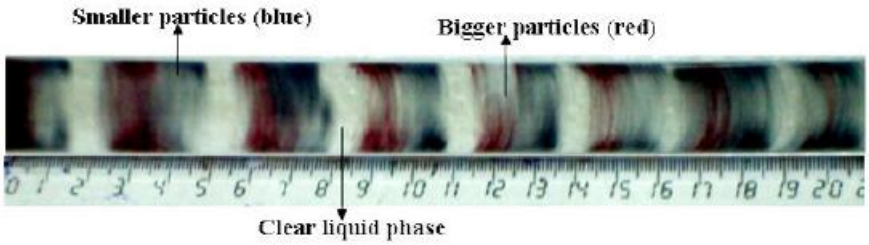

Figure 6.19: Segregation pattern in fully filled horizontally rotating cylinder in the complete centrifugal force dominated regime. The rotation rate in this case was 219.2 rpm. The alternate rings of bigger (red) and smaller particles (blue) can be observed. The bands of larger and smaller particles are adjacent to each other with clear fluid between the two sets of bands.

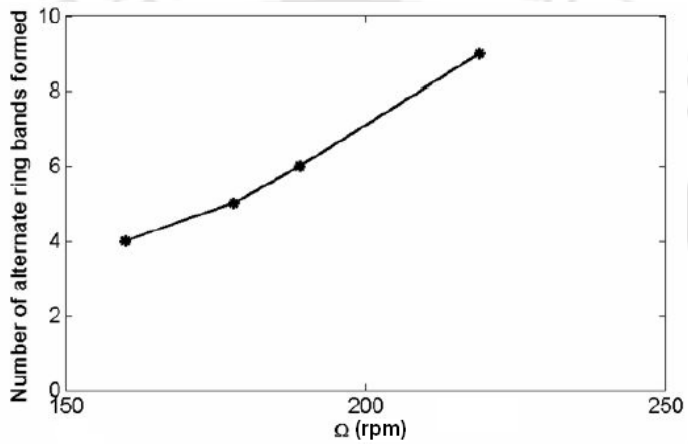

Figure 6.20: Growth of number of bands with the angular speed in the centrifugal force dominated regime.

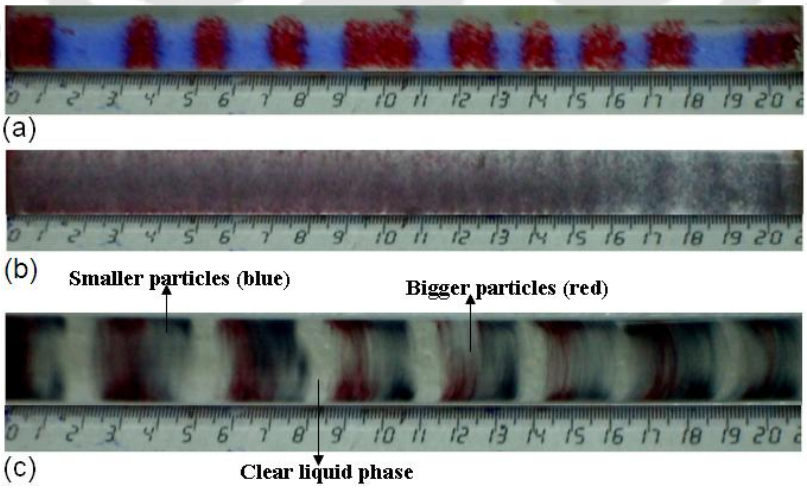

Figure 6.21: Photographs explaining the three major segregation regimes of non-neutrally buoyant system (a) gravity dominated force regime (b) partially centrifugal-gravity dominated regime and (c) Complete centrifugal force dominated regime.

The cumulative results of three major segregation patterns for non-neutrally buoyant system at different dominated forces are shown in Fig.6.21.

6.4 NEUTRALLY BUOYANT SUSPENSION IN ROTATING CYLINDER

We have also examined the dynamics pattern and free surface effect in a horizontal rotating cylinder filled with bi-dispersed non-Brownian neutrally buoyant suspensions. Experiments were conducted for various rotation rates and filling fraction. The behavior was quite different from previous studies with settling suspensions for the same condition. The same PMMA particles (203 µm as smaller and 580 µm as larger particles) were chosen for this study also. To make the neutrally buoyant suspension two kind of suspending fluid was prepared. One was 74% of glycerol and 24% of water mixture whose final density was 1.18 g/cm^3 and its viscosity was measured to be 19.5 cP at 24°C. Another was prepared by mixing 76% Triton-X-100, 16.2% Zinc chloride and 7.8% of water, with percentage based on mass. This fluid had the density of 1.18 g/cm^3 and viscosity of 4000 cP at 24°C. The particle fraction maintained were same as in previous studies, i.e. 8.08% (volume%). The experiments were conducted for the same low angular speed to higher angular speed as well as the filling fraction for 25%, 50%, 75%, 100% for the both suspension (19.5 cP and 4000 cP). The settling suspension exhibited different regime according to the angular speed and they were distinguished in the experiments by their unique flow patterns and particle distributions. In settling suspension at low rotation rate the particles lie and slide at the bottom floor of the cylinder. At medium speed of rotation, it exhibited an irregular flow pattern where both gravity and centrifugal forces were significant. At higher rotation rates, the particles experienced significant centrifugal force and both types of particles were spun with inner wall and rotating along the cylinder but moved in horizontal direction and exhibited different segregation pattern. Now, we describe the observed pattern for the neutrally buoyant system for various angular rotations as well as various filling fraction.

6.4.1 Results and discussion

6.4.1.1 Neutrally buoyant bi-dispersed particles suspended in 19 cP fluid

The neutrally buoyant systems were also subjected to the similar conditions as the settling system. The experiments were conducted for various filling fractions and various angular speeds. We started the experiment with completely filled cylinder ($X_{f=}1$) and for further

experiments the filling fraction was reduced in steps to X_f = 0.75, 0.50 and 0.25. The experiment of each filling fraction was carried out from very low rotation speeds to a maximum of 219.2 rpm. In the fully filled rotating cylinder for N<4.1 rpm, the smaller particles followed the suspending fluid motion (in full circle) but bigger particles were slowly carried up along the cylinder up to some height and then fell down. Upon further increase of rotation rate to N≥ 4.1 rpm, the smaller particles still followed the suspending fluid but the bigger particles were segregated at center line of the cylinder and created a swing-wave like movement from one end to another end (Fig.6.22a). Upon further increase of angular speed (N≥18.4 rpm), the bigger particles were segregated into a number of small rings. The formation of segregation looked like a cone-ring structure (Fig.6.22b). This kind of pattern formation was observed in settling system at N≥ 72 rpm, whereas in neutrally buoyant system this appeared at 4.1 rpm. When the rotation rate is increased further (N>40 rpm), drag force lifts the bigger particles to larger height. It was observed that the bigger particles formed rings in some places but it collapsed soon. This phenomenon is replicated along the entire length of the tube. Smaller particles did not show any significant change as they were always uniformly dispersed in suspending fluid homogeneously. Thus there was no unique segregation pattern exhibited in fully filled cylinder. All angular rotations exhibited irregular pattern formations. In the partially filled cylinder, no significant particle segregation occurred for all filling fractions as well as at any rotating speed (Fig.6.22c-e). Both smaller particles and bigger particles were sliding and rising along with the upward moving wall. The particles were dispersed again in the suspending fluid while falling along with the downward motion of the cylinder wall. This action was repeated for all the speed of rotations. Thus it can be observed that the free surface restricts the occurrences of instability in rotating suspensions of bi-dispersed particles.

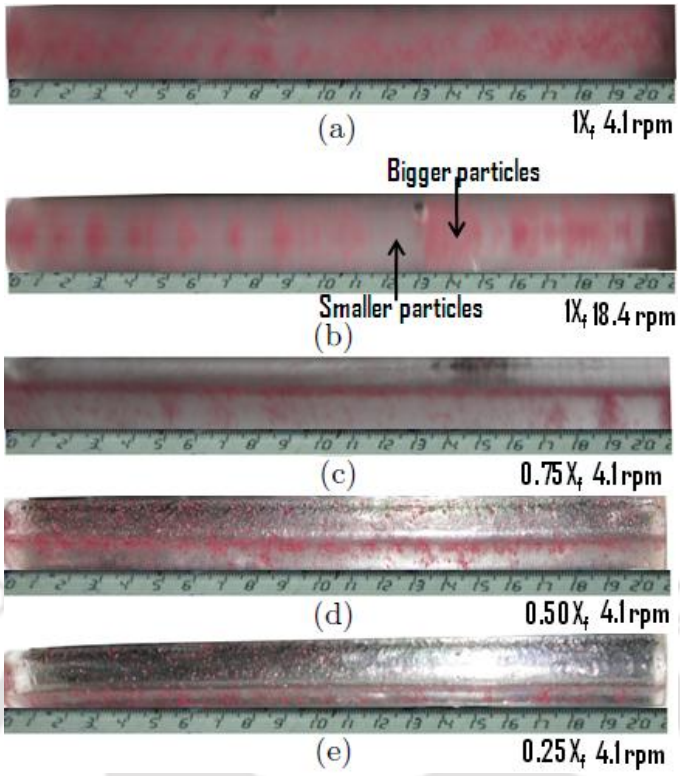

Figure 6.22: Segregation pattern of nuetrally buoyant bi-dispersed suspension in 19 cP of suspending fluid. (a) Completely filled cylinder at 4.1 rpm (swing-wave pattern), (b) Completely filled cylinder at 18.4 rpm (cone-ring pattern) (c) 75% of filled cylinder (d) 50% of filled cylinder (e) 25% of filled cylinder. Red represents bigger particles and white color (homogeneous mixed) represent the smaller particles.

6.4.1.2 Neutrally buoyant bi-dispersed particles in 4000 cP fluid

Similar conditions were applied for this study also. We did not observe any pattern formation in the result of fully filled cylinder at any speed of rotation achieved (Fig.6.23a). Both the bigger and smaller particles were moving with the suspending fluid along the cylinder wall. Due to high viscosity of the suspending fluid, the drag on both the particles was large enough to take it along the rotating cylinder walls. In the case of partially filled cylinder bigger and smaller particles appeared to stick to the wall till the free surface and the particles segregated and formed bands. The bigger (red colored) and smaller particles (blue colored) formed the bands side by side. This kind of segregation occurred in settling system for N>120 rpm. The rate of segregation and band formation increased with decrease in filling fraction as shown in Fig.6.23(b-d). It can be seen that it is mostly bigger particles that form the bands and smaller particles were stuck with wall during upward motion but dispersed in suspending fluid while falling during the downward motion of the cylinder. The smaller particles also formed bands

at filling fraction of 0.25 (clear view is shown in Fig.6.23e), but it decreased or almost no band formation from was observed for X_f= 0.5 and 0.75. Segregation rate increases with increases of angular rotation of cylinder until 5.9 rpm and for N>5.9 rpm the segregation rate decreased. At much higher speed (N>40 rpm), there was no segregation of particles in partially filled rotating cylinder. The numbers of bands formed did not change with angular rotation and filling fraction.

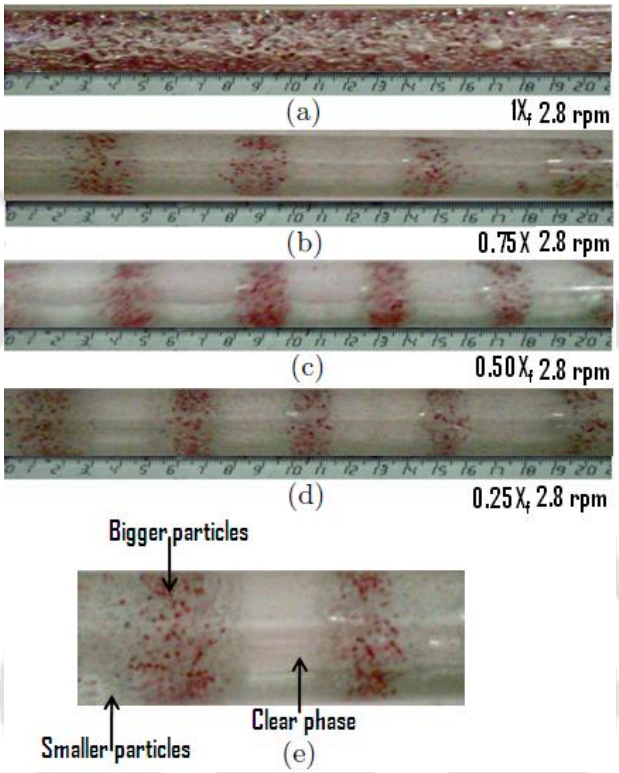

Figure 6.23: Segregation pattern of neutrally buoyant bi-dispersed for suspension of 4000 cP of suspending fluid. (a) Completely filled cylinder, (b) 75% of filled cylinder (c) 50% of filled cylinder (d) 25% of filled cylinder, and (e) close-up view of the segregation pattern. The rotation rate of the cylinder was 2.8 rpm in all the cases.

In the neutrally buoyant suspension the less viscous suspension exhibited irregular pattern formation for fully filled cylinder and no segregation was observed for partially filled cylinder. In the case of fully filled case the particles showed irregular pattern at all speed of rotation studies here. Similar pattern was observed only in the partially centrifugal force dominated regime in case of the settling suspensions. Highly viscous suspension exhibited segregation pattern at partially filled case. The rate of segregation decreased with increase of filling fraction. However, in fully filled condition no clear pattern was observed. In the partially filled cylinder, a thin layer of suspending fluid was always spun with cylinder wall.

The thickness of the layer was more for higher viscosity of suspending fluid. For more viscous fluid, more number of particles could be carried along the tube wall during upward motion which did not dispersed in the suspending fluid during the downward motion. This leads to more number of bands. Though, the rate of segregation increased until 5.9 rpm, further increase in rotating speed reduced the segregation rate. This observation was quite different from the settling suspensions.

6.5 CONCLUSION

Non-neutrally buoyant suspension of bi-dispersed non-colloidal particles in viscous fluid rotating in a horizontal cylinder displays in-homogeneities in particle distribution with alternate bands of high and low particle concentrations along the symmetric axis of the cylinder. Experiments were carried out to characterize the axial segregation in bi-dispersed suspension at various filling fraction and rotation speed of cylinder. The mixture of same particles in absence of any suspending fluid did not show any segregation. However, in case of particles suspended in water, it was observed that the rate of segregation increases with increase in filling fraction. Once the particles get segregated along the full length of the cylinder, these bands start to migrate along the tube axis finally merging to give wider bands. For a given filling fraction the rate of segregation increases with the angular speed of the rotating cylinder. When the tube is partially filled the particle segregation is observed at higher angular speed, whereas in fully filled case the segregation starts at much lower rotation speed for the same concentration of particles. The segregation pattern changes as the rotation speed is increased. At higher speed, the centrifugal force dominates over gravitational and viscous drag forces and this result into completely different segregation patterns. We have also analyzed the evolution of concentration profile from the image analysis of the particles. Experiments were conducted for dry particles (in absence of suspending fluid), partially filled and fully filled suspension in the horizontally rotating cylinder. Each experiment was run for 24 hr to observe the continuous change in the segregation pattern of particles along the axis of the tube. To examine the role of free surface on the segregation, the experiments were conducted for both fully filled and partially filled tube. The filling fractions studied were 25%, 50%, 75% and 100% respectively.

Experiments were also conducted in horizontal rotating cylinder filled with bi-dispersed of non-Brownian neutrally buoyant particles for various rotation rates and filling fraction. The behavior was quite different from settling suspension for the same conditions. In the neutrally

buoyant case both 19.5 cP and 4000 cP suspending fluid did not show any pattern in fully filled cylinder. The less viscous suspension exhibits irregular pattern formation in fully filled cylinder and did not show any pattern for partially filled case. High viscous suspension (4000 cP suspending fluid) showed segregation pattern for the partially filled case. With increase of filling fraction the rate of the segregation decreased and in fully filled condition no pattern was formed.

CHAPTER 7

CONCLUSION AND SCOPE OF FUTURE WORK

7.1 CONCLUSION

Experimental studies were carried out to study wall slip and free surface corrugation of suspensions in open channel. We have measured the apparent wall slip velocity co-efficient of concentrated suspension in plane and serrated wall open channel flow with the tool of particle image velocimetry. The suspensions consisted of various particle sizes, various suspending fluids and various particle fractions. The screw pump was used which is specifically designed to handle suspension of large particles. An Argon ion continuous laser was used as light source. The images were captured using a 1360 X 1024 pixel CCD camera in conjugation with a macro zoom lens. The camera was operated with frame rate of 19 frames/s and the duration between subsequent images was 52 ms. To get the mean velocity profiles, an average of 100 velocity vectors was taken which were obtained by cross – correlation analysis of 100 consecutive pairs of images. It was observed that the apparent wall slip velocity varies linearly with shear rate. The slip coefficient is low at moderate concentration but increases rapidly as higher concentration is reached. The slip velocity is higher for suspension of larger sized particles at the same concentration. The viscosity of suspending fluid also affects the wall slip and a lower suspending fluid viscosity shows higher values of slip velocity. These results are in qualitative agreement with the earlier findings. To verify the migration of particles across the channel we had conducted one experiment in which a small fraction of the suspending PMMA particles were dyed in black. The image of these particles showed uniform concentration across the whole channel width. This indicates that there is no appreciable migration in the *x-y* plane for which we report the velocity profiles. In our second study the effect of slip velocity on surface corrugation was studied by the analysis of the spectra of the refracted light from the free surface. These experiments were performed to study whether wall slip affects the surface corrugation pattern

or not. The surface images were taken by placing the camera above the surface and illuminating the free surface using cold light source. The light source was placed at an appropriate angle so that it reached the camera lens after refraction from the free surface. It is found that the normalized spatial and temporal spectra are similar for both plane wall and serrated wall channel. The spatial auto-correlation in flow and span-wise directions for plane and serrated channel also did not show any significant variation to make any conclusive observation. Thus, it appears that the wall slip affects the velocity profile close to the wall as well as blunting of profile but this has no apparent effect on the surface corrugation patterns. The mean height of free surface corrugation was measured by performing the flow visualization experiments in velocity-vorticity plane. The location of the interface was determined from the gradient of image intensity of the tracer particles which floated on the free surface. The velocity in the bulk (beneath the free surface) was determined by PIV technique. To locate the interface in clear vision, CCD camera was placed on one side of the channel at an appropriate angle. The contrast between the suspension and air indicates the location of the interface. The interface location was determined using an edge detection routine. The interface was visualized by illuminating the tracer particles over the free surface. The interface fluctuations are very small at low concentration of particles but increases with increase in particle concentration. There is an optimum particle concentration at which the interface fluctuation is the largest. Thereafter, it decreases with increase in particle concentration. For a given concentration of particles, the interface fluctuation increases linearly with the flow speed. The analysis of interface location and vertical velocity of the interface both showed the same trend.

We have carried out significant experimental studies on free surface flow of suspensions which is often encountered in natural settings such as flood waves carrying extremely high concentration of very fine sediments as well as in many material processing procedures such as slurry flow in open channels. The present study has very significant application potential. We have prescribed a simple experimental method for the characterization of wall slip and demonstrated how the flow visualization technique can be used to characterize wall slip in open channels where the rheological methods are not suitable for large size of particles such as debris flow, lava flow. This technique can be also be used for a large number of materials which show slip behavior such as polymers, composites, slurries, solid rocket fuel, solder paste etc. Petroleum industries often require characterization of wall slip for cement-concrete mixture during casing cementing operations. We have also characterized the free surface

deformation in open channel flow and determined the factors governing the fluctuations. This knowledge can be utilized to control surface corrugation in many food processing and material processing procedures.

Finally, we have studied the behavior of bi-dispersed neutrally and non-neutrally buoyant suspension of non-colloidal particles in a horizontally rotating cylinder. Suspension of solid rigid particles in viscous fluid present in rectangular and cylindrical conduit has many practical applications in chemical, metallurgical, plastic, food and pharmaceutical industries. Experiments were carried out at various filling and angular speed of the cylinder. Non-neutrally buoyant suspension of bi-dispersed non-colloidal particles in viscous fluid rotating in a horizontal cylinder displays in-homogeneities in particle distribution with alternate bands of high and low particle concentrations along the symmetric axis of the cylinder. The mixture of same particles in absence of any suspending fluid did not show any segregation. However, in case of particles suspended in water it was observed that the rate of segregation increases with increase in filling fraction. Once the particles get segregated along the full length of the cylinder, these bands start to migrate along the tube axis finally merging to give wider bands. For a given filling fraction the rate of segregation increases with the angular speed of the rotating cylinder. When the tube is partially filled the particle segregation is observed at higher angular speed, whereas in fully filled case the segregation starts at much lower rotation speed for the same concentration of particles. The segregation pattern changes as the rotation speed is increased. At higher speed, the centrifugal force dominates over gravitational and viscous drag forces and this result into completely different segregation patterns. We have also analyzed the evolution of concentration profile from the image analysis of the particles.

In neutrally buoyant system the behavior was quite different from previous studies for the same conditions. To make the neutrally buoyant suspension two kind of suspending fluid was prepared. One was of low viscosity (19 cP) and another of higher viscosity (4000 cP). The experiments were conducted for same conditions as was the case in non-neutrally buoyant systems (various filling fractions and various rotating speeds). In the neutrally buoyant case, both 19.5 cP and 4000 cP suspending fluid did not show any pattern in fully filled cylinder. The less viscous suspension exhibits irregular pattern formation in fully filled cylinder and did not show any pattern for partially filled case. High viscosity suspension (4000 cP suspending fluid) showed segregation pattern for the partially filled case. With increase of filling fraction the rate of the segregation decreased and in fully filled condition no pattern

was formed. It is interesting to note that the free surface fluctuations decrease with increase in the viscosity of suspending fluid. On the other hand, the experiments with rotating cylinder reveal that the higher viscosity of the suspending fluid stabilizes the segregation pattern. The fluctuation of the particles in the bulk tries to disperse the particles if they accumulate in bands and this prevents any stable band formation. This is why we did not observe any stable band formation with suspension in less viscous suspending fluid. It is to be noted that we have not measured the free surface fluctuations in the rotating cylinder. These results require further investigation to establish the exact relationship between free surface fluctuations and axial segregation.

7.2 SCOPE OF FUTURE WORK

The findings from the project have opened many possibilities for further exploration. In this thesis, we have investigated suspension of solid spherical particles in viscous Newtonian fluids. It is desired to test the proposed method for other kind of suspensions such as suspension of non-spherical particles and suspension of particles in non-Newtonian fluids. To better understand the free-surface deformation, we also need to map the whole field surface elevation using the technique of free surface gradient detector (FSDG). This technique involves color coding of different slopes of the free surface with different colors in order to establish a one-to-one correspondence between color and slope.

Measurement of stresses at the side and bottom wall of the channel will help us to formulate the proper boundary condition for slip condition. CFD simulation of free surface flow of equivalent homogeneous fluid at the same conditions at which experiments with suspensions are carried out will help us to make quantitative analysis of the non-Newtonian behavior of the suspension flow over equivalent homogeneous flow. Model can be developed to explain the observed experimental data and it can be compared with the prediction of the model. More detailed studies required on the rough wall channel flow to understand the physics of zero wall slip and effect of shear induced migration at different roughness of the wall.

In the experiments of rotating cylinder, the work can be extend to carry out particle level simulation such as Stokesian Dynamics and develop a model for bi-dispersed suspension in rotating cylinder. The experiment can be extended toward quantitative measurements and the velocity pattern for bigger and smaller particles should be measured in the bi-dispersed system for neutrally and non-neutrally buoyant suspension in rotating cylinder.

REFERENCES

Abbott, J.R., Tetlow, N., Graham, A.L., Altobelli, S.A., Fukishima, E., Mondy, L.A., Stephens, T.S., 1991. Experimental observations of particle migration in concentrated suspensions: Couette flow. J. Rheol. 35, 773-797.

Ackerson, B.J., 1990. Shear induced order and shear processing of model Hard-Sphere suspensions, J. Rheol. 34, 553-590.

Adrian, R.J., Keane, R.D., Zhang, Y., 1995. Super resolution particle-imaging velocimetry, Meas. Sci. Technol. 6, 754-768.

Ahuja, A., Singh, A., 2009. Slip velocity of concentrated suspensions in Coueete flow. J. Rheol. 53, 1461-1485.

Aral, B., Kalyon, D.M., 1994. Effects of temperature and surface roughness on time dependent development of wall slip in steady torsional flow of concentrated suspensions. J. Rheol. 38, 957-972.

Argyriadi, K., Vlachogiannis, M., Bontozoglou, V., 2006. Experimental study of inclined film flow along periodic corrugations: The effect of wall steepness. Phys.Fluids 18, 012102(1-15).

Averbakh, A., Shauly, A., Nir, A., Semiat, R., 1997. Slow viscous flow of highly concentrated suspensions-part I: Lasser Doppler Velocimetry in rectangular ducts. Int. J. Multiphase Flow 23, 409-424.

Ball, R.C., Richmond, P., 1980. Dynamics of colloidal dispersions, Phys. Chem. Liq. 9, 99-116.

Barnes, H., 1995. A review of the slip (wall depletion) of polymer solutions, emissions and particle suspensions in viscometers: its cause, character, and cure. J.Non-Newton. Fluid Mech. 56, 221-223.

Batchelor, G.K., 1969. The stress system in a suspension of force free particles. J. Fluid Mech. 41, 545-570.

Bilodeau, R., Bousefield, D., 1998. Shear thinning predictions from particle motion modeling. J. Rheol. 42, 743–763.

Bingman, C., 1996. Quantitative relationships between visible water color and ultraviolet transmission. Aqua. Front. 3, 12-16.

Brady, J.F., Carpen, I.C., 2002. Second normal stress jump instability in non-Newtonian fluids. J.Non-Newt. Fluid Mech. 102, 219-232.

Brady, M.R., Telionis, D.P., Vlachos, P.P., Yoon, R.H., 2006. Evaluation of multiphase flotation models in grid turbulence via Particle Image Velocimetry. Int. J. Miner. Process 80, 133-143.

Brauner, N., Rovinsky, J., Maron, D.M., 1996. Determination of the interface curvature in stratified two-phase systems by energy considerations. Int. J. Multiphase flow 22, 1167-1185.

Breedveld, V., Van Den Ende, D., Bosscher, M., Jongschaap, R.J.J., Mellema, J., 2002. Measurement of the full shear-induced self-diffusion tensor of noncolloidal suspensions. J. Chem. Phys. 116, 10529-10535.

Breu, A.P.J., Kruelle, C.A., Rehberg, I., 2003. Pattern formation in a rotating aqueous suspension, Eur. Phys. Lett. 62, 491–497.

Carruthers, D.J., Hunt, J.C.R., 1986. Velocity fluctuations near an interface between a turbulent region and a stable stratified layer. J. Fluid Mech. 165, 475-501.

Chapman, B.K., 1990. Shear induced migration phenomena in concentrated suspensions. PhD thesis, University of Notve Dame.

Cherlo, S.K.R., Kariveti, S., Pushpavanam, S., 2010. Experimental and numerical investigations of two-phase (liquid-liquid) flow behavior in rectangular microchannels. Ind.Eng.Chem.Res. 49, 893-899.

Chow, A.W., Sinton, S.W., Iwamiya, J.H., Stephens, T.S., 1994. Shear induced particle migration in coquette and parallel-plate viscometers: NMR imaging and stress measurements. Phys. Fluids 6, 2561-2576.

Chow, A.W., Sinton, S.W., Leighton, D.T., 1995. Particle migration of non-Brownian, concentrated suspensions in a truncated-cone-and-plate. Soc. Rheol. Meet. Sacramento, CA.

Christensen, K.T., Soloff, S.M., Adrian, R.J., 2000. Technical Report 943, Department of Theoretical and Applied Mechanics, University of Illinois at Urbana-Champaign.

Corbett, A.M., Phillips, R.J., Kauten, R.J., McCarthy, K.L., 1995. Magnetic resonance suspensions in rotating geometries. J. Rheol. 39, 907-924.

Dabiri, D., Gharib, M., 2001. Simultaneous free-surface deformation and near-surface velocity measurements. Exp. Fluids 30, 381-390.

Derakshandeh, B., Hatzikiriakos, S.G., Bennington, C.P.J., 2010. Rheology of pulp suspensions using ultrasonic Doppler velocimetry. Rheol. Acta 49, 1127-1140.

Desaubry, C., Gervais, P., 2000. Characterization of a standard CCD video camera devoted to the design of efficient particle image velocimetry instrument. Flow Meas. Inst. 11, 133-141.

Du, D., Zhang, H., Srolovitz, D.J., 2007. Properties and determination of the interface stiffness. Acta Mat. 55, 467-471.

Drazin, P., 2002. Introduction to hydrodynamic stability. Cambridge University Press.

Einstein, A., 1906. Investigation on the theory of Brownian movement. Dover publications.

Ekere N., He, D., Cai, L., 2001. The influence of wall slip in the measurement of solder paste viscosity, IEEE Trans. Comp. Pack. Technol. 24, 468-473.

Federico, V.D., 1999. Free-Surface flow of hyper concentrations. Fluid Dyn. Res. 24, 23-36.

Fielding, S.M., Wilson, H.J., 2010. Shear banding and interfacial instability in planar poiseuille flow. J. Non-Newton. Fluid Mech. 165, 196-202.

Fitch, A. W., Jian, H., Ni, X., 2005. An investigation of the effect of viscosity on mixing in an oscillatory baffled column using digital particle image velocimetry and computational fluid dynamics simulation. Chem. Eng. J. 112, 197-210.

Gadla-Maria, F., Acrivos, A., 1980. Shear-induced structure in a concentrated suspension of solid sheres. J. Rheol. 24, 799-814.

Gans, R.F., Zupanski, G., 1988. Generations of vortices in a partially filled rapidly rotating cylinder. Exp. Fluids 6, 279-282.

Govindarajan, R., Nott, P.R., Ramaswamy, R., 2003. Theory of suspension segregation in partially filled horizontal rotating cylinders. Phys. Fluids 13, 3517-3520.

Graham, A.L., Altobelli, S.A., Fukushima, E., Mondy, L.A., Stephens, T.S., 1991. NMR imaging of shear induced diffusion and structure in concentrated suspensions undergoing Couette flow. J. Rheol. 35, 191-201.

Hampton, R.E., Mammoli, A.A., Graham, A.L., Tetlow, N., 1997. Migration of particles undergoing pressure-driven flow in a circular conduit. J. Rheol. 41, 621-640.

Hay, G., Mackay, M.E., McGlashan, S.A., Park, Y., 2000. Comparison of shear stress and wall slip measurement techniques on a linear low-density polyethylene. J.Non-Newt. Fluid Mech. 92, 187-201.

Heise, M., Schmidt, S., Kruger, U., Ruckert, R., Rosler, S., Neuhaus, P., Settmacher, U., 2004. Flow pattern and shear stress distribution of distal end-to-side anastomoses. A comparison of instantaneous velocity fields obtained by particle image velocimetry. J. Bio Mech. 37, 1043-1051.

Hill, K.M., Kakalios, J., 1994. Reversible axial segregation of binary mixtures of granular materials. Phys. Rev. E 5, 3610-3613.

Hill, K.M., Kakalios, J., 1995. Reversible axial segregation of rotating granular media. Phys. Rev. E 4, 4393-4400.

Hill, K.M., Caprihan, A., Kakalios, J., 1997. Axial segregation of granular media rotated in a drum mixer: Pattern evolution. Exp. Fluids 22, 239-248.

Hill, K.M., Kakalios, J., Yamane, K., Tsuji, Y., Caprihan, A., 1997. Dynamic angle of repose as a function of mixture concentration: Results from MRI experiments and DEM simulations. Powder and Grains conference proceedings.

Hirsa, A., Korenowski, G.M., Logory, L.M., Judd, C.D., 1997. Velocity field and surfactant concentration measurement technique for free-surface flows. Exp. Fluids 22, 239-248.

Hirsa, A.H., Vogel, M.J. Gayton, J.D., 2001. Digital particle velocimetry technique for free-surface boundary layer measurements: Application to vortex pair interactions, Exp. Fluids 31, 127-139.

Hoang, K.C., Malakhov, D., Momsen, W.E., Brockman, H.L., 2006. Open microfluidic flow cell for studies of interfacial processes at gas-liquid interfaces. Anal.Chem. 78, 1657-1664.

Honig, D., Mobius, D., 1991. Direct visualization of monolayers at the air-water interface by Brewster angle microscopy. J. Phys. Chem. 95, 4590-4592.

Huang, C.T., Khomami, B., 2001. Role of dynamic modulation on stability of multilayer Newtonian and viscoelastic flows down an inclined plane. J. Non. Newton. Fluid Mech. 97, 67-86.

Jain, N., Khakhar, D.V., Lueptow, R.M., Ottino, J.M., 2001. Self-organization in slurries. Phys. Rev. Lett. 86, 3771-3774.

Jana, S.C., Kapoor, B., Acrivos, A., 1995. Apparent wall slip velocity coefficients in concentrated suspensions of non-colloidal particles, J. Rheol. 39, 1123-1132.

Jeffery, D.J., Acrivos, A., 1976. The rheological properties of suspensions of rigid particles. AIChE. J. 22, 417-432.

Jin, B., Acrivos, A., 2004. Theory of particle segregation in rimming flows of suspensions containing neutrally buoyant particles. Phys. Fluids 16, 641-651.

Joseph, D.D., Wang, J., Bai, R., Yang, B.H., Hu, H.H., 2003. Particle motion in a liquid film rimming the inside of a partially filled rotating cylinder. J. Fluid Mech. 496, 139-163.

Kadambi, J.R., Martin, W.T., Amirthaganesh, S., Wernet, M.P., 1998. Particle sizing using particle image velocimetry for Two-phase flows. Powder Tech. 100, 251-259.

Kalyankar, M.K., Matson, W.R., Ackerson, B.J., Tong, P., 2008. Dynamics of rotating suspension, Phys. Fluids 20, (083301)1-9.

Kalyon, D.M., Yaras, P., Aral, B., Yilmazer, U., 1993. Rheological behavior of a concentrated suspension: A solid rocket fuel simulant, J. Rheol. 37, 35-53.

Kalyon, D.M., 2005. Apparent slip and viscoplasticity of concentrated suspensions, J.Rheol. 49, 621-640.

Karnis, A., Goldsmith, H.L., Mason, S.G., 1966. The kinetics of flowing dispersions: Concentrated suspensions of rigid particles. J. Colloid Interface Sci. 22, 531-553.

Khakhar, D.V., McCarthy, J.J., Shindrot, T., Ottino, J.M., 1996. Transverse flow and mixing of granular materials in a rotating cylinder. Phys. Fluids 9, 31-43.

Kiger, K.T., Pan, C., 2000. PIV Technique for the simultaneous measurement of dilute two-phase flows. J. Fluid Eng. 122, 811-818.

Koh, C.J., Hookham, P., Leal, L.G., 1994. An experimental investigation of concentrated suspension flows in a rectangular channel, J. Fluid Mech. 266, 1-32.

Kumar, S., Gupta, R., Banerjee, S., 1998. An experimental investigation of the characteristics of free-surface turbulence in channel flow. Phys. Fluids 10, 437-456.

Kurada, S., Rankin, G.W., Sridhar, K., 1997. A new particle image velocimetry technique for Three-dimensional flows. Optic Laser Eng. 28, 343-376.

Krasnopol'skaya, T.S., Van Haijst, G.J.F., Voskamp, J.H., Trigger, S.A., 2003. Similarities of pattern in fluid and granulated flow inside a horizontal rotating cylinder, Int. Appl. Mech. 37, 929-934.

Krieger, I.M., Dougherty, T.J., 1959. Concentration dependence of the viscosity of suspensions. Trans. Soc. Rheol. 3, 137-152.

Kriegsmann, J., Miksis, M., Vanden-Broeck, J.M., 1998. Pressure driven disturbances on a thin viscous film. Phys. Fluids 10, 1249-1255.

Lam, Y.C., Wang, Z. Y., Chen, X., Joshi, S. C., 2007. Wall slip of concentrated suspension melts in capillary flows, Powder Technol. 177, 162-169.

Law, C.N.S., Khoo, B.C., Chew, T.C., 1999. Turbulence structure in the immediate vicinity of the shear-free air-water interface induced by a deeply submerged jet. Exp. Fluids 27, 321-331.

Lawl, A., Kalyon, D.M., 1997. Non-isothermal extrusion flow of viscoplastic fluids with wall slip, Int. J. Heat Mass Transfer. 40, 3883-3897.

Lee, J., Ladd, A.J.C., 2005. Axial segregation of settling suspension in a rotating cylinder, Phys. Rev. Letters. 95, 048001(1-4).

Leighton, D., Acrivos, A., 1987a. Measurement of self-diffusion in concentrated suspension of spheres. J. Fluid Mech. 177, 109-131.

Leighton, D., Acrivos, A., 1987b. The shear-induced migration of particles in concentrated suspension of spheres. J. Fluid Mech. 181, 415-439.

Li, H., Ewoldt, R., Olsen, M.G., 2005. Turbulent and transitional velocity measurements in a rectangular microchannel using microscopic particle image velocimetry. Exp. Therm. Fluid Sci. 29, 435-446.

Loimer, T., Nir, A., Semiat, R., 2002. Shear-induced corrugation of free interfaces in concentrated suspensions. J. Non-Newton. Fluid Mech. 102, 115-134.

Lyon, M., Leal, L.G., 1998. An experimental study of the motion of concentrated suspensions in two-dimensional channel flow. J. Non-Newton. Fluid Mech. 363, 25-56.

Matson, W.R., Ackerson, B.J., Tong, P., 2003. Pattern formation in a rotating suspension of non-Brownian settling particles. Phys. Rev. E 67, 050301(1-4).

Matson, W.R., Kalyankar, A.J., Ackerson, B.J., Tong, P., 2005. Concentration and velocity pattern in a horizontal rotating suspension of non-Brownian settling particles. Phys. Rev. E 71, 031401(1-11).

Matson, W.R., Kalyankar, A.J., Ackerson, B.J., Tong, P., 2006. Dynamics of rotating suspension. Solid state commun. 139, 605-616.

Miller, R.M., Morris, J.F., 2006. Normal stress-driven migration and axial development in pressure-driven flow of concentrated suspensions. J. Non-Newt. Fluid Mech. 135, 149-165.

Miller, N., Quinton, J.N., Barberis, E., Presta, M., 2009. Variability in the mobilization and transport of sediment and phosphorus across 13 European soils. J. Env. Quality 38, 742-750.

Mooney, M., 1931. Explicit formulas for slip and fluidity. J.Rheol. 2, 210-222.

Morris, J.F., Boulay, F., 1999. Curvilinear flows of non-colloidal suspensions: the role of normal stresses. J. Rheol. 43, 1213-1237.

Muller, J.S., 2002. Velocity measurements in complex flows of non-Newtonian fluids. Korea-Australia Rheol. J. 14, 93-105.

Nickerson, C.S., Kornfield, J.A., 2005. A cleat geometry for suppressing wall slip, J. Rheol. 49, 865-874.

Nikolov, A.D., Kralchevsky, P.A., Ivanov, I.B., 1985. Film and line tension effects on the attachment of particles to an interface. J. colloid interface sci. 112, 122-131.

Nott, P.R., Brady, J.F., 1994. Pressure driven flow of suspensions: Simulation and theory. J. Fluid Mech. 275, 157–199.

Northrup, M.A., Kulp, T.J., Angel, S.M., Pinder, G.F., 1993. Direct measurement of interstitial velocity field variations in a porous medium using fluorescent – particle image velocimetry. Chem. Eng. Sci. 48, 13-21.

Olsen, M.G., Adrian, R.J., 2000. Brownian motion and correlation in particle image velocimetry. Optic Laser Tech. 32, 621-627.

Overlez, G., Bertrand, F., Rodts, S., 2006. Local determination of the constitutive law a dense suspension of non-colloidal particles through magnetic resonance imaging. J. Rheol. 50, 259-292.

Pan, T.W., Glowinski, R., Hou, S., 2007. Direct numerical simulation of pattern formation in a rotating suspension of non-Brownian settling particles in a fully filled cylinder. Comp. Struct. 85, 955-969.

Pandey, P., Turton, R., 2005. Movement of different – shaped particles in a pan coating device using novel video – imaging techniques. AAPS Pharm. Sci. Tech. 6, 237-244.

Paul, S.S., Tachie, M.F., Ormiston, S.J., 2007. Experimental study of turbulent cross-flow in a staggered tube bundle using particle image velocimetry. Int. J. Heat. Fluid Flow 28, 441-453.

Philip, O.G., Schmidl, W.D., Hassan, Y.A., 1994. Development of a high speed particle image velocimetry technique using fluorescent tracers to study steam bubble collapse. Nucl. Eng. Design 149, 375-385.

Phillips, R.J., Armstrong, R.C., Brown, R.A., 1992. A constitutive equation for concentrated suspension that accounts for shear-induced particle migration. Phys. Fluids 4, 30-40.

Phung, T.N., Brady, J.F., Bossis, G., 1996. Stokesian dynamics simulations of Brownian suspensions. J. Fluid Mech. 313, 181-207.

Ramirez-Gilly, M., Martinez-Padilla, L.P., Manero, O., 2007. Particle image velocimetry applied to suspensions of millimetric-size particles using a vane-in-a-large-baffled-cup rheometer. J. Food Eng. 78, 1117-1126.

Rashidi, M., Hetsroni, G., Banerjee, S., 1992. Wave turbulence interaction in free-surface channel flows. Phys. Fluids 4, 2727-2738.

Roberts, G.O., Kornfeld, D.M., Fowlis, W.W., 1991. Particle orbits in a rotating cylinder. J. Fluid Mech. 229, 555-567.

Sanders, J., Joseph, D.D., Beavers, G.S., 1981. Rimming flow of a viscoelastic liquid inside a rotating horizontal cylinder. J. Non-Newton. Fluid Mech. 9, 269-300.

Singh, A., Nott, P.R., 2000. Normal stresses and microstructure in bounded sheared suspensions via Stokesian dynamics simulations. J. Fluid Mech. 412, 279-301.

Singh, A., Nott, P.R., 2003. Experimental measurements of the normal stresses in sheared Stokesian suspensions. J. Fluid Mech. 490, 293-320.

Singh, A., Nir, A., Semiat, R., 2006. Free surface flow of concentrated suspensions. Int. J. Multiphase Flow 32, 227-790.

Sinton, S.W., Chow, A.W., 1991. NMR flow imaging of fluids and solid suspensions in poiseuille flow. J. Rheol. 35, 735-772.

Slominski, C., Niedostatkiewicz, M., Tejchman, J., 2007. Application of particle image velocimetry (PIV) for deformation measurement during granular silo flow. Powder Technol. 173, 1-18.

Soltani, F., Yilmazer, U., 1998. Slip velocity and slip layer thickness in flow of concentrated suspensions. J. Appl. Polym. Sci. 70, 515-522.

Stevans, J., 1998. Axial segregation of powders in a horizontal rotating tube. J. Stat. Phys. 93, 467-475.

Tang, H.S., Kalyon, D.M., 2004. Estimation of the parameters of Herchel-Bulkley fluid under wall slip using a combination of capillary and squeeze flow viscometers. Rheol. Acta 43, 80-88.

Tatum, J.A., Finnis, M.V., Lawson, N.J., Harrison, G.M., 2005. 3-D particle image velocimetry of the flow field around a sphere sedimenting near a wall part 2. Effects of distance from the wall. J. Non-Newton. Fluid Mech. 127, 95-106.

Taylor, G.I., 1938. The spectrum turbulence. Proc. Roy. Soc. Lond. A 132, 476-490.

Thomas, P.J., Riddell G.D., Kooner, S., King, G.P., 2001. Structure of granular banding in two-phase flow. Phys. Fluids 13, 2720-2723.

Thoroddsen, S.T., Mahadevan, L., 1997. Experimental study of coating flows in a partially filled horizontally rotating cylinder. Exp. Fluids 23, 1-13.

Timberlake, B.D., Morris, J.F., 2002. Concentration band dynamics in free-surface couette flow of a suspension. Phys. Fliuids 14(5), 1580-1589.

Timberlake, B.D., Morris, J.F., 2005. Particle migration and free-surface topography in inclined plane flow of a suspension. J. Fluid Mech. 538, 309-341.

Tirumkudulu, M., Tripathi, A., Acrivos, A., 1999. Particle segregation in monodisperse sheared suspensions. Phys. Fluids. 11, 507-509.

Tirumkudulu, M, Mileo, A., Acrivos, A., 2000. Particle segregation in monodisperse sheared suspensions in partially filled rotating horizontal cylinder. Phys. Fluids 12, 1615-1618.

Tisne, P., Aloui, F., Doubliez, L., 2003. Analysis of wall shear stress in wet foam flow using the electrochemical method. Int. J. Multiphase Flow 29, 841-854.

Tsuei, L., Savas, O., 2000. Treatment of interfaces in particle image velocimetry. Exp. Fluids 29, 203-214.

Vand, V., 1948. Viscosity of solutions and suspensions. I. Theory. J. Phys. Colloid Chem. 52, 277-299.

Wang, Z.Y., 2002. Free surface instability of non-Newtonian laminar flows. J. Hydra. Res. 40, 449-460.

Wasterweel, J., 1997. Fundamentals of digital particle image velocimetry. Meas Sci. Technol. 8, 1379-1392.

Yezaz-Ahamed, G.M., Singh, A., 2011. Numerical simulation of particle migration in asymmetric bifurcation channel. J. Non-Newt. Fluid Mech. 166, 42-51.

Yilmazer, U., Kalyon, D.M., 1989. Slip effects in capillary and parallel disk torsional flows of highly filled suspensions. J.Rheol. 33, 1197-1212.

Yoshimura, A., Prud'homme, R., 1988. Wall slip corrections for Couette and parallel disk viscometers. J. Rheol. 32, 53-67.

Zarraga, I.E., Hill, D.A., Leighton, D.T., 2000. The characterization of the total stress of concentrated suspensions of non-colloidal spheres in Newtonian fluid. J. Rheol. 44, 185-220.

APENDIX - I

REYNOLDS NUMBER CALCULATIONS FOR CHANNEL FLOW

The Reynolds number was calculated using the formula: $R_{ep} = \gamma a^2 \rho/\eta$, where γ is wall shear rate, 'a' is particle radius; ρ is the suspending fluid density and η is the viscosity of the suspending fluid. The typical shear rate value was taken for the experiments with 40 % suspension.

S.No	Wall shear rate	Particle size and density	Viscosity of suspending fluid	Reynolds number
1	2.5 s^{-1}	200 µm (1.18 g/cm^3)	19.5 cP	0.0013
2	1.3 s^{-1}	200 µm (1.18 g/cm^3)	4000 cP	0.0000025
3	1.5 s^{-1}	80 µm (1.05 g/cm^3)	2.05 cP	0.0012
4	3.5 s^{-1}	250 µm (1.05 g/cm^3)	2.05 cP	0.026
5	7 s^{-1}	500 µm (1.05 g/cm^3)	2.05 cP	0.14
6	4.5 s^{-1}	500 µm (1.05 g/cm^3)	98 cP	0.0028
7	1.5 s^{-1}	500 µm (1.05 g/cm^3)	204 cP	0.00046

REYNOLDS NUMBER FOR ROTATING CYLINDER

The wall Reynolds number was computed using the formula: $R_{ew} = R^2\Omega\rho_s/\eta$, where R is radius of tube (0.6 cm), Ω is angular speed of rotation, ρ_s is the suspending fluid viscosity (1 g/cm^3) and η is the viscosity of suspending fluid (1 cP).

S.No	Rotation speed of the tube (rpm)	Wall Reynolds number
01	1.3	5.37
02	2.11	11.57
03	4.1	16.946
04	5.9	24.386
05	8.3	34.306
06	10.2	42.159
07	13.3	54.972
08	16.7	69.025
09	20.2	83.491
10	24.8	102.5
11	28.7	118.62
12	31.6	130.61
13	34.8	143.84
14	38.1	157.48
15	40.6	167.81
16	71.42	295.19
17	82.19	339.71
18	105.89	437.67
19	120	495.98
20	219.2	906.45

APENDIX - II

DYNAMIC ANGLE OF REPOSE IN ROTATING CYLINDER

Dynamic angle of repose is considered as one of the significant factor for granular particle segregation in rotating cylinder. Hill et al. 91997) have explained the dynamic angle of repose. Their schematic diagram of dynamic angle of repose is shown in the Fig. A1. When the difference in dynamic angle of repose is more for the binary particles, the rate of segregation will also be high in a rotating cylinder. However, the dynamic angle of repose can be measured only when the binary particles attained complete segregation. Since our binary particles did not attained any segregation, dynamic angle of repose for our system could not be measured. As static angle of repose was same for our system, where both particles are of same material as well as shape. Hence, it is justified to assume that dynamic angle of repose also would be the same for our system. If the dynamic angle of repose is same for such systems then other factors play a role in causing the instability in rotating cylinder. In our system buoyancy force, angular rotation speed, viscosity of suspending fluid, free surface availability are the factors which influence the particle segregation even though the static and dynamic angle of repose were same.

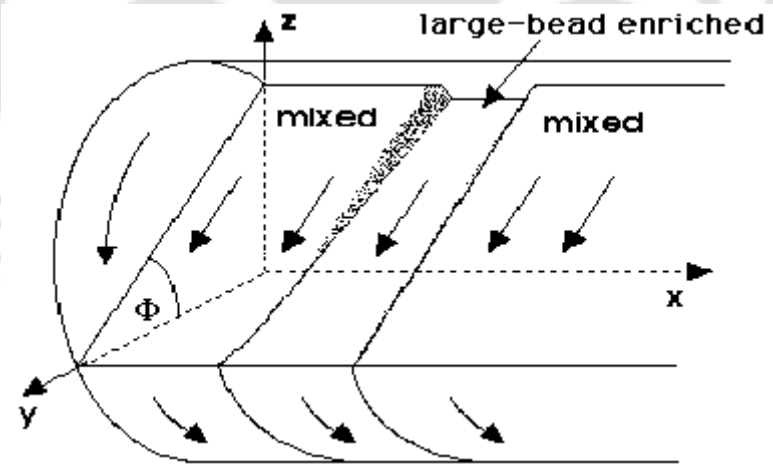

Figure A1: Schematic diagram of the dynamic angle of repose by Hill et al. (1997).

LIST OF PUBLICATIONS

INTERNATIONAL JOURNALS

1. **Kumar, A.A.,** Singh, A., 2010. Dynamics of bi-dispersed settling suspension of non-colloidal particles in rotating cylinder. Adv. Powder Technol. 21, 641- 651.
2. Medhi, B.J., **Kumar, A.A.,** Singh, A., 2011. Apparent wall slip velocity measurements in free surface flow of concentrated suspensions. J. Multiphase Flow, Article in press.
3. **Kumar, A.A.,** Medhi, B.J., Singh, A., Determination of the interface location and free surface deformation of free surface flow of various concentrated suspensions (To be submited in Physics of fluids).

INTERNATIONAL CONFERENCES

4. **Kumar, A.A.,** Singh, A., (Sep 14 - 16, 2009). Axial segregation of bi-dispersed non-colloidal suspensions in rotating drums. "*The Fourth Asian Particles Technology Symposium"*, Delhi, India.
5. **Kumar, A.A.,** Medhi, B.J., Singh, A., (May 30 - Jun 4, 2010). Measurements of apparent wall slip velocity in concentrated suspensions of non-colloidal particles in open channel flow. "*International Conference on Multi Phase Flow"*, Tampa, Florida, USA.
6. **Kumar, A.A.,** Medhi, B.J., Singh, A., (Dec 16 – 18, 2010). Determination of the interface location in free surface flow of concentrated suspension. Presented in "*4th International Conference on Fluid Power and Fluid Mechanics"* IIT Madras, India.